INFLUENCE ON BLOOD PRESSURE WAVEFORMS OF EXTERNAL PRESSURE CONSTRAINTS WITH REFERENCE TO SPHYGMOMANOMETRY

A thesis submitted for
the Degree of Doctor of Philosophy
in the Faculty of Engineering
of the University of London

by

Roger Selwyn Clist

June 1974

Engineering in Medicine Laboratory
Department of Electrical Engineering
Imperial College of Science and Technology
London S.W.7

ABSTRACT

This thesis concerns the characterization of changes in arterial blood pressure waveforms which occur during an indirect blood pressure measurement using a sphygmomanometer on the upper arm. A simple form of analysis is developed and applied to waveforms proximal and distal to the cuff in order to establish a criterion for determining the time at which the cuff pressure is equal to the diastolic pressure.

Work was carried out initially on data obtained during the course of clinical investigations. Two approaches to the analysis are described, one frequency domain, the other time domain. The results of the frequency domain approach are shown to provide an objective and well defined indicator of the diastolic point, namely the first harmonic amplitude ratio of the distal and proximal waveforms. In contrast, the results of the time domain approach were ill defined and open to subjective interpretation.

To test the generality of these results, an electrical analogue model of the vascular system of the arm was constructed and used in a simulation of an indirect blood pressure measurement. Analyses of waveforms generated by the model yielded results similar to those observed in the real situation. It was confirmed that the trend in the first harmonic amplitude ratio parameter was insensitive to small changes in waveshape or period.

The thesis concludes with a discussion of the application of this work to the design of an instrument for the non-invasive measurement of systolic and diastolic blood pressures, and with indications of what further work should be carried out.

INDEX

ABSTRACT 2

ACKNOWLEDGMENTS 5

1. INTRODUCTION 6

1.1 Arterial Blood Pressure 8

1.2 The Measurement of Blood Pressure 9

1.3 Delay Between Two Photoplethysmograms 14

1.4 Scope of the Present Study 17

2. PRESSURE AND FLOW IN BLOOD VESSELS 23

2.1 The Cardiovascular System 24

2.2 Equations of Fluid Flow 29

2.3 Solutions to the Equations 31

2.4 Flow During Indirect Blood Pressure Measurement . 35

2.5 Summary 38

2.6 Conclusion 40

3. ANALYSIS OF ARTERIAL PRESSURE WAVEFORMS DURING INDIRECT BLOOD PRESSURE MEASUREMENT 42

3.1 Aortic and Radial Waveforms 43

3.2 Features of the Data 49

3.3 Frequency Analysis 63

3.4 Impulse Response Analysis 90

3.5 Observations and Conclusions 107

4. ELECTRICAL ANALOGUE MODELLING OF THE VASCULAR SYSTEM . 115

4.1 Types of Model 116

4.2 Transmission Line Analogue of an Arterial Segment . 120

4.3 Improvements to the Simple Analogue 125

4.4 Comprehensive Modelling of the Arterial Tree . . 129

4.5 Conclusion 134

5. SIMULATION OF AN INDIRECT BLOOD PRESSURE MEASUREMENT . 137

5.1 The Model of the Arm 139

5.2 The Peripheral Terminations 145

5.3 The Cuff 153

5.4 Simulation of Indirect Blood Pressure Measurements 164

5.5 Summary 192

6. DISCUSSION 195

6.1 Partial-Beat Analyses 196

6.2 Evaluation of the Simulation 202

6.3 Theoretical Basis of the Waveform Analysis . . 205

6.4 Results of the Analyses 207

7. CONCLUSION 211

7.1 Summary of the Research 212

7.2 Considerations for an Instrument 215

7.3 Proposals for Further Work 218

APPENDICES 220

A. The Model of the Arm 221

B. Ancillary Circuits 231

C. Computer Programs 243

REFERENCES 256

ACKNOWLEDGMENTS

I acknowledge with gratitude the assistance received from the New Zealand National Research Advisory Council whose award of a Research Fellowship allowed me to study at Imperial College for $3\frac{1}{2}$ years.

I wish to thank my supervisor, Dr. J.C. Vickery, for his guidance and help in the many problems encountered during this research. I also wish to thank Professor B.McA. Sayers for his advice, particularly in matters concerning signal analysis.

The assistance of Dr. P. Bourdillon with the recording of blood pressure waveforms is gratefully acknowledged. I am also indebted to Dr. D.M. Monro for the use of his FFT and plotting subroutines.

There are several who have helped in the preparation of this thesis. In particular I wish to record my thanks to Dr. R.I. Kitney for his helpful criticism of the text, Mrs. A. Edwards for the typing, and Mrs. J. Hill for the diagrams.

I wish to express my appreciation of the help and co-operation received from the staff of the Engineering in Medicine Laboratory and my colleagues in Room 809.

Finally, special thanks are due to my wife Jeunesse not only for her assistance with the typing of the draft and the assembly of this manuscript but also for her patience, understanding, and constant encouragement throughout this period of study.

1. INTRODUCTION

1.1 ARTERIAL BLOOD PRESSURE

1.2 THE MEASUREMENT OF BLOOD PRESSURE

1.2.1 Direct Measurement

1.2.2 Sphygmomanometry

1.2.3 De Dobbeleer's Method

1.3 DELAY BETWEEN TWO PHOTOPLETHYSMOGRAMS

1.4 SCOPE OF THE PRESENT STUDY

1.4.1 The Research Proposal

1.4.2 Outline of Thesis

1. INTRODUCTION

The human cardiovascular system has been the subject of a great deal of research. As a result of this work, a parameter of great clinical significance has emerged, namely, the blood pressure. This is the driving pressure circulating blood to every part of the body in order to maintain perfusion of the tissues. The primary reason for its importance is that the level of the blood pressure reflects the state of the cardiovascular system.

The existence of the circulatory system was recognized by Harvey (1628), who concluded that the heart propelled blood in a closed system through invisible vascular connections between the arteries and veins. The first measurement of arterial blood pressure was carried out by Hales (1733) using an intra-arterial cannula, while the use of an external cuff to measure the systolic blood pressure indirectly was first demonstrated by Riva-Rocci (1896). The idea of using the auscultation of arterial sounds for the measurement of both the systolic and diastolic pressures was introduced by Korotkoff (1905). Although this is the method most widely used today, it has the disadvantage that the measurement of blood pressure relies on subjective aural judgment. Clearly there is a need for alternative non-invasive methods based upon objective criteria suitable for application in automatic monitoring systems. Unfortunately, the development of such apparatus has failed to progress as rapidly as other types of patient monitoring equipment (Greatorex, 1971).

This situation stimulated work described in this thesis, which has led to a method for the identification of the diastolic

point of the indirect measurement cycle by signal analysis. It is believed that this new method represents an advance in indirect blood pressure recording techniques, and that, after further development, it will find application in clinical monitoring equipment.

1.1 ARTERIAL BLOOD PRESSURE

The pumping action of the heart causes the arterial blood pressure to vary with every heart beat in a pulsatile manner typified by the waveform shown in Fig. 1-1. The maximum and minimum blood pressures are respectively known as the systolic and diastolic pressures, and the difference between these two pressures is referred to as the pulse pressure. In addition, the waveform is asymmetric so that the mean arterial pressure is less than the arithmetic mean of the systolic and diastolic pressures. The pressures are traditionally expressed by clinicians as the equivalent height of a mercury column in millimetres (mm Hg). For a healthy young adult, the systolic pressure is typically 120 mm Hg, the diastolic pressure 80 mm Hg, and the mean pressure 96 mm Hg (Guyton, 1966).

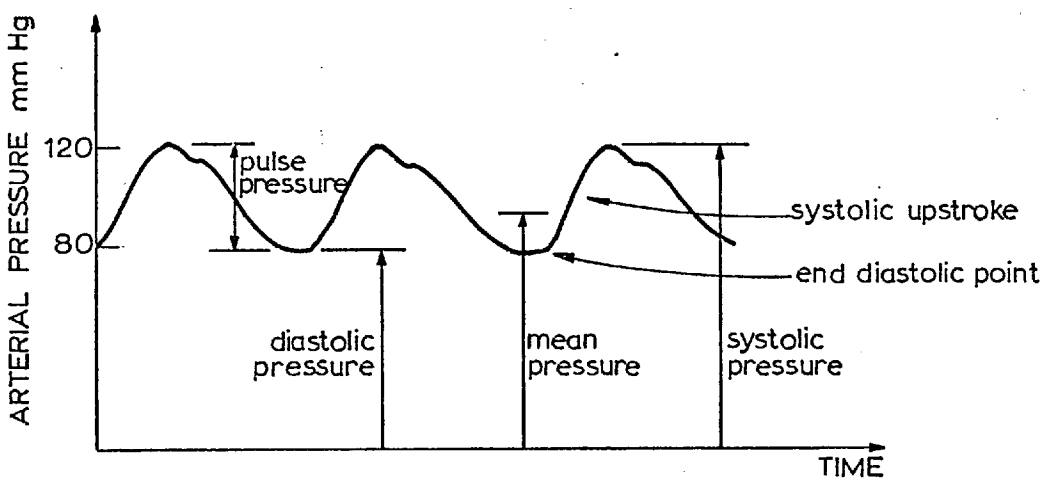


Fig. 1-1: Pressure variation in a large artery.

The pressure waveform comprises a rapid rise from diastolic to systolic levels (known as the systolic upstroke) followed by a slower undulating decrease as the heart relaxes and prepares for the following beat. The point of minimum pressure in the waveform is known as the end-diastolic point. The nature of the vascular system causes changes in the contour of the pulse wave as it travels away from the heart. This is due to several factors, including the smoothing effect of the elastic walls of the blood vessels, the superposition of waves reflected at bifurcations and from the periphery, and the differing velocities of the components of the wave. The net result is the augmentation of the pulse pressure in the peripheral arteries with only a small drop in mean pressure (3-5 mm Hg) (Guyton, 1966).

The magnitudes of the systolic and diastolic pressures are therefore dependent upon the site of measurement. Furthermore, slow variations in blood pressure arise from the regulatory control exercised by the autonomic nervous system, the kidneys, and the endocrine glands. The levels of blood pressure therefore rarely remain constant but change in accordance with the requirements of the body, being in dynamic equilibrium with many interdependent variables.

1.2 THE MEASUREMENT OF BLOOD PRESSURE

1.2.1 Direct Measurement

Blood pressure may be measured directly or indirectly. Direct measurement of blood pressure is performed by puncturing the vessel wall with a hollow needle passed through the overlying

tissues enabling the arterial pressure to be hydraulically coupled to an external pressure transducer by a fluid line filled with saline. Alternatively, a catheter can be inserted and passed along the artery so that the blood pressure may be recorded at any desired site. Although certain technical precautions are required to ensure the faithful reproduction of arterial waveforms, the technique is common surgical practice, giving the maximum amount of information possible. However, because the method necessitates penetration of tissues and artery, it can only be performed under sterile conditions. The use of the method is therefore restricted to situations requiring a high degree of absolute accuracy, maximum dynamic response, continuous monitoring, or measurement in deep regions. (Shirer, 1962).

1.2.2 Sphygmomanometry

Although the systolic and diastolic pressures can be measured accurately only from the intra-arterial waveform, clinicians require ways of estimating these levels indirectly, with minimal discomfort, inconvenience, or risk to the patient. Most indirect methods of measuring blood pressure use some means of applying external pressure to an artery in order to constrict the blood flow. Of these, the Korotkoff Sounds method is universally accepted and widely used (Greatorex, 1971). The method uses a simple apparatus known as a sphygmomanometer. This comprises an inflatable cuff enclosed within a fabric cover and connected by an air line to a mercury manometer and a rubber bulb hand pump. A stethescope is required to detect the Korotkoff Sounds.

The method is described as follows. The cuff is wrapped around the upper arm and quickly inflated to a level exceeding the systolic pressure of the subject, thus occluding the brachial artery and halting the arterial (and venous) flow in the lower arm. The pressure in the cuff is then allowed to escape slowly through a hand-controlled valve attached to the pump, the preferred rate of depressurization being constant at 3 mm Hg per second. Meanwhile the clinician listens for sounds with the stethescope positioned over the brachial artery distal to the cuff. No sounds are heard while the cuff pressure remains greater than systolic blood pressure, but as the cuff is slowly decompressed a level is reached where the systolic peak of the pressure waveform slightly exceeds the occluding pressure. At this point, the "cuff systolic point", the artery under the cuff momentarily opens and allows a brief pulse of blood to flow into the lower arm, simultaneously producing a distinctive sound usually described as being short and sharp. The pressure in the cuff at this moment is taken to be equal to the systolic blood pressure. The sounds continue to be heard with each heart beat, but as the cuff pressure steadily decreases the sounds change in character, becoming muffled before entirely disappearing. The recommended index of the diastolic blood pressure is when the sounds become muffled (Kirkendall at al., 1967). This moment will be referred to as the "cuff diastolic point". After the disappearance of the sounds, the cuff is rapidly exhausted to the atmosphere, thus completing the measurement cycle.

The measurement of systolic and diastolic blood pressures by auscultation of the Korotkoff Sounds has become widely

accepted because it is a non-invasive method using only simple equipment in a straightforward procedure. In fact the term "blood pressures", when unqualified, is understood to mean the brachial systolic and diastolic pressures measured in this manner. The method does, however, have several shortcomings which can cause marked discrepancies between directly and indirectly recorded blood pressures. The principal objection is that the readings are dependent on the skill, experience, and acuity of hearing of the observer. Recommendations for the implementation of the technique are given by Bordley et al., (1951), and Kirkendall et al., (1967). The relationship between the dimensions and construction of the cuff and the accuracy of the measurement is discussed by Karvonen et al., (1964) and Simpson et al., (1965). It appears that although any one measurement may be inaccurate, errors are small when averaged over a large number of measurements (Weinman, 1972).

The genesis of the Korotkoff Sounds is not well understood although many theories have been suggested, as listed by McCutcheon and Rushmer (1967). It has been shown by Anliker and Raman (1966), in a theoretical analysis that the Korotkoff Sounds at the cuff diastolic point are a phenomenon of the dynamic instability of fluid-filled shells, induced by the application of a pressure cuff. They postulate that local flow disturbances are hydraulically amplified to the point of audibility.

A number of factors contributing to measurement inaccuracy are common to all methods utilizing cuffs. For example, it is known that the transmission of the cuff pressure to the arterial wall is affected by the intervening tissues of the limb (Vierhout, 1963). In addition, the systolic and diastolic readings are

taken at different times during the deflation of the cuff and can therefore never relate to the same cardiac cycle. Also, the maximum resolution in the measurement of systolic and diastolic blood pressures is equal to the drop in cuff pressure between heart beats. Assuming a heart rate of approximately one beat per second, the resolution is about 3 mm Hg if the observer maintains linear cuff deflation at the recommended rate.

1.2.3 De Dobbeleer's Method

A different method of indirect blood pressure measurement has been proposed by De Dobbeleer (1963; 1965). In this method, the standard clinical arm cuff is replaced by a double cuff of similar external dimensions, both chambers of the cuff being connected to the same pressure source. The minor pulsations in the volumes of the cuffs caused by the passage of blood pulses in the constricted artery are detected by thermistors mounted in a special chamber in the air line to the cuffs. The pressure in the cuffs is raised and lowered in a manner identical to that performed in the Korotkoff Sounds method. Systolic blood pressure is registered when a pulse is first detected in the distal cuff, this first pulse being delayed with respect to the pulse sensed by the proximal cuff. As the pressure in both cuffs steadily diminishes, this delay becomes pregressively smaller until it disappears completely, a phenomenon often referred to as "phase shift".

This phenomenon is believed to be caused by the opening of the artery being delayed until the instantaneous blood pressure exceeds the cuff pressure. Hence there is no delay when cuff pressure is less than diastolic blood pressure because the artery

is then patent for the complete pressure cycle, and pulsations detected from both cuffs are in phase. The diastolic blood pressure is taken to be equal to the pressure in the cuffs when the phase shift between the pneumatic pulses first becomes zero.

It is therefore seen that the measurement of systolic blood pressure by De Dobbeleer's method is somewhat similar to that of the Korotkoff Sounds technique, whereas the diastolic blood pressure measurement is based on a unique criterion bearing no relationship to previous methods. The objective character of pulse detection makes De Dobbeleer's method suitable for automatic operation, and commercial equipment based on this technique is reported to achieve good correlation with simultaneous Korotkoff Sounds results (Greatorex, 1971).

1.3 DELAY BETWEEN TWO PHOTOPLETHYSMOGRAMS

The method of De Dobbeleer has been extended in an attempt to measure blood pressures indirectly from the finger using photoplethysmograms, i.e. pulsatile waveforms detected by a light-dependent resistor placed in contact with the skin above transilluminated tissues. One waveform is detected at a site distal to a miniature cuff on the finger, whilst a continuous reference waveform is monitored proximal to the cuff (Clark and Gowen, 1969), or from an adjacent finger (Clist, 1970). The finger cuff is inflated and deflated in an identical manner to that of the normal indirect measurement on the arm while the two waveforms are electronically examined for delay between them. To do this, the waveforms are filtered, amplified, and used to gate logic circuitry in order to obtain a rectangular output pulse

with width proportional to the delay between the waveforms.

It was found that a decreasing time delay could be repeatedly detected between the two waveforms in a sequence similar to that described by De Dobbeleer. Therefore it was postulated that the onset and disappearance of the delay marked the registration of the systolic and diastolic blood pressures. The maximum delay (occurring with the first flow pulse under the cuff) was of the order of 100 ms ; with successive heart beats the delay became progressively smaller. However, a point of "zero delay" between the two waveforms could not be identified because of what appeared to be "random delays" of up to ± 5 ms occurring under resting conditions. Hence the registration of the diastolic pressure was taken to occur when the decreasing delay first became less than a minimum threshold value (10 ms).

A comparison of the results with simultaneous blood pressures measured on the upper arm showed poor correlation (Clist, 1970). The discrepancies were thought to arise from three sources: (i) the physiological differences between the blood pressures in the finger and the arm, (ii) the nature of the photoplethysmographic waveform and its filtering for timing purposes, and (iii) uncertainty in the basic postulate that the time delay vanishes at the diastolic point.

The nature of the input signals appears to be the greatest unknown factor. Weinman et al., (1973) have shown that the generation of photoplethysmograms is more complex than is generally thought. Photoplethysmograms from a diffuse vascular bed yield signals directly related to the blood volume: an increase in blood volume reduces the amount of light received

by the photosensor, and vice versa. However, photoplethysmograms are sometimes 'inverted' when monitoring larger arteries, in the sense that more light at the sensor concurs with an increase in arterial blood volume. Although this inversion can be avoided by careful positioning of the transducer, the suspicion remains that all photoplethysmograms contain a mixture of inverted and non-inverted signals (Weinman, 1972).

A photoplethysmographic waveform detected by a light-dependent resistor is a pulsatile signal of a few millivolts amplitude at a D.C. level of several volts. The magnitude of the D.C. level depends on the static resistance of the light-dependent resistor; this may vary over a range of more than ten times from person to person, owing to different light attenuations in the finger tissues. In addition to this variability, for any given monitoring situation the D.C. level appears to drift at very low cyclic frequencies, the drift amounting to some tens of millivolts. It is therefore necessary to remove the slowly-varying D.C. component before amplifying the pulsatile signal to a level of a few volts for triggering purposes. The filter used by Clist (1970) was a 2-stage high-pass filter whose parameter values were chosen to remove the very low frequency drift and also to serve as a differentiator emphasizing the leading edges of the pulsatile signals. The filtered signals were then of a suitable shape for the operation (after amplification) of the peak detection circuits which triggered the time delay measurement logic. The filter performed well in that suitable output signals were given for a wide range of input signal shapes and heart rates, and it had a fast settling time after the occurrence of transients

caused by finger movement. Subsequent work described in this thesis has thrown new light on the filtering requirements. This is discussed further in Chapter 6, where it is shown that the rejection of the low frequencies destroys a significant proportion of the waveform delay information and that the emphasis given to the higher harmonics largely contributes to the unreliability of this method of indirect blood pressure measurement.

1.4 SCOPE OF THE PRESENT STUDY

1.4.1 The Research Proposal

In summary, it may be said that the indirect measurement of blood pressure by the Korotkoff Sounds technique is widely practised and found to give adequate correlation with direct pressures. The mechanism by which the sounds are generated is known to be complex, and a certain amount of mystery surrounds the events taking place beneath the cuff. The influence of the tissues between the cuff and the brachial artery is unknown, but it is recommended that the cuff be 20% wider than the diameter of the limb on which it is to be used (Kirkendall et al., 1967).

De Dobbeleer's phase shift criterion is a unique method for estimating the diastolic blood pressure. The use of time delay measurements makes the method more suitable for implementing in the design of automatic equipment than techniques requiring subjective judgments. However, there is still a need for the reliable non-invasive measurement of blood pressure causing less interference to the patient than an inflated arm cuff.

The extension of De Dobbeleer's method to the use of finger photoplethysmographic waveforms showed that the phase shift phenomenon was present, but measurements were too unreliable

to be used clinically. Nevertheless, the possibility of blood pressure measurement from the finger is very attractive, particularly if it can be achieved with miniaturized equipment permitting patient monitoring in a non-clinical environment. There is therefore much to be gained by a detailed study of the phase shift phenomenon in order that its clinical importance might be realistically assessed and its limitations recognized.

It was proposed that the following work be undertaken to clarify the value of the phase shift phenomenon and its relevance to indirect blood pressure measurement:

(1) that direct arterial waveforms be recorded proximal and distal to a cuff during a normal indirect blood pressure measurement on the arm

(2) that signal analysis techniques be applied to the waveforms in an attempt to characterize the changing delay in a new manner

(3) that any results obtained be shown to be consistently present in the general case.

An inflated cuff makes an incursion into arterial hydrodynamics that becomes less severe as the pressure is released. It was expected that signal analysis techniques would prove sensitive in identifying the point in the indirect blood pressure measurement cycle where certain features of the waveform cease to be modified by the cuff and revert to their pre-occlusion values. This point should coincide with the first pulse for which the artery is patent over the whole cardiac cycle, indicating that the cuff pressure is at diastolic blood pressure.

1.4.2 Outline of Thesis

Chapter 2 contains a brief description of the cardiovascular system and a review of the different techniques which have been adopted in the solution of the equations of fluid motion for the particular case of arterial haemodynamics. Previous waveform analyses were found to deal only with steady-state conditions, whereas the waveforms of interest (those recorded distal to an occlusive cuff) are of an essentially transient nature. The relatively small amount of work specifically related to flow in vessels constrained by external pressure is largely confined to the reporting of experimental observations. This emphasizes the need for an analytical approach to the evaluation of waveforms under these conditions, and it is proposed that Fourier analysis be applied to blood pressure waveforms recorded proximal and distal to an arm cuff. The chapter closes with a discussion of the requirements for recording practical waveforms.

The recording and analysis of aortic and radial blood pressure waveforms are described in Chapter 3. The data are digitized, edited, and divided into successive beats using the E.C.G. peaks as delimiters. The delay between the waveforms is studied initially by making appropriate time measurements in each beat, but no distinct changes are observed by which the diastolic blood pressure may be measured reliably. Although a trend of decreasing delay is seen as the cuff is being deflated, it is concluded that methods relying on the disappearance of a time delay between waveforms are poor indicators of the diastolic point.

In contrast to this finding, harmonic analysis is shown to give a more accurate measurement of the diastolic blood pressure.

Several variations of analysis are compared, all of which show that the most reliable information concerning the cuff diastolic point is contained in the first harmonic amplitude ratios of the distal and proximal waveforms. The results of the analyses are largely presented in graphical form, giving emphasis to the corner point in the trends where the results return to their steady-state values. This corner point is seen to occur when the cuff pressure is close to diastolic blood pressure in each of the five cycles of indirect measurement that were recorded, thus suggesting an objective criterion for measuring the diastolic blood pressure. It is pointed out that confirmation of the generality of the results is required before the analysis procedure can be taken as the basis of a clinical method of indirect blood pressure measurement. Chapter 3 closes with a discussion of the need for a model of the vasculature of the arm with which the effects of an external pressure cuff may be simulated and further waveforms generated for observation and analysis.

In Chapter 4, various types of cardiovascular model are discussed and the electrical analogue approach is selected as being most appropriate for modelling the haemodynamics of an arm during an indirect blood pressure measurement. This form of modelling is described in detail, and it is shown how several important features of pulsatile flow may be incorporated into a complex model based on transmission line theory. However, it was decided to construct a simple model of nineteen 3-component segments, omitting certain refinements which would increase the number of components beyond this minimum.

The design of the electrical analogue model is described

in Chapter 5. It was found necessary to include damping in the peripheral terminations in order to reduce unrealistic resonances in the transmission amplitude response. The cuff is modelled by switches which interrupt the venous and arterial flow whenever the cuff pressure is greater than the proximal blood pressure. Switching instability occurs during changes of state and relates to oscillatory action reported to occur in simulations using hydraulic models. This instability is thought to explain inflections seen in the systolic upstrokes of practical pressure waveforms recorded distal to a cuff.

The programs for time measurements and frequency analyses were repeated on the simulated waveforms and the results were compared with those obtained using practical data. There was close agreement between the results except for the phase differences in the region of the cuff diastolic point. The simulation was repeated with an input containing variable interbeat intervals. Although the shapes of the input waveforms were somewhat unreal, frequency analyses confirmed the validity of the first harmonic amplitude ratio parameter as an indicator of the cuff diastolic point.

The inconsistencies between the phase differences of the practical and simulated waveforms are investigated further in Chapter 6. By performing analyses on truncated sections of each blood pressure beat it is shown that the nature of the trend of this parameter near the cuff diastolic point is obscured by minor changes in waveshape. A second feature revealed by these analyses is the relative insensitivity of the trend of the first harmonic amplitude ratios to small changes in both waveshape and period. This is further evidence of the importance of this

parameter as a reliable indicator of the cuff diastolic point.

Chapter 6 also contains an evaluation of the simulation and its importance to the present study. It is pointed out that although certain aspects of the simple model could be improved, the use of a more refined model would not lead to significantly different conclusions. The use of harmonic analysis in this thesis is compared to the treatment of evoked responses in neurological studies. It is stressed that the vital feature in the analysis is the division of the data into beats beginning at the time of occurrence of the QRS peak of the E.C.G. Sectioning the waveforms in this manner ensures that the entire pressure pulse is always contained within the period of analysis.

Chapter 7 contains comments on the practicability of using the amplitude ratio parameter in an instrument to measure blood pressure indirectly. It is proposed that the research be continued by applying the analyses to waveforms recorded non-invasively.

The appendices contain practical details of the design and construction of the model of the arm, circuit diagrams, and descriptions of the computer programs and subroutines.

2. PRESSURE AND FLOW IN BLOOD VESSELS

2.1 THE CARDIOVASCULAR SYSTEM

2.1.1 The Heart

2.1.2 The Arteries and Veins

2.1.3 The Small Vessels and Microcirculation

2.1.4 Direct Measurement of Pressure and Flow

2.2 EQUATIONS OF FLUID FLOW

2.2.1 Steady Flow

2.2.2 Oscillatory Flow

2.3 SOLUTIONS TO THE EQUATIONS

2.3.1 Womersley's Solution

2.3.2 Solution by the Method of Characteristics

2.3.3 Flow Waveform Generation by Analogue Computer

2.4 FLOW DURING INDIRECT BLOOD PRESSURE MEASUREMENT

2.4.1 Flow in Collapsible Vessels

2.4.2 Experimental Studies with Simulated Arteries

2.5 SUMMARY

2.6 CONCLUSION

2. PRESSURE AND FLOW IN BLOOD VESSELS

In recent years considerable attention has been given to the study of blood pressure and flow. This has not only resulted in a better understanding of the operation of the cardiovascular system, but also has aided clinicians in the diagnosis of disease in the heart and blood vessels. The supply of blood to the organs and tissues of the body is the prime function of the cardiovascular system, and blood flow is therefore a more important quantity than the blood pressure necessary to sustain circulation. However, since blood pressure is technically easier to measure, there has been a large amount of work devoted to methods of computing blood flow from the pressure gradient.

A brief description of the cardiovascular system is given in this chapter. This is followed by a discussion of the hydrodynamic equations and their importance in understanding circulatory effects. Three approaches to the solution of the equations are discussed, as well as the assumptions required to make the equations mathematically tractable. Finally a review is given of previous work dealing with indirect blood pressure measurement and its elucidation.

2.1 THE CARDIOVASCULAR SYSTEM

2.1.1 The Heart

Blood serves as a transport and exchange medium for many physiological processes, two important functions being the supply of fuel to tissue cells and the removal of their waste products. Blood is pumped by the heart and is distributed to every part of

the body by a closed circulatory system.

The heart is a large muscular organ whose action is pulsatile and approximately periodic, the heart rate being subjected to neural and hormonal control. Each cardiac cycle consists of a period of contraction (systole) followed by a longer period of muscular relaxation (diastole). The systolic phase of the cardiac cycle is normally initiated by an action potential emanating from a special group of cells which exhibit spontaneous depolarization; these cells, situated in the sino-atrial node of the heart, are often referred to as the "pacemaker". The electrocardiogram (E.C.G.) is the record of the electrical activity of the heart measured at the body surface.

During systole, blood is forced from the left ventricle of the heart into the aortic artery, and the arterial blood pressure quickly rises to a maximum (the systolic pressure). After full contraction is achieved, there is a brief period of reverse flow into the heart from the aorta, which causes closure of the aortic valve, preventing further back flow. During diastole, the heart relaxes as its chambers fill with blood. Prior to the next systole, the pressure in the aorta drops towards a minimum (the diastolic pressure) as the blood is circulated through the smaller distributing arteries to the capillaries. The pressure in the arteries is therefore pulsatile, varying regularly with every heart beat from systolic to diastolic levels. These levels do not necessarily remain constant, but may vary as a result of other influences, e.g. respiration.

After physiological exchanges have taken place in the capillaries, the blood is collected and returned to the right heart by the venous system. However, it is not immediately

pumped back into the systemic arteries, but is first passed through the pulmonary system where further physiological processes take place in the lungs.

2.1.2 The Arteries and Veins

The arteries and veins are the pipes of the circulatory system conveying blood between the heart and the tissue exchange vessels. The arteries form the high pressure supply to the tissue vessels and the veins constitute the low pressure return. Both portions of the cardiovascular circuit are networks of branching tubes commonly referred to as 'trees'. The diameters of the vessels diminish with distance from the heart, although there is a net increase in total cross-sectional area with every subdivision.

The properties of the arteries greatly influence cardiovascular fluid dynamics. The arterial wall is viscoelastic with differing static and dynamic moduli. Arteries close to the heart are more distensible than those further away, and their diameters change significantly with the pressure pulsations of each heart beat. The change in volume represents temporary storage of blood, so that the intermittent flow pulses from the heart are converted into continuous, though pulsatile, arterial flow.

The repetitive action of the heart sustains the oscillations of arterial pressure and flow. As the pulse travels away from the heart the systolic pressure increases and the diastolic pressure decreases, with little drop in mean pressure. This augmentation of the pulse pressure is partly due to wave

reflections at branch points and arterial terminations. Changes in waveshape may also be attributed to the frequency dependence of the pulse wave velocity, higher harmonics being propogated at a great velocity than lower frequencies.

Flow in the veins is almost steady, except in the vena cava where it is influenced by the periodic filling of the heart. Venous diameters are greater than those of their corresponding arteries, and the walls are more distensible. The veins are normally partly collapsed, so that the body can accommodate changes in total blood volume by altering the amount of venous storage.

2.1.3 The Small Vessels and Microcirculation

Linking the arteries to the veins are the small arteries, arterioles, capillaries, venules, and small veins. Because the greatest pressure drop in the circulation occurs in these vessels they are collectively represented by what is known as the peripheral resistance.

The damping of the arterial pressure wave first occurs in the small arteries terminating the major arterial branches. A major drop in mean pressure then occurs in the arterioles, where the pulsatile waveform is damped to such an extent that capillary flow is practically non-pulsatile (Selkurt, 1966). It is in the capillaries that the physiological exchanges between blood and tissue take place, and the diameters of these vessels are often less than the diameter of a red blood cell. The other components of the microcirculation, the arterioles and venules, not only are larger in diameter but also have walls of smooth muscle. The contraction and relaxation of these muscular walls is a phenomenon

known as vasomotion, by means of which large changes in the perfusion of tissue beds are possible. Hence the blood flow to the various parts of the body does not necessarily remain constant but varies with the physiological requirements of the dependent tissues.

2.1.4 Direct Measurement of Pressure and Flow

The direct measurement of blood pressure in the large arteries using a catheter and transducer requires arterial puncture. Measurement is accurate and waveforms are faithfully reproduced provided care is taken to remove all air bubbles from the saline-filled catheter. Otherwise, the overall frequency response can be considerably degraded. The magnitudes of systolic and diastolic pressures depend on the site of measurement. A reference level is required to account for hydrostatic pressure differences.

The blood velocity waveform has been experimentally observed by McDonald (1960). Small bubbles of oxygen were injected into a blood vessel and their movement photographed through the vessel wall by high-speed cinematography. The curve of average velocity is constructed by tracing the path of a bubble from the film. A calibrated blood flow waveform may be obtained from this provided the internal cross-sectional area of the blood vessel is known. To obtain an accurate quantitative result, the internal radius of the blood vessel needs to be precisely measured, an error of 0.1 mm resulting in a peak flow rate error of approximately 30% (McDonald, 1955). Using this method in arteries of about 4 mm diameter, it is seen that the peak of the flow curve precedes that of the pressure pulse, and

there is a period of back flow (McDonald, 1960).

Electromagnetic flowmeters may be used for the measurement of pulsatile blood flow in exposed vessels; such instruments are capable of measuring flow in small arteries. Blood flow is observed to be oscillatory in arteries of 1 mm diameter, but the peaked flow pattern is considerably damped and there is no back flow (Attinger, 1966).

The measurement of flow is hampered by the calibration and stability difficulties of flowmeters. These problems are more pronounced with miniature pressure and flow transducers designed for intra-arterial use, where position across the blood stream becomes an important factor in making calibrated measurements.

2.2 EQUATIONS OF FLUID FLOW

2.2.1 Steady Flow

The pressure-flow relationship for steady flow of a fluid in a rigid tube is expressed by Poiseuille's equation (Eq.2.1) (Guyton, 1966).

$$Q = \Delta P . \frac{\pi r^4}{8 \mu l} \qquad (2.1)$$

where Q = flow rate

ΔP = pressure gradient along the vessel

r = vessel internal radius

l = vessel length

μ = viscosity of the fluid

The most significant factor in Poiseuille's equation is the proportionality of flow to the fourth power of the vessel

radius. Hence the diameter of a blood vessel largely determines the rate of blood flow through it. This is the reason for the effective regulation of local blood flow by vasomotor control of the diameter of the arterioles.

Equation 2.1 assumes the steady, laminar flow of a Newtonian (constant viscosity) fluid. Blood exhibits an anomalous viscosity which becomes significant both at low flow velocities and in small vessels. This is thought to be due to the particle nature of the blood (Burton, 1965).

2.2.2 Oscillatory Flow

A basic law of fluid motion may be formed by relating the inertial forces of acceleration of a blood mass and the frictional forces of viscous flow to the associated pressure gradient along the stream. This law is expressed mathematically by the Navier-Stokes equations, which are second-order partial-differential equations in 3 dimensions. Equations 2.2 and 2.3 are the Navier-Stokes equations for an incompressible Newtonian fluid flowing with cylindrical symmetry (Attinger, 1968). Further equations are required to describe the behaviour of the vessel wall. All mathematical analyses of flow involve simplifications so that these fundamental equations can be solved for specific conditions. For example, for the special case of steady flow in rigid tubes, the equations reduce to Poiseuille's equation.

$$\frac{\delta V_z}{\delta t} + V_r \frac{\delta V_z}{\delta r} + V_z \frac{\delta V_z}{\delta z} = F_z - \frac{1}{\rho}\frac{\delta P}{\delta z} + \nu\left(\frac{\delta^2 V_z}{\delta r^2} + \frac{1}{r}\frac{\delta V_z}{\delta r} + \frac{\delta^2 V_z}{\delta z^2}\right) \qquad (2.2)$$

$$\frac{\delta V_r}{\delta t} + V_r \frac{\delta V_r}{\delta r} + V_z \frac{\delta V_r}{\delta z} = F_r - \frac{1}{\rho}\frac{\delta P}{\delta r} + \nu\left(\frac{\delta^2 V_r}{\delta r^2} + \frac{1}{r}\frac{\delta V_r}{\delta r} - \frac{V_r}{r^2} + \frac{\delta^2 V_r}{\delta z^2}\right) \qquad (2.3)$$

where r = radial coordinate
z = longitudinal coordinate
t = time
p = pressure
v = velocity
ν = kinematic viscosity = $\frac{\mu}{\rho}$
ρ = density of fluid
μ = viscosity of fluid
F = the sum of external body forces

2.3 SOLUTIONS TO THE EQUATIONS

2.3.1 Womersley's Solution

A technique for solving the Navier-Stokes equations for pulsatile flow was developed by Womersley between 1954 and 1957. The initial assumptions were constant diameter rigid tubes and laminar flow of a constant viscosity homogeneous fluid (Womersley, 1955a). The analysis was later extended to include the viscoelastic properties of the arterial wall (Womersley, 1955b, 1957a). Finally the concept of a 'tethered' artery was introduced, i.e. the artery was assumed to be constrained from moving longitudinally by the connective tissue (Womersley, 1957b). The restriction of a thin-walled vessel was removed by Jager in a more generalized treatment (Noordergraaf, 1969).

The first step in the calculation of the flow waveform is the experimental measurement of the pressure gradient. The pressure gradient is a difficult quantity to measure with precision, and an error of 1 mm Hg/cm can result in a peak flow error of 30% (McDonald, 1955). Theoretically the pressure gradient should be measured at a point, but in practice it is the differential pressure measured over a short segment of artery. The transducer error would be minimized by making the arterial segment long, but to avoid errors due to the inclusion of reflected components, the measurement is made over as short a

segment of artery as possible. Of course there can be no side flows from this segment.

A steady heart rate is assumed so that the pulsatile pressure and flow waveforms may be considered to represent a condition of steady-state oscillation. Fourier Analysis is applied to the pressure gradient waveform to obtain the amplitudes and phase angles of the fundamental and its harmonics. For each discrete frequency the corresponding flow curve is calculated from the equations, using tables of Bessel Functions with complex arguments. The arterial pressure-flow relationship is assumed to be linear, and the flow waveform is taken to be the sum of the flow curves individually calculated. In practice it is unnecessary to go beyond the sixth harmonic, as further harmonics modify the composite flow waveform to an extent less than the errors involved in the approximations. There is close agreement between the waveforms calculated by Womersley's method and those observed experimentally by cinematography (McDonald, 1960). The errors due to the assumptions are therefore small.

2.3.2 Solution by the Methods of Characteristics

The method of characteristics is a technique that is suitable for digital computer solution of partial differential equations with non-linear terms. When applied to arterial flow, this approach uses the continuity and momentum equations together with an empirical equation defining the behaviour of the vessel wall. By prescribing initial and boundary conditions, these relationships permit flow and pressure to be predicted as functions of time and distance along the vessel. Account is taken of reflections at bifurcations by satisfying the equations

at closely spaced intervals along the vessel for small time increments.

The flow is assumed to be laminar and uni-dimensional, i.e having a flat velocity profile. Viscous losses are taken to be proportional to velocity, and higher for reverse flow. Side flows may be simulated by including a term in the continuity equation to represent a distributed outflow along the length of the vessel. The method permits a wide choice of assumptions of vessel wall behaviour. Lambert (1958) assumes non-linear wall elasticity, whereas Streeter et al. (1963, 1964) assume that the vessel walls are linearly elastic and tethered along the length of the vessel. The method has been extended by Vander Werff (1971) to remove the need for a distal boundary condition.

The waveforms published by Streeter et al. (1964) do not agree very well with simultaneous flowmeter waveforms, particularly in the region of back flow. However, some of the discrepancies may be due to inadequate experimental techniques (Attinger, 1968). The principal limitations of the method are the assumption of uni-dimensional flow and the empirical equation describing the wall (Vander Werff, 1971).

2.3.3 Flow Waveform Generation by Analogue Computer

A method of generating the instantaneous and continuous flow waveform from the pressure gradient has been developed by Fry (1959). The technique is applicable to the ascending and upper thoracic aorta, where the flow velocity profile may be assumed, on average, to be flat. The flow is visualised as a solid cylindrical bar of liquid sliding in a viscous sleeve.

For this case the Navier-Stokes equations can be reduced to

$$-\frac{\delta p}{\delta z} = L\frac{\delta Q}{\delta t} + RQ \qquad (2.4)$$

where p = pressure, Q = flow, z = distance, t = time, and

$$R = 1.6\frac{8\mu}{\pi r^4} \qquad (2.5)$$

$$L = 1.1\frac{\rho}{\pi r^2} \qquad (2.6)$$

where r = internal radius of vessel

μ = viscosity of fluid

ρ = density of fluid

An analogue circuit may be used to solve Eq. 2.4 to provide a continuous flow waveform using the pressure gradient as a forcing function. The bracketed constants in Eq. 2.5 and 2.6 have been determined empirically by matching the analogue computer solution to the simultaneous waveform of a flowmeter (Fry, 1959). The inertial and frictional constants (L and R respectively in Eq. 2.4) therefore take into account deviations from the assumed flat velocity profile, and compare favourably with constants obtained from Womersley's theory (Greenfield and Fry, 1965). Experiments indicate that in large arteries, where the inertial term dominates the differential equation, the results given by the analogue computer do not differ appreciably from those predicted by Womersley's method. However, Womersley's method gives better results for small arteries, as the frictional component is more closely estimated (Greenfield, 1966). Gabe (1965a, 1965b) has used Fry's method for the measurement of flow in the iliac artery.

2.4 FLOW DURING INDIRECT BLOOD PRESSURE MEASUREMENT

2.4.1 Flow in Collapsible Vessels

The situation during an indirect blood pressure measurement is one where the walls of the artery under the cuff are forced by the external pressure to undergo large deformations. Flow in the veins occurs under similar conditions, and although the characteristics of venous and arterial walls differ, comparisons may be drawn between the two situations.

Conrad (1969) has studied the pressure-flow relationship in collapsible tubes for both steady and non-steady flow. It was found that steady flow through a short length of thin-walled rubber tube surrounded by external pressure was a multiple-valued function that could be separated into three regions corresponding to the open, partially collapsed, and almost completely collapsed tube. The pressure drop between inlet and outlet determined the flow, whereas the transmural pressure and the stresses in the wall determined the tube geometry. The flow was varied by changing the upstream pressure while the external pressure and downstream circuit were held constant. Poiseuille's law was obeyed when the tube was either widely open or almost collapsed. In both cases the tube behaved as if it had rigid walls, but the fluid resistance for the collapsed state was 100 times greater than when widely open.

In many experiments the tube was observed to oscillate when partly collapsed, due to the dynamic resistance becoming negative at a critical transmural pressure. The point of instability is determined by the tube geometry and the elasticity of the wall, and is independent of the rate of flow. However, flow influences collapse through an increase in transmural

pressure by the Bernouilli effect (the local reduction of internal pressure caused by increased fluid velocity at a constriction). Conrad proposes that the equivalent circuit for the tube is a flow-controlled non-linear resistance with series inertance and shunt compliance, all parameters being volume dependent.

Vessel stability is also discussed by Burton (1951, 1965). Analysis of the stability of vessels having both active tension (of smooth muscle) and elastic tension (of elastin and collagen fibres) shows that equilibrium is possible over a wide range of lumen size. For a given active tension, if the transmural pressure is lowered the vessel can reach a point of instability (the "critical closing pressure") and is forced to close completely. This will also happen for a given transmural pressure if the active tension rises above a critical value. This effect is seen in the vasomotor control of arteriolar flow, and is probably only of minor importance to flow in the large arteries, where the ratio of smooth muscle to elastin is small.

2.4.2 Experimental Studies with Simulated Arteries

An experimental apparatus to reproduce the generation of Korotkoff sounds has been described by Sacks et al. (1963). In this apparatus a rubber tube was used to represent the artery and a surrounding pressure chamber to simulate the cuff. The input to the model was a sinusoidal pressure generator. Arterial wall displacements and wave velocities measured from the model were in close agreement with the theoretical results of Womersley except during transient changes in mean pressure level. The auscultatory systolic and diastolic pressures were

found to be consistently higher than the corresponding maximum and minimum intra-arterial pressures by an amount dependent on the stiffness and thickness of the arterial wall.

The apparatus described above was modified by Anliker and Raman (1966) to observe the characteristic behaviour of the vessel wall and fluid. They found that there was an established flow prior to the actual onset of Korotkoff sound production. Furthermore, at diastolic cuff pressures the simulated artery underwent only small deformations and essentially retained its circular cross-section during the whole cardiac cycle. It was suggested that this was due to the external pressure exceeding the intra-luminal pressure for too short a time to allow the prevailing forces to induce the collapse of the vessel. Flow visualization using dye tracers did not reveal any turbulent bursts or vortex shedding. Anliker and Raman also showed that the application of a pressure cuff can change the system locally from one that is dynamically stable to one that is intermittently unstable and capable of mechanically amplifying certain vibrations. They concluded that the Korotkoff sounds at diastole are a phenomenon of the dynamic instability of the brachial artery, the instability being introduced by the application of the pressure cuff.

McCutcheon and Rushmer (1967), using cineangiograms and plastic casts of canine arteries, demonstrated that as the wall is unloaded by decreased transmural pressure the arterial lumen under the cuff is primarily tapered and its circumference shrinks considerably before becoming roughly elliptical and flattening completely. As a result, they doubt that rubber tubes constitute

adequate models for arteries in vivo, arguing that rubber tubes become unstable and flatten into a binodal configuation when externally compressed.

2.5 SUMMARY

The equations of oscillatory fluid flow are non-linear and are mathematically intractable. While the equations of steady flow (modified by appropriate coefficients to account for turbulence, etc.) are satisfactory for general hydraulic engineering calculations, the analysis of arterial flow requires a more detailed treatment because of the high proportion of pulsatility. In addition, blood is a complex heterogeneous fluid with anomalous viscosity, and in many situations the deviations from Newtonian behaviour cannot be ignored.

A search of the literature has shown that up to the present the main interest in cardiovascular fluid dynamics has been the computation of flow waveforms from the pressure gradient. Comparisons between different sites in the arterial tree have been mainly in terms of fluid impedance and wave velocity. A large proportion of the work concerns the aorta, where parameters may be measured with less error than in smaller vessels. Most of the properties of the arterial wall have been determined from excised arteries, and although the materials of the wall have stable physical properties, considerable dimensional changes take place when a vessel is removed from the body (McDonald, 1960), because it is no longer tethered to the surrounding tissues.

Womersley's theory appears to be the reference with which all other approaches to steady-state oscillatory flow are compared.

His extensive work on the linearization of the Navier-Stokes equations has resulted in the definition of a non-dimensional parameter (Eq. 2.7) often referred to as the "Womersley alpha". Because of difficulties in manipulating Bessel functions with complex arguments, early investigators were limited to situations where α was either large or small compared to unity, thus excluding part of the range of physiologic interest (Noordergraaf, 1969). Womersley, using a digital computer, was able to remove this restriction, and show that for all values of α the calculated waveforms agree closely with flowmeter waveforms.

$$\alpha = r \sqrt{\frac{\omega}{\nu}} \qquad (2.7)$$

where r = internal vessel radius

ω = angular frequency

ν = kinematic viscosity of blood

α = "Womersley's alpha", non-dimensional parameter

Fry's method is an attractive way of obtaining the instantaneous flow curve from the pressure gradient using simple instrumentation. Being an analogue computer solution of a differential equation, it can deal with transient as well as steady-state cases. However, its application to the measurement of the flow waveform either side of a cuff during an indirect blood pressure measurement is limited in that the differential equation being solved becomes an invalid representation of the physical situation. Fry (1959) states that the vessel must not pulsate greatly and entering flow must not be from an expanding jet. The assumption of uni-dimensional flow also restricts the application; similarly in Streeter's method, although the method of characteristics can deal with large wall movements and other

non-linearities.

These techniques of solving the equation of pulsatile flow have been undertaken to elucidate the relationships of arterial haemodynamics. No analyses relative to transient conditions have been found, except in the study of sphygmomanometry from a stability viewpoint by Anliker and Raman (1966). Little work has apparently been done on the events taking place beneath an inflated arm-cuff, which is a complex situation worthy of closer attention.. The purpose of the present study is to characterize the alterations in waveforms imposed by a changing external pressure constraint produced by a cuff. Certain characteristics have been displayed in the hydraulic model of Sacks et al. (1963), but the input waveform used was sinusoidal and not representative of blood pressure.

2.6 CONCLUSION

The review of cardiovascular analyses given in this chapter has revealed the complexity of establishing pressure-flow relationships on a theoretical basis under steady-state conditions. The situation occurring during an indirect blood pressure measurement is much more complicated, making the theoretical approach even less attractive. It is concluded that an analytical approach based on in vivo measurements would be fruitful in characterizing the transient situation. A cuff imposes a gross disturbance on the arterial system, and a frequency analysis of vascular waveforms is certain to show deviations from normal values during the changing waveshapes that occur during cuff depressurization. A Fourier description of harmonic amplitudes and phase angles would highlight transient time delays.

There is therefore a need for directly recorded waveforms with which to explore Fourier techniques. Whilst the ideal measurements would be of flow in the vessels proximal and distal to an arm-cuff, direct pressure waveforms are much easier to obtain, and it is proposed to use these as a basis for analysis. The proximal waveform could be approximated by a recording of aortic arch pressure such as is commonly performed in the course of clinical investigations. Similarly, the distal waveform could be approximated by a recording of radial blood pressure. By accepting these waveforms, it would be possible to obtain recordings from a patient undergoing aortic catheterization with the additional intervention of a radial puncture. The recording and use of these waveforms to investigate such features as time delays, spectral content, and the accuracy of systolic and diastolic measurements is outlined in the following chapter.

3. ANALYSIS OF ARTERIAL PRESSURE WAVEFORMS DURING INDIRECT BLOOD PRESSURE MEASUREMENT

3.1 AORTIC AND RADIAL WAVEFORMS

3.1.1 Analogue Recording of Data

3.1.2 Digitizing the Data

3.1.3 Editing of Data

3.2 FEATURES OF THE DATA

3.2.1 Blood Pressure Waveforms

3.2.2 Sequence of Events

3.2.3 Systolic and Diastolic Pressures

3.2.4 Timing Measurements

3.3 FREQUENCY ANALYSIS

3.3.1 The Fourier Series and Discrete Fourier Transform

3.3.2 The Fast Fourier and Chirp-Z Transforms

3.3.3 Fixed Period Analysis

3.3.4 Waveform Levelling

3.3.5 Interbeat-Interval Period Analysis

3.4 IMPULSE RESPONSE ANALYSIS

3.4.1 The Cuff as a Filter

3.4.2 Filtered Impulse Responses

3.5 OBSERVATIONS AND CONCLUSIONS

3.5.1 The Waveforms

3.5.2 Time Relations of the Waveforms

3.5.3 Application of Signal Analysis Techniques

3.5.4 The Need for a Model

3. ANALYSIS OF ARTERIAL PRESSURE WAVEFORMS DURING INDIRECT BLOOD PRESSURE MEASUREMENT

This chapter describes the analysis of aortic and radial artery blood pressure waveforms recorded during a normal indirect blood pressure measurement on the upper arm. The results of analyses in both the frequency and time domains show several interesting features that occur during cuff depressurization. Curves of phase differences between corresponding harmonics of the two waveforms plotted versus beat number show a corner point in the trends when the cuff pressure is approximately equal to an elevated distal diastolic pressure that occurs prior to the cuff diastolic point. On the other hand, corresponding curves of the amplitude ratio of the distal and proximal fundamental components are shown to indicate the cuff diastolic point more accurately. These features are observed consistently in all the records analysed, contrasting with the unreliable nature of the results of direct time measurements on the same data. This suggests that signal analysis techniques could be exploited in an instrument to provide an objective method of locating the cuff diastolic point.

3.1 AORTIC AND RADIAL WAVEFORMS

3.1.1 Analogue Recording of Data

The recording took place in the Catheter Room of Hammersmith Hospital, at the termination of a left-heart catheterization. The patient, a male aged 36 years, was diagnosed as having aortic stenosis and regurgitation, i.e. the aortic valve was abnormally narrow, and leaked. The catheter (inserted via the

femoral artery) was withdrawn from the heart and positioned in the ascending aorta, but unfortunately, due to the patient's condition the blood pressure waveform at this site exhibited ringing at the systolic peaks. However, despite the presence of distortion, this waveform later proved to be satisfactory for the purposes of the current study.

A 19-gauge needle was inserted into the radial artery at the left wrist and a standard blood pressure cuff (width 13 cm across the fabric) was wrapped around the left arm in the normal position over the brachial artery. During recording the patient was supine on the operating table with his arm horizontal at heart level. The radial blood pressure was transmitted to a Statham P23GB strain-gauge pressure transducer through an Alexa catheter (length 180 cm), whereas the aortic blood pressure was transmitted to an identical transducer through a Judkin's catheter (length 120 cm). The outputs of both transducers were connected to a multi-channel oscillographic recorder for display; a third channel was used to display the patient's E.C.G. The balanced outputs of the three display channels were amplified by simple differential amplifiers with a gain of 10, and the single-ended outputs recorded on three frequency modulated channels of an instrumentation tape recorder (P.I.6208) at 3.75 inches per second. The air pressure in the cuff was monitored by a differential-transformer transducer (S.E.75/8) connected to a portable transducer amplifier (S.E.905) and recorded simultaneously on a fourth channel of the instrumentation tape recorder.

The pressure in the cuff was raised and lowered as in the usual indirect blood pressure measurement, the deflation rate

being approximately 3 mm Hg per second. This cycle was repeated a total of five times in 7½ minutes, after which the needle in the radial artery was withdrawn. At this point it was realised that the severe ringing that had been observed in the aortic waveform could have been reduced by moving the catheter away from the heart. The catheter was therefore moved approximately 15 cm to the aortic arch, and a further recording of 30 seconds made. The position of the catheter was checked using an X-ray monitor.

The experiment was completed by recording zero and calibration levels on the three pressure channels. A water column equivalent to a pressure of 80 mm Hg was available for calibrating the Statham transducers. The cuff pressure channel was calibrated at 200 mm Hg.

3.1.2 Digitizing the Data

The analogue data was digitized by the IBM 1800 computer in the Engineering in Medicine Laboratory, using an Analogue to Digital Conversion program to create a digital (ADC) tape of the data as multiplexed integer words of 11-bit precision. The four channels digitized were (1) the aortic blood pressure, (2) the radial blood pressure, (3) the E.C.G., and (4) the cuff pressure. Sampling was carried out at a rate of 200 Hz per channel, this figure being chosen according to the following considerations:-

(1) If the sampling rate is too low, information about detailed fluctuations of the continuous waveform is lost. If the sampling rate is too high, the number of data samples is unnecessarily large. The minimum sampling rate for the adequate representation of a continuous signal is specified by the sampling theorem, namely, a sampling frequency twice that of the highest frequency

present in the signal (Nyquist, 1928).

(2) Of the four channels digitized, the E.C.G. was the waveform containing the highest frequencies. By experiment, it was found that the E.C.G. could be low-pass filtered with a 3 dB cut-off frequency of a minimum of 48 Hz (30 dB/octave attenuation outside the pass band) without visible alteration to the shape of the QRS segment (refer Fig. 3-1). It was important that no distortion of the QRS shape occurred, as the reference times for each beat were based on the times of occurrence of the QRS peaks in the digitized E.C.G. (Section 3.1.3).

(3) Assuming that the E.C.G. is band-limited to 48 Hz, the minimum sampling rate permitted by the sampling theorem is 96 Hz. If sampling was carried out at this rate, the peak of the QRS segment could be located precisely by a complex signal reconstitution procedure to obtain inter-sample data points. However, this procedure can be avoided if the sampling rate is increased sufficiently. It was therefore decided to sample the waveforms at 200 Hz per channel so that the location of the peak of the QRS segment could be determined within $\pm$ 2.5 ms without the requirement for interpolation. This proved to be sufficiently accurate for present purposes.

The tape was played at 10 times the recording speed, and the external synchronization of the analogue-to-digital converter was set to 8 KHz, i.e. an effective real-time sampling rate of 200 Hz per channel. The cuff pressure channel was low-pass filtered by the tape recorder output filter, with a cut-off frequency of 100 Hz (10 Hz real-time frequency). Both blood pressure channels were low-pass filtered by double K section

passive filters (Allison Laboratories, Model 2AB) with cut-off frequencies of 480 Hz (48 Hz). The E.C.G. channel was band-pass filtered by a similar passive filter, the cut-off frequencies being 15 Hz and 480 Hz (1.5 Hz, 48 Hz). The lower cut-off frequency of the pass band was necessary to remove low frequency drift and produce a stable base line.

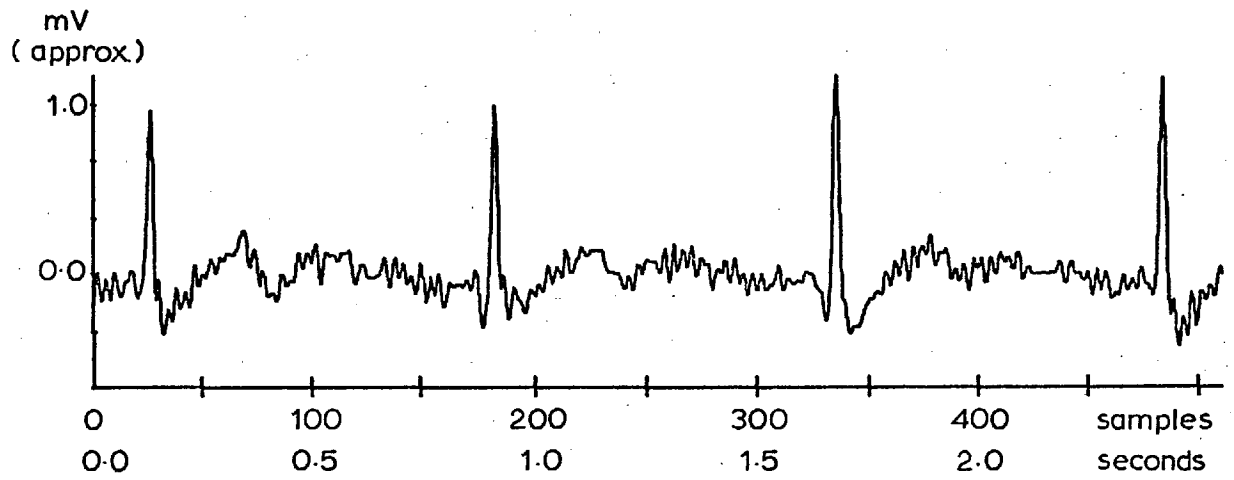


Fig. 3-1: Digitized E.C.G. Waveform

3.1.3 Editing of Data

It was decided to do most of the data processing on the CDC 6400, the main College computer, and to use the IBM 1800 in the Engineering in Medicine Laboratory for minor programs, particularly for interactive programs when oscilloscope display, or use of the ADC tape was required. The data were transferred between machines in compressed binary form, 75 12-bit integer words being packed to an 80-column punched card. This allowed the full 11-bit precision of the ADC data to be passed to the CDC machine.

Since both the aortic and radial blood pressure waveforms are related to a common generator, the heart, it was decided to analyse the data on a beat-by-beat basis, using the E.C.G. peaks as timing markers. The positions of the E.C.G. peaks in the sampled data are therefore the only information required from this channel thus condensing the data considerably. A similar large reduction in data may be made by sampling the cuff pressure channel only once per beat. Although the cuff pressure changes by 3 mm Hg each second, a sampling rate of once per beat corresponds to the same resolution as given by the usual indirect blood pressure measurement method, and it is therefore acceptable. Hence the minimum data to be transferred to the CDC machine comprises the two sampled blood pressure records, the times of occurrence of the QRS peaks, and the cuff pressure samples at these instants.

An editing program was written for the IBM machine to perform this task directly from the ADC tape. In this program, large portions of data were read from the tape, demultiplexed, and put into appropriate core memory arrays for the four channels. The program then scanned the E.C.G. array and located the QRS peaks by firstly detecting the crossing of a pre-set threshold and then searching for the following maximum. The E.C.G. waveform was then displayed on the oscilloscope with the selected peak values brightened. If the program failed to detect a peak because its height did not exceed the threshold, the omitted peak could be inserted by shifting a movable bright spot to the appropriate position on the screen. However, this facility was rarely required as the QRS had a stable amplitude.

Finally, both pressure waveforms were simultaneously displayed on the oscilloscope with the samples occurring at the QRS peaks brightened. This was to check for abnormalities in the data. Three records of binary punched cards were then produced. The first record (one card) contained the cuff pressure samples and the indices of the QRS peaks relating to the following two records (approximately 28 cards each) of the sampled aortic and radial blood pressures. This procedure covered a data length of 10, 11, or 12 heart beats, and was repeated to produce consecutive records of punched cards until the cycle of cuff inflation had been completed. The program was repeated for all five cycles of cuff pressure, and was also used for a small section of the aortic arch blood pressure waveform.

3.2 FEATURES OF THE DATA

3.2.1 Blood Pressure Waveforms

Fig. 3-2 shows the data of the final cuff pressure cycle. There are 67 heart beats occurring in 52.5 seconds, plotted as six consecutive records. The aortic pressure waveform may be differentiated from the radial waveform by the spurious ringing on systolic peaks. The vertical lines on the plots indicate the sample numbers of the QRS peaks. The line representing the cuff pressure appears discontinuous in places because it is drawn as a succession of straight lines joining samples taken at the time of occurrence of the QRS peaks.

Fig. 3-3 shows a section of the aortic arch waveform recorded after the radial needle had been withdrawn. Even with a small shift in the aortic catheter position, the ringing seen in

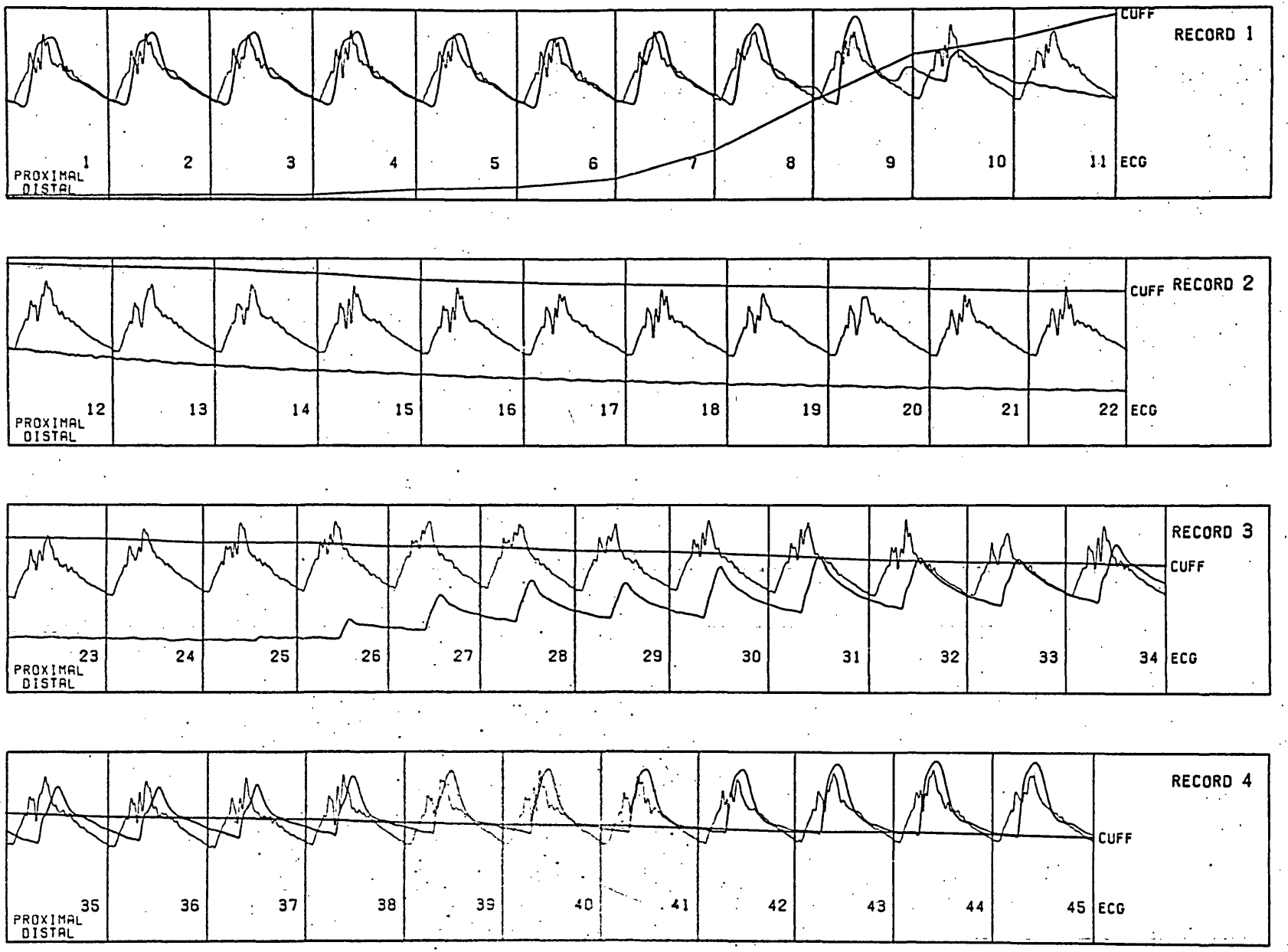

RECORD 1
CUFF
ECG
PROXIMAL
DISTAL
1
2
3
4
5
6
7
8
9
10
11
RECORD 2
CUFF
ECG
PROXIMAL
DISTAL
12
13
14
15
16
17
18
19
20
21
22
RECORD 3
CUFF
ECG
PROXIMAL
DISTAL
23
24
25
26
27
28
29
30
31
32
33
34
RECORD 4
CUFF
ECG
PROXIMAL
DISTAL
35
36
37
38
39
40
41
42
43
44
45

Fig.3-2 (page 1)

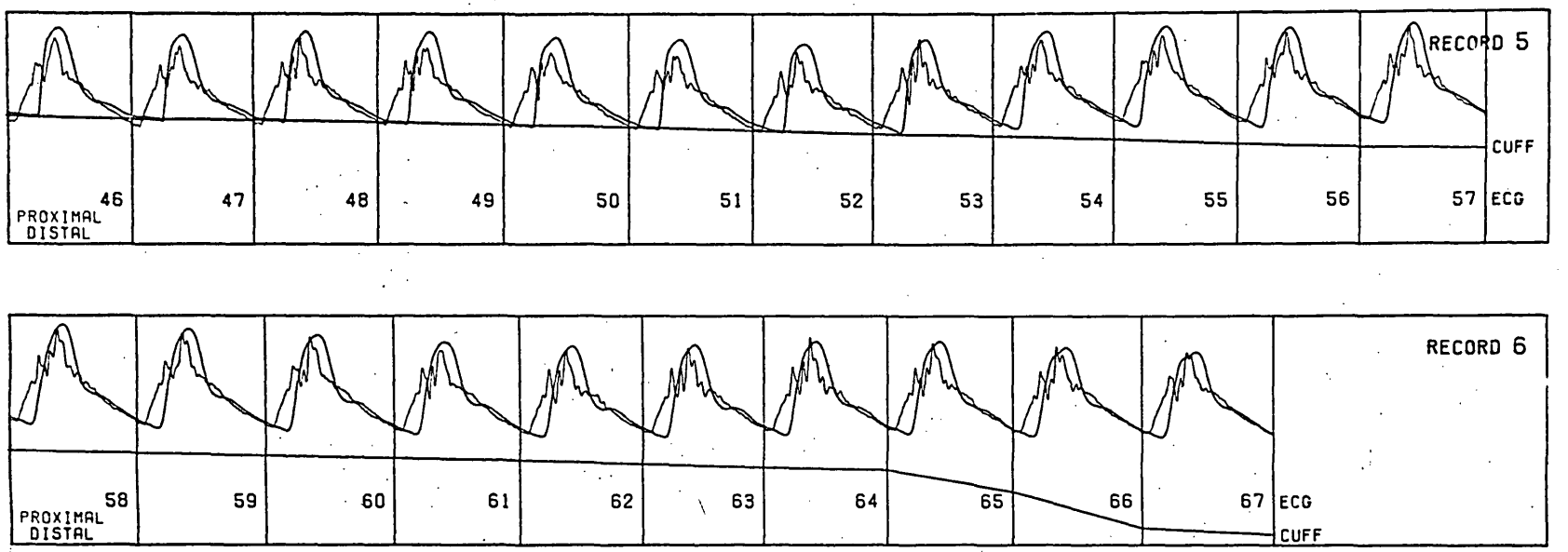


Fig.3-2. (page 2): Ascending aorta and radial blood pressures recorded during an indirect blood pressure measurement.

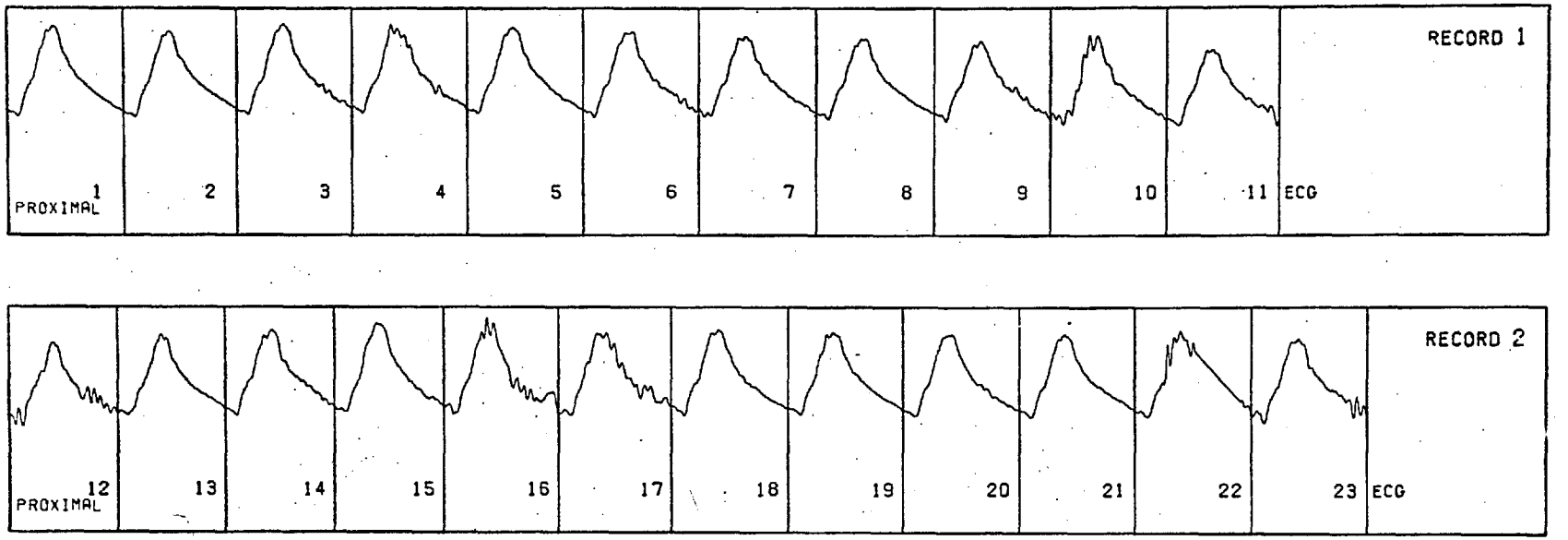


Fig. 3-3: Aortic arch blood pressure waveform.

the ascending aorta waveform has largely been removed. The spectral amplitudes of several aortic arch beats were compared with typical ascending aorta beats, and it was found that the ascending aorta waveform contained more energy in the higher harmonics than the aortic arch waveform, as would be expected from the presence of the ringing. This is seen by comparing Figs. 3-4 and 3-5, which show 26 harmonic amplitudes for the first three beats of Fig. 3-3 (aortic arch blood pressure) and Fig. 3-2 (ascending aorta blood pressure) respectively. The computation of these amplitudes assumed that the interbeat interval was the period of the fundamental, in accordance with the procedure outlined in Section 3.3.5. The mean pressure has been removed from each beat, so that the fundamental appears as the largest component, the next in magnitude being the second harmonic. It will be noticed from Fig. 3-5 that the ascending aorta waveform has little energy in the third harmonic. This led to some difficulties in the impulse response analysis, as described in Section 3.4.2. However, this low content of third harmonic is not thought to be unusual. McDonald (1960) has investigated the variation in the spectral amplitudes of the blood pressure waveform recorded at different sites in the canine aorta, and reports that a minimum in the third harmonic occurs approximately 2 cm distal to the aortic valves, believed to be caused by the complex nature of wave reflections in the arterial tree.

Fig. 3-6 shows the spectral amplitudes of the radial blood pressure waveform for the same beats as in Fig. 3-5, when the cuff was at zero pressure. It is seen that most of the waveform energy is contained in the fundamental and second

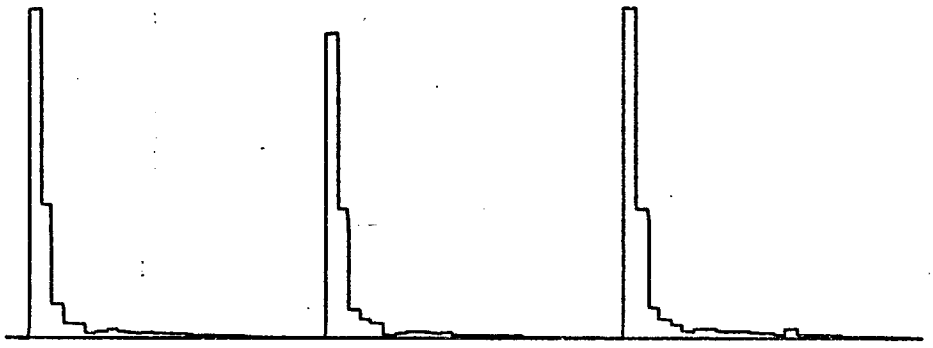


Fig. 3-4: Aortic arch blood pressure amplitude spectra.
(Beats 1, 2, 3 of Fig. 3-3).

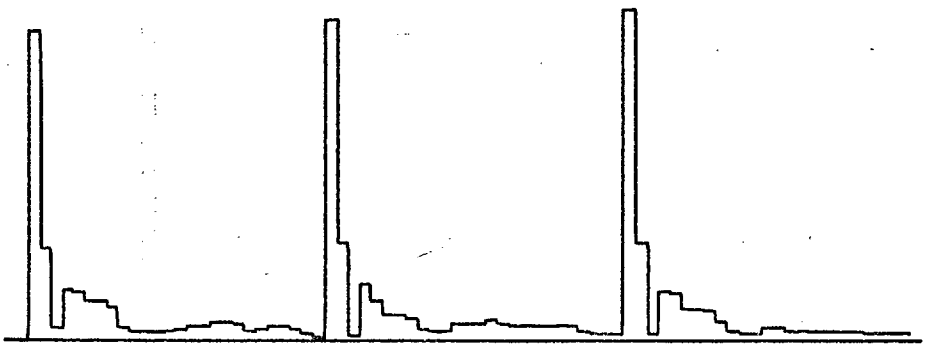


Fig. 3-5: Ascending aorta blood pressure amplitude spectra.
(Beats 1, 2, 3 of Fig. 3-2).

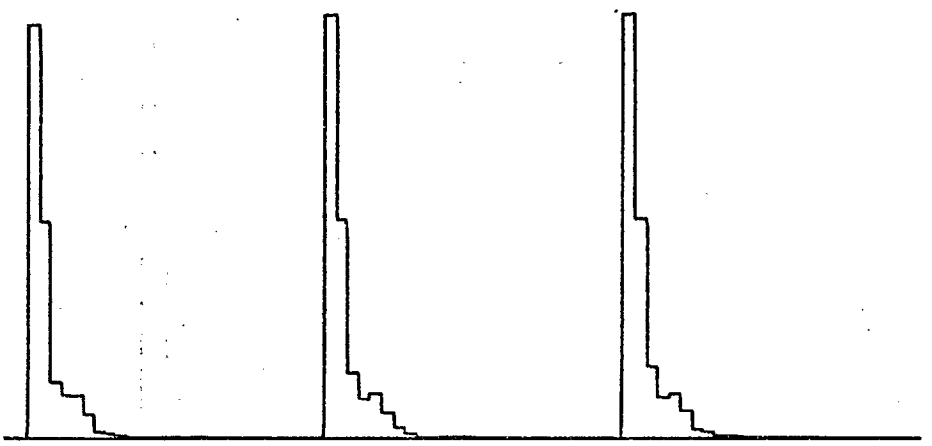


Fig. 3-6: Radial blood pressure amplitude spectra.
(Beats 1, 2, 3 of Fig. 3-2).

harmonic waves. The amplitudes of the higher harmonics are relatively small, and both the amplitudes and phase angles of harmonics above the fourth were found to vary from beat to beat, representing minor changes in waveshape. The minor variations in waveshape are caused by a number of factors, including changes in the ejection pattern of the heart, and varying peripheral loads. As a result of the unreliable nature of the higher harmonics, most of the discussions of the analyses undertaken during the course of this work are limited to trends seen in the fundamental and second harmonic frequencies.

3.2.2 Sequence of Events

The sequence of events occurring during the 6 records of Fig. 3-2 may be outlined in conjunction with Fig. 3-7. The cuff is at zero pressure until beat 3 at which point it is quickly inflated to above systolic blood pressure, reaching a maximum of 160 mm Hg by beat 11. The effect of this inflation on the radial diastolic blood pressure becomes apparent in beats 9 and 10 where the radial diastolic blood pressure becomes elevated (possibly because normal arterial back-flow under the cuff is prohibited) and by beat 11 the radial pulse has completely disappeared.

For the subsequent 40 seconds, the cuff pressure is deflated at a constant rate from 160 mm Hg to 50 mm Hg, giving a deflation rate slightly less than the standard clinical rate of 3 mm Hg per second. It is then quickly deflated to zero at beat 65. At the start of the deflation, the radial blood pressure diminishes in an essentially exponential manner (Record 2, Fig. 3-2), as flow continues through the distal peripheral

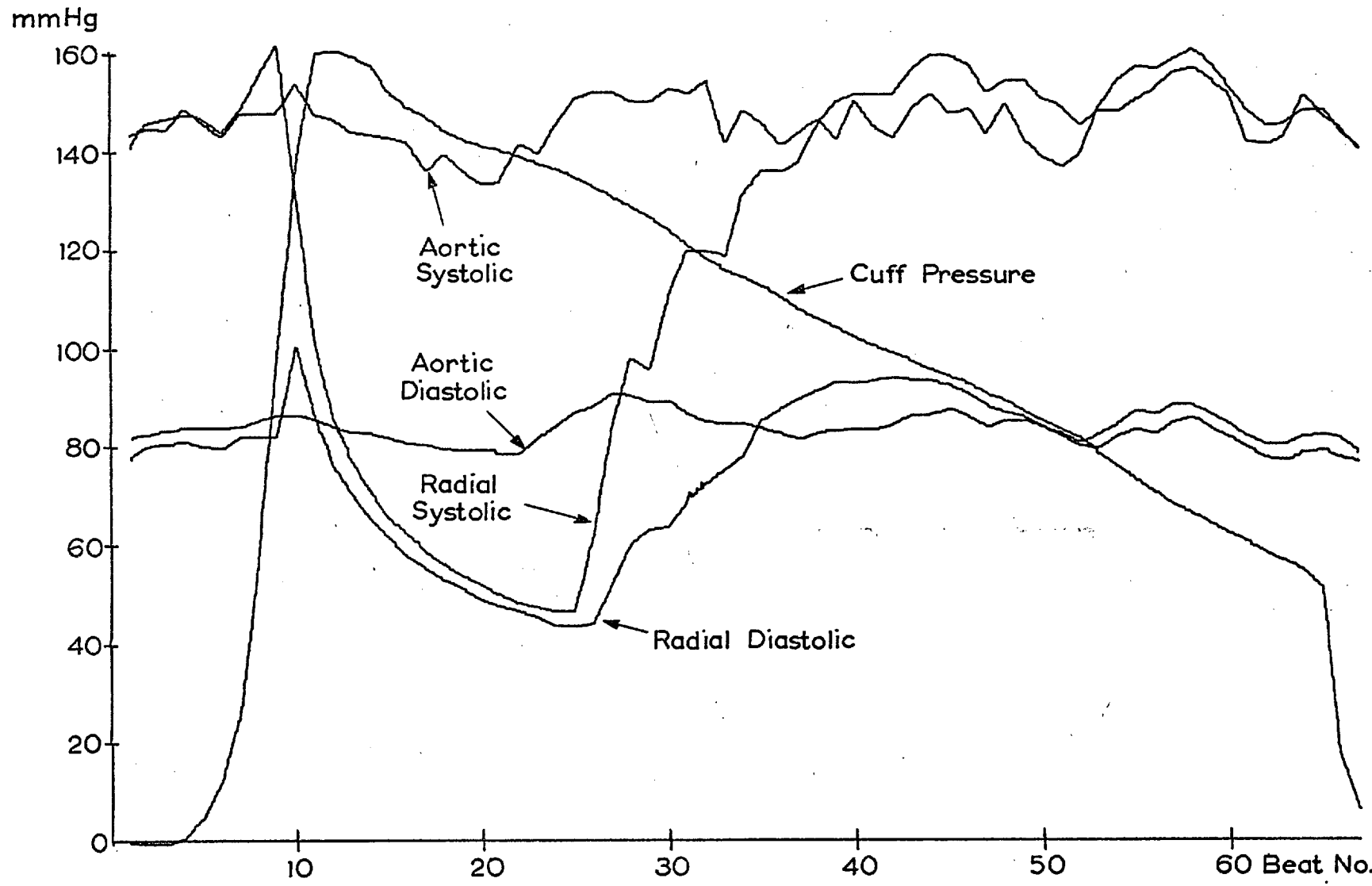


Fig. 3-7: Variation in Systolic, Diastolic, and Cuff Pressures.

resistance and blood accumulates in the veins. The minimum radial pressure is 43 mm Hg at beat 24. Blood flow under the cuff does not resume until beat 25 when a small pulse is visible in the radial waveform. This radial pulse increases in magnitude quite rapidly at first (Record 3) until a steady-state appears to have been reached (Records 5 and 6). The shape of the radial waveform at the beginning of Record 1 is not recovered in all details until the beats at the end of Record 6, when the cuff pressure is released. This indicates that there is still an influence exerted by the cuff on the waveform even when the cuff pressure is sub-diastolic, a condition reached towards the end of Record 5.

The delay between the aortic and radial waveforms is most strikingly seen at the end-diastolic points, where there is a relatively well defined change of slope. This delay is maximum at beat 25, and becomes progressively smaller until the end of Record 5, when it returns to the value it had before the cuff was inflated. Measurements of this time delay are discussed in Section 3.2.4.

An interesting inflection occurs in the radial systolic upstrokes of beats 31 to 39, the significance of which is discussed in detail in Sections 5.3.4 and 5.4.2. In short, it is thought to be due to the momentary closure of the artery after flow has resumed beneath the cuff.

3.2.3 Systolic and Diastolic Pressures

Fig. 3-7 shows the variation of systolic and diastolic blood pressures in both the aortic and radial arteries, as well as the cuff pressure. During the period of total brachial artery

occlusion, the radial pulse is lost and the distal systolic and diastolic pressures cannot be defined; the maximum and minimum distal pressures as plotted in this period result in a pair of decaying curves.

When the radial pulse first appears (beat 25), the cuff pressure is said to be just below systolic blood pressure according to the method of indirect blood pressure measurement. It is apparent from Fig. 3-7 that at this point, the cuff systolic point, there is a discernable difference between the aortic systolic pressure and the cuff pressure. However, the true aortic systolic pressure is obscured by the ringing.

When the cuff pressure has decreased to the approximate level of diastolic blood pressure, the radial diastolic blood pressure tends to follow the fall in cuff pressure for several beats (beats 44 to 52 in Fig. 3-7). The radial blood pressure is elevated above its pre-occlusion level to which it slowly reverts during these beats. This phenomenon was also observed in three of the other four cycles of cuff pressure, the odd case being when the cuff was deflated too quickly and exhausted to zero when still at a pressure close to diastolic blood pressure. The elevation of radial blood pressure after a cuff inflation has been previously reported by London and London (1967).

3.2.4 Timing Measurements

An estimate of delay between the pressure waveforms may be obtained directly from the digitized data. Consequently, a program was written to count the number of samples in each beat from the QRS peak to the end-diastolic point for both the aortic and

radial pressures. The results are shown in Fig. 3-9. At the sampling rate used there are only a few samples in these intervals and therefore the time measurements have coarse resolution. Uncertainty is also introduced when the foot of the pressure wave is not marked by an abrupt change of slope. However, taking these factors into account, it may be assumed from Fig. 3-9 that the time from the QRS peak to the aortic end-diastolic point is very nearly constant. This interval extends from the time when the QRS impulse initiates contraction to the time when the ventricular pressure has risen sufficiently to open the aortic valve (Guyton, 1966). Hence this interval remains relatively constant if the heart maintains a regular contractile force and the diastolic blood pressure does not vary greatly.

When the cuff is at zero pressure, the equivalent time delay measurement for the radial waveform is also constant, its magnitude being greater than for the aortic waveform because of the propagation delay of the pressure pulse as it travels peripherally. When the pressure in the cuff is between systolic and diastolic blood pressures, the radial pressure pulse is further delayed because for each beat the occluded artery cannot open until the instantaneous blood pressure exceeds the cuff pressure. Therefore a decreasing delay is seen during the release of cuff pressure as the radial end-diastolic point shifts closer to the time of the QRS peak. There is a short plateau in the trend during beats 46 to 53 (Fig. 3-9) followed by a step when the radial end-diastolic point delay returns to a value slightly greater than what it was before the cuff was inflated. When Fig. 3-8 (which shows the cuff pressure and diastolic blood pressure variations) is

compared with Fig. 3-9, it is seen that the plateau and step occur when the cuff pressure is close to diastolic blood pressure, suggesting that the trend in the delay stabilizes at the cuff diastolic point. However, contrary to what might be expected, measurements made for the other cycles of cuff pressure did not show a similar alteration in the delay when the cuff pressure was in the region of the diastolic blood pressure, and the tendency was for the delay to continue to decrease until low cuff pressures were reached. This is illustrated in Fig. 3-12, where measurements of delay are plotted for the cycle of cuff pressure shown in Fig. 3-11.

The program was repeated with measurements of the intervals from the QRS peak to the point located one quarter of the way up the systolic upstroke. This point is easier to locate than the end-diastolic point since it lies on a steeply rising wave front. The results for both cycles of cuff pressure are shown in Figs. 3-10 and 3-13, respectively. It is seen that there is very little difference from the plots of Figs. 3-9 and 3-12. Certainly no distinct change occurs by which the cuff diastolic point may be located precisely, although the trend of decreasing delay is clearly evident.

These measurements show that timing a feature of the radial waveform with respect to the QRS peak (or some such reference marker in a waveform unaffected by the measurement) does not give a reliable indication of diastolic blood pressure. Although the time measurement can be resolved only to one inter-sample period ($\pm$ 2.5 ms), a finer resolution would merely produce a smoother curve. There are therefore doubts as to the

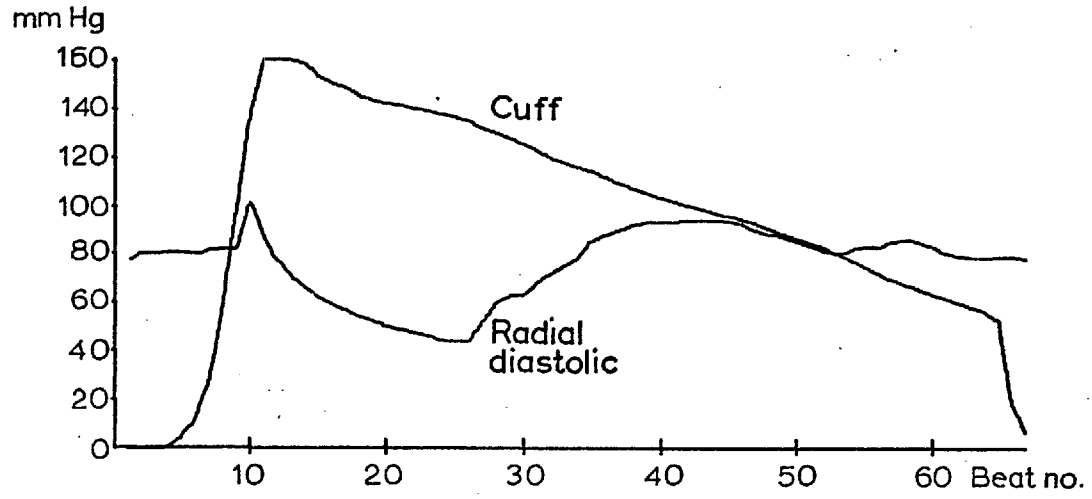


Fig. 3-8: Cuff pressure and radial diastolic pressure.

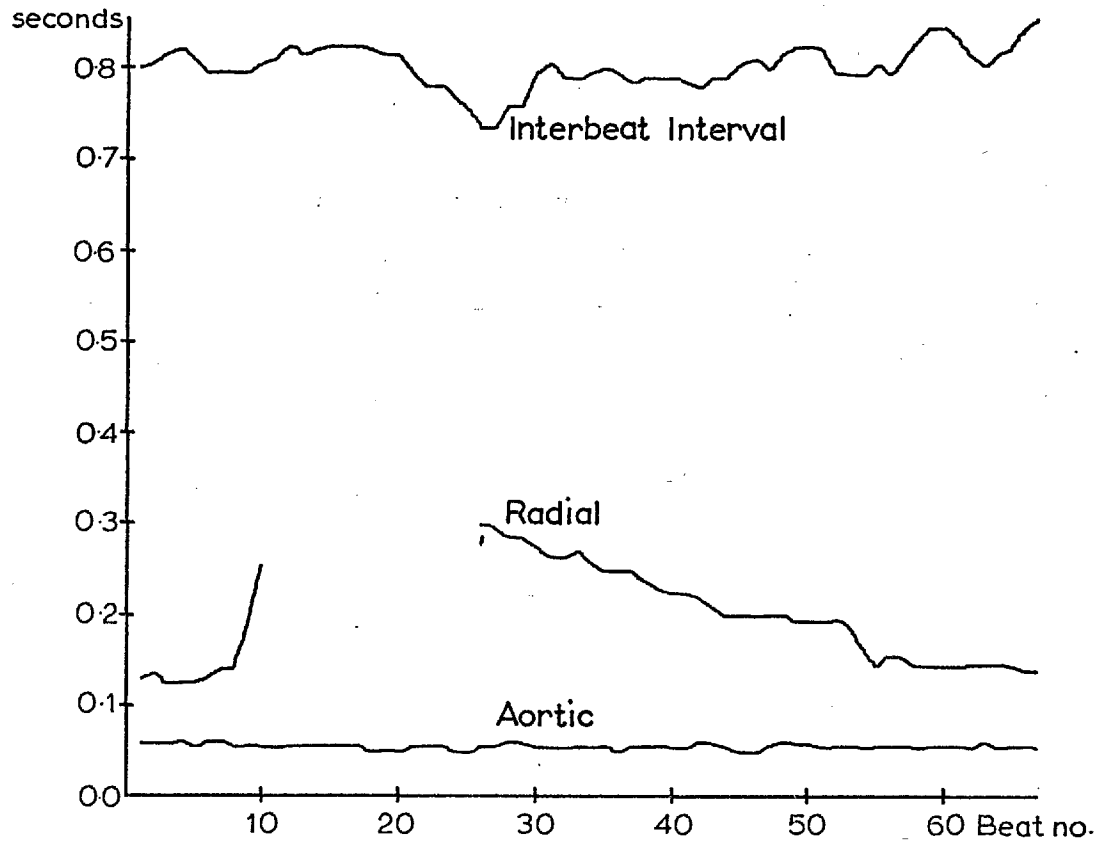


Fig. 3-9: Intervals from QRS to end-diastolic point.

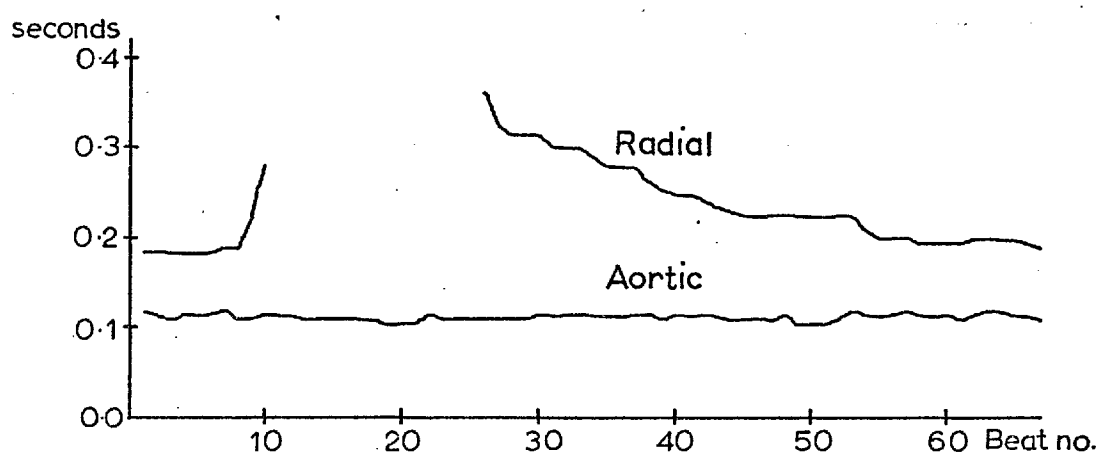


Fig. 3-10: Intervals from QRS to systolic upstroke.

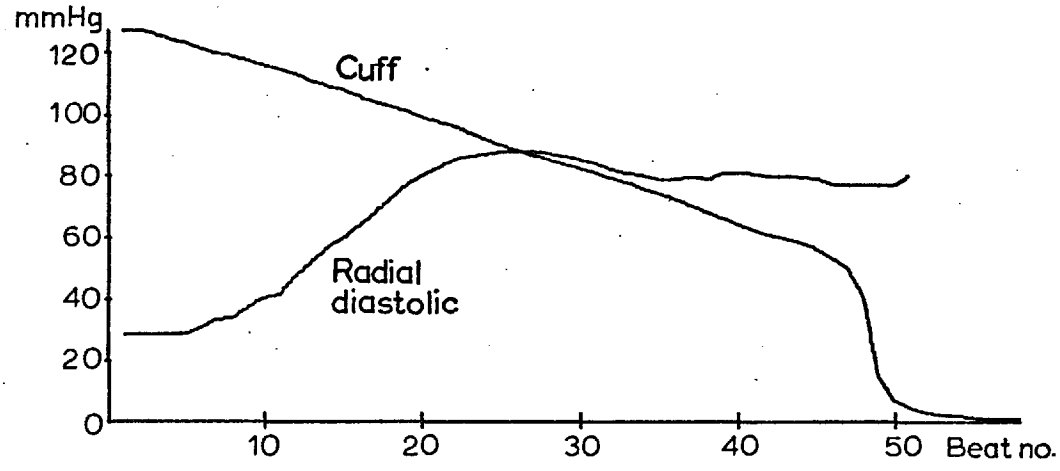


Fig.3-11: Cuff pressure and radial diastolic pressure.

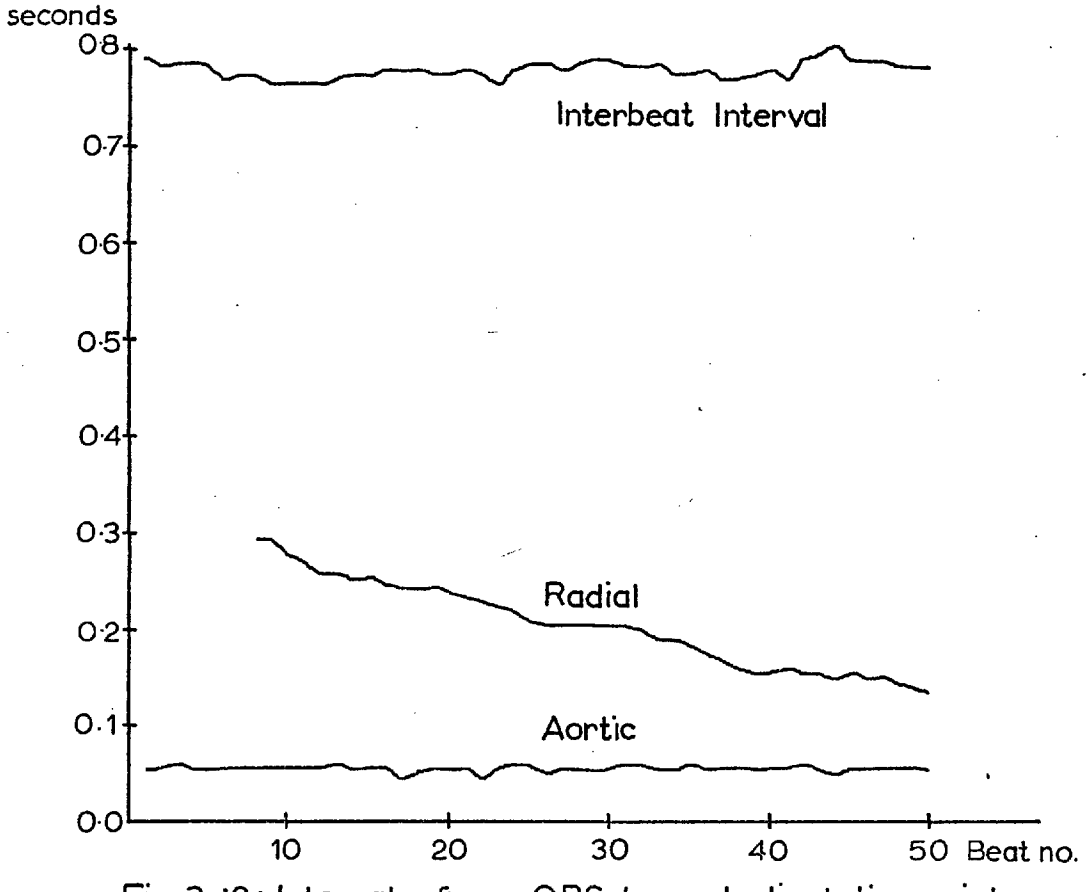


Fig.3-12: Intervals from QRS to end-diastolic point.

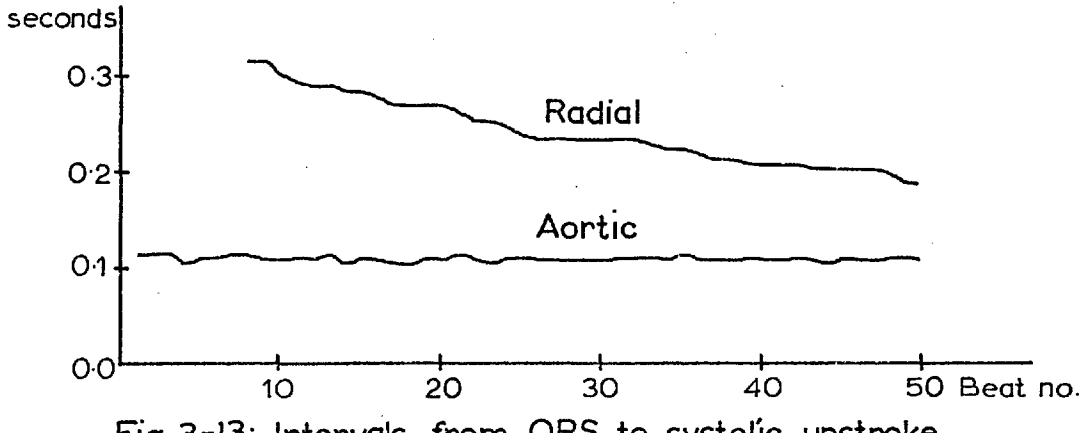


Fig.3-13: Intervals from QRS to systolic upstroke.

reliability of any blood pressure measuring apparatus based on the timing of waveforms. Furthermore, these measurements have confirmed the continuing influence of the cuff on the transmission of the blood pressure pulse even when the cuff pressure has fallen below diastolic pressure. Other techniques of examining the data are therefore sought.

3.3 FREQUENCY ANALYSIS

3.3.1 The Fourier Series and Discrete Fourier Transform

A periodic waveform can be analysed into a set of harmonically-related sinusoidal waves known as a Fourier series provided that the integral of the waveform is finite over a complete period, and that the number of discontinuities in any finite interval is also finite (Stuart, 1961). These conditions do not exclude any waveform of practical interest from being represented by a Fourier series (Lynn, 1973). Eq. 3.1 is the Fourier series representation (for all t) of a periodic signal f(t) with a period equal to T.

$$f(t) = \tfrac{1}{2}A_0 + \sum_{n=1}^{\infty}\left(A_n \cos\frac{2\pi}{T}nt + B_n \sin\frac{2\pi}{T}nt\right) \qquad (3.1)$$

Thus f(t) is considered to comprise a steady level ($\frac{1}{2}A_0$) plus a number of sine and cosine waves of different frequencies, the lowest frequency being the 'fundamental' (n=1) with a period equal to T. The remainder of the waves are harmonics of this frequency. A non-periodic function defined over a finite range $t_o \leq t \leq t_o+T$

is also represented by Eq. 3.1, but outside the range in which f(t) is defined the expression represents a periodic extension of f(t).

The Fourier coefficients A_n, B_n are computed by integrating f(t) over one complete period according to Eqs. 3.2, 3.3, and 3.4.

$$A_o = \frac{2}{T}\int_{t_o}^{t_o+T} f(t)\,dt \qquad (3.2)$$

$$A_n = \frac{2}{T}\int_{t_o}^{t_o+T} f(t)\cos\frac{2\pi}{T}nt\,dt \qquad (3.3)$$

$$B_n = \frac{2}{T}\int_{t_o}^{t_o+T} f(t)\sin\frac{2\pi}{T}nt\,dt \qquad (3.4)$$

$$n=1,2,3\ldots$$

The spectral composition of a sampled-data signal is generally referred to as the Discrete Fourier Transform (DFT), and a sequence of N equally-spaced data values f(k) can be expressed by Eq. 3.5 provided that the sampled version adequately represents the underlying continuous signal (Lynn, 1973). In this case the N pairs of coefficients are evaluated by summation according to Eqs. 3.6 and 3.7. These coefficients may be combined to form N complex coefficients C_n (Eq. 3.8).

$$f(k)=\sum_{n=0}^{N-1}\left(A_n\cos\frac{2\pi}{N}nk + B_n\sin\frac{2\pi}{N}nk\right) \qquad (3.5)$$

$$k=0,1,2\ldots N-1$$

$$A_n = \frac{1}{N}\sum_{k=0}^{N-1} f(k)\cos\frac{2\pi}{N}nk \qquad (3.6)$$

$$B_n = \frac{1}{N}\sum_{k=0}^{N-1} f(k)\sin\frac{2\pi}{N}nk \qquad (3.7)$$

$$C_n = A_n - jB_n \qquad (3.8)$$

$$n=0, 1, 2 \ldots N-1$$

C_o is a unique term in that it represents the D.C. level and is therefore wholly real. Of the remainder of the coefficients, only the first half need be computed as the second half are the complex conjugates of the first half taken in reverse order. This is a result of the data being real, and hence the total power of each harmonic is equally shared between the mirrored conjugates. The n^{th} harmonic may therefore be represented by a sinusoid having an amplitude equal to $2\sqrt{A_n^2 + B_n^2}$ and a phase angle of arctan $-(B_n/A_n)$. The phases of these harmonic sinusoids are defined at n=0 with respect to a zero-phase fundamental, i.e. a cosine wave of period N with maximum positive amplitude at points n=0 and n=N. If N is odd, the highest harmonic is given when $n=\frac{N+1}{2}$, but if N is even, the highest harmonic for which phase information is available is when $n=\frac{N}{2}$. This is because the term $C_{\frac{N}{2}+1}$ is unique in that the addition of the conjugates at this frequency doubles the real part but destroys the imaginary part. Provided that the sampling theorem has been satisfied, the superposition of all the sinusoids results in an exact reconstruction of the original waveform (Lynn, 1973).

A DFT subroutine was written to compute the Fourier

coefficients A_n, B_n from any given length data sequence using Eq. 3.6 and 3.7. A second subroutine was used to compute the amplitudes and phases of the harmonics from the Fourier coefficients. Both subroutines were tested with waveforms of known harmonic content. It was found useful to express the harmonic phase angles as coefficients of Pi radians.

3.3.2 The Fast Fourier and Chirp-Z Transforms

The most convenient and efficient method of computing the Fourier coefficients is to use the Fast Fourier algorithm, commonly referred to as the Fast Fourier Transform (FFT). This algorithm is used to calculate the full set of N complex coefficients from N data samples in $N\log_2 N$ operations, compared to N^2 operations for the conventional DFT. The FFT is not an approximation to the DFT, but provides the same result with some improvement in accuracy due to the greatly reduced number of calculations contributing to round-off error (Monro, 1971). However, use of the FFT is restricted to data sequences where the number of samples is a power of two, or at least factorable into small prime numbers (Singleton, 1969). If this requirement cannot be met, the so-called Chirp-Z Transform may be used to perform the identical task on a general length sequence. However, the processing requirements of this algorithm are considerably greater than those of the FFT, e.g. 4 times as much core memory data storage, and 8 times as much central processor time. A useful set of Fourier subroutines is given by Munro (1972), and these were used for transformation by the FFT or Chirp-Z algorithms. These subroutines may be used in the forward or

inverse modes, transforming respectively from the time domain to the frequency domain and vice versa.

Transformation using Monro's Chirp-Z subroutines is done in two stages. The first subroutine calculates and transforms a weighting function known as the "chirp" function, whereas the second subroutine performs the remainder of the calculations. If more than one forward or inverse transform of the same length is required, the first subroutine need only be called once, thus achieving a considerable saving of computing time.

3.3.3 Fixed Period Analysis

The object of the analysis is to observe beat-to-beat changes in the blood pressure waveforms during an indirect blood pressure measurement. It was therefore thought reasonable to perform a frequency analysis of successive beats and compare the spectral estimates to reveal differences which occur as the cuff pressure changes. This form of analysis assumes that each beat constitutes one period of an imaginary repetitive waveform differing from the waveforms formed from neighbouring beats. The justification for assuming repetitive waveforms rather than single transients is discussed in Chapter 6. By assuming repetition a considerable simplification of the analysis is achieved.

Since each beat in the digitized data contained approximately 160 samples (variations in interbeat interval causing minor deviations about this figure) the FFT could not be applied, and analysis programs used the Chirp-Z or DFT subroutines to compute the spectra. The choice of subroutine was determined by the program. If only one blood pressure waveform was to be analysed, the DFT subroutine was used if the number of harmonics

to be computed was less than 16. For 16 or more harmonics it was quicker to use the Chirp-Z subroutine and compute all the harmonics. However, if both the aortic and radial waveforms were to be analysed concurrently, it was found to be faster to compute all harmonics with the Chirp-Z subroutine if the required number of harmonics was 12 or greater. This was because the Chirp-Z initialization subroutine needed to be executed only once before transforming the simultaneous aortic and radial waveforms of each beat.

As previously stated, a beat-by-beat analysis requires the separation of the blood pressure waveforms into intervals representing successive independent beats. The beginning of each interval is indicated by the QRS peak of the E.C.G., as it marks the start of a new cycle of cardiac activity; the logical end of the interval is indicated by the following QRS complex. However, the physiological variability of the heart rate means that the results of an analysis using the interbeat interval as the period of the fundamental frequency cannot be compared on a true time basis, although loose comparisons may be made between corresponding harmonic numbers. Such an analysis is described in Section 3.3.5.

To avoid this difficulty, a specific fundamental period is used for each beat, timed from the QRS peak; this period cannot be longer than the minimum interbeat interval found in the recording. Three of the five indirect blood pressure measurement cycles were analysed in this way, using a fixed period of 0.7 seconds. A section of data recorded when the cuff was at zero pressure was also analysed, the spectra of which are shown in Fig. 3-14. In this figure, and similar ones that follow, the

aortic and radial waveforms are alternatively named as proximal and distal waveforms. The amplitudes are plotted to an arbitrary scale, and the phase angles are plotted within the limits of 0.0 and 2.0 representing a range of 2 Pi radians. Note that in interpreting the phase plots, a decreasing angle represents an increasing phase lag.

From Fig. 3-14 it is seen that the fundamental and second harmonic amplitudes of the aortic waveform are variable, whereas the corresponding phase angles remain relatively stable throughout the data. The amplitude variations may be attributed to changes in the pulse pressure. The stability of the phase angles indicates that the bulk of the waveform maintains a constant time relationship with respect to the QRS peaks. These observations also apply to the radial spectra, the major differences between the aortic and radial results being that the radial amplitudes are greater than the aortic amplitudes, and the phase angles are smaller, indicating greater phase lag. Both these effects are consequences of the transmission line character of the arterial tree, an analogy which is discussed in Chapter 4. As a result, the amplitude and phase characteristics of the transfer function of pressure to any point in an artery are dependent on the position of measurement. The practical effect of this behaviour is that the pulse pressure increases in amplitude but becomes further delayed in time as it travels peripherally. As the frequency domain representation of a pure time delay is a phase shift proportional to frequency, it is expected that the second harmonic phase shift will be greater than that of the fundamental. This is indeed seen to be the case in Fig. 3-14 but the phase

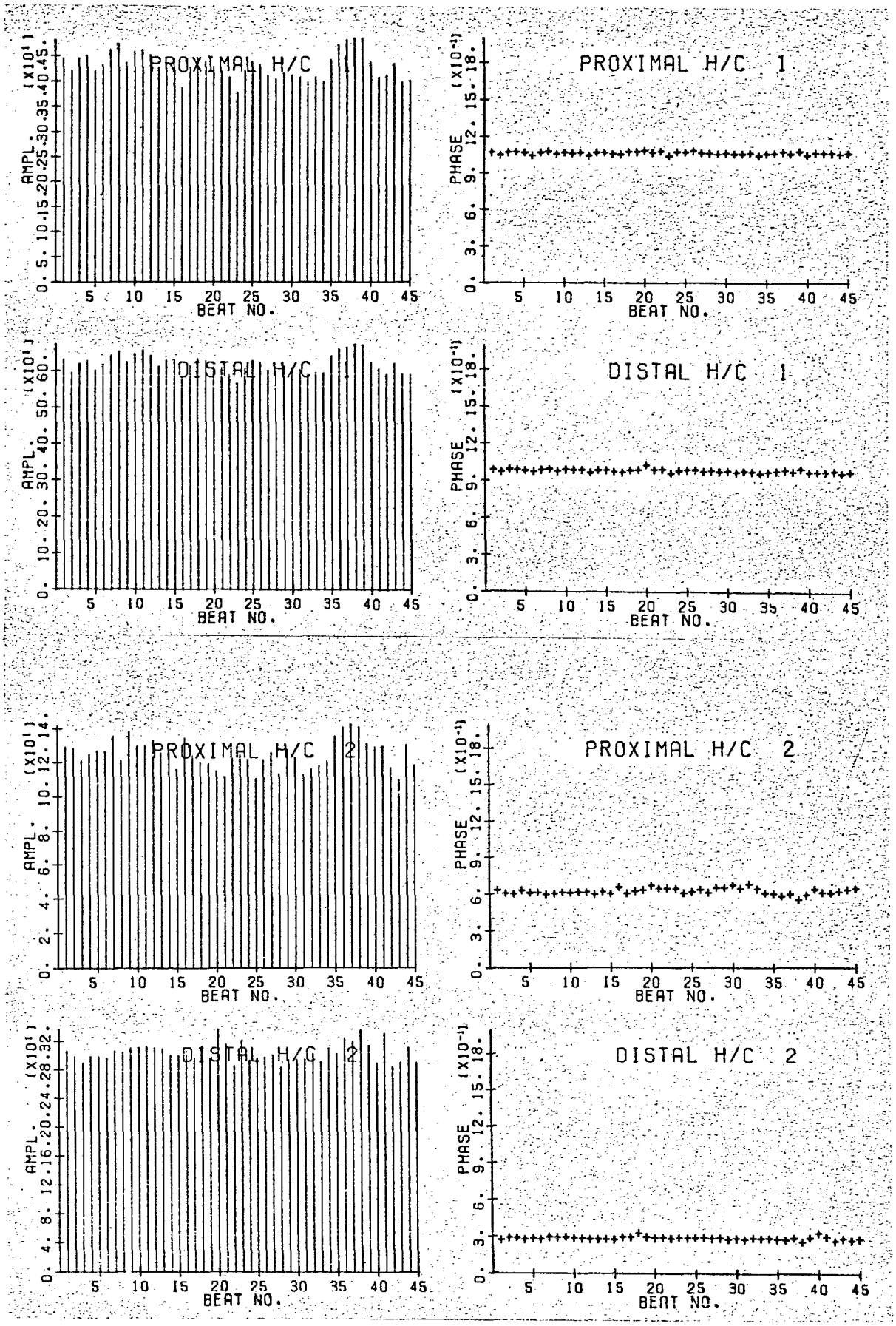


Fig. 3-14: Spectra computed using a fixed period of 0·7 seconds.

shift is not directly proportional to frequency as reflections from branch points and the periphery, together with losses in the arterial wall and the fluid, lead to a complex behaviour, especially at high frequencies.

During an indirect blood pressure measurement, the distal waveform is further delayed when the cuff pressure is between systolic and diastolic blood pressures, as the artery under the cuff cannot open until the instantaneous proximal pressure exceeds the cuff pressure. Hence it is expected that this delay will be seen as a further phase shift in the spectra of beats occurring during this period. Furthermore, as the cuff pressure changes slowly, changes in the spectra should form a smooth progression back towards the pre-occlusion values, with the point of complete recovery being at the cuff diastolic point.

The spectra computed for a complete cuff pressure cycle are shown in Fig. 3-15, the data being those of Fig. 3-2, which have been discussed previously in Section 3.2. It is seen that the aortic spectra are not very different from those shown in Fig. 3-14, whereas the influence of the cuff pressure is clearly visible in the radial spectra. During the period of complete arterial occlusion (beats 11 to 25), the radial amplitudes and phases bear no relationship to the previous spectra. In fact, the spectra computed during the first part of the occlusion period are virtually those of a negative ramp, causing phase angles of approximately 1.5 Pi to be computed for all harmonics. This arises because the exponential drop of distal pressure during this period is approximately linear over the course of one beat. However, the amplitudes eventually drop to below the noise level,

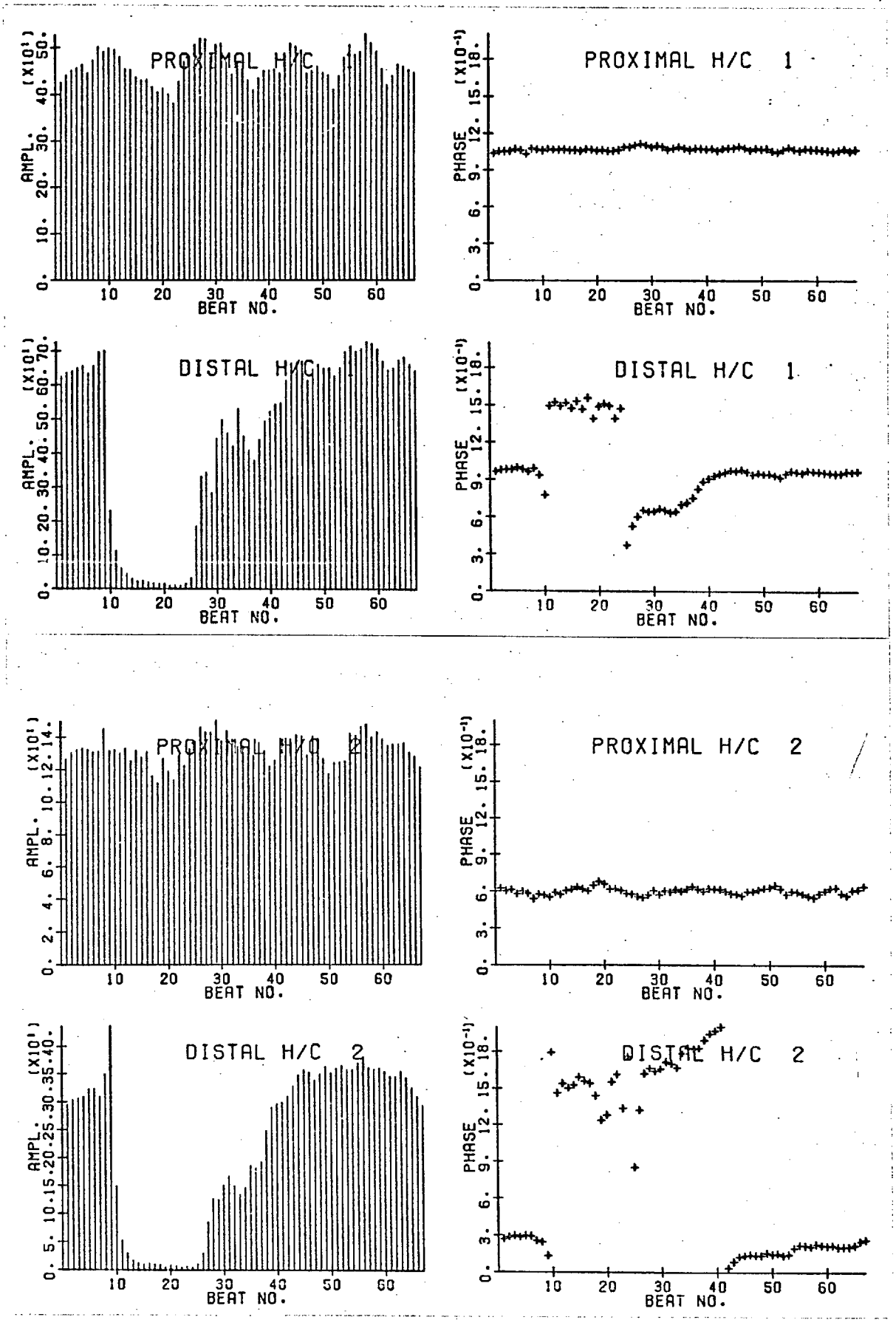


Fig. 3-15: Spectra of the data of Fig. 3-2 (fixed period analysis).

causing meaningless phase angles to be calculated.

When flow resumes in the artery at beat 26, the radial phase angles are considerably different from their pre-occlusion values, showing the additional delay that is imposed on the waveform by the cuff when at the systolic point. Trends are observed during successive beats as the phase angles revert towards their original values, the positive slopes of the trends showing that a relative phase advance is occurring, i.e. successive beats of the radial waveform are progressively shifting to the left, as seen in Record 3 of Fig. 3-2. For the second harmonic of the radial waveform, the phase angles begin at approximately 1.5 Pi at beat 26 and increase to 2 Pi, where there is an apparent discontinuity. This is caused by the computing algorithm, which limits the range of phase angles between zero and 2 Pi. In fact, there is no discontinuity and the phase angles continue to advance smoothly.

The differences between the spectra of the two waveforms can be emphasized by dividing the amplitudes of corresponding harmonics and subtracting their phase angles. Fig. 3-16 shows the distal:proximal amplitude ratios and the proximal-distal phase differences for the fundamental and second harmonic frequencies plotted versus the beat number. The phase difference plot for the fundamental has a distinct corner point at beat 44, although the pre-occlusion phase difference is not completely recovered until the cuff pressure has been released. However, the amplitude ratio of the fundamental is still increasing at beat 44, and does not reach its pre-occlusion value until beat 52. The second harmonic plots, although of

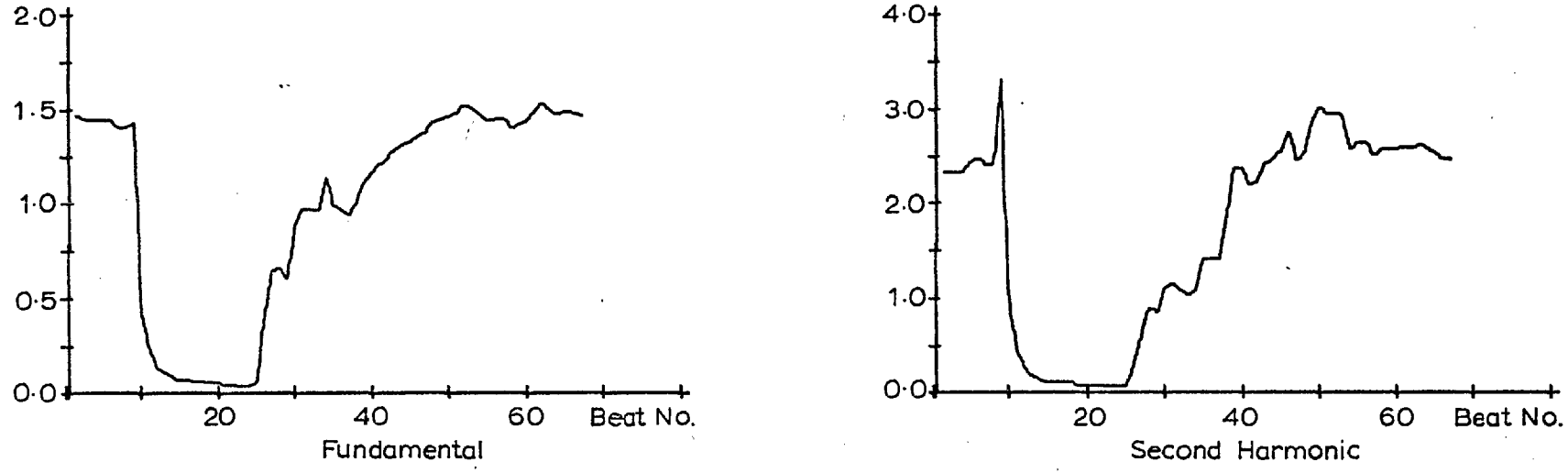


Fig. 3-16a: Distal : Proximal Amplitude Ratios.

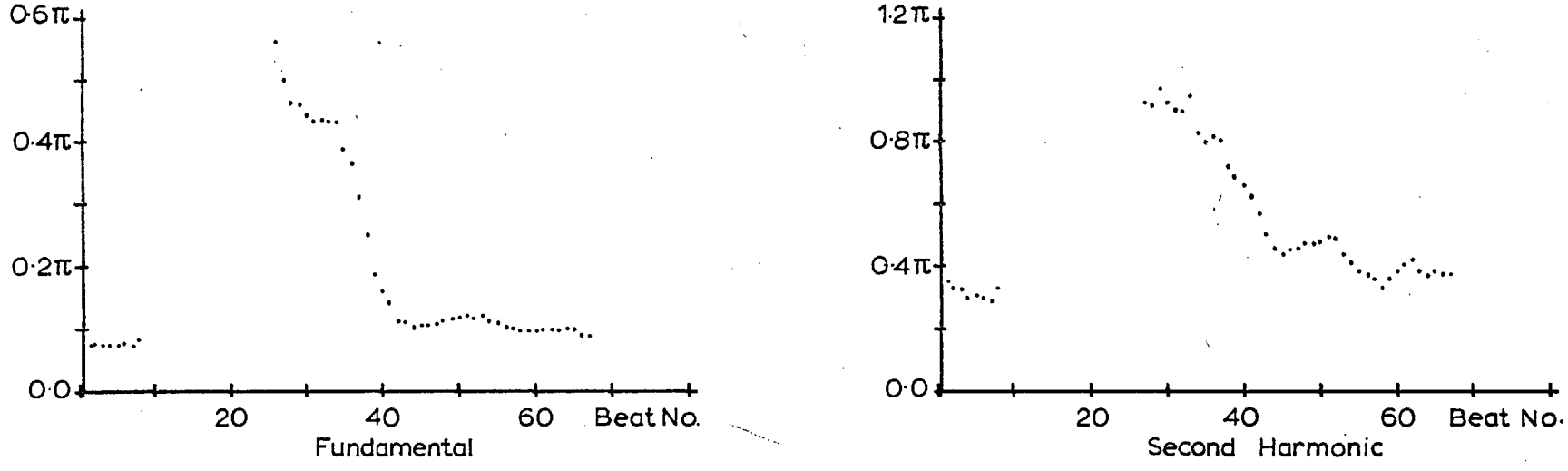


Fig. 3-16b: Proximal - Distal Phase Differences. Fixed Period Analysis.

similar overall shape, are not so smooth as those of the fundamental, thus making it more difficult to identify important points of interest. These results are typical for all the cycles of cuff pressure analysed.

With reference to Fig. 3-7, it is seen that during beats 44 to 52 the cuff pressure and the radial diastolic blood pressure tend to track together quite closely, the radial diastolic pressure rising to meet the cuff pressure at beat 44 and subsequently diverging from it at beat 52. The true diastolic blood pressure is therefore indicated by the cuff pressure at this point of divergence. This is supported by diagrams given by Geddes (1970), which show that the Korotkoff sounds continue during the period of elevation of the distal diastolic pressure and cease at the point of divergence from the cuff pressure.

It therefore appears that the best indication of the cuff diastolic point is given when the amplitude ratios of the fundamental components of the distal and proximal pressure waveforms stabilize to pre-occlusion values. The trend in the fundamental phase differences (which may be taken as an indirect indication of the changes in relative waveform delay) is quite marked and shows a distinct corner point occurring when the cuff pressure is close to the distal diastolic blood pressure. However, at this point the distal diastolic pressure is elevated by about 10 mm Hg above both the pre-occlusion and post-occlusion levels. It is therefore apparent that an elevated diastolic pressure would be registered if the phase difference corner point was taken to indicate the cuff diastolic point. This premature stabilization of the phase angle differences was consistently

observed in the other analyses, whereas the stabilization of the fundamental amplitude ratio was found to be a more accurate index of the true diastolic pressure. This suggests that analyses applied to indirect waveforms obtained proximal and distal to a cuff might reveal a similar trend in fundamental amplitude ratios that would prove valuable in locating the cuff diastolic point.

3.3.4 Waveform Levelling

Since Fourier analysis assumes an identically repeating data sequence, the segmentation of the data into fixed sections will in general produce a disparity in the levels at the two ends. If this step change is large, a considerable spread of unwanted spectral energy is generated as the data are no longer band-limited and do not conform with the requirements of the sampling theorem. This is illustrated in Fig. 3-17a, where 25 harmonic amplitudes are shown for six consecutive radial beats from Records 1 and 2, Fig. 3-2. From Fig. 3-2 we see that beat 12 has no pulse present whatsoever, yet its amplitude spectrum in Fig. 3-17a could mislead one into thinking that a pulse was present. However, under normal non-occluded conditions, the beginning and end of a selected beat occur towards the end of the diastolic run-off where the discontinuity is usually small, and its effect on the lower harmonics may be neglected.

This level disparity at the end of the data sequence may be thought of as resulting from the summation of a linear trend and a pulsatile wave. If the linear trend is subtracted, the features of the pulsatile wave may be examined alone, there

now being no step discontinuity although there could be a slight difference in slopes at the ends of the data sequence. The effect of this non-linear filtering on the radial waveform of Fig. 3-2 may be seen in Fig. 3-18, where the trend for each beat has been removed forwards in time, bringing the end of the wave to the same level as the beginning. Thus the leading portion of the wave is not changed as much as the latter part. The most significant alteration in the data is in the non-pulsatile region of the radial waveform, which appears as a continuous straight line since the mean level has been removed as well. The effect in the amplitude spectrum is seen in Fig. 3-17b, and it is now obvious that there is no pulse present in beats 11 and 12.

The plots of sequential amplitude ratios and phase differences for this form of analysis were very similar to the results obtained previously, when the linear trends were not removed from the data. There was improved rejection of non-significant results during the non-pulsatile region, and changes in the results for the radial beats occurring immediately after the cuff systolic point, where the waveform recovers most rapidly and the linear trend is relatively large. However, there was very little alteration in the results for beats occurring near the cuff diastolic point, but the plots were less smooth than previously. As this is the region of greatest interest in the analysis, it is concluded that the removal of the linear trend is unnecessary, unless complete suppression of the non-pulsatile region is required. This form of analysis may prove useful however, in examining trends in waveforms containing drift, e.g. photoplethysmograms.

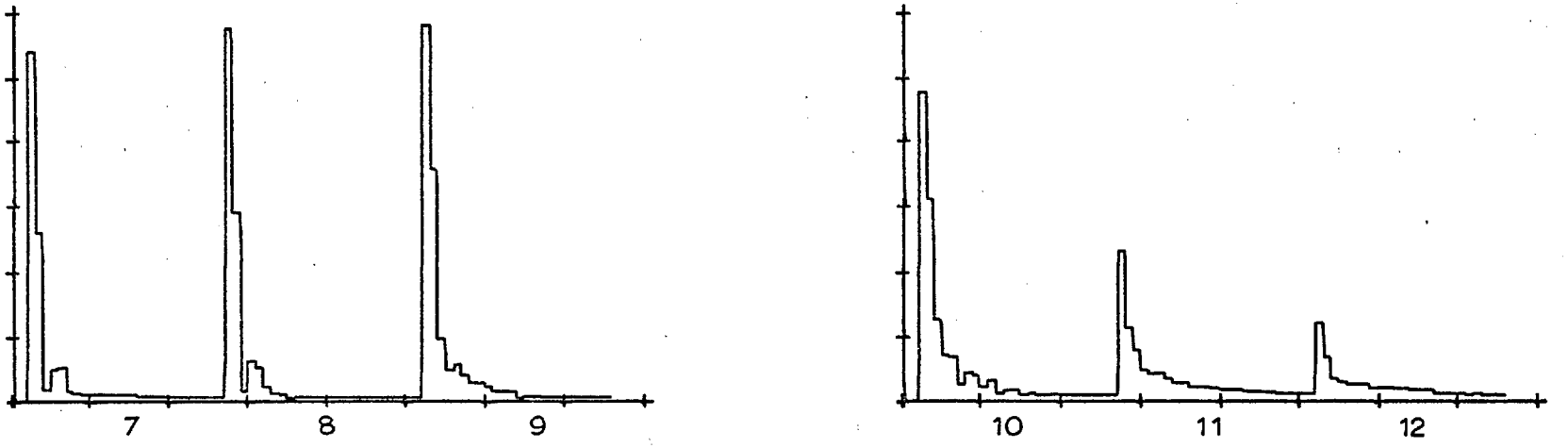


Fig. 3-17a: Radial blood pressure amplitude spectra without waveform levelling.
(Beats 7 to 12 of Fig. 3-2)

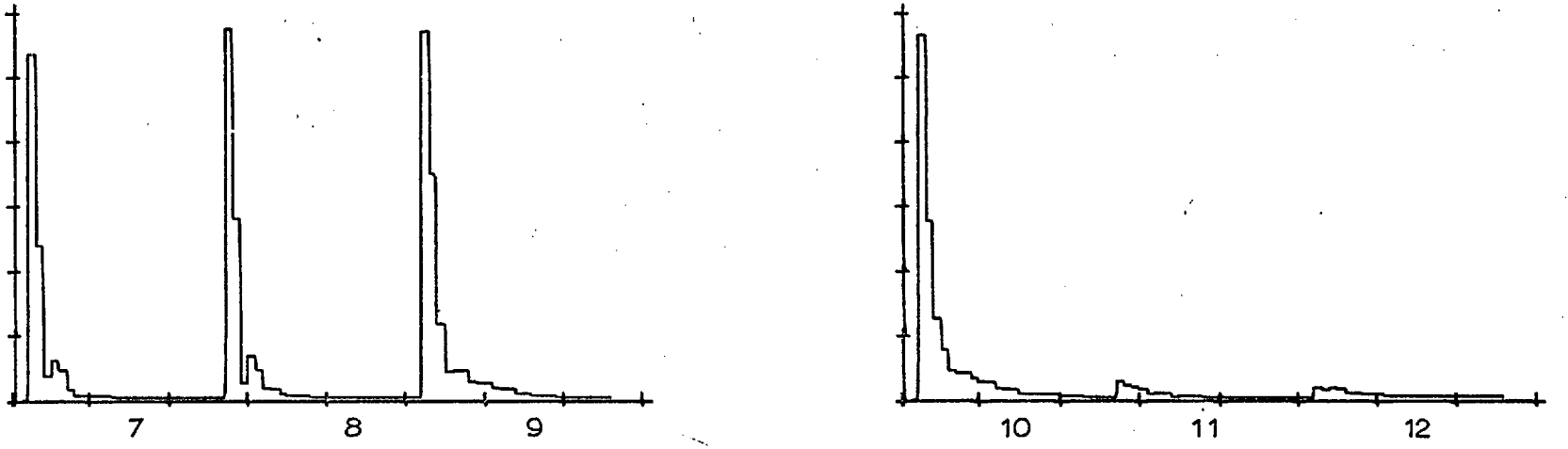


Fig. 3-17b: Radial blood pressure amplitude spectra with waveform levelling.
(Beats 7 to 12 of Fig. 3-2)

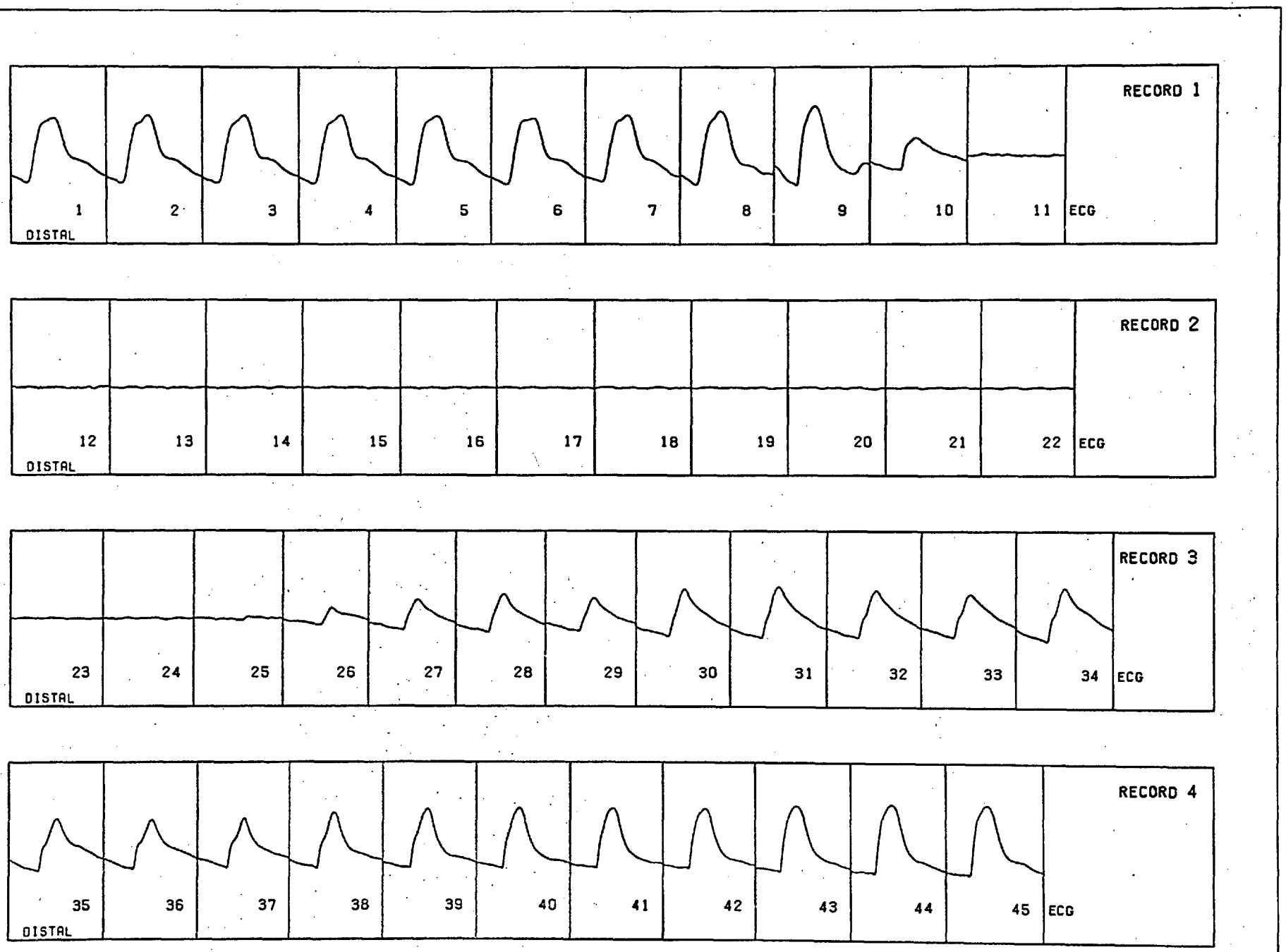


Fig. 3-18 (page 1)

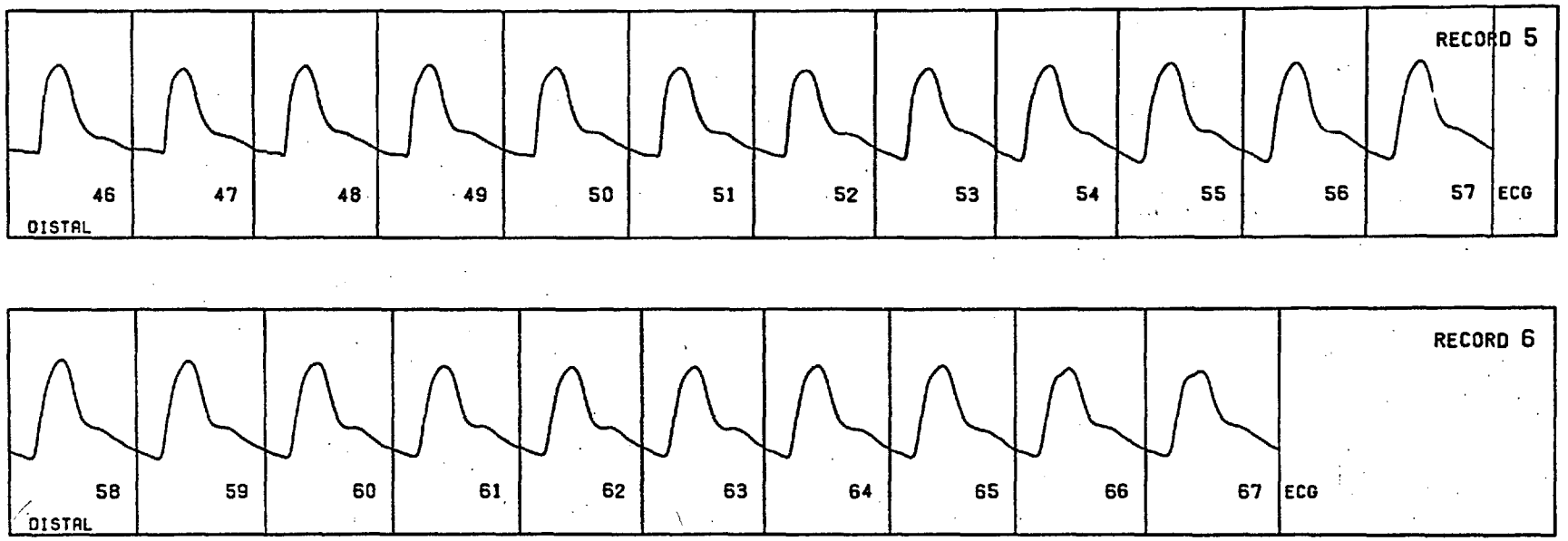


Fig.3-18 (page 2): Removal of linear trend and mean level from the radial blood pressure waveform of Fig.3-2.

3.3.5 Interbeat-Interval Period Analysis

An alternative approach to the analysis is the seemingly straightforward one of treating each beat as if it repeated with a fundamental period equal to its interbeat interval. As before, analysis can proceed on the basis of examining the phases and amplitudes of harmonic frequencies. However, when making beat-to beat comparisons of corresponding harmonic numbers, a difficulty arises in that these harmonics do not necessarily represent the same absolute frequencies. Thus the interpretation of sequential phase shifts in terms of equivalent time delay is no longer straightforward but requires that each phase value is weighted according to the absolute frequencies of that beat. If such considerations are ignored and a plot is made of amplitudes and phase angles versus beat number, the curves shown in Fig. 3-19 are obtained. These are for the data recorded at zero cuff pressure, and may be compared with the results of the previous analysis using a fixed-length period (Fig. 3-14). It is particularly noticeable that the phase angles of Fig. 3-19 are more irregular than those of Fig. 3-14. This irregularity is largely caused by the computation of the phase angles being for different absolute frequencies represented by the changing interbeat interval. The variation may be examined by plotting the phase angles versus the corresponding interbeat intervals with a suppressed-zero time axis, as in Fig. 3-20. Linear variations with positive slopes are revealed, which are indicated by the superposed lines of best fit. These characteristics arise for the same reason as was given for the stability of the phase angles calculated in the fixed period analysis, namely, that the

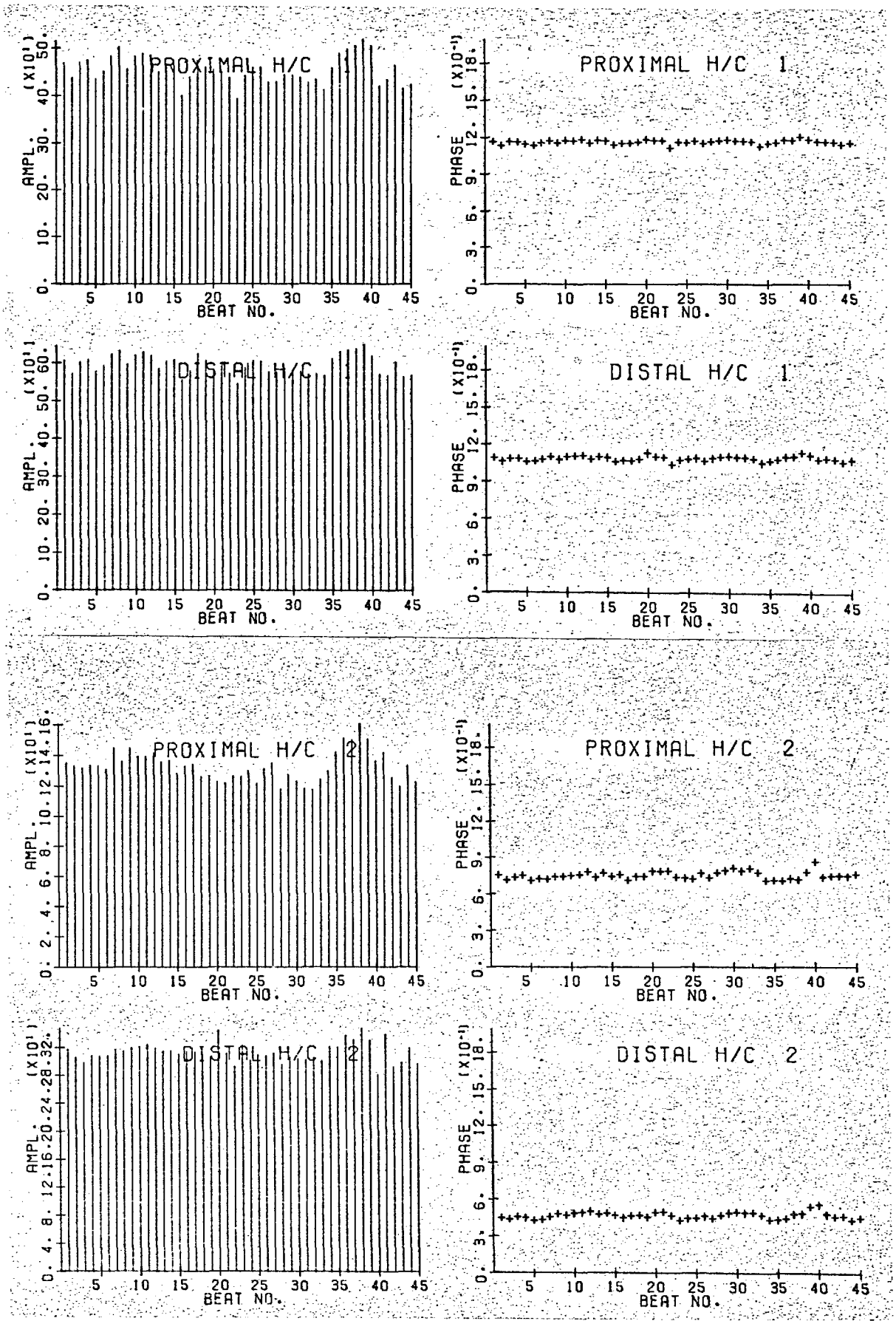


Fig. 3-19: Spectra computed using a period equal to the interbeat interval.

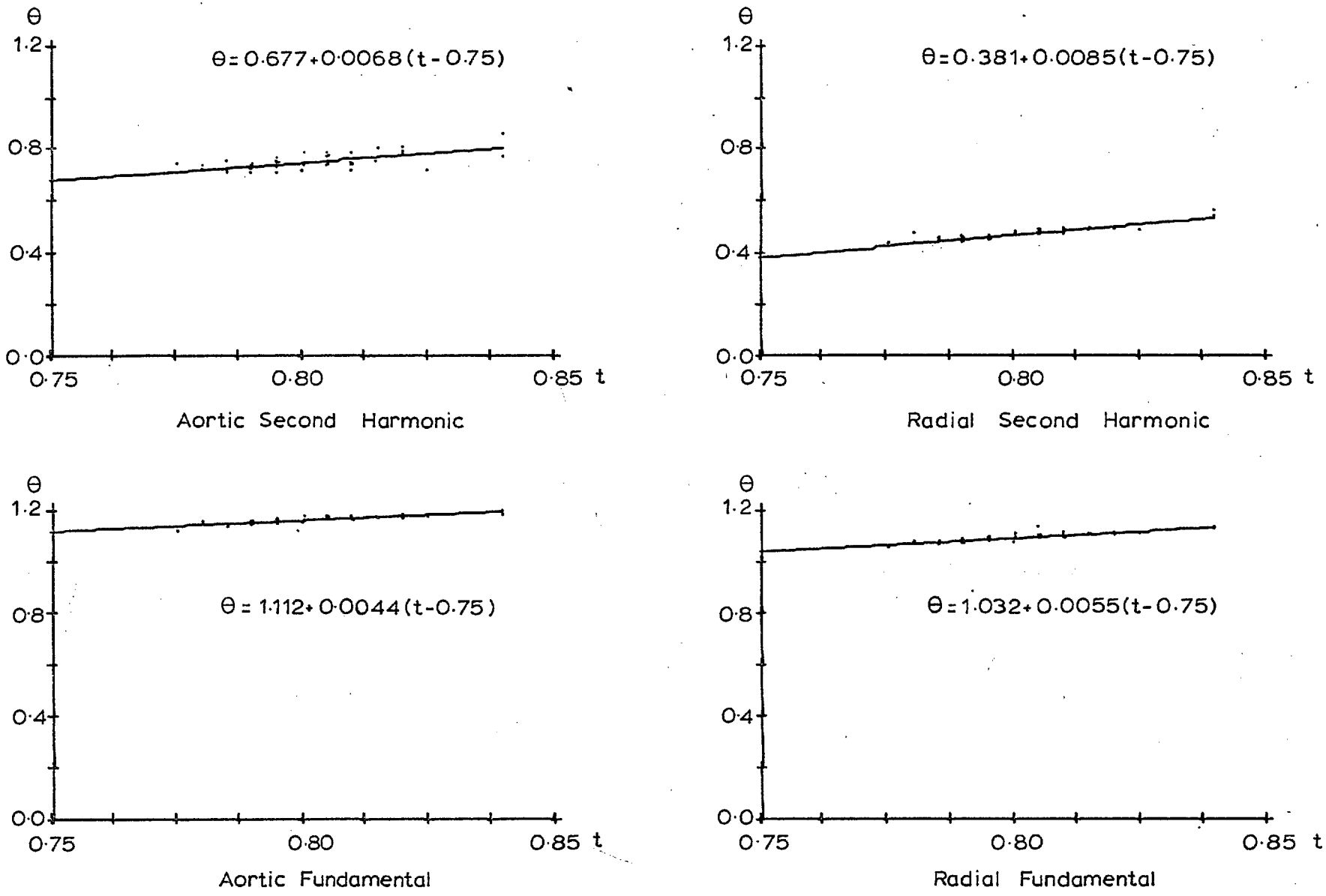


Fig. 3-20: Variation of harmonic phase angle θ (in units of π radians) with Interbeat Interval t (seconds).

bulk of the blood pressure waveform maintains a constant time relationship with the QRS peaks. Hence this constant time appears as a linearly changing phase angle when the analysis is carried out using fundamental periods of increasing lengths, as phase is directly proportional to time. The positive slope indicates a phase advance with increasing period, i.e. as the interbeat interval increases, the bulk of the waveform still remains at the left-hand side of the data sequence being analysed, in a fixed position with respect to the QRS peak.

It is therefore possible to convert phase angles (expressed as coefficients of Pi radians) into equivalent time shifts of each harmonic (measured from the QRS peaks) by multiplying each harmonic phase angle by a factor equal to the time interval represented by Pi radians for that harmonic, i.e. by the interbeat interval divided by twice the harmonic number. If it could be assumed that the pressure waveform did not change shape significantly (at least as far as the phase spectrum is concerned) but was purely delayed when recorded at increasingly distal locations, then the obvious effect of changing the recording site would be to alter the numerical value of the time shifts. On this basis, the phase difference between harmonics of waveforms recorded at two sites can be weighted by this factor to give the delay between the harmonics corrected for the changes of interbeat intervals. The distal waveforms would be delayed in time more than the proximal waveforms, and thus their computed phase angles exhibit a larger lag. Changes of the phase angle with interbeat interval will also be larger in consequence. This is borne out by the fact that the slopes of the radial

harmonic lines in Fig. 3-20 are slightly steeper than those of the aortic harmonics, and the difference in the gradients is greater for the second harmonic than for the fundamental. However, the measured gradients of the best fit lines in Fig. 3-20 do not exactly correlate with the theoretical predictions based on the simple delay assumption. This is because the real situation is more complex and the propagation velocities of the harmonics in the artery vary with frequency and position. This behaviour can be attributed to reflections (particularly at high frequencies) and to effects caused by changes in the arterial wall parameters (McDonald, 1960).

The spectra of the data of Fig. 3-2 computed using the interbeat interval as the period of analysis are shown in Fig. 3-21. These spectra are not as smooth as those obtained when a fixed analysis period was used (Fig. 3-15), although differences between the amplitude spectra of the two cases are not as noticeable as the variations in the phase spectra. The situation is improved if, as before, the results are presented in comparative rather than absolute form, as in Fig. 3-22, which shows the amplitude ratios and phase differences calculated from the spectra of the proximal and distal waveforms. Further improvement is obtained if the phase differences are compensated for the variations in interbeat interval, as discussed above. The resulting harmonic time delays are shown in Fig. 3-23, and although these plots are only slightly smoother than the phase difference curves of Fig. 3-22, the value of performing this conversion lies in the fact that the harmonic time delays are expressed to a constant time scale independent of the absolute

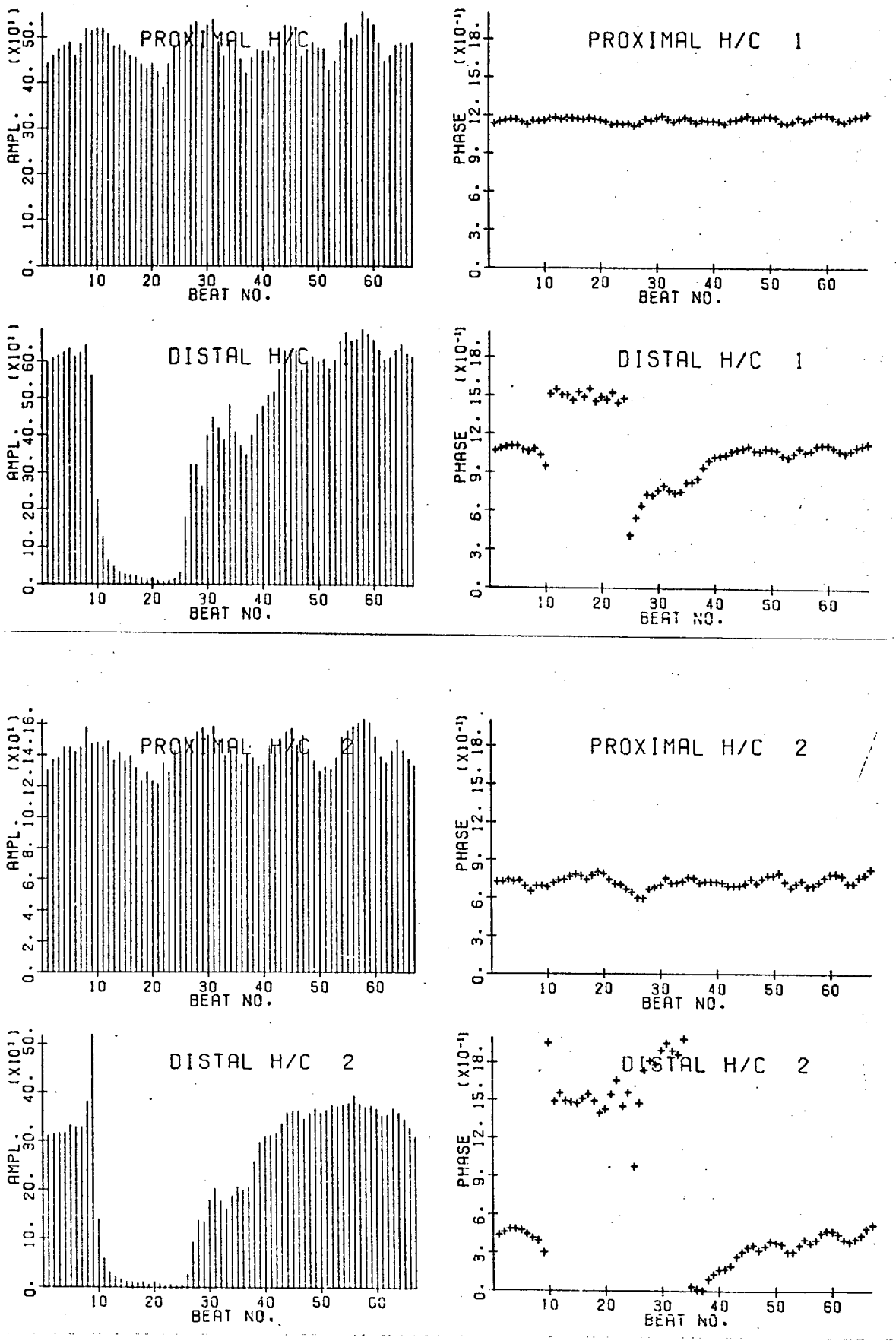


Fig. 3-21: Spectra of the data of Fig. 3-2 (interbeat-interval period analysis).

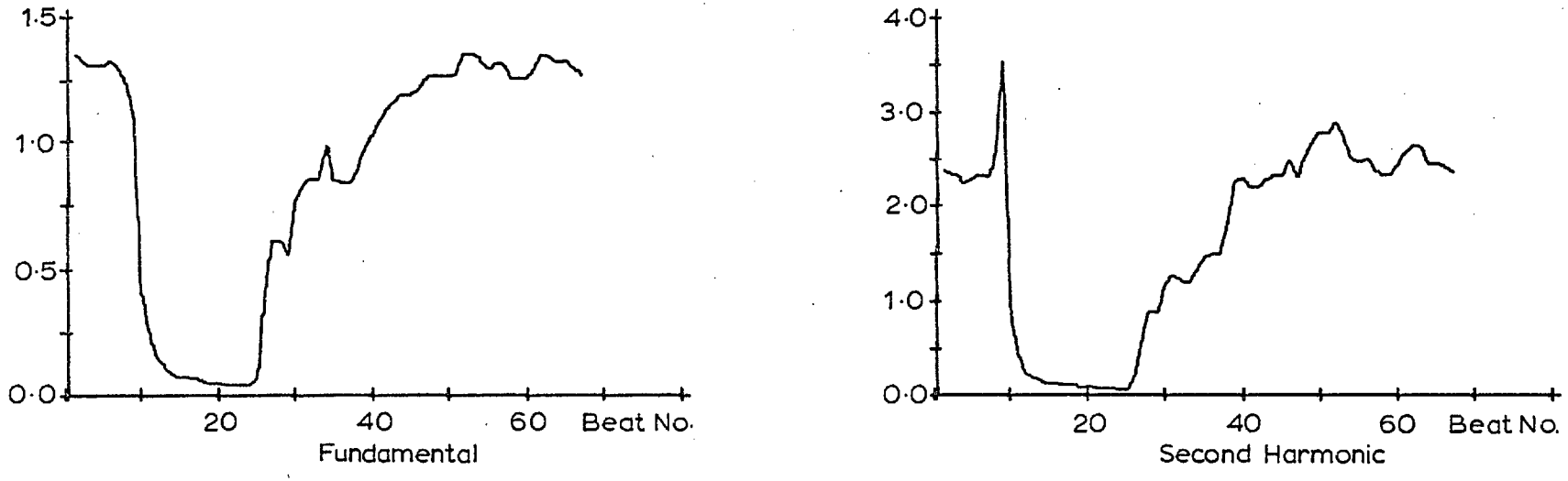


Fig. 3-22a: Distal: Proximal Amplitude Ratios

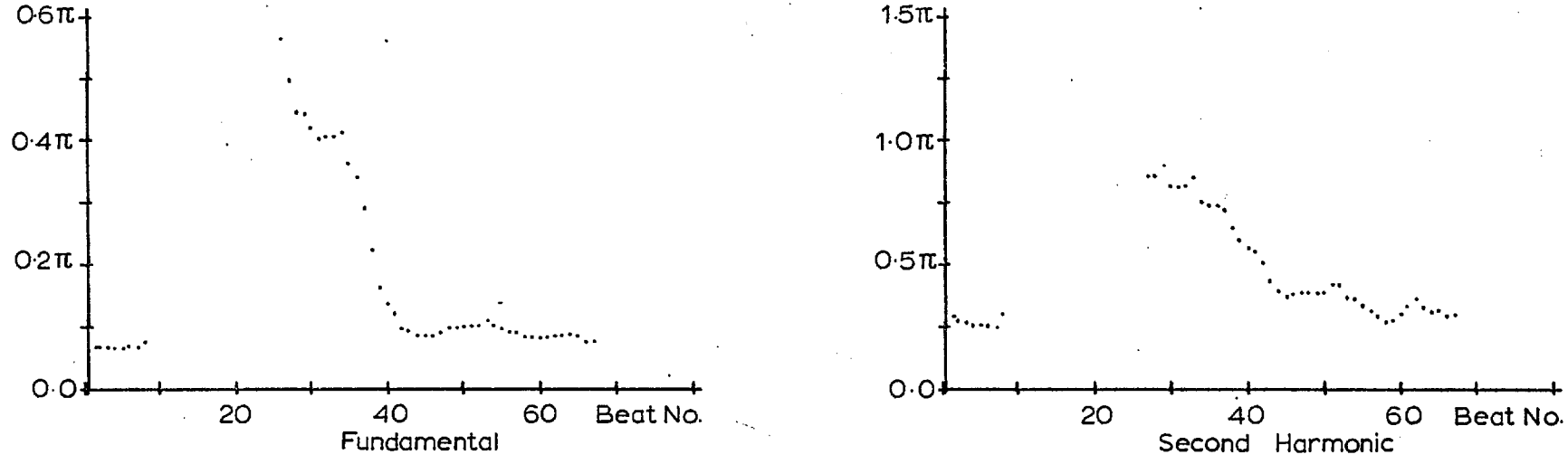


Fig. 3-22b: Proximal-Distal Phase Differences. Interbeat-Interval Period Analysis.

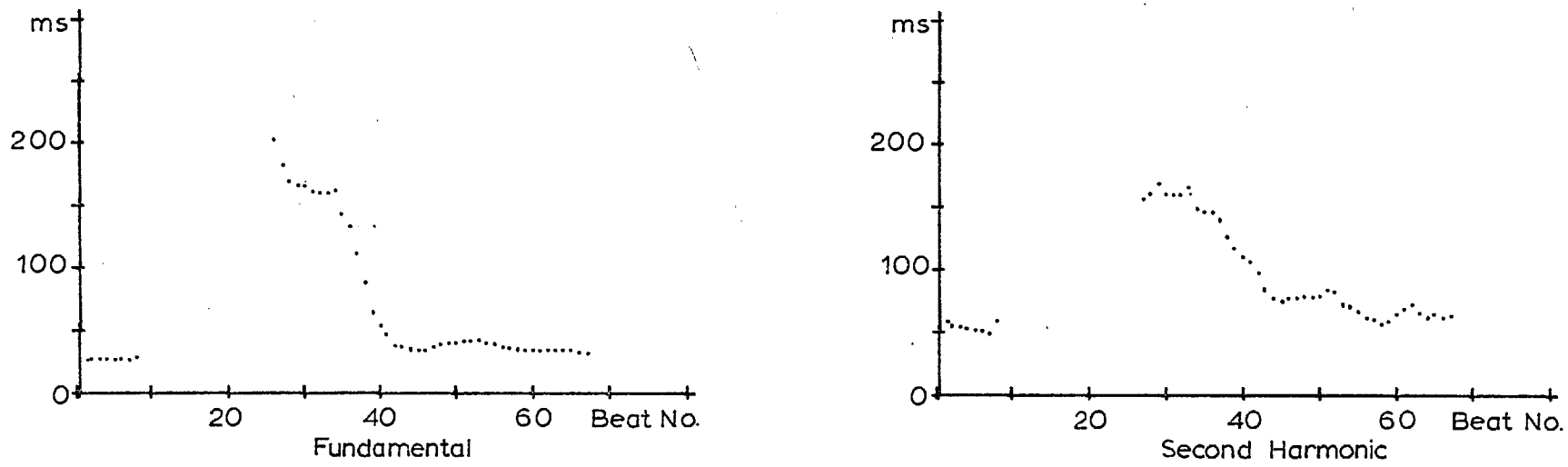


Fig. 3-23: Harmonic time delays computed from phase differences. Interbeat - Interval Period Analysis.

frequencies involved.

The results of this form of analysis do not reveal any new features in the spectra. At the cuff systolic point (beat 26) the harmonics of the radial waveform are delayed with respect to the aortic waveform by about 170 ms, this delay decreasing during successive beats towards the pre-occlusion value of 25 ms for the fundamental frequency and 60 ms for the second harmonic. As expected, a corner point is seen at beat 44 in the time delay plot for the fundamental, with a similar (though not so distinct) change occurring in the time delay of the second harmonic. The fundamental amplitude ratio appears to stabilize at beat 52, when the cuff is at true diastolic blood pressure.

This type of analysis was carried out on all five cycles of cuff pressure that were recorded, and the results discussed in this section are typical of the results of the other analyses. The characteristics of the spectra were such that the cuff systolic and diastolic points could be located from the spectral plots in each case, except for the measurement cycle when the cuff was deflated prematurely. Although the results of analyses using the interbeat interval as the fundamental period are slightly inferior to the results of the fixed period analysis, this approach is likely to be useful with other signals where the fundamental period may vary over an unknown range, or the data are being analysed "on line". It is recommended that the fixed period analysis be used for recorded data since the interpretation of the spectra is then straightforward and not complicated by changes in absolute frequencies.

3.4 IMPULSE RESPONSE ANALYSIS

3.4.1 The Cuff as a Filter

The amplitude ratios and phase differences calculated in the previous section can be thought to represent the transfer function of a notional filter which has the proximal waveform as input, and the distal waveform as output (Fig. 3-24). An alternative approach to the frequency analysis is to characterize this filter in the time domain by computing its impulse response. As the pressure in the cuff changes so do the characteristics of the filter, and its changing impulse response may be calculated from the aortic and radial waveforms for each beat provided conditions are assumed to be constant during a beat, with stepwise changes occurring at the QRS instants.

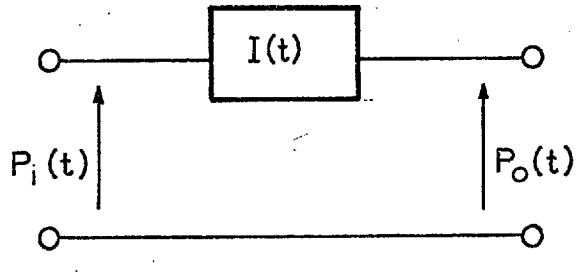


Fig 3-24: The cuff as a filter.

$$P_o(t) = \int_{-\infty}^{\infty} I(\tau)\, P_i(t-\tau)\, d\tau \qquad (3.9)$$

where $P_i(t)$ = proximal pressure waveform

$P_o(t)$ = distal pressure waveform

$I(t)$ = impulse response of section of artery with cuff

t = time

τ = dummy time variable

Eq. 3.9 is the convolution equation describing the system shown in Fig. 3-24 (Lathi, 1965). This equation may be stated as follows: the output waveform equals the input waveform convolved with the impulse response of the filter. Therefore when the input and output waveforms are known, an "inverse convolution" or "deconvolution" is required to obtain the unknown impulse response. To do this, Eq. 3.9 is transferred to the frequency domain to obtain Eq. 3.10, which may be stated as follows: the frequency spectrum of the output waveform equals the frequency spectrum of the input waveform multiplied by the frequency response of the filter.

$$P_o(j\omega) = P_i(j\omega) \cdot W(j\omega) \qquad (3.10)$$

where $W(j\omega)$ = frequency response of filter

ω = angular frequency

Rearranging,

$$W(j\omega) = \frac{P_o(j\omega)}{P_i(j\omega)} \qquad (3.11)$$

Hence the frequency response of the filter may be computed by dividing the frequency spectrum of the output waveform by the frequency spectrum of the input waveform. The impulse response I(t) is then given by the inverse transform of the frequency response of the filter. This procedure gives a valid impulse response provided all output frequencies are adequately represented in the input waveform. With practical waveforms this criterion is not necessarily satisfied, and it is possible for some of the harmonics in the divisor of Eq. 3.11 to be so small as to fall below the noise level, introducing considerable error into the result for these harmonics. In such a case the impulse response is dominated by components for which the numerator in

Eq. 3.11 is large compared with the denominator.

With sampled data, the practical evaluation of the impulse response of spectra computed by the DFT effectively changes the integration over infinite limits in Eq. 3.9 to a summation over the period of the data. As a result, the impulse response computed by discrete frequency domain deconvolution is repetitive since the DFT assumes a repetitive data sequence. Furthermore, if this response has not decayed to zero within a time equal to the period of the data, only a part of the complete impulse can be evaluated. Such is the case with the present data, as the vascular system is re-excited before the response to the current beat has ceased. Hence the responses in this section are not strictly true impulse responses as they are computed on a beat-by-beat basis; nevertheless they represent valid parameters for describing the system.

A program was written to implement the deconvolution procedure outlined above, and the impulse response of the filter representing the section of artery and the cuff was computed for each beat during two of the indirect blood pressure measurements. As before, the DFT or Chirp-Z subroutines were used to compute the real and imaginary parts of the required number of lower harmonics, using a fixed period of 0.7 seconds. These values were placed in the correct positions in a power-of-2 length array with all other harmonics set to zero and an inverse FFT subroutine used for the transformation into the time domain. In this way, the resulting impulse responses may be considered as filtered, since they contain only the chosen number of lower harmonics. For each harmonic the complex division effectively

divides the amplitudes of the output and input waveforms, but subtracts their phase angles. This form of analysis therefore combines the transmission characteristics of as many harmonics as desired into a single function for each beat. Plotting the impulse response is therefore a compact method of presenting both amplitude and phase information simultaneously.

3.4.2 Filtered Impulse Responses

It was found that the most acceptable results were obtained when the waveforms were levelled (using the procedure described in Section 3.4.4), and the impulse responses were filtered to contain only the fundamental and second harmonic frequencies. Fig. 3-25 shows the results for the level-corrected data of Fig. 3-18. For visual convenience time t=0 has been placed in the central position of the impulse response by interchanging the right and left halves of the data array computed by the inverse FFT. This is permissible as the impulse response as computed is a repetitive function.

In Fig. 3-25 the impulse response is relatively stable from beat 1 to beat 8, and then is quickly reduced to an insignificant level as the cuff is inflated. Nothing substantial is seen until flow recommences under the cuff at beat 26, the response for this beat being small in amplitude and considerably displaced to the right. From beat 26 there are gradual changes towards the pre-occlusion shape of the impulse response, while from beat 44 there are only minor changes in position not forming part of the previous well-ordered shifting to the left. However, the peak-to-peak amplitudes continue to increase until

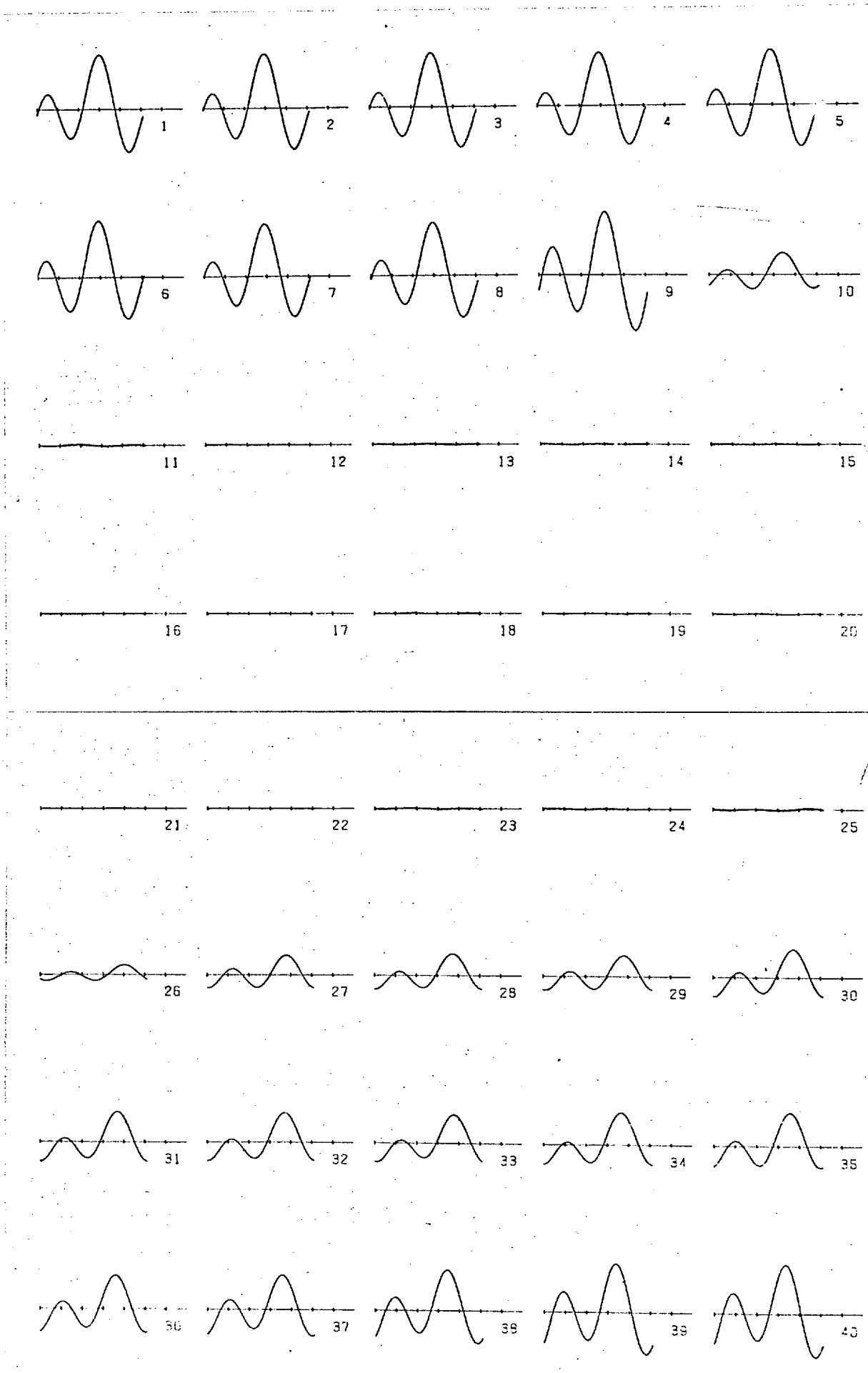


Fig. 3-25 (page 1).

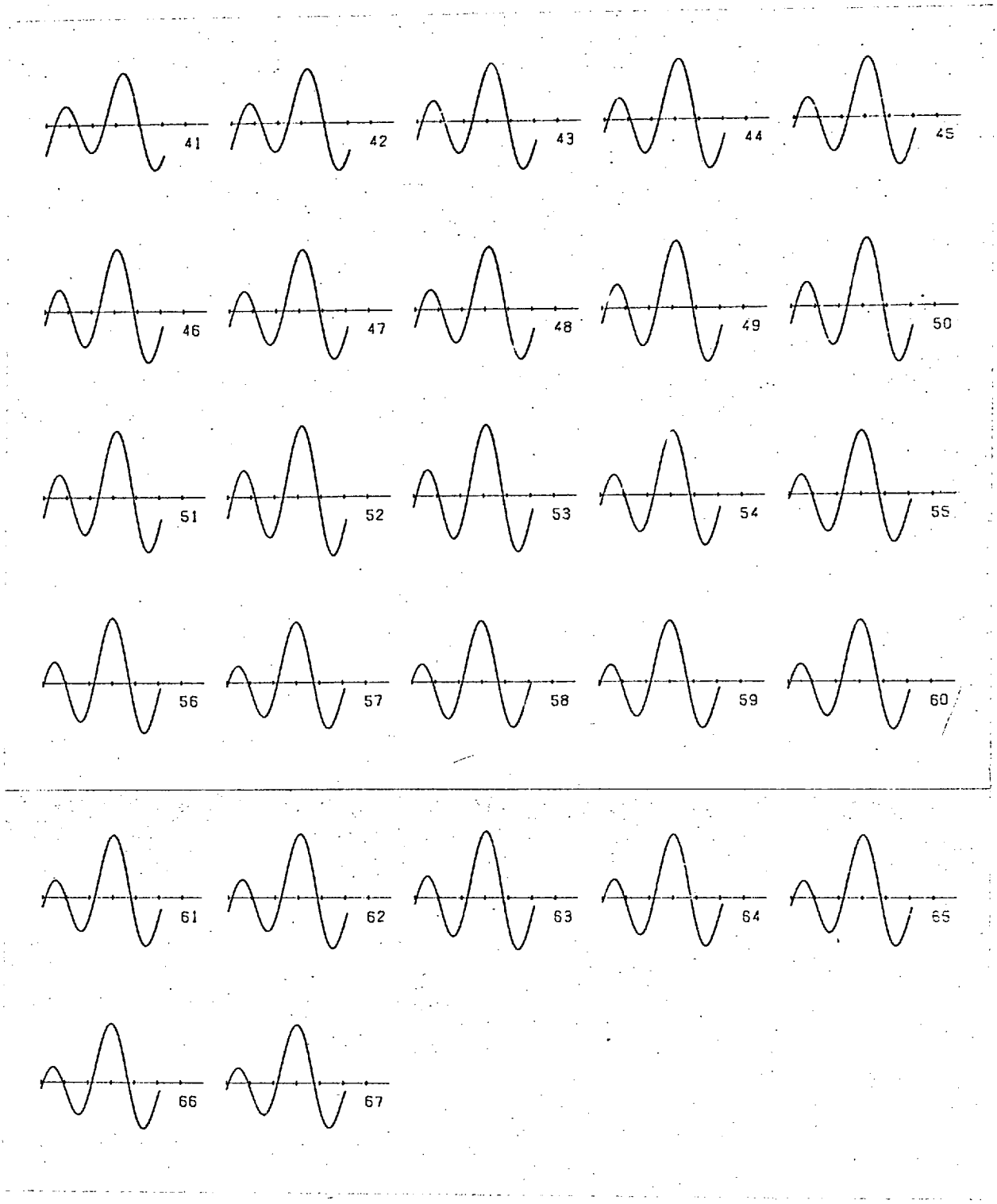


Fig. 3-25 (page 2): Filtered impulse responses of the data of Fig. 3-2.

a maximum is reached at beat 52, after which only minor changes in amplitude and position occur. In the light of the results of the frequency analyses of Section 3.3, it is not surprising that such features are seen in the impulse responses at beats 26, 44 and 52.

Clearer impressions of the changes in the filtered impulse responses are given by 3-dimensional representations. In Figs. 3-26 and 3-27 the successive responses are considered as a deck of cards viewed from the left and right respectively. This form of presentation allows the set of responses computed for all the beats occurring during an indirect blood pressure measurement to be shown in a single plot. The pre-occlusion beats are at the front, followed by the flat total occlusion period. As time passes, the responses reappear at beat 26 when intermittent flow resumes beneath the cuff during the deflation portion of the measurement cycle. The changes in amplitude and position of these responses are evident from both viewpoints, as the influence of the cuff diminishes and the pre-occlusion shape is regained by the impulses towards the rear of the diagram. However, it is difficult to identify special features which would indicate the cuff diastolic point with confidence.

The shift towards the left-hand side is revealed more clearly in Fig. 3-28, in which the successive impulse responses are shown as if stacked directly one behind the other. However, although this presentation provides a distinct picture of changes in phase, the amplitude changes are not so obvious. The contour plot of Fig. 3-29 is an alternative presentation giving equal weight to both phase and amplitude changes. In

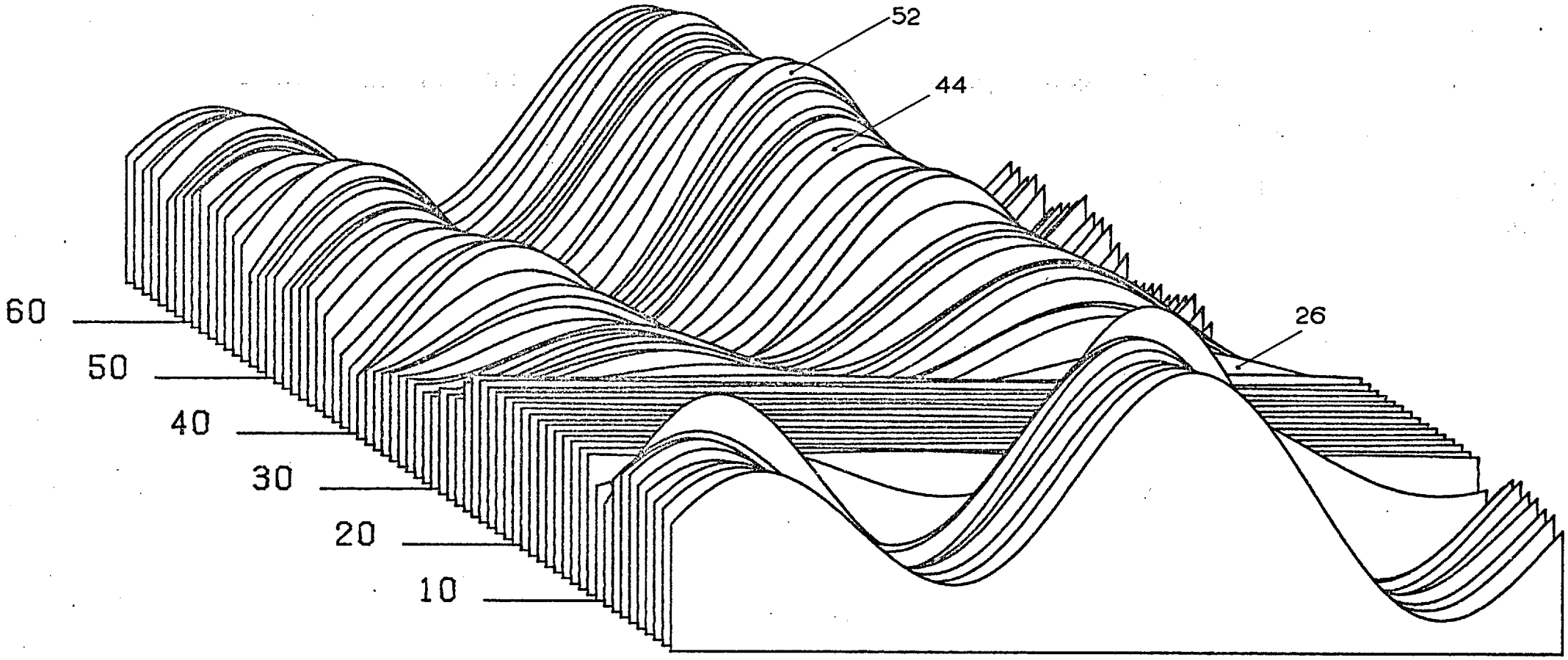


Fig. 3-26: Successive filtered impulse responses (left view).

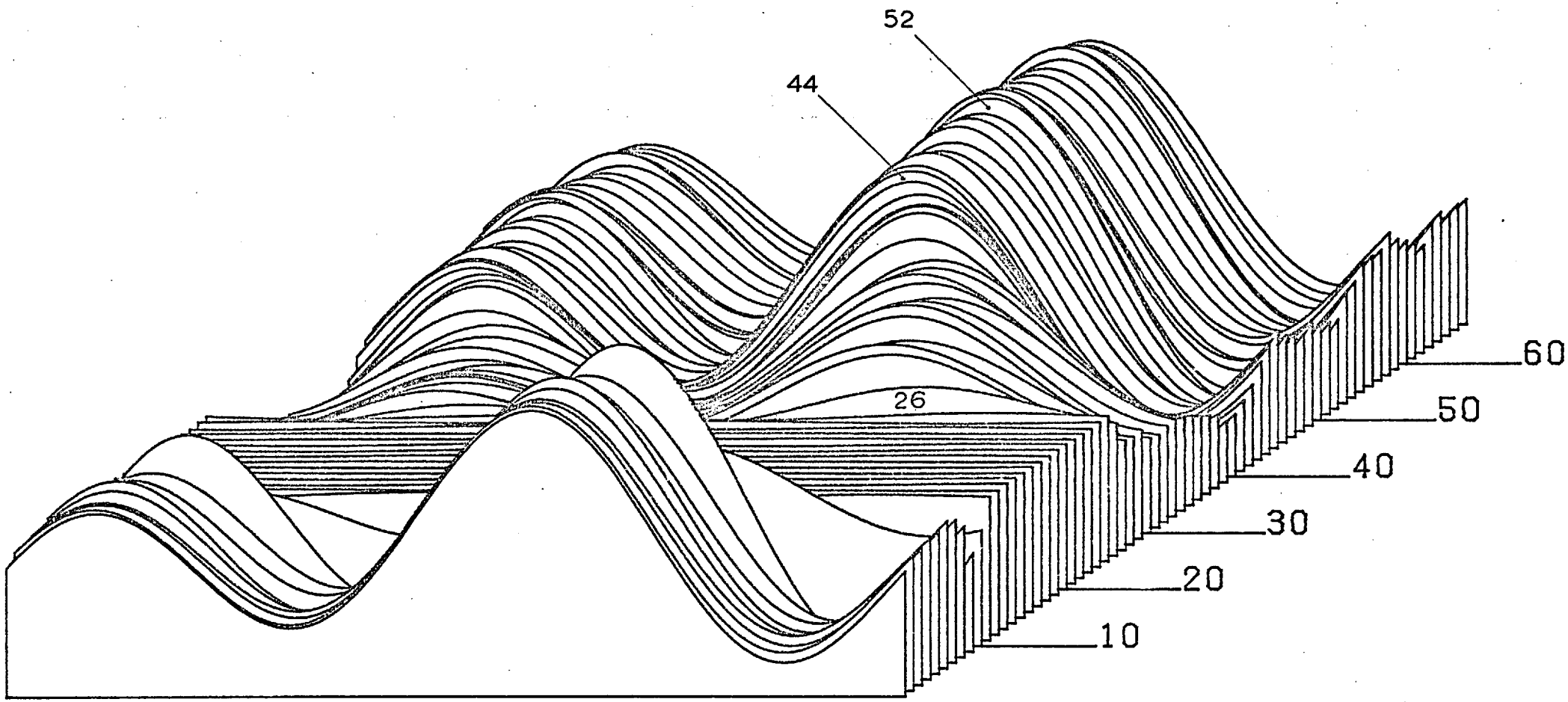


Fig.3-27: Successive filtered impulse responses (right view).

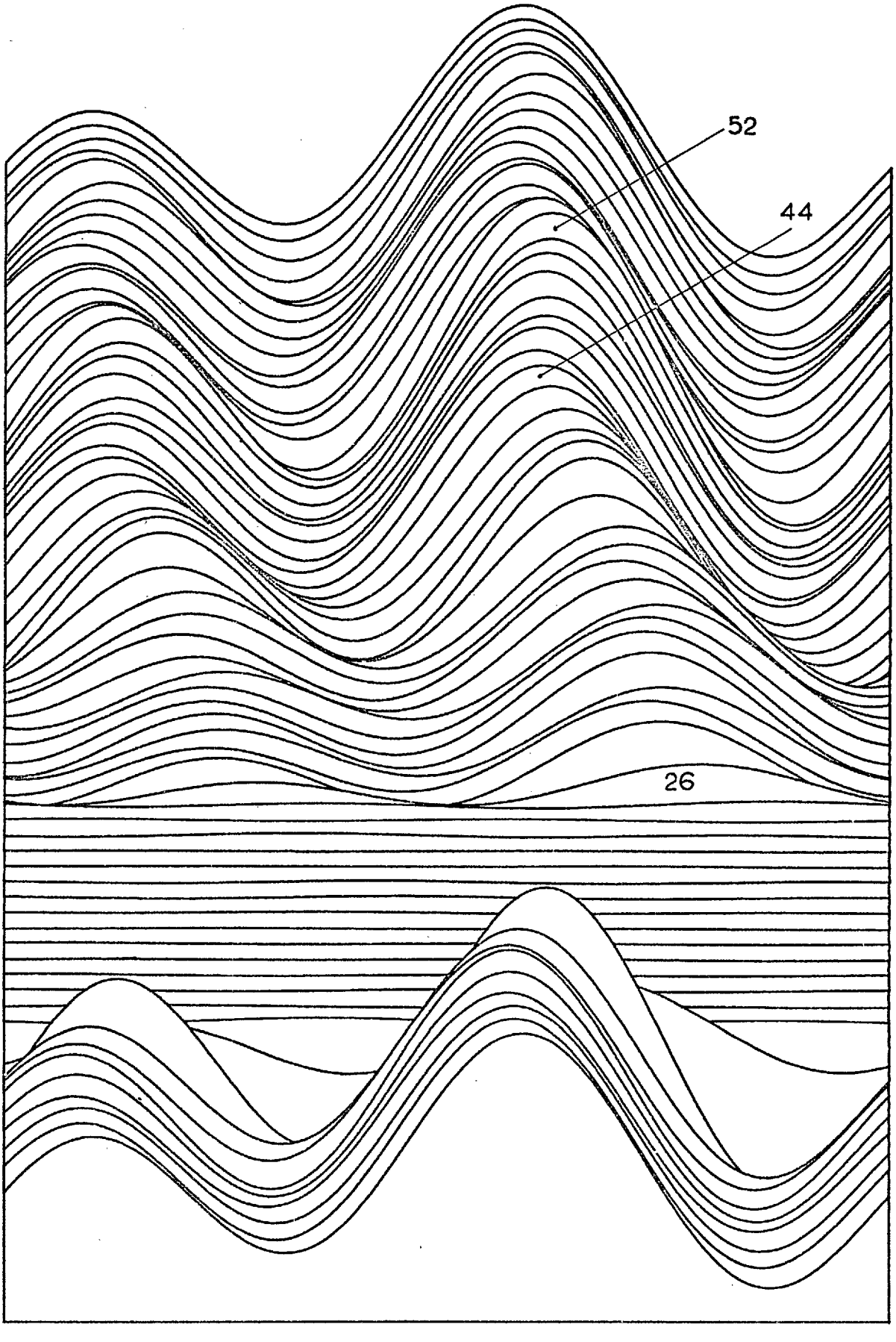


Fig.3-28 : Successive filtered impulse responses (front view).

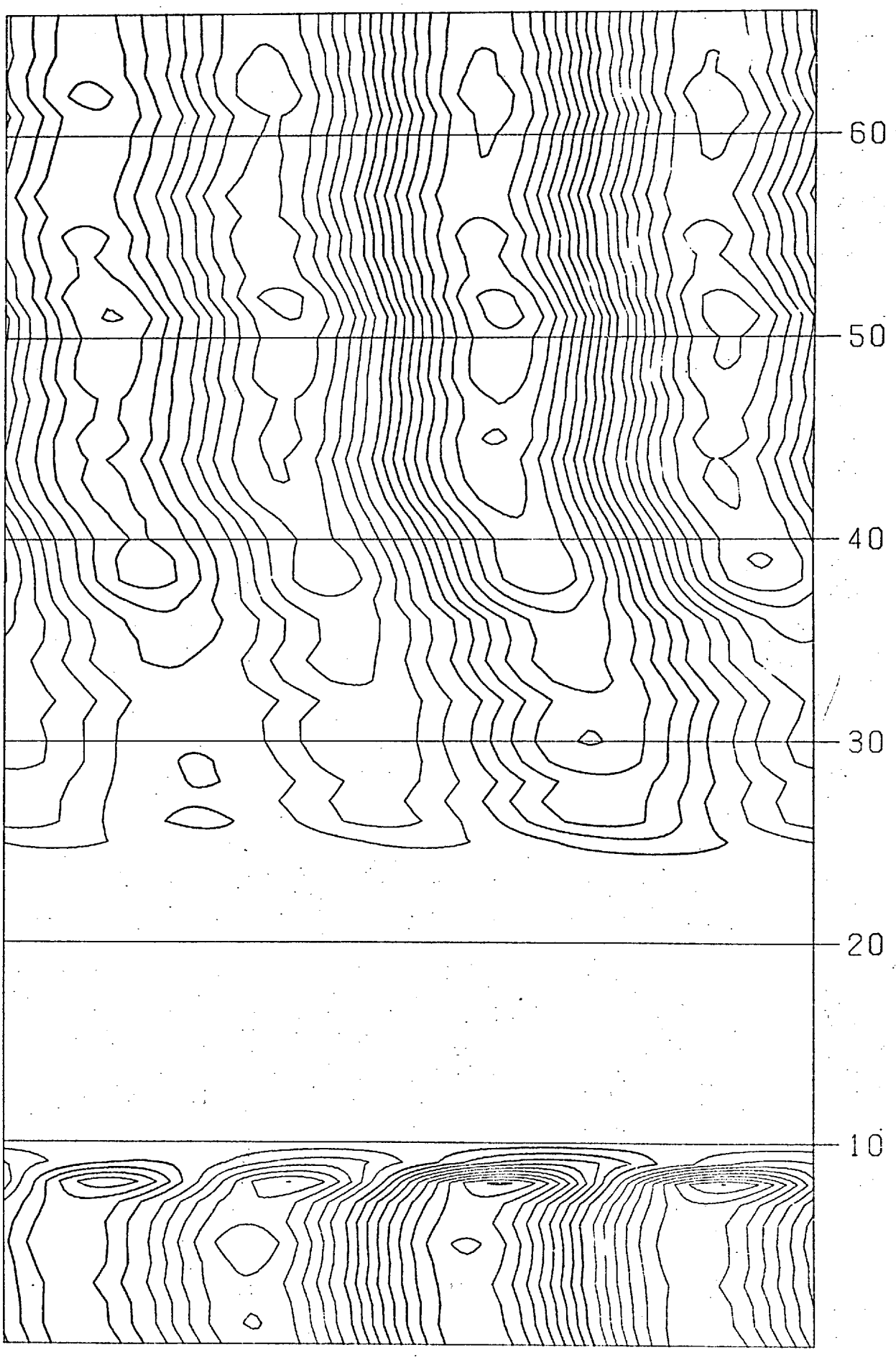


Fig. 3-29: Contours of successive filtered impulse responses.

this diagram the darker lines represent equi-spaced contours of the "hills", whilst the finer lines are used to show the contours of the "valleys". It is seen that the shift towards the left stabilizes at about beat 44, whereas the amplitudes continue to increase until about beat 52, as indicated by the additional contours in this region. This area of the plot corresponds to the cuff diastolic point in the original data. The cuff systolic point is indicated by the onset of the contours at beat 26. Although quantitative information is perhaps more clearly portrayed in a contour plot than in perspective diagrams (because the axes are rectangular and the contours are equi-spaced), it is thought that not much reliance can be placed on this form of presentation as the interpretation is still somewhat subjective.

When the impulse response was filtered to contain only the fundamental frequency, a progression was still seen between beats 26 and 44, but the beat-to-beat changes were harder to detect. When the filtering was expanded to include the third harmonic, meaningless plots were produced because of the low third harmonic amplitude of the aortic waveform compared to the third harmonic amplitude of the radial waveform. For many beats the third harmonic output:input amplitude ratio was greater than 10, and the impulse response was dominated by the relatively high gain at the third harmonic, completely obscuring the significant trend in beats 26 to 52. However, ignoring transmission of the third harmonic, inclusion of higher harmonics also detracted from the orderly trend, as shown in Fig. 3-30, where the filtering has been extended to include the fourth and fifth harmonics. There is considerable variation in the impulse

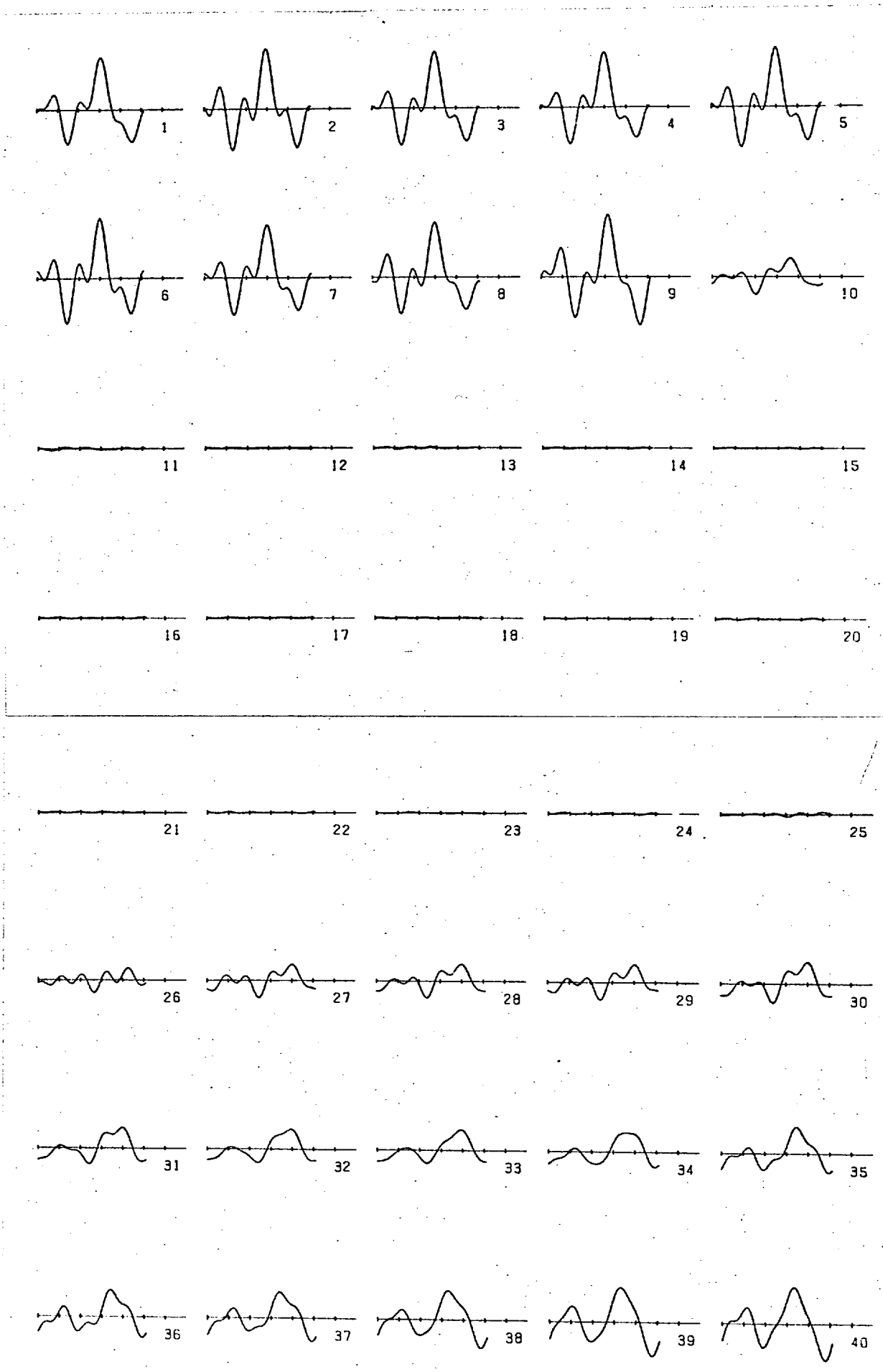


Fig. 3-30 (page 1)

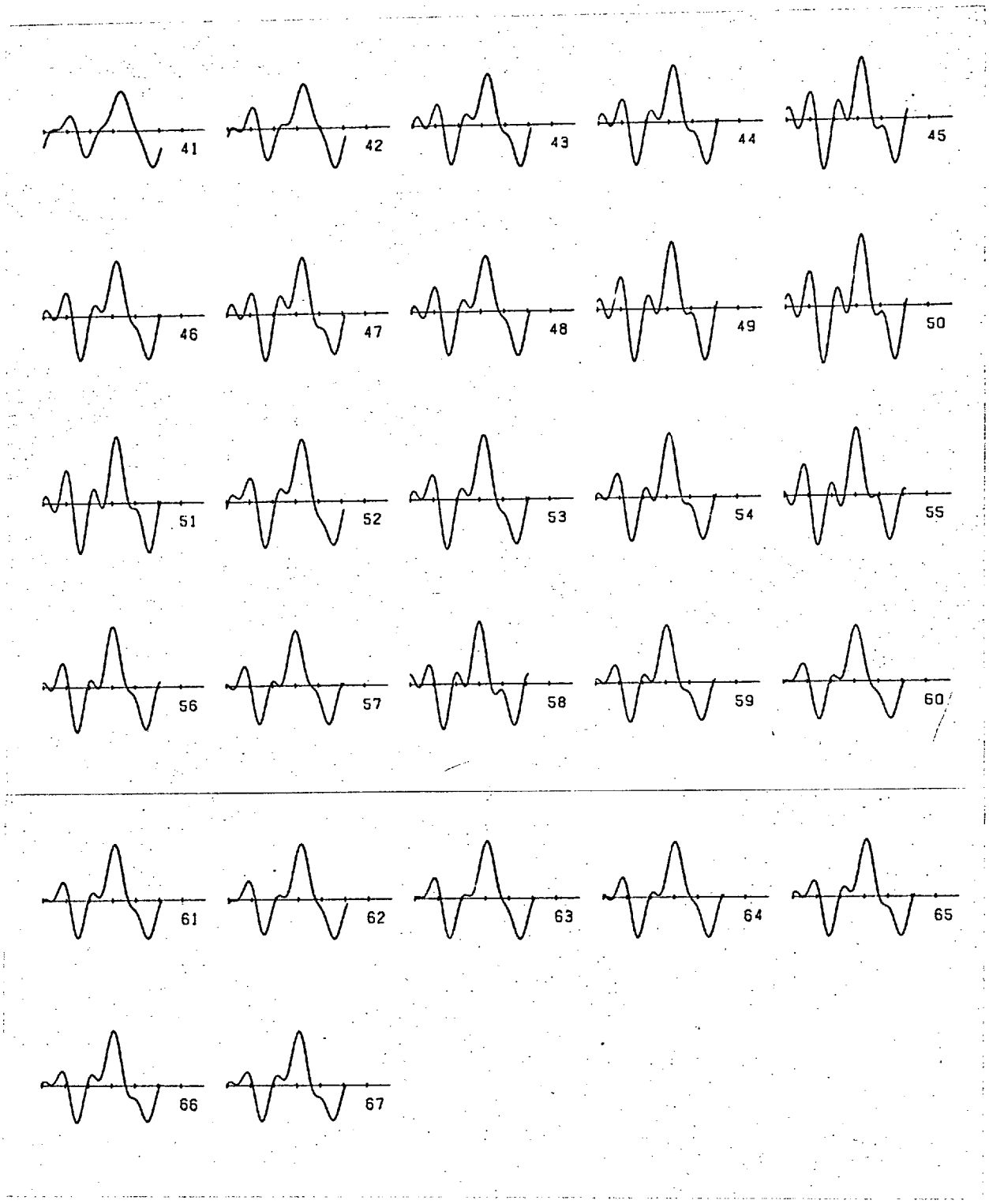


Fig. 3-30 (page 2): Inclusion of 4th and 5th harmonics in the impulse responses.

responses for beats 1 to 8, i.e. before the cuff is inflated, and no striking feature is seen when the cuff pressure is near diastolic blood pressure (beats 41 to 55). It appears from these results that minor differences of waveshape mask the underlying time relationship of the input and output waveforms.

All the impulse responses discussed up to this point have been computed from data that have had the linear trend removed from each beat. If this procedure is not carried out, responses such as are shown in Fig. 3-31 are obtained, where the filtering is the same as for the responses of Fig. 3-25, i.e. they contain only the fundamental and second harmonic frequencies. There is little alteration to the impulse responses for beats where there is an adequate radial pulse pressure; however, during arterial occlusion (beats 11 to 26) the impulse response is initially non-zero, due to the decline of distal pressure. It is therefore preferable to remove the linear trend before computing the impulse response in order to suppress spurious responses during the non-pulsatile region.

The filtered impulse response technique outlined in this section enables the amplitude ratio and phase difference results of Section 3.3 to be combined into one plot independent of the number of beats or harmonics being considered. It should be noted that in contrast to the frequency analysis, the non-significant phase differences computed during the period of total occlusion do not contribute to the responses because the amplitude ratios are virtually zero. Also, harmonic phase shifts greater than 2 Pi radians do not appear as discontinuities.

The computed responses represent the total of all the

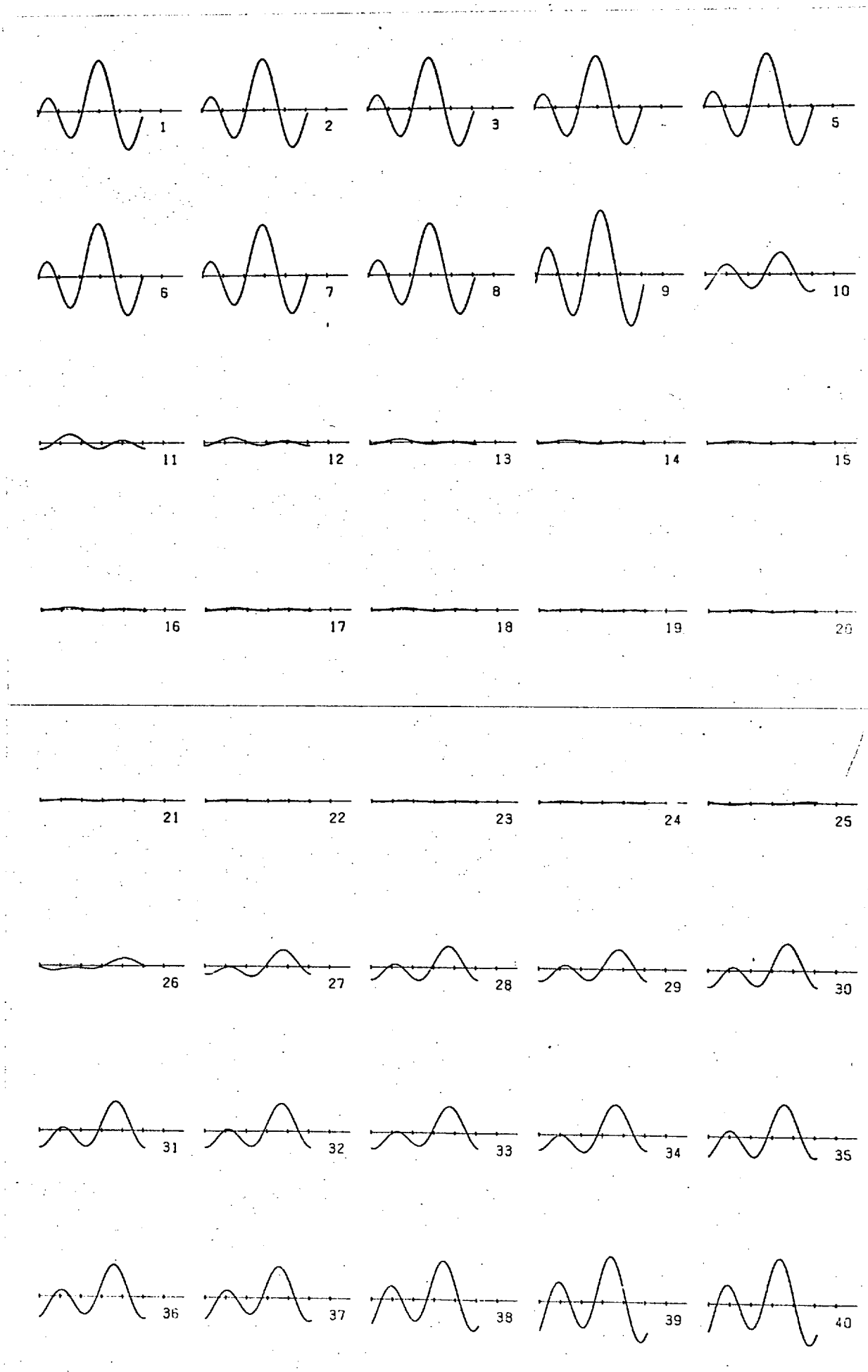


Fig. 3-31 (page 1).

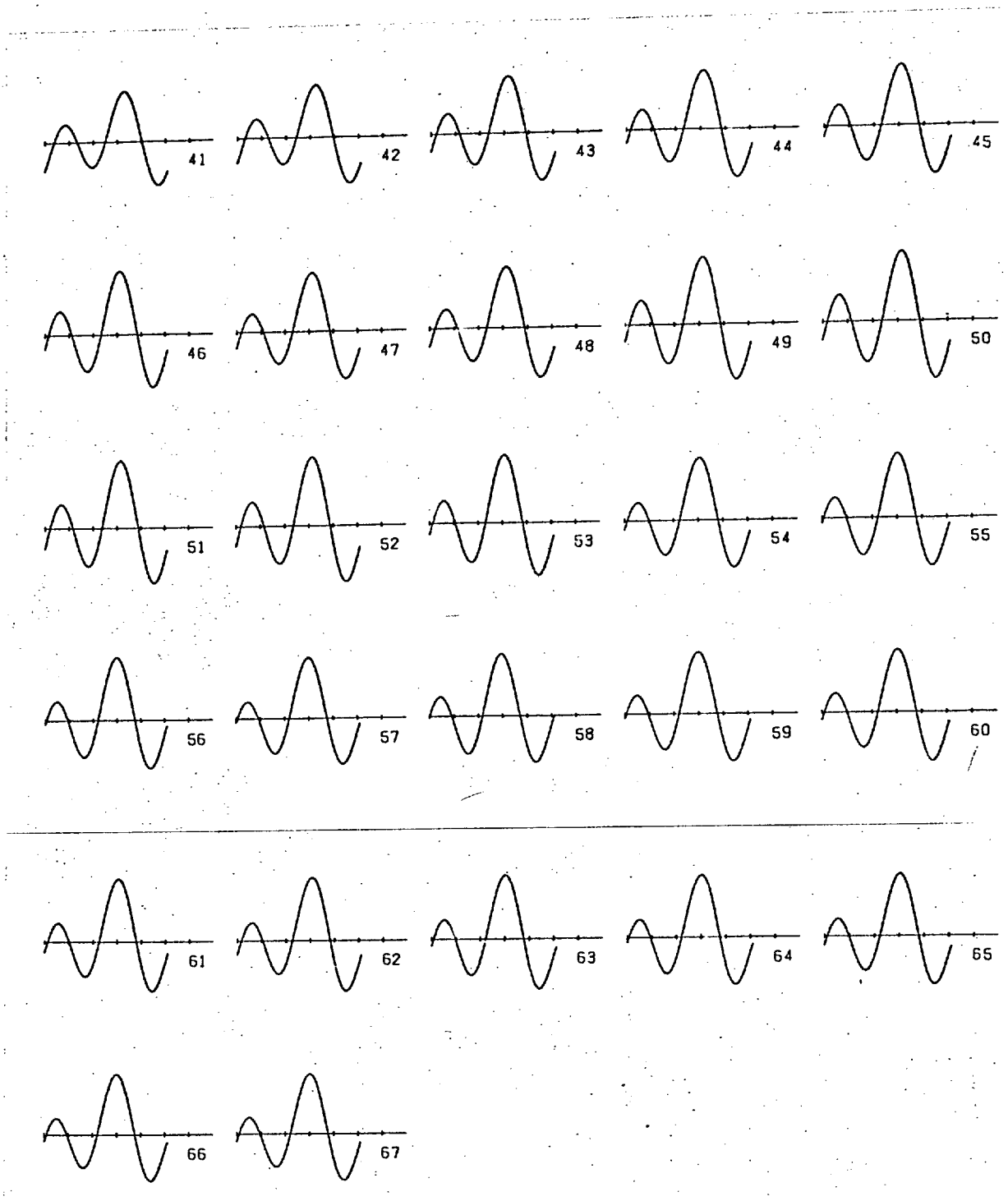


Fig. 3-31 (page 2): Filtered impulse responses without removal of linear trend from the data.

effects causing the distal waveform to differ from the proximal. When the cuff is at zero pressure, the filtering action of arterial transmission is seen alone. Deviations from this response indicate the effect of the inflated cuff. Of the several forms of plot used, the contour diagram is probably the most meaningful because the contours and both axes can be readily calibrated. Although 3-dimensional methods of presentation contain all the information available for locating the cuff systolic and diastolic points, the total effect is subjective and judgments based on these diagrams appear to be unreliable.

3.5 OBSERVATIONS AND CONCLUSIONS

3.5.1 The Waveforms

The recordings discussed in this chapter are similar in most respects to those of the brachial pressure distal to the cuff described by London and London (1967). In particular, the following points of agreement are noted.

(1) The systemic arterial pressure does not change significantly during the indirect measurement.

(2) There is a rise in distal diastolic pressure accompanying inflation of the cuff.

(3) Following occlusion, the pressure in the distal artery levels off to approximately 40 mm Hg.

(4) After the occurrence of the cuff systolic point, the distal diastolic pressure rises to a maximum which is greater than the resting value. As the cuff pressure continues to fall, there is an accompanying drop in the distal diastolic

pressure until the cuff diastolic point is reached.

(5) During cuff deflation there is a sequentially changing delay in the onset of the distal pressure wave.

The following discussion relates to the preceding points.

(1) It was found that although the aortic pulse contour remained relatively stable, the aortic diastolic pressure rose during the re-establishment of brachial flow. The recordings also suggested an accompanying rise in the aortic systolic pressure but this could not be accurately determined because of the ringing at the peaks.

(2) The rise in distal diastolic pressure as the cuff is inflated is doubtless due to the occlusion of the artery during the diastolic phase of two or three beats. The situation would be markedly different if the cuff pressure was applied to the arm at a faster rate than the risetime of the arterial pulse pressure. However, the rate of application of cuff pressure is unlikely to affect the measurement of cuff systolic and diastolic pressures because the distal pressure drops in an approximately exponential manner towards a constant level.

(3) The stabilization of distal pressure to a level between 40 and 50 mm Hg while the cuff pressure exceeds systolic blood pressure was the consistent observation of London and London (1967). However, it should be noted that the waveforms given by these authors show a cuff deflation rate faster than normal, so that the cuff systolic point is reached while the distal arterial pressure is still decreasing. Nevertheless, similar levels were reached in the data discussed in this chapter, even though a much slower cuff deflation rate was used. This shows the

essentially exponential character of the arterial pressure drop as the veins fill with the continuing capillary flow.

(4) The elevation of the distal diastolic pressure prior to the cuff diastolic point occurs as follows. When the proximal waveform falls below cuff pressure the artery is occluded and the distal pressure, which is no longer influenced by the proximal wave, decreases because of continuing flow into the periphery. This decrease is not as rapid as it would be if the distal wave was coupled to the proximal wave. With each successive beat the point at which the exponential fall commences follows the cuff pressure, and hence the distal diastolic pressure maintains a level slightly less than the cuff pressure until the cuff diastolic point is reached.

(5) The distal pressure wave rises when the proximal wave exceeds the cuff pressure. This point advances in time as the cuff pressure decreases, due to the finite slope of the systolic upstroke.

Although the recorded aortic waveform was considerably distorted at the peaks, it has proved to be adequate for the purposes of this investigation. This is because the bulk of the waveform energy lies in the fundamental and second harmonic (the main frequencies of interest) which are below the frequency range of the ringing. However, the presence of the ringing has obscured the true aortic systolic pressure in these recordings.

The cuff systolic point is sharply indicated by the first pulse beneath the cuff, and its accuracy is not really in question. This topic has been discussed extensively in the literature (Karvonen et al., 1964; Simpson et al., 1965;

Kirkendall et al., 1967; London and London, 1967; Weinmann, 1972). The accuracy of the cuff diastolic point is assessed by comparison with the direct pressure recordings. Although the recordings were made at sites some distance from the cuff, it is known that the diastolic pressure decreases only slightly in the main arteries as the pulse travels away from the heart (Guyton, 1966). For example, in these data the difference between the diastolic pressures at the two sites was about 4 mm Hg, and the diastolic pressure in the brachial artery could be taken as approximately midway between the proximal and distal values. Although the blood pressures can change significantly during an indirect blood pressure measurement, the results of any cuff method should be compared with the systolic and diastolic pressures at the times of the cuff systolic and diastolic points respectively.

3.5.2 Time Relations of the Waveforms

The QRS complex of the E.C.G. is a most convenient chronological occurrence marking as it does the beginning of the electrical and mechanical events of each heart beat. The effect of the cuff is clearly seen in a parallel recording of the E.C.G. and the distal pressure wave. Although a decreasing delay is observed between the QRS and the onset of the distal pulse the eye cannot judge when this delay stabilizes to its resting value because of minor changes in beat-to-beat waveshape. For the same reason the simple timing of a waveform feature does not reveal any reliable change at the cuff diastolic point although the decreasing delay is exposed more clearly than can

be discerned by eye. This has been demonstrated by time measurements using two criteria, as described in Section 3.2.4.

As time delay measurements taken from direct pressure waveforms were found to be unreliable, it was therefore concluded that such measurements based on indirect waveforms would be even worse. It is suggested that the measure of correlation achieved by the method of De Dobbeleer (1963) is largely due to the low-pass filtering action of the pneumatic circuitry of the thermistor pulse detectors. Furthermore, the random delays seen between two photoplethysmograms monitoring the pulse at different (though not widely separated) sites may be attributed to the emphasis given to the higher components of the waveforms by the filtering employed (Clist, 1970).

3.5.3 Application of Signal Analysis Techniques

Frequency analysis has been shown in this chapter to give a better estimate of the cuff diastolic point than that given by time measurements made directly from the data. The decomposition of the waveforms by Fourier analysis has shown that most of the spectral power of each blood pressure beat lies in the fundamental and second harmonic frequencies. The higher harmonics represent minor shape details which were found to vary considerably from beat to beat even when the arterial system was undisturbed. It is suggested that this is due to the complex nature of reflections set up by a varying peripheral load, as well as minor changes in the ejection pattern of the heart. Computation of the third and higher harmonic coefficients did not yield significant information concerning the cuff

diastolic point, although trends of delay could be seen during the cuff depressurization consistent with the rotation of the phase angles of certain harmonics through more than 2 Pi radians.

Several variations of analysis have been tried. In effect, Fourier analysis has been used to discriminate against the high frequencies, enabling the fundamental and second harmonic components to be isolated and examined in detail. Special attention has been given to the plots of phase differences between corresponding harmonics of the proximal and distal waveforms. As the cuff pressure is released, a trend is seen which, in the case of the fundamental frequency, shows a distinct corner point when the phase differences stabilize to pre-occlusion values. It was found that this corner point occurred before the cuff pressure had decreased to the resting level of diastolic blood pressure. Instead, it was found that the corner point occurred when the cuff was approximately equal to the elevated distal diastolic pressure, a phenomenon which occurs prior to the cuff diastolic point. It is shown that a better estimate of the cuff diastolic point is given by the fundamental amplitude ratio of the distal and proximal waveforms. This parameter continues to increase after the phase difference corner point has occurred, and stabilizes when the distal diastolic pressure becomes no longer elevated above the resting diastolic pressure. The amplitude ratio therefore appears to be the parameter of greater value in locating the cuff diastolic point, and may prove useful as an objective criterion for the design of a blood pressure measurement apparatus.

The features discussed above were apparent in every

variation of the analysis. The smoothest trends were obtained from fixed period analyses, but the disadvantage of this approach is that the minimum interbeat interval must be known or estimated prior to analysis, since the conditions of the succeeding beat cannot be allowed to influence the analysis of the current beat. If the interbeat interval is used as the period of analysis, the phase differences may be corrected and expressed as time delays to reduce the effect of changes in the fundamental period. It was not found necessary to correct for level disparity between the ends of each beat, as apart from the non-pulsatile region of the distal waveform, there is little alteration in the significant low frequency components.

The filtered impulse response technique combines many parameters into one plot, conveying an impression of the amplitude ratio and phase difference changes occurring throughout a complete measurement cycle. The most meaningful presentation appears to be a contour plot of successive impulse responses positioned one behind the other. Nevertheless, the results are still judged subjectively, and the positions of the cuff systolic and diastolic points cannot be located with confidence.

3.5.4 The Need for a Model

The analyses discussed in this chapter have given rise to several ideas which need further investigation. In particular, it must be established that the observed changes occur in the general case and are not artefacts of a specific recording on a single subject. The reported observations of signal delay between waveforms obtained indirectly (De Dobbeleer, 1963; Gowen, 1963;

London and London, 1967; Clist, 1970) suggest that these changes do occur in the general case. Further direct recordings of blood pressure could be taken from a wider selection of subjects, but the subjects available for this purpose have cardiovascular defects and their waveforms would not necessarily represent an improvement on the data discussed in this chapter. Recordings of pressures closer to the cuff would be desirable, but this is clinically inconvenient as it requires further interference with the subject.

In order to check the generality of the results of the analyses, it was proposed that an arterial model be used to simulate an indirect blood pressure measurement. In such a model one has full control of all parameters, and the analogues of pressure and flow may be measured at different points in the system while other parameters (e.g. heart rate, and systolic and diastolic pressures) are held constant. It is also possible to make measurements and observations using a model that are impracticable in the course of clinical investigations.

A survey of previous work on cardiovascular modelling is given in the following chapter. The different approaches to the subject are discussed, with the result that an analogue electrical model is selected as being most appropriate for the generation of waveforms on which the analyses of this chapter may be duplicated.

4. ELECTRICAL ANALOGUE MODELLING OF THE VASCULAR SYSTEM

4.1 TYPES OF MODEL

4.1.1 Lumped and Distributed Models

4.1.2 Computer Models

4.1.3 Physical Models

4.2 TRANSMISSION LINE ANALOGUE OF AN ARTERIAL SEGMENT

4.2.1 The Telegraph Equations

4.2.2 The Simplified Equations of Fluid Flow

4.2.3 Performance of the Electrical Analogue

4.3 IMPROVEMENTS TO THE SIMPLE ANALOGUE

4.3.1 The Longitudinal Impedance

4.3.2 The Transverse Impedance

4.4 COMPREHENSIVE MODELLING OF THE ARTERIAL TREE

4.4.1 Anatomical and Physiological Data

4.4.2 Peripheral Resistance Models

4.4.3 Performance of Arterial Analogues

4.5 CONCLUSION

4. ELECTRICAL ANALOGUE MODELLING OF THE VASCULAR SYSTEM

In this chapter, the discussion principally relates to the modelling of the arteries. Several types of vascular model are described from which the electrical analogue form is selected as being the most convenient to simulate an indirect blood pressure measurement. An outline of the simple lumped-parameter transmission line analogue of a short segment of artery is given, followed by a discussion of refinements to the simple analogue and the performance of practical models. The chapter concludes with a discussion of the design features of a model of the vessels of the arm with the addition of switches to simulate the effects of a cuff.

4.1 TYPES OF MODEL

4.1.1 Lumped and Distributed Models

There are several approaches to modelling the circulation, each having certain advantages for specific applications. Broadly, they are classified into two distinct categories; lumped and distributed. In the lumped model the spatial distribution of response is ignored and only the bulk properties of the system are represented, as in studies of overall cardiovascular behaviour. In the distributed model consideration is given to propagation delays and other effects which occur along the length of the system. In the present study a distributed model is required to represent the changes in the pressure and flow waveforms as they travel peripherally.

In practice, a distributed model is approximated by

division into a series of lumped-parameter segments. The difference between distributed and lumped models therefore reduces to the fineness of the division, or in other words, the degree of lumping. Most distributed models of the vascular system are designed with lumped-parameter segments equivalent to a few centimetres of artery, and are implemented mathematically using computers, or physically using hydraulic or electrical analogues.

4.1.2 Computer Models

As will be shown in Section 4.2, with certain assumptions the equations of fluid motion in a short length of artery can be reduced to a pair of partial differential equations. Therefore a set of interconnected vascular segments can be represented by a corresponding set of equations which may be solved by analogue or digital computation. The nature of the analogue computer is that it solves these equations simultaneously thus making the computation time independent of the complexity of the problem. A digital computer can be programmed to solve the same equations (Kitney and Sheldrake, 1973), but because the calculation procedures are carried out in a step-by-step manner the computational effort increases rapidly with the number and complexity of the equations.

For a moderately complex situation, the analogue computer is satisfactory and has been used by Snyder et al. (1968) for the aorta (13 segments) and De Wit (1973) for the arm (4 segments). The factor restricting the use of analogue computers to relatively simple models is the limitation to the number of integrators available.

For the simulation of an indirect blood pressure measurement the effects of a cuff need to be included in a model of the vessels of the arm. In an analogue computer model the cuff could be represented by a switch or relay between two modelled segments of the brachial artery, while in a digital computer model it could be simulated by a non-linear element. However, even assuming that suitable machines were available, considerable effort would be required to develop programs and computational techniques, and it is shown in the next section that there is a more convenient method of modelling.

4.1.3 Physical Models

Hydraulic models are sometimes used to study the arterial system, as they possess some features not found in the other types of analogue, e.g. the use of a fluid with properties similar to those of blood automatically includes effects due to viscosity, turbulence, and boundary layers. Other features however, are very difficult to implement and virtually prohibit the use of such models for extensive arterial systems. For instance, it is not easy to obtain the rubber tube equivalent of a vessel with a given radius, taper, wall thickness, and modulus of elasticity or a pump producing the correct physiological waveforms. Furthermore, it is very difficult to change parameters once the system has been constructed.

A hydraulic model of the brachial artery has been used by Sacks et al. (1963) to study the production of Korotkoff sounds, the cuff being simulated by a surrounding pressure chamber (Section 2.4.2). The scaling factors involved in

simulating physiological parameters resulted in a very large apparatus which contained 250 gallons of fluid. The size of an apparatus for a more extensive arterial simulation and the difficulties involved in obtaining representative physiological pressure waveforms make this form of analogue unattractive for the present study.

An alternative physical model is the electrical analogue of the hydraulic system. As it is composed solely of resistors, capacitors, and inductors this form of model can accommodate large numbers of segments in a relatively small space. Voltage and current (the analogues of pressure and flow) may be measured simultaneously at any node in the model. The choice of time scale is determined largely by the need for the components to have convenient values; such models typically operate at one thousand times real frequency. A disadvantage of this type of model is that it is a major task to change the vascular parameters once the model has been constructed.

The literature contains considerable information on electrical analogue modelling. Of particular value is the model of Noordergraaf (1956) which has been extended and modified by Jager et al. (1965), Westerhof et al. (1969), and Westerhof and Noordergraaf (1970b). This model (subsequently referred to as the Westerhof-Noordergraaf model) has 121 segments representing the 27 major systemic arteries, the segment length being about 5 cm, i.e. small with respect to the wavelength of the fundamental frequency (approximately 5 metres). A similar detailed model of the vascular system has been described by De Pater (1966).

The electrical analogue seems particularly suited to the

study of wave transmission problems in the arterial tree. The analogy is intuitive, simple in concept, and inexpensive to construct and operate. The effects of a cuff can be represented crudely by semiconductor switches, one in series with the brachial artery, the other in the venous return.

On consideration of the characteristics of the various types of model, it was decided to proceed with the electrical analogue as being the simplest and most convenient for a simulation of an indirect blood pressure measurement.

4.2 TRANSMISSION LINE ANALOGUE OF AN ARTERIAL SEGMENT

4.2.1 The Telegraph Equations

The analogy between the transmission of a pressure pulse in an elastic tube and a voltage pulse along a telegraph cable has been recognized for many years (Noordergraaf, 1969). Both systems have distributed parameters and exhibit transmission delay, i.e. the input wave travels along the cable (or tube) with finite velocity.

Fig. 4-1 shows an incremental length Δz of a uniform 2-conductor transmission line. Over this short length, the distributed parameters of the line may be represented by series resistance $R\Delta z$ and inductance $L\Delta z$, and shunt conductance $G\Delta z$ and capacitance $C\Delta z$, where R, L, G, and C are the values per unit length. The resistance represents the wire resistivity and the conductance represents the leakage between the conductors. The inductance and capacitance relate to energy storage in the magnetic and electric fields associated with waves on the line. At any instant t in time, the voltage V and current I vary only

with the distance z along the line. Hence by applying Kirchhoff's voltage and current laws to the circuit of Fig. 4-1, Eq. 4.1 and 4.2 are obtained.

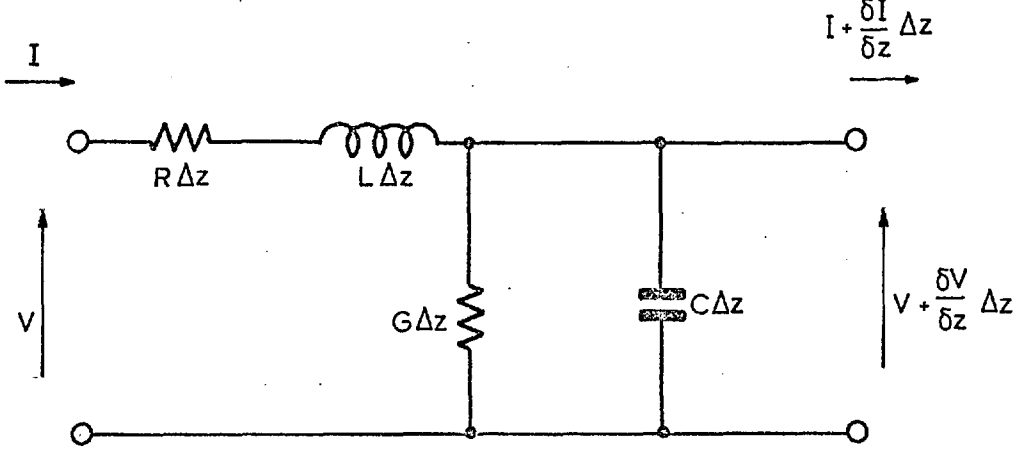


Fig.4-1: A short segment of a transmission line.

$$V - (V+\frac{\delta V}{\delta z}\Delta z) = R\Delta z I + L\Delta z\frac{\delta I}{\delta t} \qquad (4.1)$$

$$I - (I+\frac{\delta I}{\delta z}\Delta z) = G\Delta z V + C\Delta z\frac{\delta V}{\delta t} \qquad (4.2)$$

Dividing by Δz and simplifying, we obtain Eq. 4.3 and 4.4, commonly known as the telegraph equations (Skilling, 1952).

$$-\frac{\delta V}{\delta z} = R I + L\frac{\delta I}{\delta t} \qquad (4.3)$$

$$-\frac{\delta I}{\delta z} = G V + C\frac{\delta V}{\delta t} \qquad (4.4)$$

4.2.2 The Simplified Equations of Fluid Flow

The considerations leading to the development of the haemodynamic-electrical analogue may be outlined as follows (Noordergraaf, 1969). Firstly, a simpler equation of motion is derived from the Navier-Stokes equations by neglecting the non-linear terms and assuming that the tube has a constant circular cross-section and has walls that are homogeneous, isotropic, purely elastic, and constrained from moving longitudinally. Furthermore, it is assumed that for the inertial term the longitudinal velocity is not a function of radius, i.e. that the velocity profile is flat. On the other hand, it is assumed that for the viscous terms the longitudinal velocity profile is parabolic, i.e. Poiseuille-type flow. With these assumptions, the resulting equation of motion is given by Eq. 4.5.

A second equation is obtained by considering the arterial segment to be short and equating the difference between inflow and outflow with the sum of the flow absorbed by the radial expansion of the tube and the leakage flow lost through side branches. The resulting equation of continuity for the segment is given by Eq. 4.6.

$$-\frac{\delta P}{\delta z} = \frac{8\mu}{\pi r^4} I + \frac{\rho}{S} \frac{\delta I}{\delta t} \qquad (4.5)$$

$$-\frac{\delta I}{\delta z} = WP + \frac{dS}{dP} \frac{\delta P}{\delta t} \qquad (4.6)$$

where P = pressure; r = radius of artery

I = flow; ρ = density of blood

t = time; μ = viscosity of blood

z = axial coordinate; W = leakage through side branches

S = cross-sectional area of artery = πr^2

At this stage the simplified equations of fluid flow (Eq. 4.5 and 4.6) are compared with the telegraph equations (Eq. 4.3 and 4.4) and found to be of the same form. A short segment of artery can therefore be represented by the 4-element passive network of Fig. 4-1, the analogous quantities in the hydraulic and electrical systems being as follows.

Pressure	P	Voltage	V
Flow	I	Current	I
Resistance	$\frac{8\mu}{\pi r^4}$	Resistance	R
Leakage	W	Conductance	G
Inertance	$\frac{\rho}{S}$	Inductance	L
Compliance	$\frac{dS}{dP}$	Capacitance	C

Furthermore, the compliance $\frac{dS}{dP}$ may be expressed in terms of the geometric and elastic parameters of the vessel (Horeman and Noordergraaf, 1958). Since the arterial wall can be considered isovolumetric (Patel and Vaishnav, 1972), Poisson's ratio is 0.5 and the expression for the compliance reduces to Eq. 4.7.

$$\left[C = \right] \frac{dS}{dP} = \frac{3S(a+1)^2}{E(2a+1)} \qquad (4.7)$$

where $a = \frac{r}{h}$

h = wall thickness

E = Young's modulus for the wall

Hence given the segment length Δz, the numerical values of the four elements of the electrical analogue (Fig. 4-1) can be calculated from anatomical data r and h, and physiological data E, ρ, μ, and G (the leakage into side branches). A model of an artery is constructed from several segments in series, thus permitting the introduction of a stepwise geometric taper whilst maintaining constant arterial radius within each segment. The degree of lumping (i.e. the choice of Δz) must be such that the segment length is short compared with the wavelength of the fundamental frequency (Noordergraaf, 1969).

4.2.3 Performance of the Electrical Analogue

Noordergraaf (1969) and Westerhof et al. (1969) have commented on the performance of models formed from the simple analogue of Fig. 4-1. With such models there is a realistic time delay and change in the contour of the pressure pulse as it travels distally, but the increase in the pulse pressure is greater than that observed in the living system. In addition, the input impedances of either a single artery or the entire arterial tree are more sensitive to changes in frequency than in reality and the pulse wave velocity is too small in the more

peripheral vessels.

Several possible explanations have been suggested for these discrepancies: the contradictory flow profile assumptions in the derivation of the simplified equations of fluid flow; too much lumping, i.e. the segment length too long; inappropriate values of anatomical and physiological parameters; and too much linearization. A considerable amount of work has been carried out to evaluate the effect of these assumptions with the result that certain corrections may be applied, as described in the next section. However, the simple analogue of Fig. 4-1 has formed the basis for most, if not all, of the more detailed electrical analogues.

4.3 IMPROVEMENTS TO THE SIMPLE ANALOGUE

4.3.1 The Longitudinal Impedance

The network of Fig. 4-1 is the simplest representation of an arterial segment which exhibits transmission line properties. However, in the derivation of the analogy, contradictory flow profiles have been assumed in simplifying the equation of motion, namely a flat velocity profile for the inertial term and a parabolic velocity profile for the viscous term. These assumptions were made so that the inductive and resistive elements in the longitudinal impedance are independent of frequency. In effect, the viscous and inertial forces are assumed to be superposed without interaction. However, Womersley (1957) has shown that for a sinusoidal pressure gradient the velocity profile is neither flat nor parabolic, but is described by a time-varying expression containing Bessel functions. The true shape of the

velocity profile resembles a mixture of both flat and parabolic profiles, and depends on the vessel radius and the frequency of the pressure gradient. Hence blood flow profiles are even more complex in shape because the arterial pressure gradient comprises several frequencies as well as a steady component.

It has been shown by Jager et al. (1965) that the simple network of Fig. 4-1 may be modified to include the interaction of viscous and inertial forces by replacing the longitudinal impedance by resistive and inductive elements whose values are functions of frequency. Furthermore, it is shown that the correct frequency-dependent characteristics can be obtained with the simple passive network of Fig. 4-2 (excluding R_o), the component values being specified by Eq. 4.8.

$$L_m = \frac{\rho}{S}\,\frac{1}{2m-1},\quad R_m = \frac{8\mu}{\pi r^4}\quad m \qquad (4.8)$$

$$m = 1,2,3\ldots$$

By putting m=1 in Eq. 4.8, it is seen that L_1 and R_1 in Fig. 4-3 are the same as L and R defined in Section 4.2.2 for the simple analogue of Fig. 4-1.

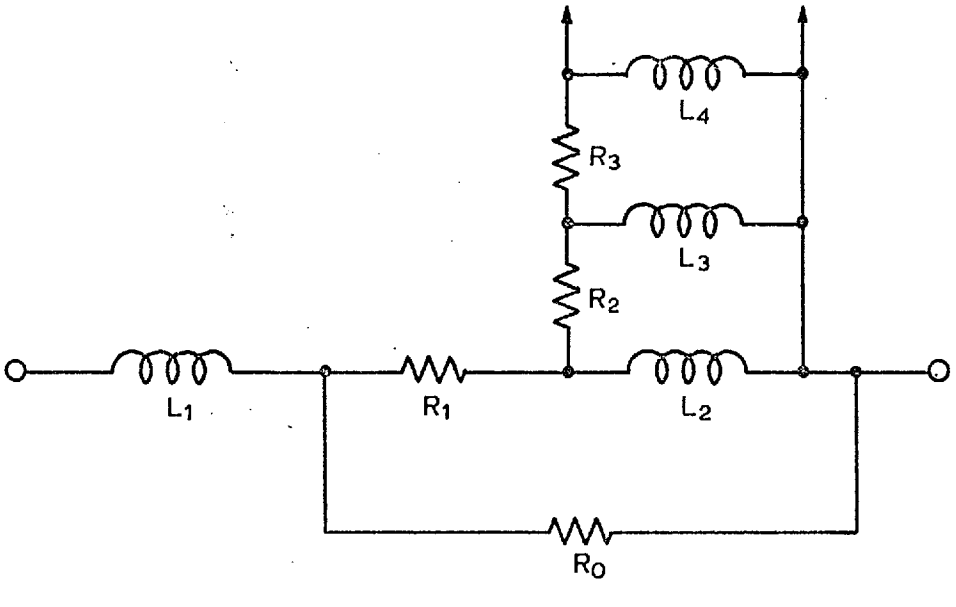


Fig. 4-2: Improved longitudinal impedance.

Therefore components with $m \geq 2$ may be considered to form a correction network accounting for true velocity profiles. The number of elements required in the correction network depends on the vessel radius and the maximum error permissible at the highest frequency to be transmitted. For the major human arteries, m typically varies between 3 and 5 (Westerhof et al., 1969).

Another effect unaccounted for in the simple analogue of Fig. 4-1 is that due to the anomalous viscosity of blood. Blood is a suspension of corpuscles in plasma and consequently there is a non-linear relationship between the applied pressure gradient and the rate of flow. It is therefore incorrect to assume that blood is a Newtonian fluid, except in large vessels where flow rates are high (Attinger, 1968). No attempts have yet been made to include non-Newtonian behaviour into a model, although it may be necessary to do so when the small vessels are studied in greater detail (Noordergraaf, 1969). However, there is a related effect which has been studied by Jager et al. (1965). This is the tendency for red cells to congregate along the axis in small arteries giving a relatively cell-free layer at the vascular wall, the viscosity of which is significantly less than that of the main stream. It is shown that this effect can be represented by the addition of an extra resistance R_o in the longitudinal impedance, as in Fig. 4-2. However, lack of information as to the size and viscosity of the boundary layer has prevented this correction from being implemented up to the present (Noordergraaf, 1969). It is fortunate that arteries to be modelled are sufficiently large for the effects of anomalous viscosity to be

negligible (Westerhof et al., 1969). Taylor (1959) has reported that the effect becomes important for arteries with diameters less than about 0.5 mm.

4.3.2 The Transverse Impedance

In the design of the simple analogue (Section 4.2.2) it has been assumed that the arterial wall is purely elastic, contrary to experimental evidence (Bergel, 1961a,b). The modelling of the viscous properties of the arterial wall is discussed by Westerhof and Noordergraaf (1970b), who show that a 5-element network (Fig. 4-3) in place of the single capacitor of the simple analogue (Fig. 4-1) simulates all known aspects of arterial viscoelasticity, namely the frequency variation of Young's modulus, stress relaxation, hysteresis, and creep. As the value of C_1 is given by Eq. 4.7 as previously, the network formed by C_2, R_2, C_3, and R_3 may be

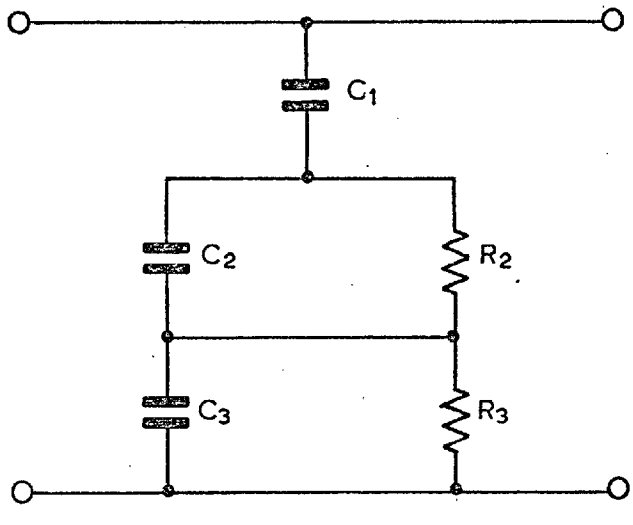


Fig. 4-3: Improved transverse impedance.

considered as a correction network accounting for the losses imposed on the propagating arterial wave by the viscous damping of the wall. From experimental measurements, the component values for arteries other than the aorta are given by the following equations (Westerhof and Noordergraaf, 1970b).

$$C_2 = 2.1\ C_1 \qquad C_2R_2 = 170 \text{ ms}$$
$$C_3 = 1.6\ C_1 \qquad C_3R_3 = 14 \text{ ms} \qquad (4.9)$$

Another improvement affecting the transverse impedance is to change the configuration of the network from the inverted-L type to the symmetrical (Pi) type. This is done by placing half of the computed transverse impedance at each end of the longitudinal impedance. The effect is to reduce errors at branch points (De Pater, 1966) and errors introduced by lumping, especially at higher frequencies (Westerhof et al., 1969). Although the overall improvement in an extensive model is small, the effect is essentially similar to an increase in the number of segments (i.e. less lumping) and the arterial geometric tapering is more realistically simulated (Noordergraaf, 1969).

4.4 COMPREHENSIVE MODELLING OF THE ARTERIAL TREE

4.4.1 Anatomical and Physiological Data

The determination of parameter values is a problem encountered by all investigators. Because the spread of values is quite large, anatomists tend to provide qualitative descriptions only and consequently quantitative data on the human arterial system is difficult to find. The anatomical tables provided by Westerhof et al. (1969) appear to be the most

extensive currently available.

The internal radii of arteries need to be estimated with special care. As Poiseuille's equation (Eq. 2.7) shows, small errors in radius can produce large changes in calculated flow rates, since the resistance of an arterial segment is inversely proportional to the fourth power of the radius. The radii of the larger vessels are of great importance in arriving at a model which accurately represents the real situation (Westerhof et al., 1969). One problem contributing to measurement difficulties is that, although the physiological properties of the wall remain fairly stable, considerable changes in dimensions take place when an artery is excised (McDonald, 1960).

In the Westerhof-Noordergraaf model, peripheral arteries are given a Young's modulus four times as great as that of the aorta, and intermediate arteries double. This was done because there is experimental evidence that the Young's modulus of the arterial wall increases with the distance from the heart, a feature referred to as "elastic taper". Also, in this model the conductances representing leakage through small branches are omitted from most arterial sections. It was necessary to include this component only for certain aortic segments where there is significant outflow into the coronary and intercostal arteries. Because interest is centred primarily on the pulsatile nature of the circulatory system, no account is taken of the influence of gravity on the mean pressure level. The model may therefore be considered as representing a supine subject.

4.4.2 Peripheral Resistance Models

The smallest arteries separately modelled in the

Westerhof-Noordergraaf model have radii of about 1.3 mm. All vessels smaller than this figure are lumped together with the peripheral resistance into a single resistor terminating the final sections of the branches of the arterial tree. The value of this terminal load is calculated by dividing the mean pressure at the periphery by the mean flow for each region.

A more detailed approach is taken by De Pater (1966). In his model each peripheral circulation is formed by 7 transmission-line type segments representing the main branches, secondary branches, terminal arteries and arterioles, capillaries, venules and terminal veins, secondary veins, and main veins. The values of the components of these segments are quoted in terms of "muscle-units" and "skin-units", both units having defined values of series inductance and resistance, and shunt conductance and capacitance. The segments representing the arterioles, capillaries, and venules do not have inductors because the longitudinal impedance is dominated by the resistance.

Raines et al. (1971) discuss the problem of mis-match between the termination and the line in the digital modelling of the arteries of the leg. Since the length of the arterial model is a significant fraction of the wavelength of the pressure pulse, undamped wave reflections of the higher harmonics would manifest themselves as superimposed undulations on the pressure pulse. As such undulations are not observed physiologically, it is argued that a practical scheme must be developed for arterial models in which reflected waves are avoided or highly damped. In their view it is essential that at least some distensibility of the small vessels be included in the peripheral

termination. This can be done by dividing the peripheral resistance into two parts and placing a lumped compliance (capacitance) in parallel with the more distal part. The value of the compliance is chosen to give a realistic reflection coefficient for the fundamental frequency. In this manner, the higher harmonics are damped to an even greater degree than the fundamental.

4.4.3 Performance of Arterial Analogues

The performance of any analogue is judged by comparison with the behaviour of the living system under similar conditions. For cardiovascular analogues the features compared include input impedance, pulse wave velocity, and wave shapes occurring at specific sites. In the living system these measurements may be made only at the heart rate fundamental frequency and the harmonics thereof, whereas in the analogue model, frequency can be a continuously variable parameter.

As discussed in Section 4.2.3, the response of the simple analogue (Fig. 4-1) is distinctly different from that of the living system in several ways. The input impedance parameter has been used for a great number of comparisons, and this was found to be more strongly frequency-dependent in the model than in the living system, particularly above 2 Hz. However, the simple analogue has been successively modified by (i) including the velocity profile correction network, (ii) changing the segment configuration from an inverted-L network to a symmetrical (Pi) network, (iii) modifying the Young's moduli to account for the elastic tapering effect, (iv) revising the arterial radii,

and (v) adding the correction network for arterial wall viscoelasticity. With each modification the frequency characteristics of the magnitude and phase of the input impedance became progressively smoother and closer to measurements of the living system, but no single modification produced a major difference (Westerhof et al., 1969). However, the introduction of wall damping (viscoelasticity correction network) was found to shift the maxima and minima of the impedance to slightly higher frequencies whereas the fluid damping (velocity profile correction network) left the maxima and minima at essentially the same frequencies (Westerhof and Noordergraaf, 1970b).

Westerhof and Noordergraaf conclude that the degree of lumping in their model is acceptable and that the model is valid for frequencies up to 15 Hz. As in the living system, the pulse pressure increases in magnitude as the pulse travels peripherally, with a corresponding decrease in the amplitude of the flow waveform. This is primarily due to closed-end type reflections of the lower harmonics at the periphery (length of system shorter than wavelength).

The Westerhof-Noordergraaf model has been used to simulate old age hypertension (i.e. high blood pressure caused by a general decrease of arterial distensibility) and essential hypertension (i.e. high blood pressure caused by an increase of the peripheral resistance). This model has also proved useful for demonstrating the presence of significant errors in the measurement of hydraulic input impedance when pressure and flow are not measured at the same site (Westerhof and Noordergraaf, 1970a).

4.5 CONCLUSION

The electrical analogue form of modelling has been used successfully in the past to demonstrate many features of the arterial system. It is a physical model representing the distributed living system by a series of lumped-parameter segments, each designed using authentic estimates of vascular parameters. Since the model resembles a transmission line, it is particularly suited for the study of wave propagation. Most interest in electrical analogues concerns the entire vascular system and the conditions existing in the major arteries, notably the aorta. However, Westerhof et al. (1969) have compared the input impedance of the leg with measurements obtained in the living system, finding good agreement. Although similar studies for the arm were not described, there is no evidence to suggest that the behaviour of the modelled arm is inferior to that of the leg. The literature contains no references describing attempts to include the effects of a cuff in an electrical analogue.

The vasculature of the left arm begins at the junction of the aortic arch and the subclavian artery, and continues peripherally via the axillary, brachial, ulnar, and radial arteries (Johnston and Whillis, 1947). An electrical analogue of these vessels based on the geometry, lumping, and physiological data of the Westerhof-Noordergraaf model would comprise 19 segments. The action of the cuff can be included in this model by the addition of two switches, one situated between two segments of the brachial artery, and the other in the venous portion of the peripheral circulation. The state of each switch is determined by a circuit comparing the waveform representing

the cuff pressure to the waveform immediately proximal to the switch. Vessel occlusion is therefore simulated by an open switch whenever the cuff waveform is greater than the magnitude of the proximal waveform.

The recordings discussed in Chapter 3 have shown that large changes are produced in the distal waveforms during total or partial occlusion of the brachial artery. It was therefore anticipated that the simulation of a cuff would dominate the waveforms of the model and swamp the effects of the refinements discussed in Section 4.3. Noordergraaf (1969), commenting on the inclusion of the velocity profile correction network, states that "On the whole, the difference has proved not to be large, and so the contradictory assumptions originally made concerning velocity profiles had no devastating effect." However, Westerhof et al. (1969) indicate that measurements relating to different parts of the system, e.g. a leg or an arm, show more sensitivity to the improvements (especially to elastic tapering) than the entire system. For these reasons it was proposed initially to use the simple model of Fig. 4-1 and omit the correction networks of Figs. 4-2 and 4-3 until more precise quantitative results were required. Since no increase in the total number of components was involved, the elastic taper and symmetrical (Pi) refinements were retained.

With respect to the peripheral resistance, it is necessary to model the venous compliances if the action of the cuff in occluding the veins is to be simulated meaningfully. Similarly, small artery and arteriole compliances are necessary to model the damping of the pressure pulse as it passes through

the periphery. In effect this is the approach adopted by Raines (1972), except that some component values are calculated from physiological data and others estimated on the basis of realistic damping. In view of the decision to use the simple analogue, it was thought that the complexity of De Pater's (1966) model of the peripheral vasculature was not warranted.

The construction of an electrical analogue model of the arm is described in Appendix A. The design of the peripheral terminations and the inclusion of switches for the simulation of a cuff during an indirect blood pressure measurement are described in Chapter 5.

5. SIMULATION OF AN INDIRECT BLOOD PRESSURE MEASUREMENT

5.1 THE MODEL OF THE ARM

5.1.1 The Arterial Segments

5.1.2 Performance of the Model

5.2 THE PERIPHERAL TERMINATIONS

5.2.1 Subdivision of the Peripheral Resistance

5.2.2 Estimation of the Venous Compliance

5.2.3 The Damping Capacitors

5.2.4 Performance of the Improved Model

5.3 THE CUFF

5.3.1 Modelling Concepts and Assumptions

5.3.2 The Venous Switch

5.3.3 The Arterial Switch

5.3.4 Instability of Switching

5.4 SIMULATION OF INDIRECT BLOOD PRESSURE MEASUREMENTS

5.4.1 Practical Operation of the Model

5.4.2 Analogue Waveforms

5.4.3 Time Measurements

5.4.4 Frequency Analyses

5.4.5 Variable Interbeat Intervals

5.5 SUMMARY

5. SIMULATION OF AN INDIRECT BLOOD PRESSURE MEASUREMENT

This chapter describes the model used to simulate the conditions which occur in the vascular system of the upper arm during an indirect blood pressure measurement. The model consists of a number of passive networks representing the arterial segments and the peripheral resistances of the arm with additional circuits to simulate the effects of an inflatable cuff. Initially the peripheral vessels are modelled by resistors, but damping capacitors are found to be necessary in order to obtain more realistic behaviour. The input impedance and transmission characteristics of the model with the improved peripheral terminations are shown to be similar to measurements in a model of the leg.

The cuff is simulated by two semiconductor switches, one in the brachial artery, the other in the venous return path. This simulation of vascular occlusion is shown to produce arterial instability at the instants representing the opening or closing of the vessels and offers an explanation for inflections seen in practical waveforms. Typical waveforms recorded during the simulation of an indirect blood pressure measurement are shown, and the results of analyses are compared with those obtained from the practical waveforms discussed in Chapter 3. It is found that although there are differences between the shapes of the phase difference plots, the plots of the first harmonic amplitude ratios are similar to those obtained previously and may be used to locate the cuff diastolic point with reasonable accuracy.

5.1 THE MODEL OF THE ARM

5.1.1 The Arterial Segments

The major arteries supplying the left arm may be described as follows (Hamilton, 1956). The left subclavian artery has its source at the summit of the aortic arch from where it curves upwards and outwards, giving off some branches at the root of the neck, the largest of which is the vertebral artery to the head. The subclavian artery continues as the major arterial supply to the upper limb, being named the axillary artery in the region of the shoulder and the brachial artery in the upper arm. Immediately below the elbow, the brachial artery divides into the radial and ulnar arteries: a short distance beyond this junction (approximately 2 cm), the interosseous artery branches off from the ulnar artery. These arteries terminate in the network of smaller vessels and anastomoses of the hand. The connections of the arteries are shown in Fig. 5-1.

Using the anatomical data of Westerhof et al. (1969), an electrical analogue model of the arteries of the arm was designed and constructed. The model consists of nineteen segments and four peripheral terminations. Each segment is modelled by a network of three components whose values were computed using the equations of the simple transmission line analogy. The model is designed to operate at one thousand times real frequency so that the values of the reactive components fall in convenient ranges. Further details of the practical design and construction of the model are given in Appendix A together with a complete circuit diagram and tables of component values.

The normal input to the model was a voltage waveform representing the aortic arch blood pressure. Such a waveform

was obtained by isolating a single beat from a digitized record of a practical blood pressure recording, and performing digital to analogue conversion at the appropriate frequency using the IBM 1800 computer. In effect, the computer was used as a waveform synthesizer generating the desired signal continuously at a rate determined by external synchronization. This method of obtaining an input signal for the model allowed prior manipulation of the waveform, e.g. digital filtering to remove unwanted higher harmonics. The waveform thus generated was recorded on a tape loop so that a continuous signal was available for operating the model off-line. Most of the studies of the performance of the model used input waveforms generated in this manner; however, for input impedance and transmission measurements the input was connected to a variable frequency sine wave oscillator. Amplitude and phase angle measurements were then made directly from the oscilloscope screen.

5.1.2 Performance of the Model

No measurements of the haemodynamic characteristics of either the living arm or its model could be found in the literature. Hence, in order to assess the present model its input impedance was compared with that of the Westerhof-Noordergraaf model of the leg (Fig. 5-2). To make the comparison more valid, the peripheral vessels were represented by resistors as in the Westerhof-Noordergraaf model.

The frequency characteristics of the input impedance of the model of the arm are shown in Fig. 5-3. The variations of modulus and phase angle are considerably greater for the arm than for the model of the leg, although the general shapes of

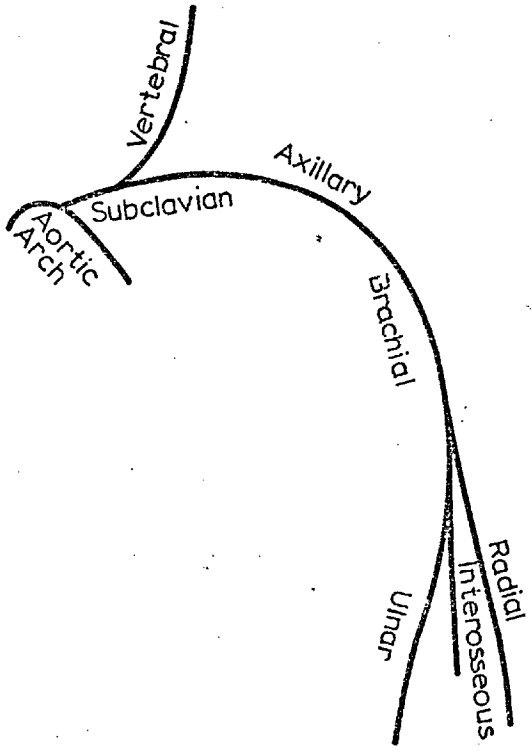


Fig. 5-1 : The arteries of the upper limb.

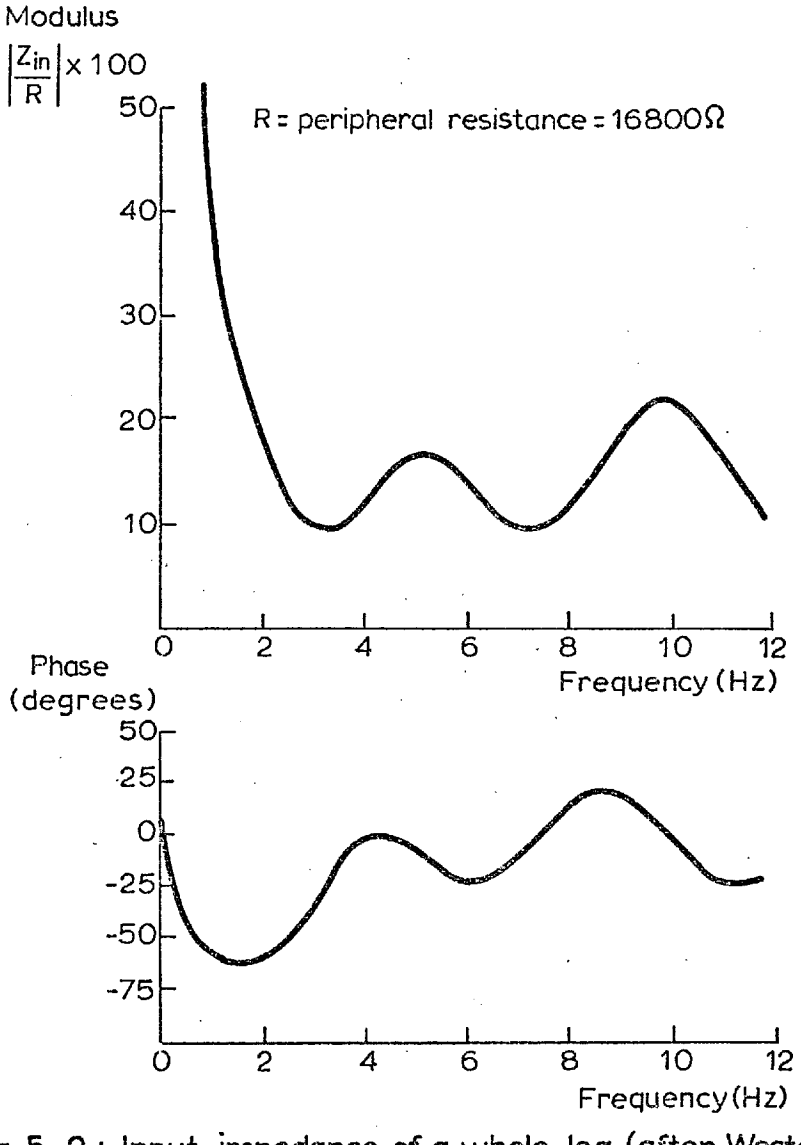


Fig. 5-2 : Input impedance of a whole leg (after Westerhof et al., 1969).

the curves are similar with maxima and minima occurring at corresponding frequencies. The variations with frequency were found to continue to 30 Hz (30 KHz in the model) at which point the input impedance rose asymptotically to infinity. Similar variations with frequency were observed in the transmission characteristics. Fig. 5-4 shows the frequency variation of the modulus and phase angle of the transfer function from the input at the subclavian artery to the radial peripheral resistance. The responses at the other peripheral resistances were found to be similar.

The amplitude response shows the presence of several resonances, three of which lie within the frequency spectrum of blood pressure waveforms, namely at 3.5, 8, and 12 Hz. The moduli at these frequencies (approximately 8) caused peripheral waveforms to differ considerably from the expected physiological waveforms if the input wave had significant components near the resonance points. It was found that acceptable peripheral waveforms could not be produced unless the input blood pressure waveform was filtered to contain the fundamental and second harmonic frequencies only. Even if this was done, attempts to include the operation of a cuff (modelled as a switch in the brachial arterial line in the manner described in Section 5.3) gave rise to uncontrollable oscillations throughout the model.

It was thought that this unsatisfactory situation was related to reflections in the arterial line. Noordergraaf (private communication, 1973) confirmed that reflection from the terminations plays a dominant role in the formation of waveshapes, and that the inclusion of correction networks and other refinements in the segments reduced the reflections. However,

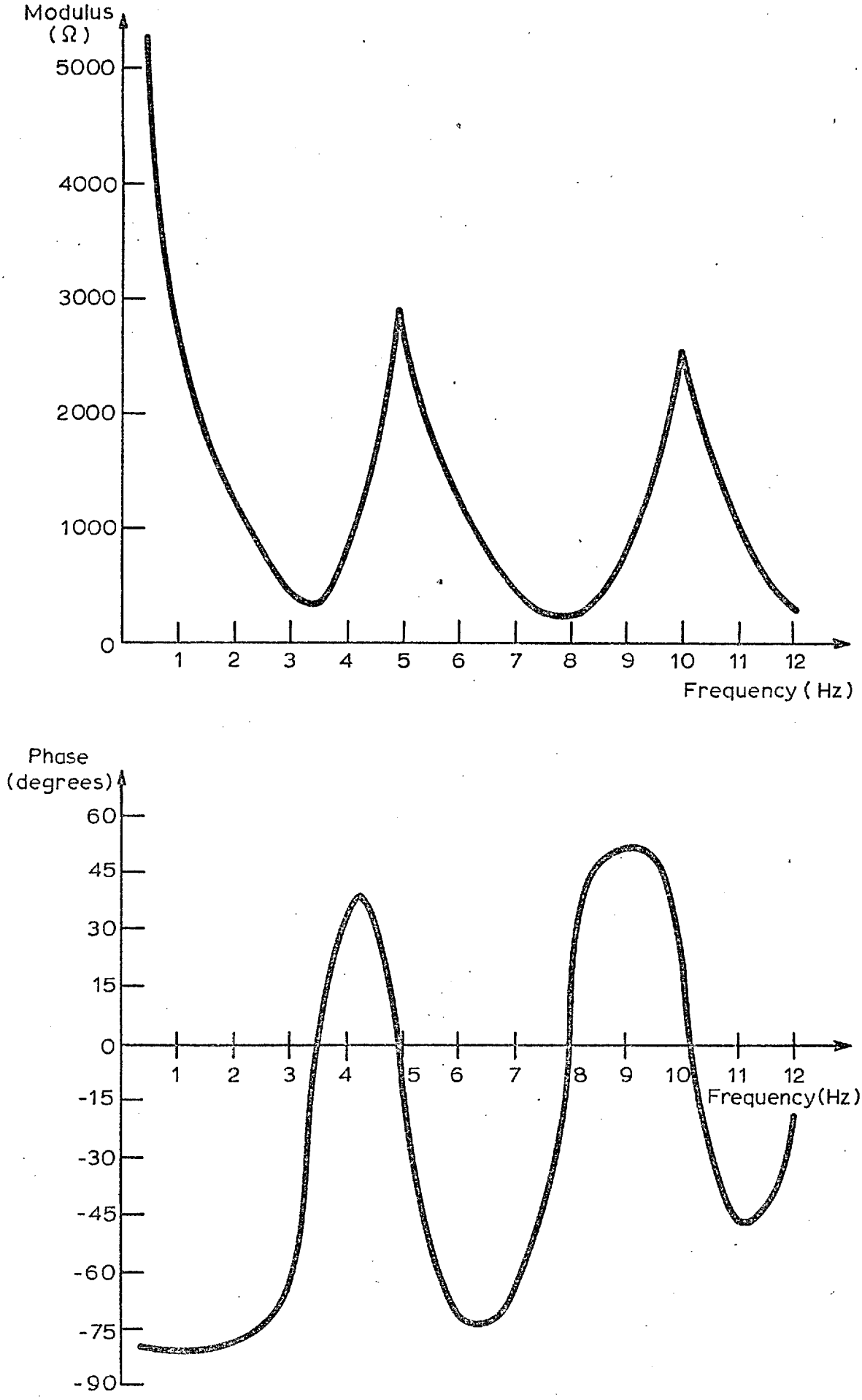


Fig. 5-3: Input impedance of the model of the arm with resistive peripheral terminations.

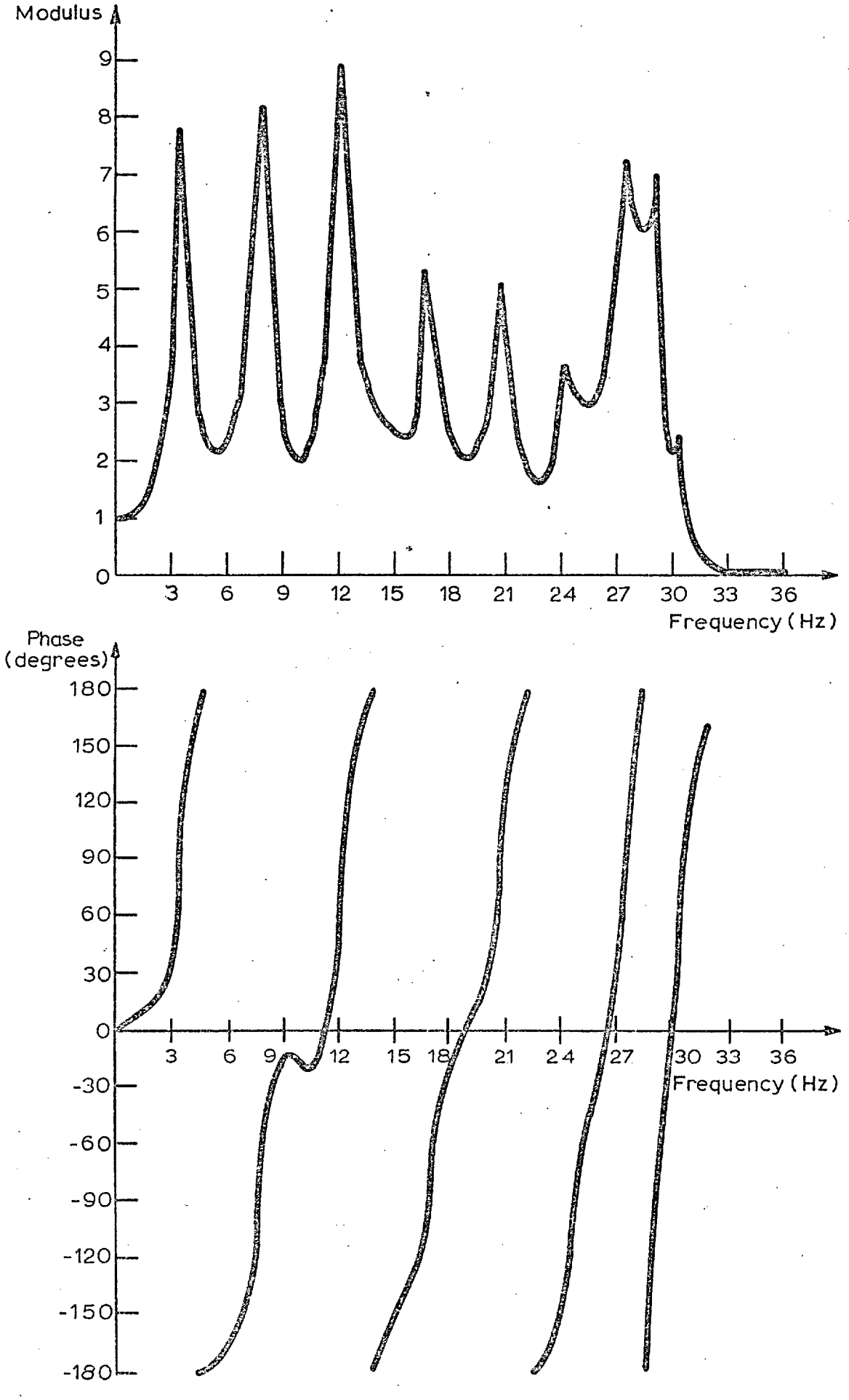


Fig. 5-4: Transfer function of the model of the arm with resistive peripheral terminations.

the reflections were still greater than expected and it was concluded that the peripheral vessels required a more detailed representation than a single resistor.

5.2 THE PERIPHERAL TERMINATIONS

5.2.1 Subdivision of the Peripheral Resistance

As discussed in Section 4.4.2, the peripheral resistance represents the combined effect of all vessels too small to be modelled by separate R-L-C segments. If a single resistor is used to model the entire peripheral circulation of an artery, no account is taken of the damping of the pressure wave known to occur in the vessels joining the small arteries and the small veins. As with transmission lines, reflections occur at the periphery because the terminations do not match the characteristic impedances of the arteries. The question of partial reflection and damping of the pressure wave at the periphery is discussed by McDonald (1960) and Guyton (1966). Although quantitative details are expressed in round figures, sufficient description is given to enable the peripheral circulation to be subdivided into sections suitable for individual modelling. It must be remembered that the peripheral resistance is subjected to several physiological influences and any model which attempts to represent it in detail must be regarded as being approximate.

The resistive components of the peripheral circulation may be estimated by dividing the mean fall in pressure in each of the different classes of vessels by the mean flow. Since the mean flow is not altered, it is only necessary to estimate the pressure differences and divide the peripheral resistor into parts in the same ratios. The pressure drops in the constituents of the

peripheral circulation are approximately 12 mm Hg in the small arteries, 55 mm Hg in the arterioles, 20 mm Hg in the capillaries, and 10 mm Hg in the veins (Guyton, 1966). Accordingly, each terminating resistor of the model was replaced by four resistors in series having the same total resistance but with individual ratios of 12:55:20:10 to represent the overall resistance to flow of the small arteries, arterioles, capillaries, and veins respectively.

5.2.2 Estimation of the Venous Compliance

To model the storage properties of the venous system distal to the cuff, a capacitor representing the venous compliance was added to each peripheral circuit. The value of the venous compliance was estimated in the following manner: referring to Eq. 4.7, the compliance per unit length is given by the slope $\frac{dS}{dP}$ where S is the cross-sectional area of the vessel and P is the transmural pressure. Approximating this slope by a finite-difference gradient, the value of a lumped compliance is therefore given by the increase in cross-sectional area divided by the corresponding increase in pressure and multiplied by the total length, i.e. the ratio of the change in volume to the change in pressure. These data were obtained from an experiment described by Guyton (1966) in which the blood flow through the forearm is estimated using a plethysmograph. In this experiment the forearm is placed in the chamber of the plethysmograph and an airtight seal is made near the elbow. A cuff at this site is suddenly inflated to 40 mm Hg so that the veins are occluded but blood continues to flow through the arteries. As a result, the volume of the forearm increases and the air displaced from the

chamber is recorded by the plethysmograph. After a few seconds the blood vessels of the forearm become distended and exert a considerable amount of back pressure which opposes further inflow. From the plethysmographic record shown, it appears that an air volume of 30 cm^3 would be displaced if the venous pressure was allowed to rise from its normal value (10 mm Hg) to the pressure of the cuff (40 mm Hg), i.e. an increase of 30 mm Hg.

Therefore total forearm venous compliance $= \frac{30\ cm^3}{30\ mm\ Hg}$

$= \frac{30\ cm^3}{30 \times 1333\ dyne/cm^2}$

$= 0.75 \times 10^{-3}\ g^{-1} cm^4 sec^2$

However, in the present study the estimate of venous compliance needs to relate to the arm distal to the normal position of the blood pressure cuff and not just to the forearm. It therefore seems reasonable to increase the forearm compliance by 20% to obtain a total distal venous compliance of $0.9 \times 10^{-3}\ g^{-1} cm^4 sec^2$.

As described in Appendix A, a capacitor was added to each of the three peripheral circuits distal to the cuff at the junction of the resistors representing the capillary and venous systems. The sum of the three capacitors was equal to the scaled value of the total compliance; this value was apportioned to each peripheral circuit in the ratio of the peripheral flows, i.e. in the inverse ratio of the venous resistors. The venous capacitor in the vertebral peripheral circuit was made the same value as that of the ulnar since the flows in both arteries are equal.

Venous compliances estimated in the manner outlined above can be considered only as very approximate. Firstly, technical difficulties in the use of plethysmographs can cause measurement inaccuracies of 50% or more (Guyton, 1966). In addition, no account has been taken of storage of blood in the small arteries,

arterioles and capillaries, nor have non-linearities in the compliance been considered, such as a decrease in distensibility at high venous pressures. However, in the absence of specific data this is a reasonable approach to adopt. Subsequent results taken from the model showed that the arterial waveforms were in any case not sensitive to these components.

5.2.3 The Damping Capacitors

No quantitative information could be found for the compliances of the small arteries and arterioles apart from a figure given by Guyton (1966), reproduced in Fig. 5-5. From this figure it may be inferred that the fundamental of the pressure pulse (considered to have an amplitude of 100% as it leaves the large arteries) is reduced to 50% amplitude by the small arteries, to 98% by the arterioles, and to 100% by the capillaries. Consequently the peripheral circuit was modified to give such attenuations by adding two empirically-determined capacitors, one at the junction of the resistors representing the small arteries and the arterioles, and the other at the junction of the arterioles and the capillaries. The circuit of the modified peripheral resistance is shown in Fig. 5-6; the component values of the four peripheral terminations of the model are given in Appendix A.

5.2.4 Performance of the Improved Model

The effect of adding capacitors to the peripheral resistance is to present a complex termination to the arterial line, and consequently the amount of reflection occurring at the periphery depends on the frequency. This causes significant changes to the input impedance of the model, as shown by comparing

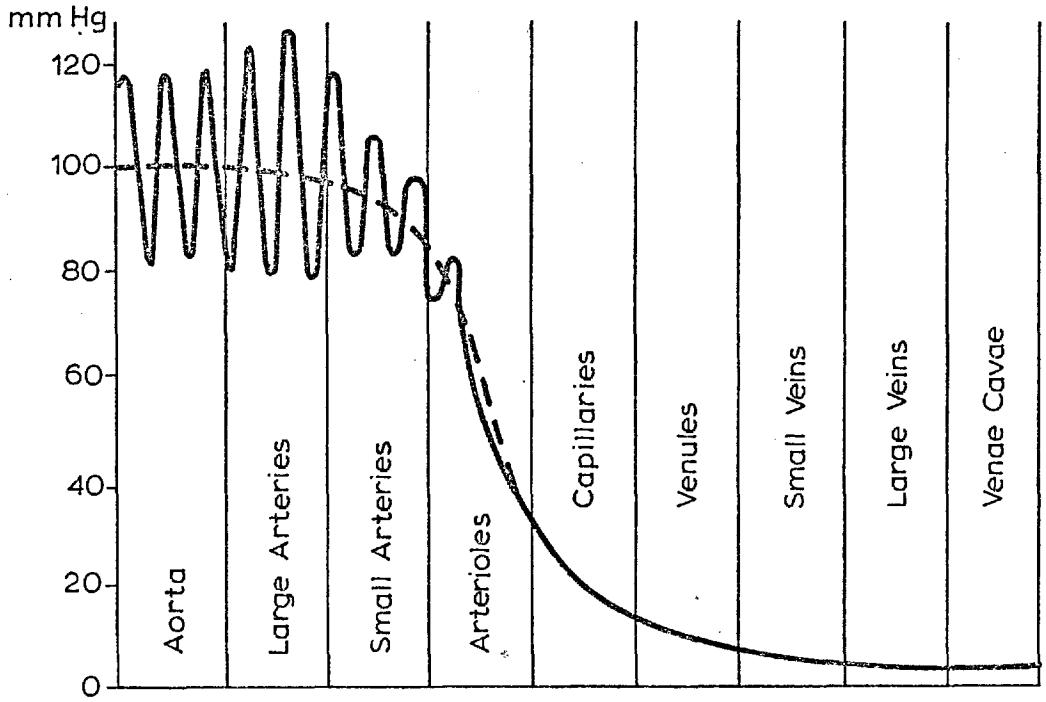


Fig. 5-5: Blood pressures in the systemic circulatory system (after Guyton, 1966).

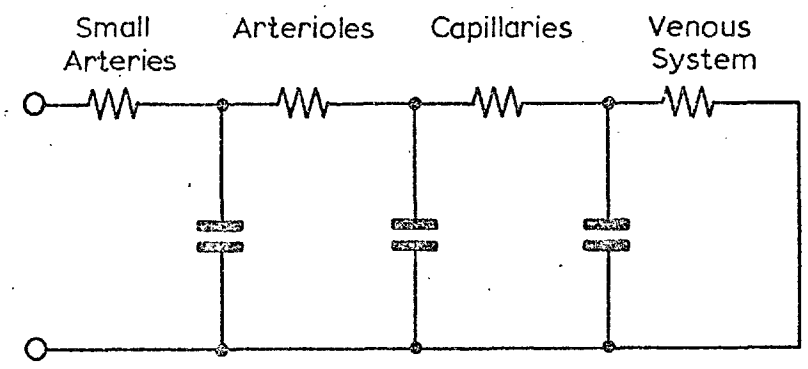
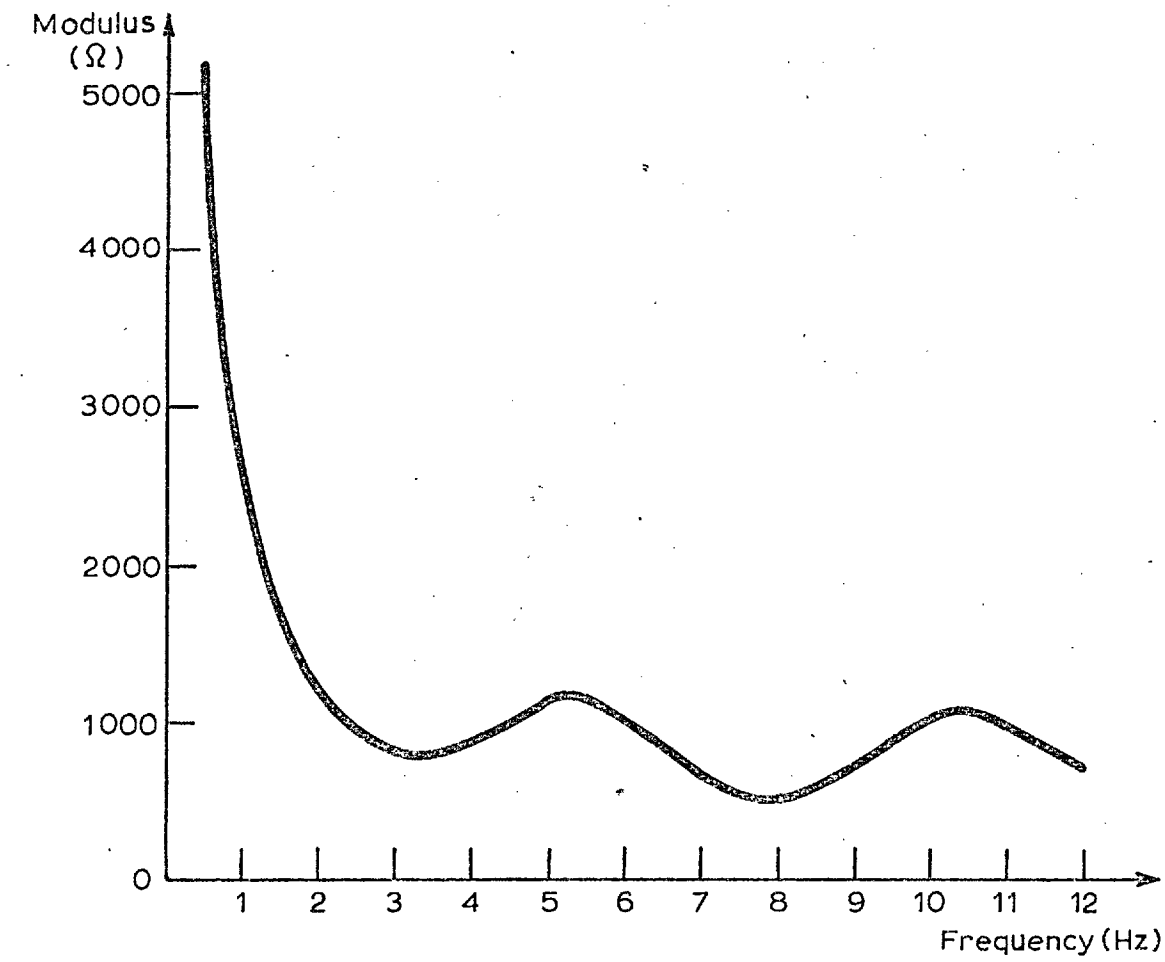


Fig. 5-6: The damped peripheral termination.

the amplitude and phase plots of Fig. 5-7 with the previous measurements of Fig. 5-3. Although resonances are still present at the same frequencies as before, the peak-to-peak variations in both amplitude and phase are greatly reduced and the shapes of the curves now closely resemble those of the model of the leg (Fig. 5-2).

The transmission characteristics of the model with the modified peripheral terminations are shown in Fig. 5-8. By comparing these plots with the previous measurements of Fig. 5-4 it is apparent that the moduli at the resonant frequencies have been reduced from approximately 8 to about 2.5. The phase characteristic for the case of the modified peripheral termination is remarkably linear throughout the passband, indicating that the arterial system is basically acting as a time delay network. When tested with practical input waveforms, the modified model did not exhibit the gross waveform abnormalities observed when the peripheral resistance was modelled by a single resistor provided frequencies above the fourth harmonic were filtered from the input waveform. Instead, the model response exhibited the augmentation of the pulse pressure that is known to occur at the periphery (McDonald, 1960) with the increase in systolic pressure being greater than the decrease in diastolic pressure. Using the aortic arch waveform of Chapter 3 (filtered to contain the fundamental, second, third, and fourth harmonic frequencies) as the input, the peripheral waveshapes closely resembled the waveforms recorded clinically in the radial artery.

The use of the more detailed model of the peripheral circulation was a great improvement, bringing the overall behaviour of the model much closer to reality. Moreover, the inclusion of



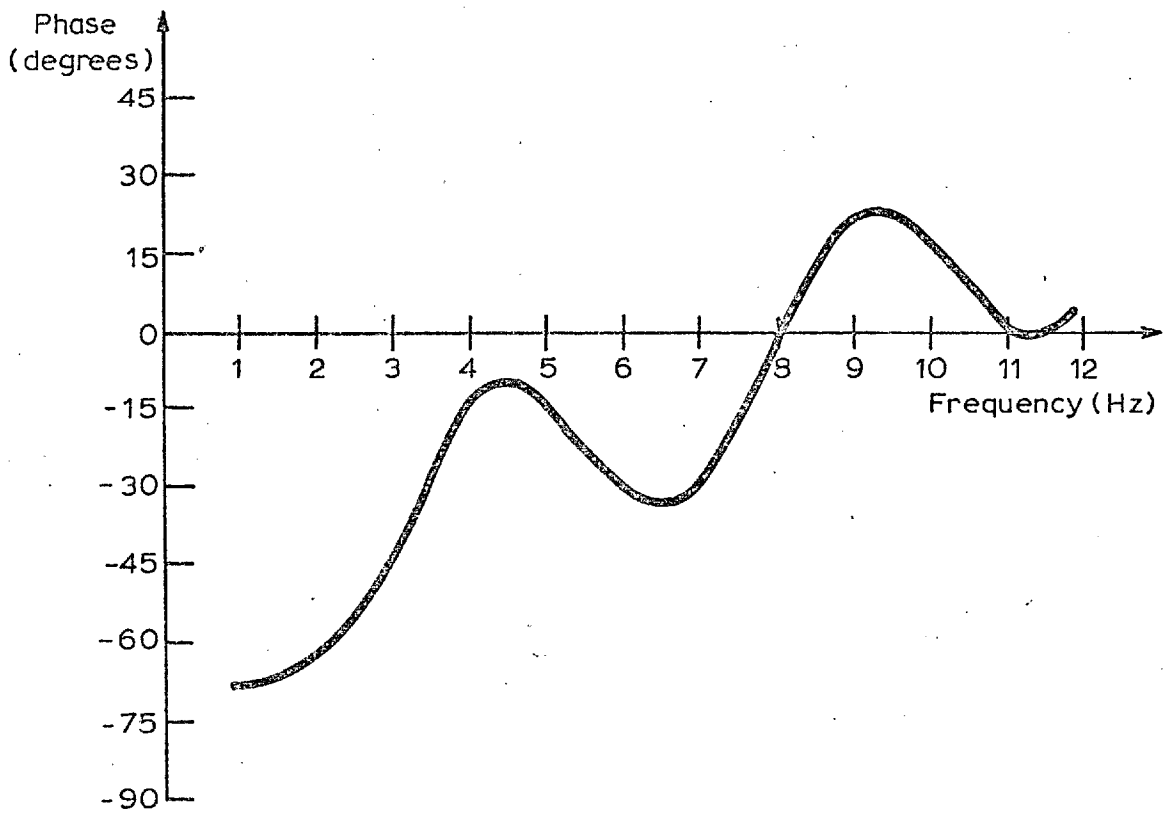


Fig. 5-7 : Input impedance of the model of the arm with complex peripheral terminations.

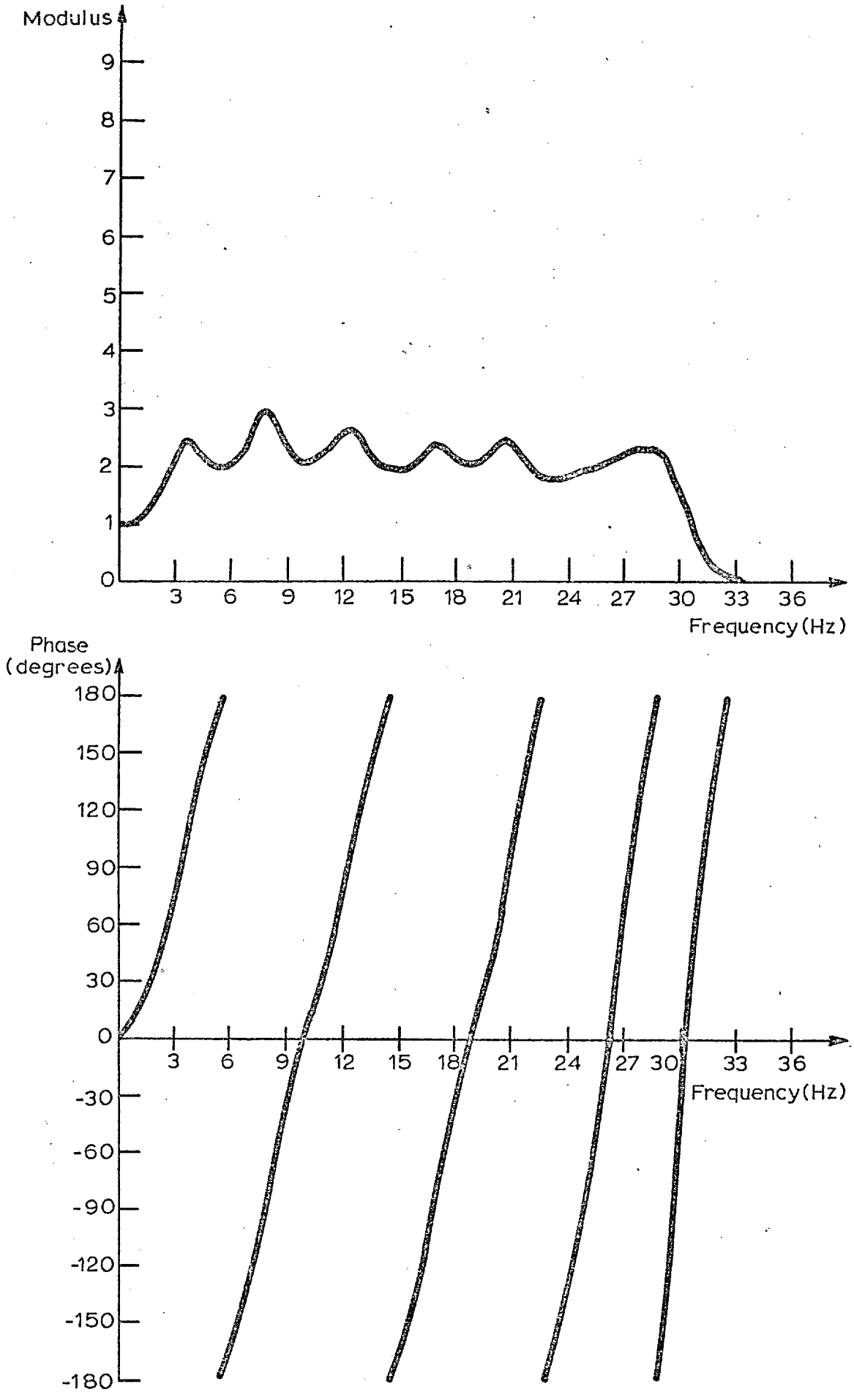


Fig. 5-8 : Transfer function of the model of the arm with complex peripheral terminations.

the operation of an arm cuff as a switch in the brachial arterial line now gave sensible results, although some difficulties were still encountered with switching transients as described in the following section.

5.3 THE CUFF

5.3.1 Modelling Concepts and Assumptions

The general concept of the action of a cuff is that underlying vessels are occluded whenever the blood pressure falls below the cuff pressure. Accordingly, a simulation of an indirect blood pressure measurement can be performed by inserting switches in the venous and arterial lines of the electrical analogue model of the arm, the instants of switching being determined by comparators monitoring the transmural pressure of the vessels. This representation of the influence of a cuff assumes that the following conditions apply:

(a) the cuff is a pressure source having zero impedance

(b) the cuff has negligible length

(c) the full cuff pressure is transmitted to the arterial wall by the intervening tissues, and is constant around the circumference

(d) the artery is completely open when blood pressure exceeds the cuff pressure and fully occluded when the cuff pressure is greater than the arterial pressure, the transitions between these states being instantaneous.

The following discussion relates to the foregoing assumptions.

(a) Small oscillations of the sphygmomanometer mercury column may be observed during the deflation period of an indirect blood

pressure measurement, indicating that the cuff is changing in volume as the blood pressure pulse passes beneath it. This implies that the cuff has a non-zero impedance of a compliant, or capacitive, nature. However, as the oscillations are only about 1 mm Hg in amplitude when the cuff pressure is approximately 100 mm Hg, this effect is negligible within the limits of accuracy being considered.

(b) The standard arm cuff is 13 cm wide and therefore covers a length of brachial artery equivalent to two segments in the analogue model. It is known that the ratio of the width of the cuff to the diameter of the arm influences the accuracy of the measurements (Karvonen et al., 1964; Simpson et al., 1965). This factor is ignored in the present model since the cuff pressure is assumed to act at a single cross-section. The most noticeable changes produced by the inclusion of a distributed switching action in the model would be expected to occur in the distal waveforms immediately following the cuff systolic point. This is because the time taken for the pulse to travel beneath the cuff is comparable to the time during which the artery is patent. As most interest in the present simulation concerns the cuff diastolic point (when the artery is patent for almost the entire cardiac cycle) it is reasonable to model occlusion at a specific location.

(c) The action of the cuff is to compress (and distort) the brachial artery which, at the site of the cuff, is midway between the skin and the humerus bone. The transfer of the cuff pressure through the tissues of the limb to the artery has been discussed by Vierhout (1963). As shown in Fig. 5-9, the pressure at the site of the artery is less than the cuff pressure, with the difference greater at the periphery than under the centre of the

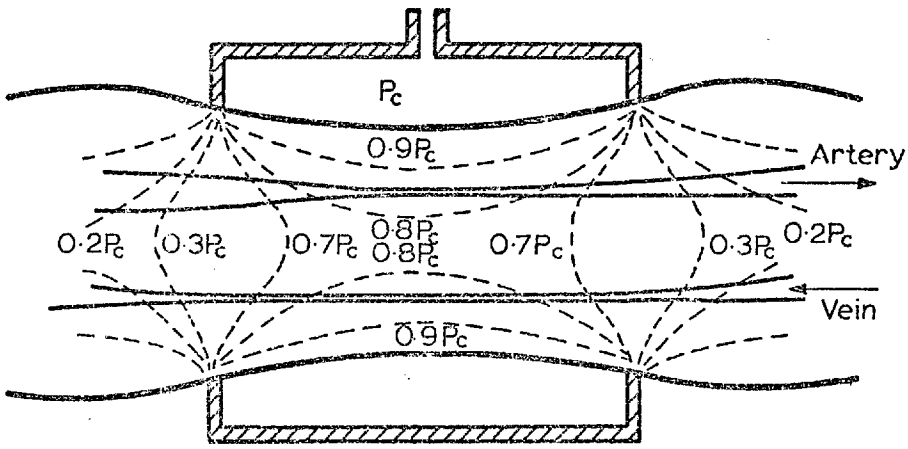


Fig. 5-9: Transfer of cuff pressure to the brachial artery (after Vierhout, 1963).

cuff. The assumption that the cuff pressure equals the pressure on the arterial wall is therefore in error by an amount dependent on the depth of the artery and the distribution of pressure in the limb. This error is normally accepted as inherent with cuff methods and no attempt is being made to elucidate the problem with the present model.

(d) Due to wall viscoelasticity, a finite time is required to change the vessels from their patent to their occluded condition. It is generally thought that the application of external pressure progressively changes the lumen from circular, to oval, to figure-of-eight, and finally to a flat cross-section in a manner similar to the behaviour of rubber tubes. However, McCutcheon and Rushmer (1967) have shown that a vessel tapers beneath a compression cuff (Section 2.4.2) and remains partially compressed until the cuff pressure is reduced below diastolic blood pressure. Furthermore, at cuff pressure levels slightly above systolic blood pressure the fluid column penetrates partway under the cuff with each systole. It therefore follows that the cuff acts in a gradual, rather than instantaneous, manner. However, for reasons similar to those given for (b), this effect would be more important near the cuff systolic point than the cuff diastolic point. Hence the assumption that the artery opens and closes instantaneously is justifiable for present purposes.

In the model, the switching functions were performed by junction field-effect transistors (FETs) having low "on" resistances (120 Ω) and near infinite "off" resistances. These gave effective isolation of the control voltage from the current path being switched. Full details and diagrams of the switching circuits are given in Appendix B.

5.3.2 The Venous Switch

There are two major veins in the upper arm, the basilic which lies parallel to the brachial artery, and the cephalic which is close to the skin. There is also a minor collateral vein in the humerus bone which is not occluded by the cuff (London and London, 1967). However, in the model all flow in the arm is considered to return through a single path beneath the cuff. Hence only one venous switch was required for the three peripheral terminations of the lower arm, inserted between the junction of the venous resistors and the circuit earth as shown in Fig. 5-10. As the voltages on the venous capacitors were equal, a single comparator was used to monitor the pressure difference between the cuff and one of the veins (the ulnar).

Fig. 5-11 shows the venous, cuff, and distal pressure waveforms occurring during a simulation of an indirect blood pressure measurement. A special circuit was used to generate the cuff pressure waveform, as described in Appendix B. The slope representing the deflation of the cuff has a gradient equivalent to the recommended clinical rate of -3 mm Hg per second. The input to the model was a recording of the aortic arch blood pressure at a frequency of 1 KHz (i.e. representing one beat per second). The variations in the distal systolic and diastolic pressures occur as a result of the action of the arterial switch.

The changes in the venous waveform may be described as follows. The waveform is at a steady value of 0.2 V (10 mm Hg) until the simulation begins with the rise of the cuff pressure waveform. When the cuff pressure exceeds the venous pressure the venous switch opens, but flow continues in the arteries for three or four beats until the systolic pressure is exceeded (170

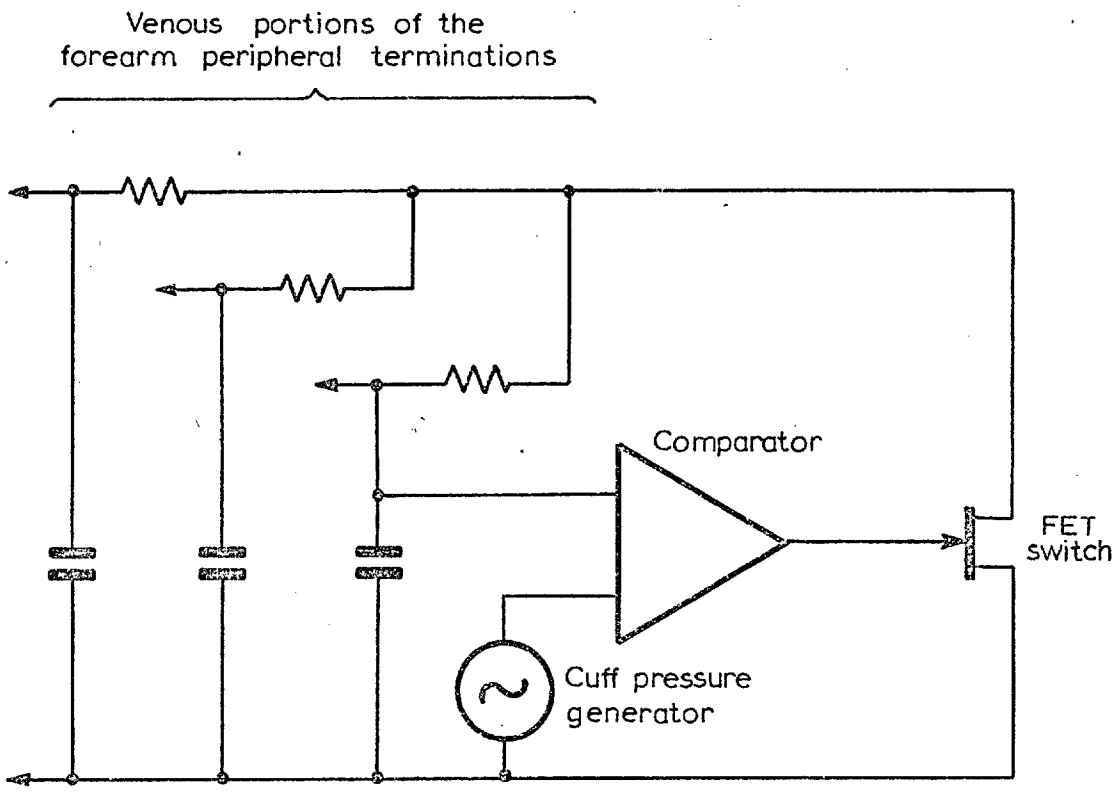


Fig. 5-10 : Schematic diagram of the venous switch.

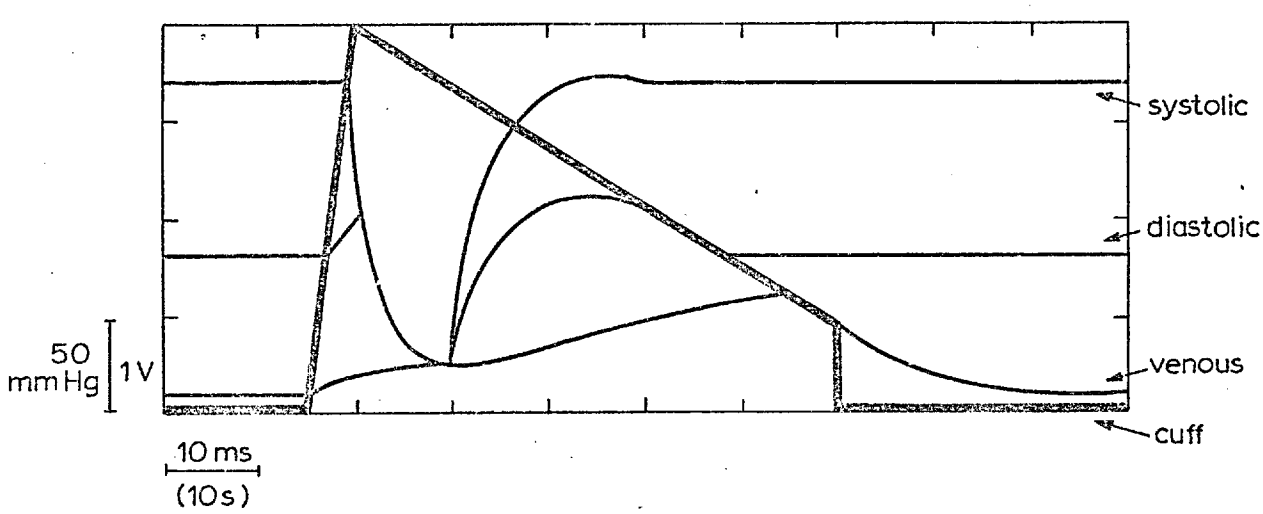


Fig. 5-11 : Simulated venous, cuff, and distal pressures.

mm Hg). Consequently the venous pressure rises during the period of continuing arterial flow until the arterial capacitors have discharged to the same voltage as the venous capacitors (0.4 V, i.e. 20 mm Hg). The venous waveform remains at this level until intermittent arterial flow recommences at the cuff systolic point. At this point the venous waveform again rises, slowly at first but more rapidly as the periods of arterial occlusion diminish, reaching a value of 55 mm Hg by the time the cuff pressure has decreased to the diastolic pressure (80 mm Hg). The venous waveform continues to rise until it exceeds the cuff pressure at about 65 mm Hg. At this point the venous switch closes and the venous capacitors begin to discharge. As the rate of discharge is greater than the decrease of the cuff pressure, the venous switch remains closed only for a brief period until the venous pressure is again less than the cuff pressure. The continuing peripheral flow causes the venous pressure to rise, and hence an oscillatory switching action occurs simulating bursts of venous flow under the cuff. As a result the venous pressure decreases at the same overall rate as the cuff pressure until at 50 mm Hg the cuff pressure returns to zero and the venous waveform decays to its normal value of 10 mm Hg in a time corresponding to 30 seconds.

The operation of the venous switch was not found to influence the waveforms at the terminal arteries. This is to be expected, since the peripheral waveforms are damped almost to 100% before reaching the venous networks, and the venous pressure does not rise as high as diastolic pressure in the terminal arteries. Although the venous switch proved to be relatively unimportant to the operation of the model, its implementation has shown that

during an indirect blood pressure measurement the venous pressure rises to several times its normal value. The maximum pressure reached is dependent on the time of venous occlusion, and a slow cuff deflation rate could possibly elevate the venous pressure to diastolic blood pressure causing an erroneous indirect measurement to be made. This also suggests why indirect measurements utilize a slow cuff deflation rather than inflation. If the latter course were taken, the early congestion of the veins could lead to a build up of back pressure opposing inflow and distorting the arterial waveforms.

5.3.3 The Arterial Switch

A cuff is usually placed around the upper arm centrally between the armpit and the elbow. Accordingly, the switch in the arterial line of the model was inserted midway along the brachial artery, the end capacitors of the segments either side of the switch being returned to the cuff pressure generator output rather than the circuit earth. The voltage across the proximal capacitor therefore represented the transmural pressure proximal to the cuff. This voltage was monitored by a comparator, the output of which determined the state of the series switch. Hence, the opening and closing of the artery under the cuff was simulated by the respective closing and opening of the switch. The circuit of the arterial switch is shown schematically in Fig. 5-12.

Since the cuff pressure generator has negligible output impedance and its waveform may be considered as a slowly-varying D.C. signal with respect to the heart rate frequency, the presence of this source does not affect signal transmission along the arterial line. The only measurable effect produced by the

insertion of the FET was that frequencies above 20 KHz were slightly attenuated. This was of no consequence as the frequencies affected were well removed from the frequencies of interest (1-4 KHz). However, several precautions had to be taken to ensure that the line was not loaded or otherwise altered by the addition of the switch and its control circuitry. For example, the comparator (an open-loop operational amplifier) required to be driven from a low impedance source to achieve fast switching with negligible hysteresis. Hence it was necessary to buffer the arterial line input to the comparator with a FET-input operational amplifier. A similar device was required to follow the voltage on the distal terminal of the switch. Its output was combined with the output of the comparator to form a gate switching voltage that prevented forward-biassing of the FET junction when the channel was in its conducting state. Thus the control of the switch did not interfere with current flow along the line, and the gate of the FET was effectively isolated from its channel. The complete circuit of the arterial switch is given in Appendix B.

5.3.4 Instability of Switching

The operation of the arterial switch during a simulation of an indirect blood pressure measurement produced transient oscillations as the switch changed states for each beat occurring while the cuff pressure was between systolic and diastolic blood pressure levels. The oscillations persisted for the complete duration of conduction for beats immediately following the systolic point, but became progressively less pronounced as the cuff pressure decreased. One or two cycles of oscillation were still present in each pulse until full conduction throughout the

heartbeat cycle was attained at the diastolic point. This action occurs because the circuit is inherently unstable at the times of switching. This instability may be demonstrated by considering the operation of the circuit of Fig. 5-13. At time t=0, V_A=E=0 and the switch is open. As time passes, V_A remains equal to E as no current is yet flowing. The switch does not close until V_A=V_B at which point current begins to flow, causing a voltage drop in R_S. V_A momentarily becomes less than V_B and the switch opens. Meanwhile E is rising so that V_A is again greater than V_B and the switch closes. The voltage drop in R_S again causes the switch to open and oscillatory action continues until E is greater than V_B by an amount equal to the voltage drop in R_S. Steady current now flows until V_A falls below V_B as E decreases, when similar transient oscillations take place. The transient oscillations will occur provided that the switching times of the comparator and switch are short compared to the time taken for the source to change by an amount equal to the voltage drop in R_S when passing through the comparator switching level.

The foregoing example illustrates instability in a simple resistive circuit. The oscillations observed in the more complex circuit of the arterial analogue are therefore to be expected. It is improbable however, that the artery itself would oscillate to the same extent because of the viscoelastic losses in the wall. Nevertheless, oscillations have also been observed in hydraulic models simulating indirect blood pressure measurements, even when flow inside the modelled artery is initially steady (Sacks et al., 1963; Anliker and Raman, 1966; Conrad, 1969). Further evidence of instability may be seen in the recordings of radial direct blood pressure previously discussed in Section 3.2. To assist

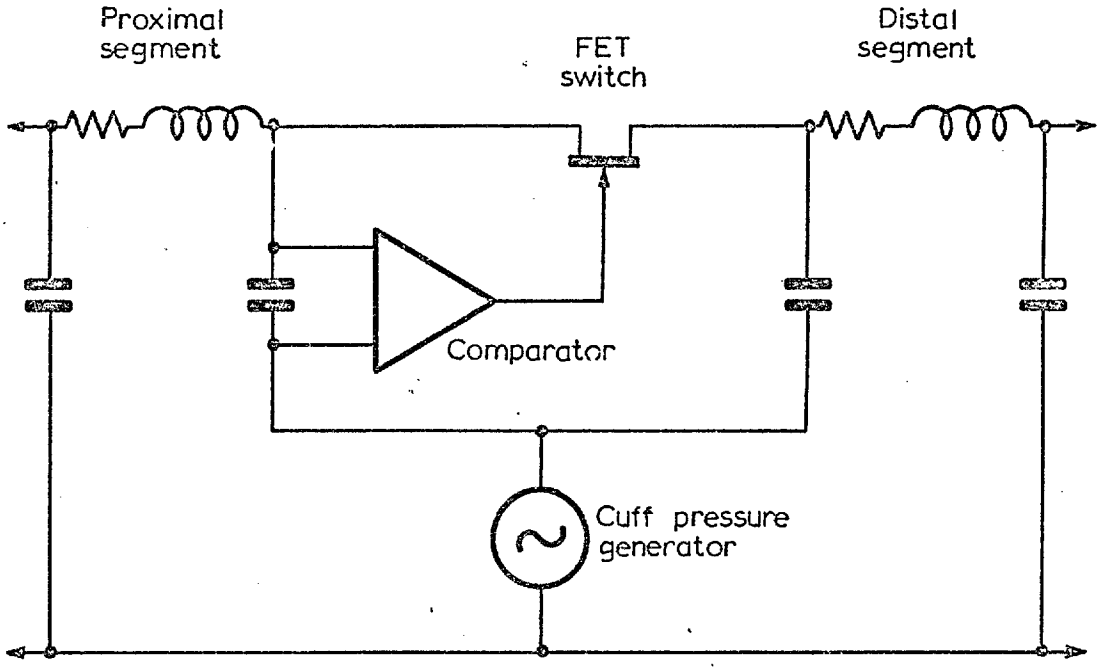


Fig. 5-12 : Schematic diagram of the arterial switch.

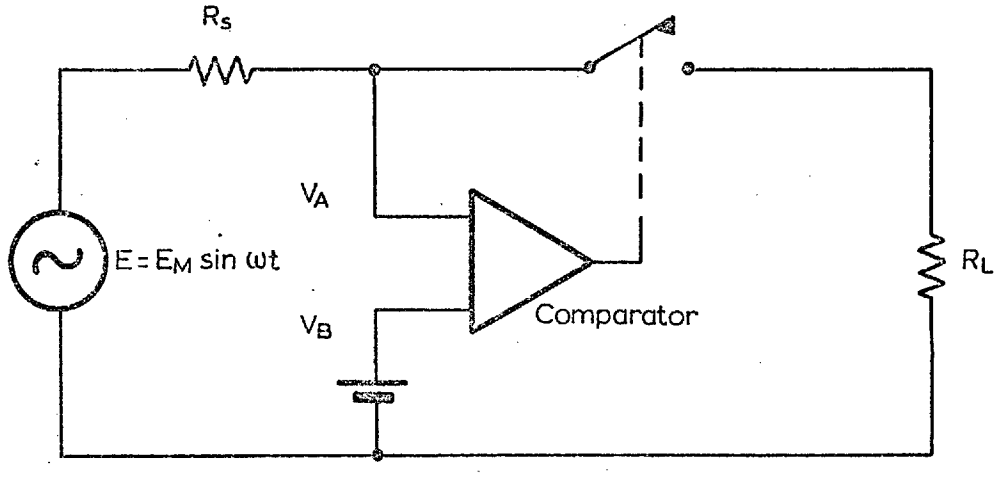


Fig. 5-13: Circuit with switching instability.

the reader, part of the radial pressure waveform of Fig. 3-2 has been redrawn in Fig. 5-14; points of inflection are clearly visible on the systolic upstrokes of beats 31 to 39, when the cuff pressure is intermediate between systolic and diastolic pressures. These inflections are not considered to be artefactual; McCutcheon and Rushmer (1967) have also reported that with the cuff inflated to a point midway between systolic and diastolic pressures, the flow velocity waveform detected by a Doppler ultrasonic transducer positioned beneath the cuff often has a convex inflection on the upstroke. In the light of the oscillatory action of the model, it is suggested that the inflections observed in practical waveforms are caused by momentary reclosure of the artery after the flow has resumed beneath the cuff. This intermittent instability is over-emphasized in the present model because no account is taken of the time required to change the geometry of the vessel walls. In the simulation the brachial artery is assumed to be either fully occluded or completely patent without intermediate stages of partial occlusion. The arterial segments distal to the switch smoothed the transients considerably, and except for a few beats occurring after the systolic point in the indirect measurement cycle, the peripheral waveforms gave little indication of oscillations further up the line.

5.4 SIMULATION OF INDIRECT BLOOD PRESSURE MEASUREMENTS

5.4.1 Practical Operation of the Model

Fig. 5-15 shows the 3-stage procedure that was used to obtain digitized waveforms analogous to the practical waveforms described in Chapter 3. It was not possible to connect the model

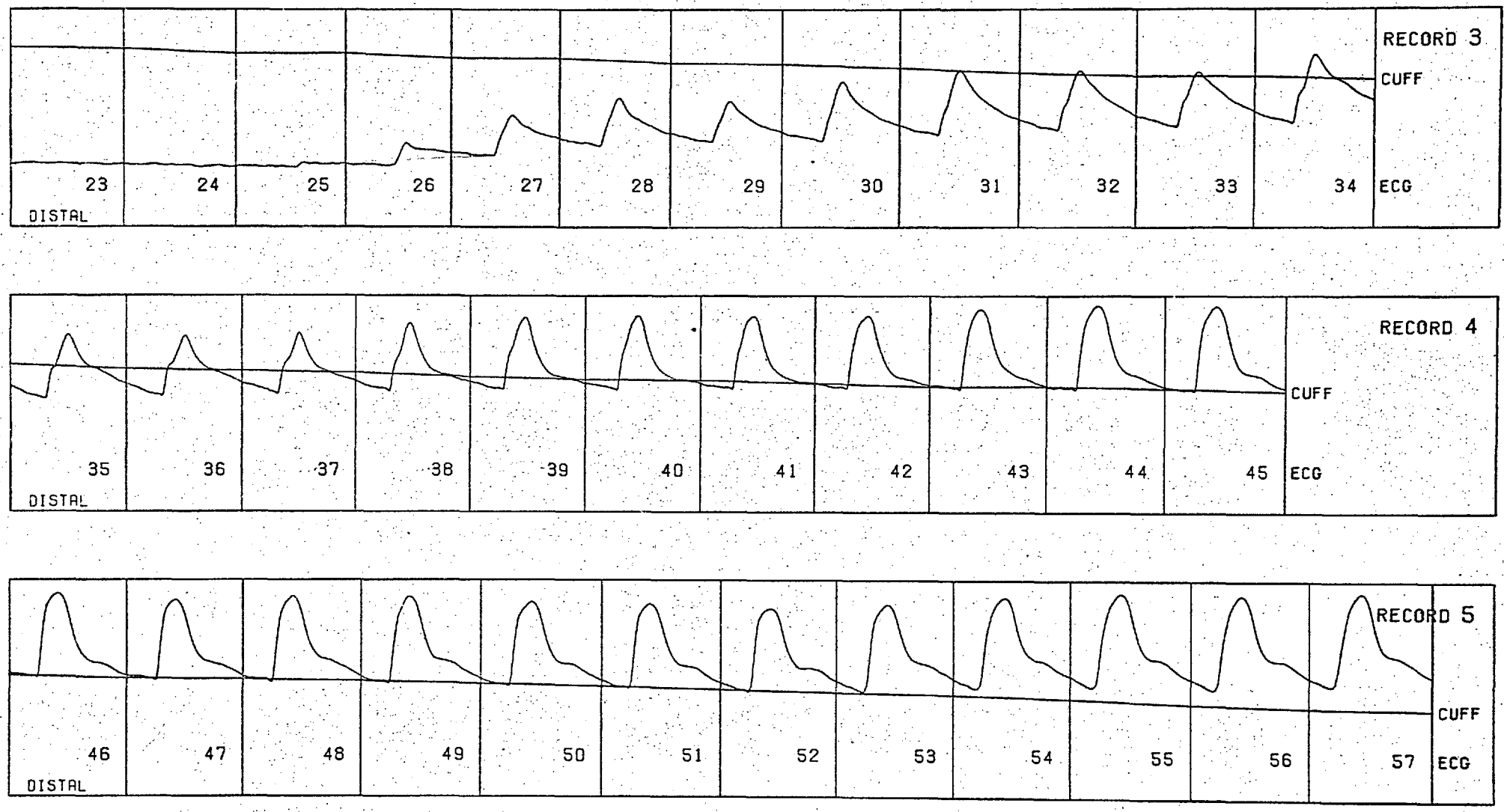


Fig. 5-14: Inflections in the systolic upstrokes of the radial blood pressure recording (from Fig. 3-2).

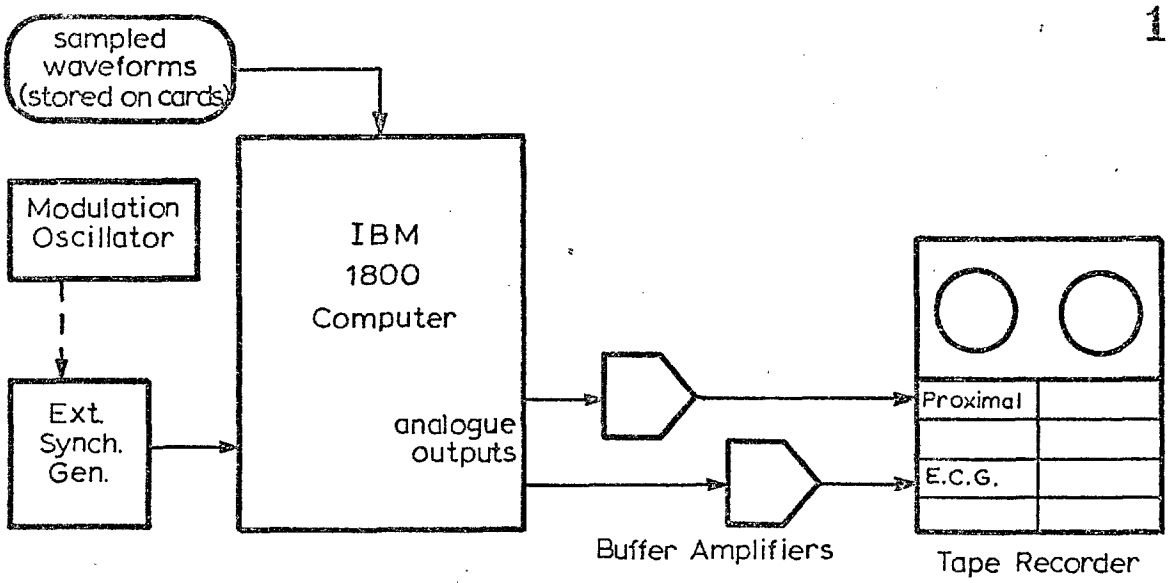


Fig. 5-15a: Input waveform generation.

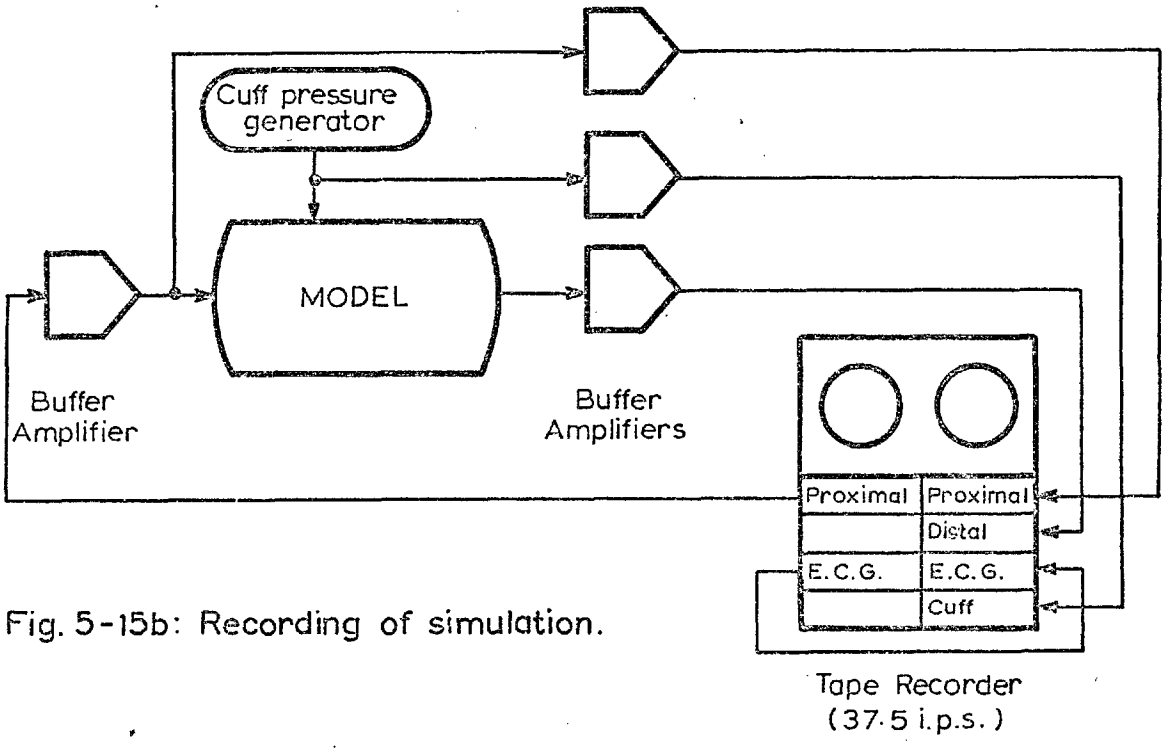


Fig. 5-15b: Recording of simulation.

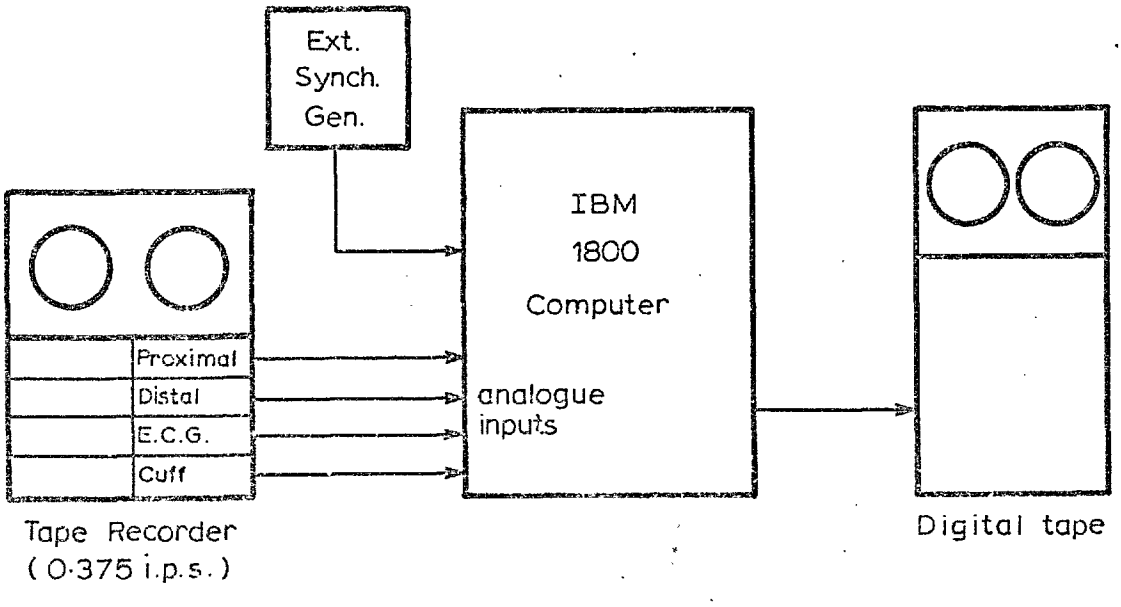


Fig. 5-15c: Digitization of waveforms.

directly to the IBM 1800 computer as the frequency scaling of the model (1000 times real frequency) required a digitization rate in excess of the maximum permissible. To overcome this difficulty, an analogue instrumentation tape recorder (P.I. 6208) was used to change the time scales of waveforms passed from the computer to the model and vice versa.

Although operation of the model required only an input waveform analogous to aortic arch pressure, a simultaneous E.C.G. was necessary to make the data compatible for use with programs developed previously for the analysis of the practical waveforms. The two waveforms required for model simulations were obtained in the following manner from a section of the digitized recording of simultaneous E.C.G. and aortic arch pressure mentioned in Section 3.1.1.

A suitable beat (150 samples, 0.75 seconds duration) was selected from the data and the Fourier coefficients of the low order harmonics of both channels were computed using a DFT subroutine. It was then possible to filter each channel in the frequency domain by placing the wanted harmonic coefficients in a 128-point array before using an inverse FFT subroutine for transformation back to the time domain. After transformation, the samples of the filtered aortic arch waveform and the simultaneous E.C.G. of the selected beat were contained in separate data arrays. To obtain continuous electrical waveforms, a subroutine was written to perform high speed digital to analogue conversion of two channels using external synchronization. The digital to analogue converter was normally triggered at a constant pulse rate as most work with the model was performed

with a constant simulated heart rate. However, it was also possible to frequency modulate the synchronizing pulse generator and produce a waveform with a variable interbeat interval as described in Section 5.4.5.

The waveforms generated by the computer were then recorded (via level-shifting buffer amplifiers) on two frequency modulated channels of a continuous tape loop, as shown in Fig. 5-15a. As the maximum conversion rate of the computer was not high enough for both channels to be simultaneously generated at 1000 Hz, the mid-range recording speed of 3.75 inches per second was used with the external synchronization of the computer adjusted for a waveform repetition rate of 100 Hz. Once this recording had been made, the speed of the tape recorder was increased 10 times to 37.5 inches per second to provide an input waveform for the model at the required repetition rate of 1000 Hz. At this speed, the recording channels have a flat response from D.C. to 10 KHz ($\pm$1 dB), which was adequate for the pressure waveforms but only marginally acceptable for the E.C.G. For this reason it was necessary to exclude frequencies below the fourth harmonic in the digital filtering of the E.C.G. waveform, so that the E.C.G. was still of an acceptable shape for timing purposes after a recording of the recording had been made.

The output of the aortic arch channel of the tape recorder was connected to the model via a low output impedance buffer amplifier with variable gain and adjustable D.C. output level. This enabled the model to be driven by an input waveform scaled to the same calibration levels as the cuff pressure generator (0 V = 0 mm Hg, 4 V = 200 mm Hg). The resonances in the amplitude transfer characteristic of the model made it necessary for

harmonics above the fourth to be omitted from the aortic arch waveform in the frequency domain filtering prior to the digital to analogue conversion. Although this did not produce great changes in the shape of the aortic arch waveform, the filtering was required to avoid non-physiological waveforms appearing at the periphery.

An additional four frequency modulated channels of the tape recorder were used to record simultaneous waveforms during simulations of indirect blood pressure measurements with the model. One channel was used to record the E.C.G. by direct connection to the E.C.G. playback channel while the other three channels were used to record the input waveform to the model, the waveform analogous to radial arterial blood pressure, and the waveform from the cuff pressure generator. These three channels were calibrated identically so that pressure comparisons could be made directly on the data.

As before, the digitization of the waveforms was carried out using the IBM 1800 computer. It was necessary to slow down the speed of the recorder by a factor of 100 times to 0.375 inches per second in order to bring the required sampling rate within the range of the analogue to digital converter. At this speed the fundamental frequency of the model waveforms is 10 Hz, and it was possible to connect the tape recorder outputs directly to the analogue inputs of the computer, with the output filters of the tape recorder set to cut off at 100 Hz. The waveforms were stored on digital magnetic tape so that editing and analysis could be carried out using the same programs as were used for the processing of the practical waveforms described in Chapter 3.

5.4.2 Analogue Waveforms

The digitized waveforms for a simulation using an input waveform of constant frequency are shown in Fig. 5-16. In this case the digitization rate was 100 samples per beat, the interbeat interval being equivalent to one second in real time. The sequence of events is the same as that described for the practical waveforms shown in Fig. 3-2. The simulated cuff pressure is at zero for beats 1 to 13, after which it quickly rises to above systolic pressure so that the radial pulse is completely obliterated in beat 19. During the period of complete arterial occlusion the decline of the simulated radial pressure waveform is marked by a small amount of extraneous noise. This represents the extent of signal degradation when using a tape recorder as a waveform buffer.

The cuff systolic point is reached at beat 30. As the simulated cuff pressure continues to decrease, the distal pressure wave builds up rapidly at first and then more gradually as the pre-occlusion shape is regained. An inflection can be seen in the systolic upstroke of many of the beats, this feature being particularly noticeable in the beats immediately following the cuff systolic point (beats 30 to 38). These inflections arise from the peripheral smoothing of transient oscillations occurring when the arterial switch changes state and are similar to inflections observed in the practical waveforms (Fig. 3-2, beats 31 to 39). This similarity led to the suggestion that the brachial artery momentarily closes after the onset of a flow pulse beneath the cuff (Section 5.3.4).

The systolic, diastolic, and cuff pressures for the data of Fig. 5-16 are shown in Fig. 5-17. This figure is similar in

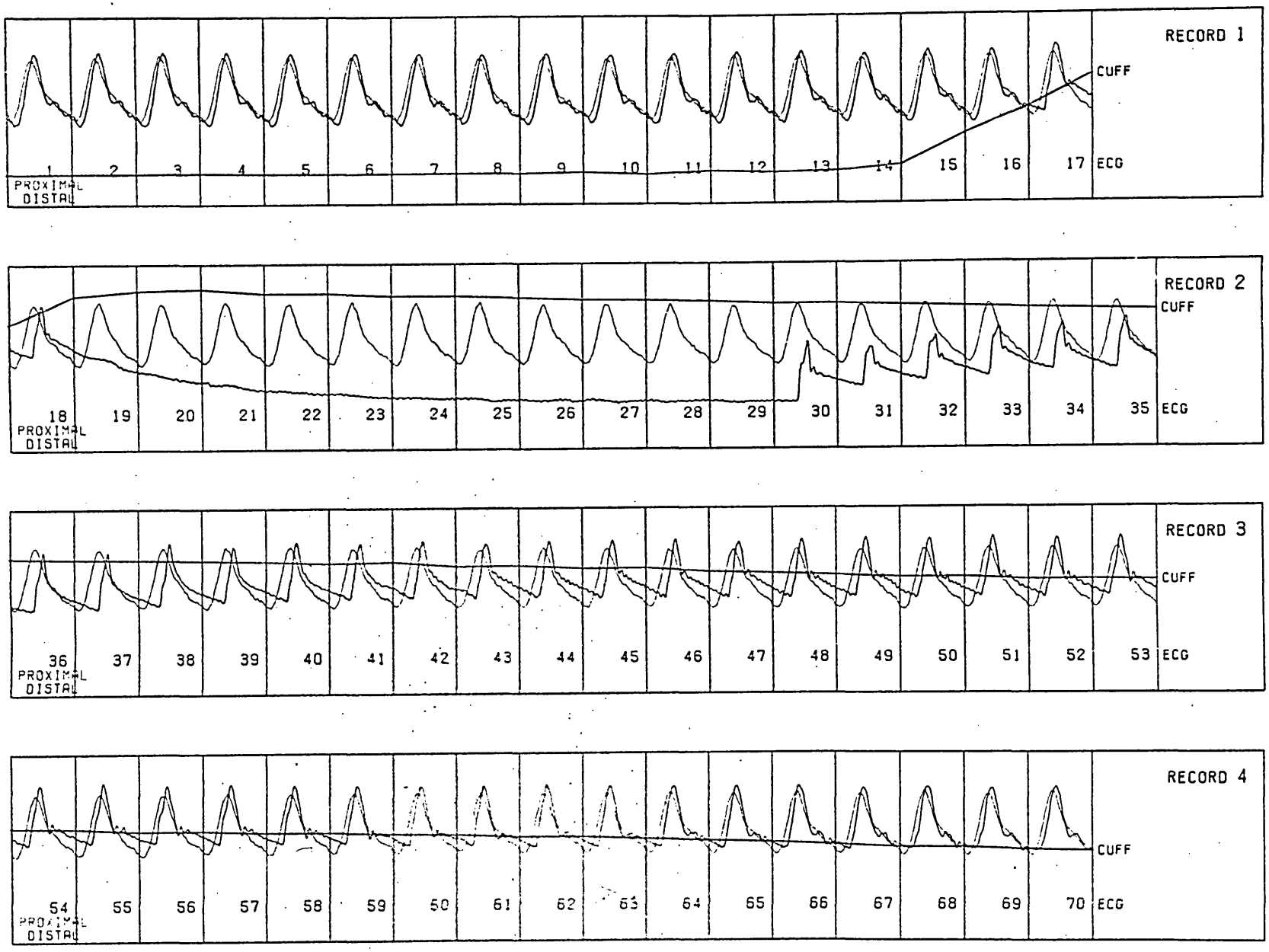


Fig. 5 - 16 : (page 1)

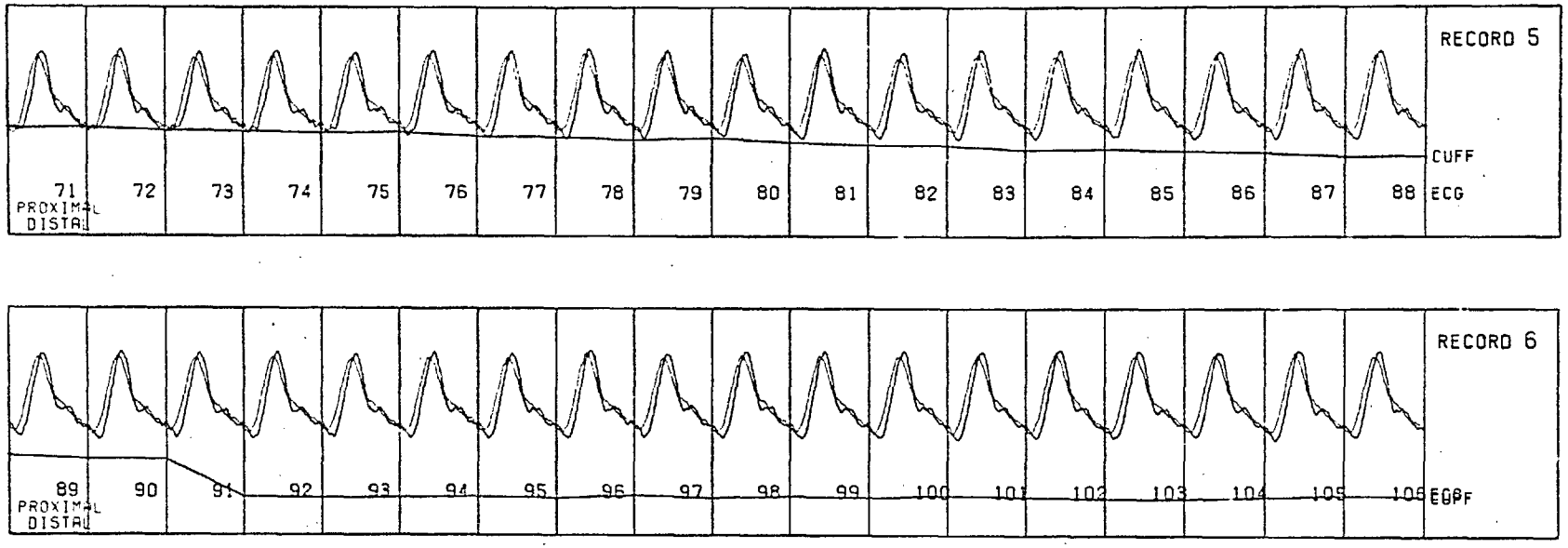


Fig. 5-16 (page 2) : Waveforms recorded during a simulation of an indirect blood pressure measurement.

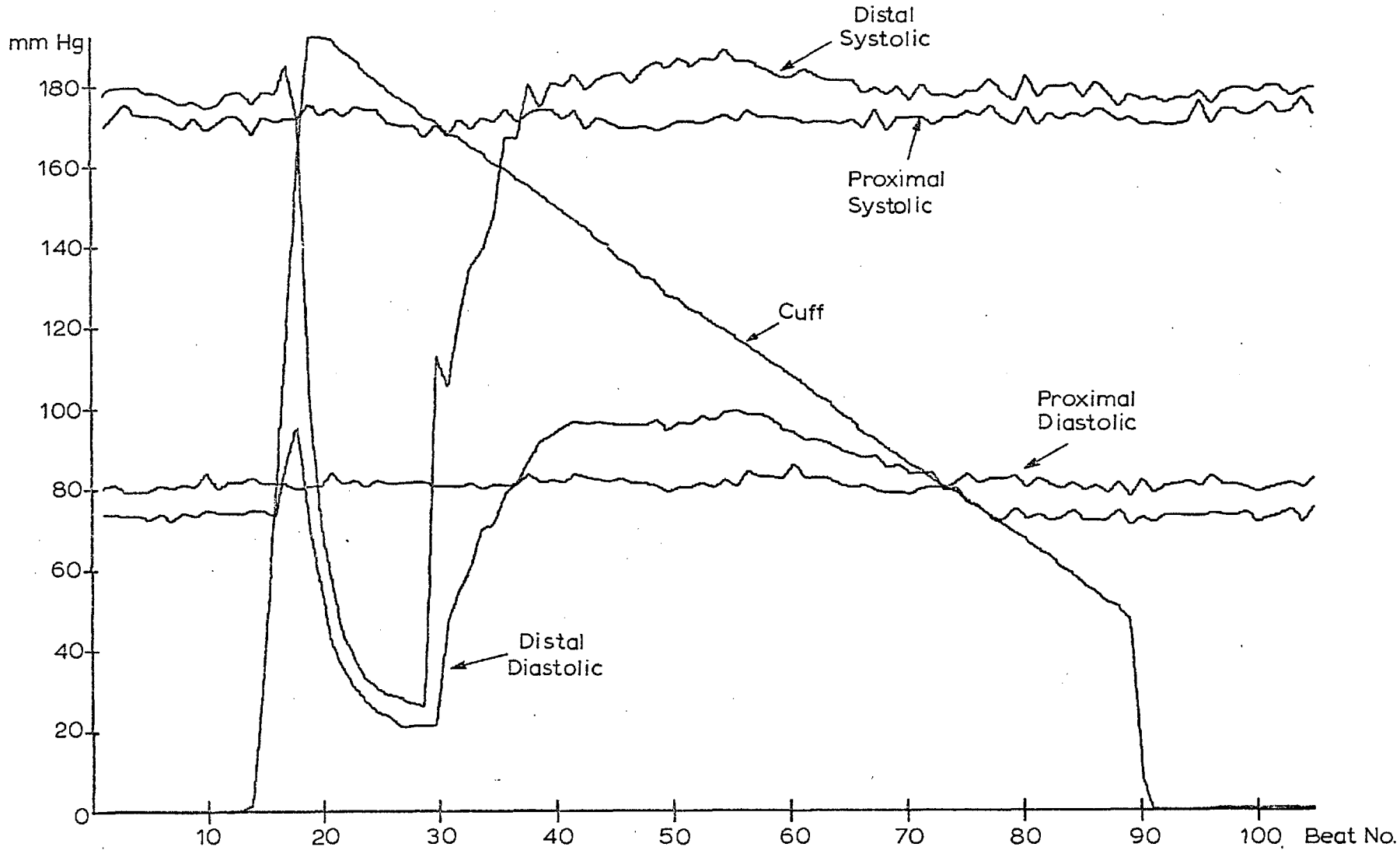


Fig. 5-17: Systolic, diastolic, and cuff pressures during the simulation.

many respects to the corresponding plot for the practical data (Fig. 3-7). During the period of total occlusion the arterial pressure drops in an approximately exponential manner towards the venous pressure (which rises above its normal value as the veins absorb the remaining peripheral flow). After the cuff systolic point has occurred (beat 30) the blood pressures rise rapidly and become elevated above their normal values, to which they slowly revert during the subsequent beats. As with the practical waveforms, the radial diastolic pressure remains equal to the cuff pressure for several beats before the divergence at the cuff diastolic point (beat 76). The reason for this phenomenon has been discussed previously in Section 3.5.1.

5.4.3 Time Measurements

The programs described in Section 3.2.4 were reapplied to the data of Fig. 5-16, and the results are shown in Figs. 5-19 and 5-20. The time measurements from the QRS peaks to the end-diastolic points contain a high proportion of irregularity, whereas the measurements from the QRS peaks to the points located one quarter of the way up the systolic upstroke are considerably smoother. The irregularities in the curves of Fig. 5-19 arise because the end-diastolic points are somewhat obscured by noise. On the other hand, the systolic upstrokes are clearly defined and consequently the curves of Fig. 5-20 show more orderly trends, the remaining irregularities being largely due to the quantization of the measurement, as interpolation between samples was not carried out.

The trend in the distal curve of Fig. 5-20 stabilizes to its pre-occlusion value at beat 73, which occurs shortly

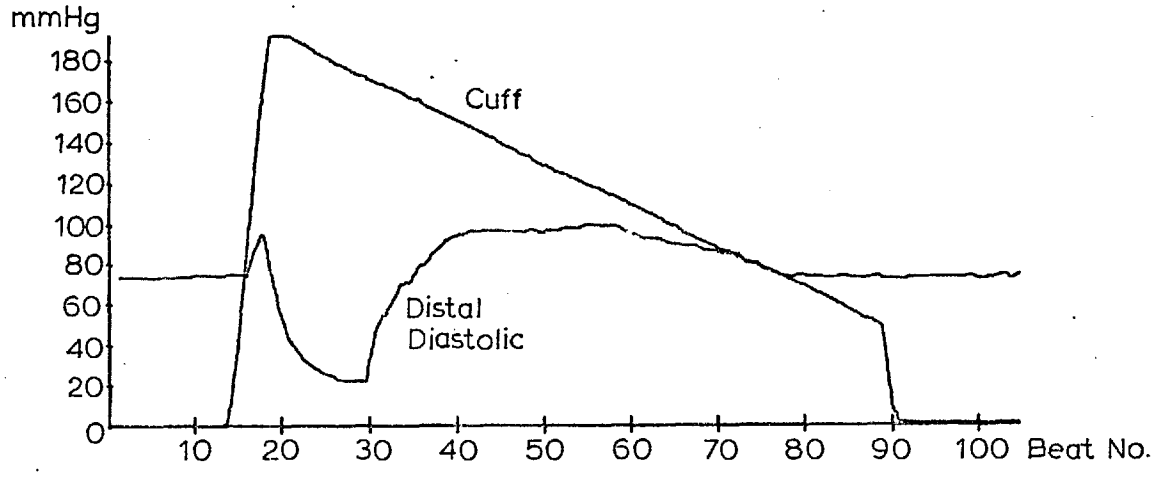


Fig. 5-18: Cuff pressure and distal diastolic pressure.

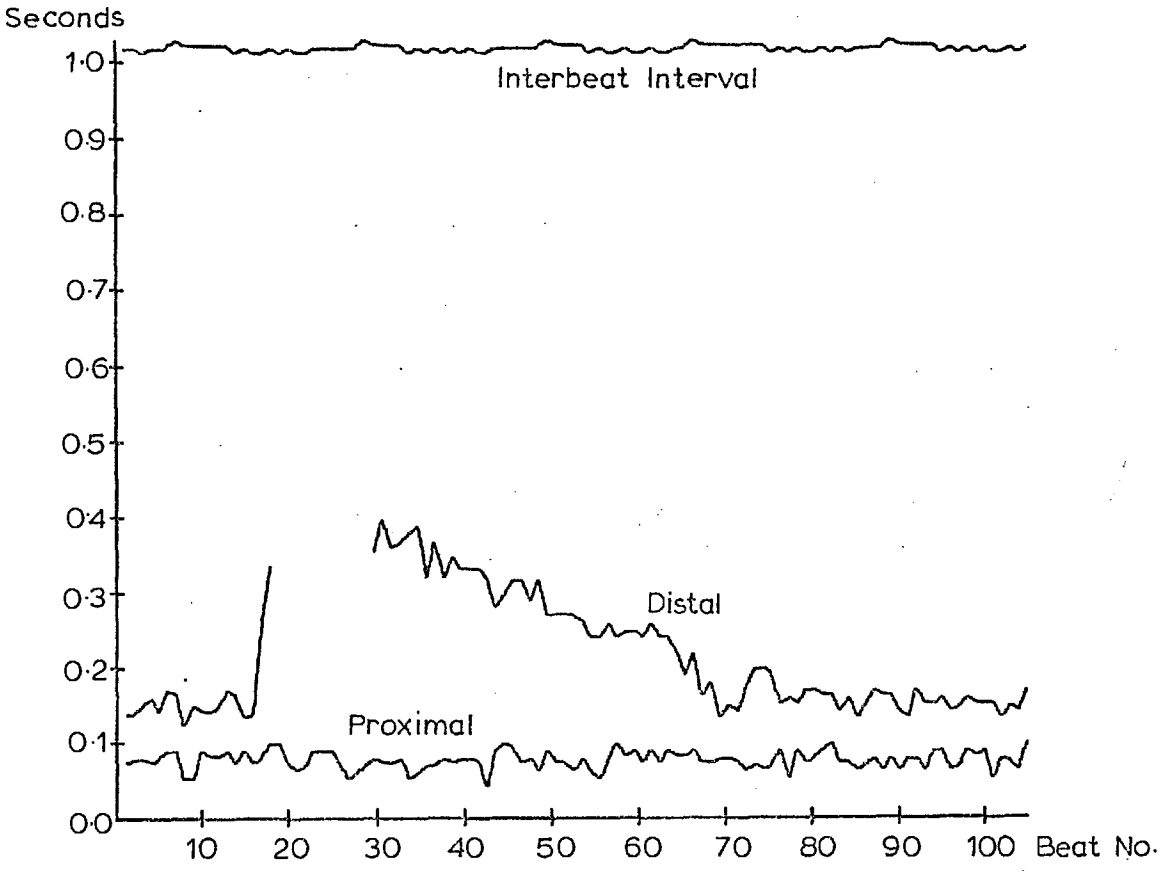


Fig. 5-19: Intervals from QRS to end-diastolic point.

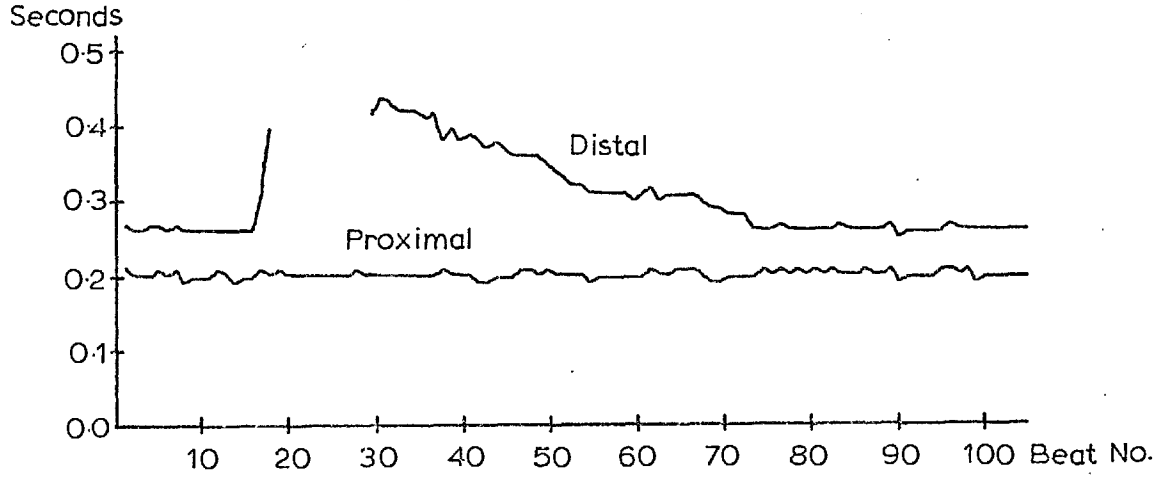


Fig. 5-20: Intervals from QRS to systolic upstroke.

before the cuff diastolic point (beat 77, Fig. 5-18). This corner point in the time measurements is relatively distinct because subsequent measurements have constant values as there are virtually no changes in the simulated waveforms once the cuff pressure is below diastolic blood pressure. The cuff pressure at the time of occurrence of beat 73 is 80 mm Hg; the brachial diastolic pressure at this instant is about 76 mm Hg (i.e. a value approximately midway between aortic and radial diastolic pressures). It would therefore appear that the cuff diastolic point could be located with reasonable accuracy from time measurements made on a waveform recorded distal to the cuff. However, measurements on practical direct pressure waveforms did not reveal a corner point in the trends with sufficient clarity to positively identify the cuff diastolic point (Section 3.2.4). It is therefore concluded that beat-to-beat variations in waveshape tend to mask the corner point making this method unsuitable for use with practical waveforms.

5.4.4 Frequency Analyses

The spectral results for the data of Fig. 5-16 are shown in Fig. 5-21, the period of analysis being equal to the interbeat interval (constant, 1.0 second). The input to the model is supposedly constant, but there are minor irregularities in the amplitudes and phases of harmonics of the proximal wave. These irregularities may be attributed to signal degradation caused by the use of a tape recorder to transfer waveforms to and from the model.

As in the analysis of the practical waveforms, during the period of total arterial occlusion the harmonic amplitudes of the distal waveform are almost zero and the corresponding

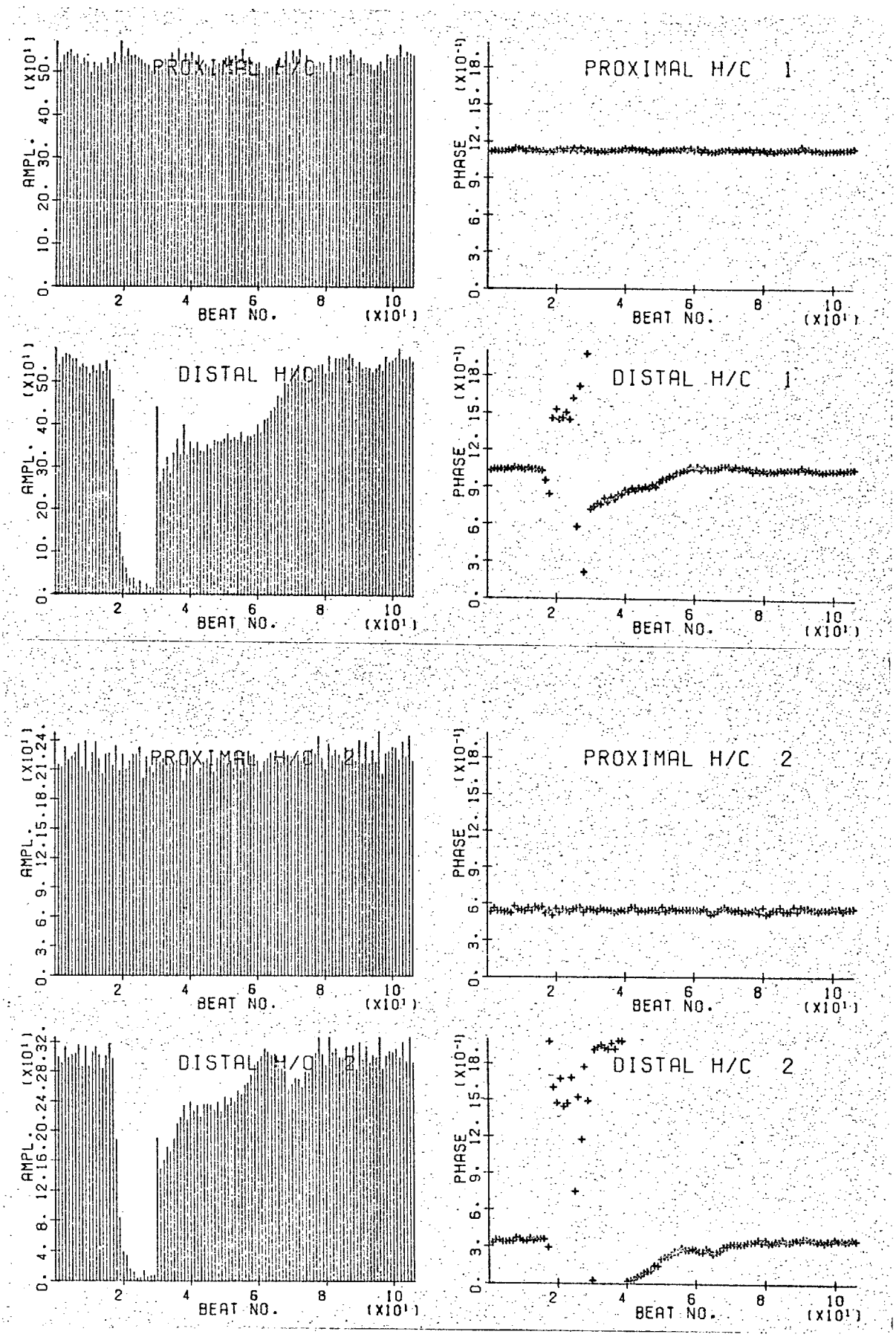


Fig. 5-21 : Spectra computed during a simulation of an indirect blood pressure measurement (constant interbeat interval).

phase angles are random. When intermittent flow resumes at the cuff systolic point (beat 30) the distal harmonic amplitudes are reduced and the phase angles are displaced. The trends which occur in the results for the subsequent beats are made more apparent in the amplitude ratio and phase difference plots of Fig. 5-22, from which it is seen that the plots for the second harmonic are more irregular than for the fundamental. The corresponding plots for the third and fourth harmonics showed even greater variations. This result is consistent with previous analyses which showed that the higher harmonics were unpredictable in practical waveforms (Section 3.5.3).

Although the phase difference plots of Fig. 5-22b both show a linear trend for the beats following the cuff systolic point (beats 30 to 56), the curves differ in the manner in which they approach their pre-occlusion values at the cuff diastolic point (beats 57 to 77). During the latter period the phase differences for the fundamental frequency "overshoot" the resting value with a reversal of slope in the trend; conversely, the second harmonic phase differences display a monotonic trend of decreased gradient. The overshoot of the first harmonic phase differences was somewhat puzzling, as this feature was not observed in the analyses of practical waveforms (e.g. Fig. 3-16b). The cause of this anomalous result was traced to small differences between the simulated and practical waveforms, as discussed in Chapter 6.

A comparison of the amplitude ratio plots of the simulated and practical waveforms (Figs. 5-22a and 3-16a respectively) shows that after the cuff systolic points the ratios for the model increase more rapidly than in the real case. This

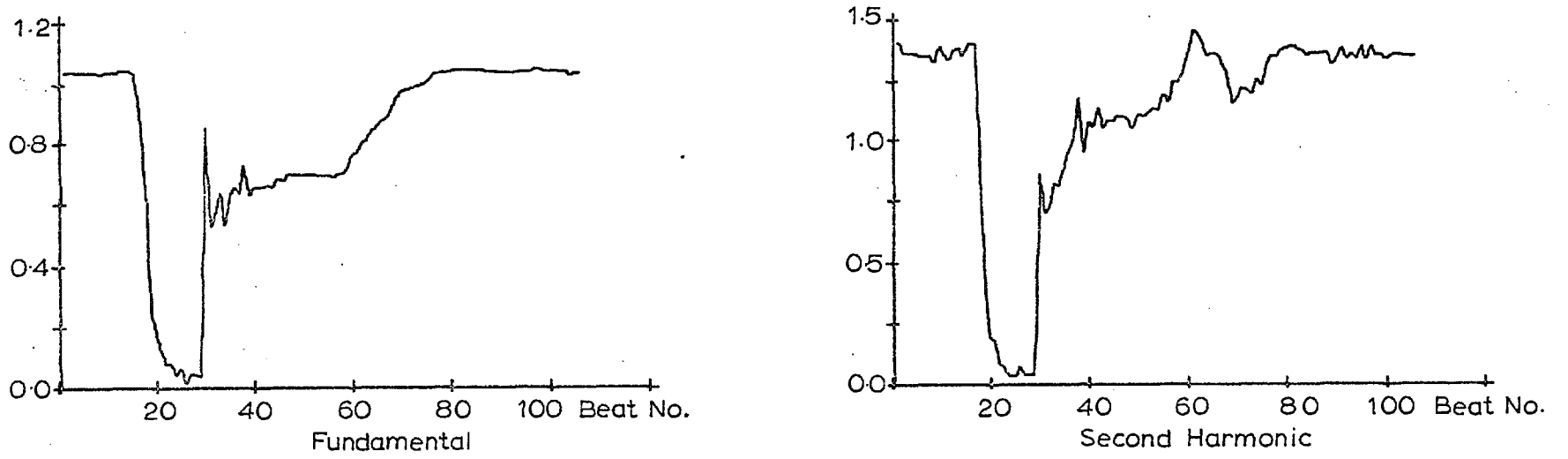


Fig. 5-22a: Distal: Proximal Amplitude Ratios.

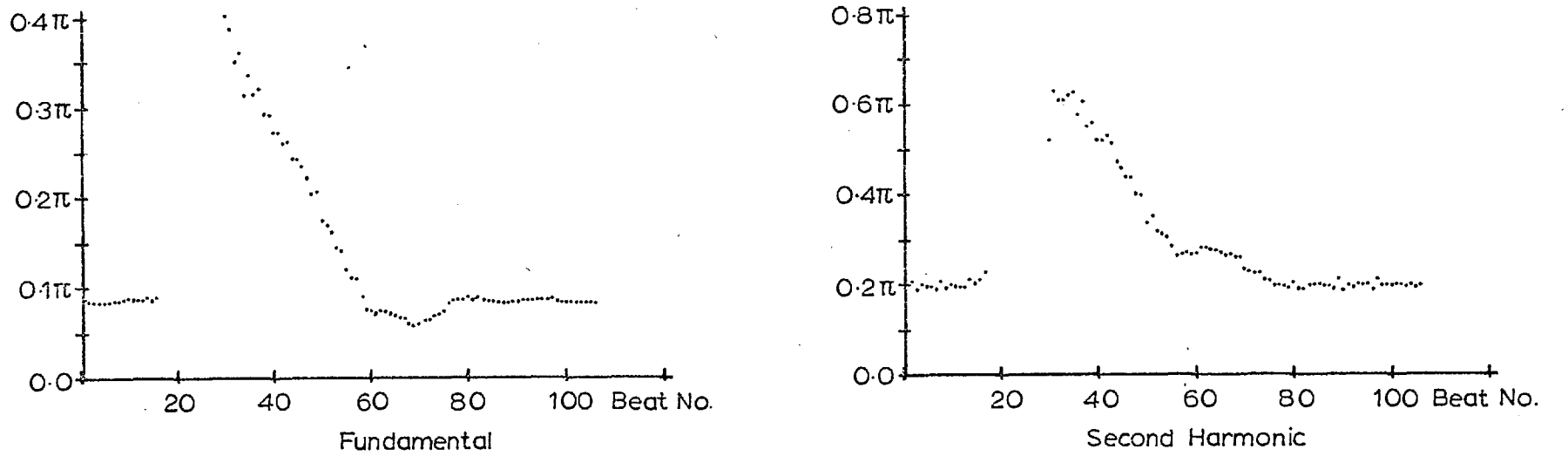


Fig. 5-22b: Proximal-Distal Phase Differences
(Simulation with constant interbeat interval).

discrepancy is attributed to the simulation of the action of the cuff; in the model, arterial conduction is either inhibited or unimpeded with no intermediate stages of resistance to flow. However, as the interest in performing the simulation concerns the location of the cuff diastolic point rather than the results in the region of the cuff systolic point, this defect of the simulation is unimportant for present purposes.

Referring to the results for the fundamental frequency of the model waveforms (Fig. 5-22), it is seen that during the period of phase difference overshoot the amplitude ratio increases sharply until the pre-occlusion value is attained at the cuff diastolic point (beat 77). This increase is caused primarily by the steady decrease of the distal diastolic pressure from its elevated value. The corresponding increase in the distal pulse pressure which occurs during this period (beats 57 to 77, Fig. 5-17) results in a significant increase in the amplitude of the distal fundamental component (refer Fig. 5-21). The clearest indication of the cuff diastolic point is therefore given by the stabilization of the first harmonic amplitude ratio after the phase difference parameter has decreased from its initial large displacement to a value much closer to the pre-occlusion phase shift. The use of the amplitude ratio parameter ensures that changes in the absolute amplitude of the proximal fundamental component are eliminated from the results. Consequently, the effect of the cuff is seen as a smooth trend, and the occurrence of the cuff diastolic point may be identified readily. This confirms what was observed in the results of the analyses of the practical waveforms (Section 3.3.3).

The filtered impulse responses of the cuff were also computed from the simulated waveforms. As with practical waveforms, the filtering had to be restricted to include only the fundamental and second harmonic frequencies for orderly trends to be apparent. However, no fresh information of consequence was revealed in the perspective diagrams and contour plots of the successive responses. Because of the subjective nature of the presentation of the results, this form of analysis will not be discussed further.

5.4.5 Variable Interbeat Intervals

The waveforms of a second simulation are shown in Fig. 5-23. In this case the input waveform has been frequency modulated by a triangular waveform, so that the simulated heart rate varies linearly between 1.0 and 1.4 beats per second with a period of 10 seconds. When digitizing the waveforms, the external synchronization was set to give a higher real-time sampling rate of 125 Hz; this ensured a convenient number of samples per beat (83 to 125). The triangular variation of the interbeat interval is shown in Fig. 5-24.

Although the interbeat intervals vary over a practical range, the resulting shapes of the waveforms generated with triangular frequency modulation are somewhat non-physiological in that the beats are either linearly expanded or contracted in time. With practical waveforms the leading portion of each beat maintains a fairly constant time relationship with respect to the QRS peak of the E.C.G.; it is during diastole that the period tends to alter. This was demonstrated by the linearity of the phase angles in the results of the analyses using the

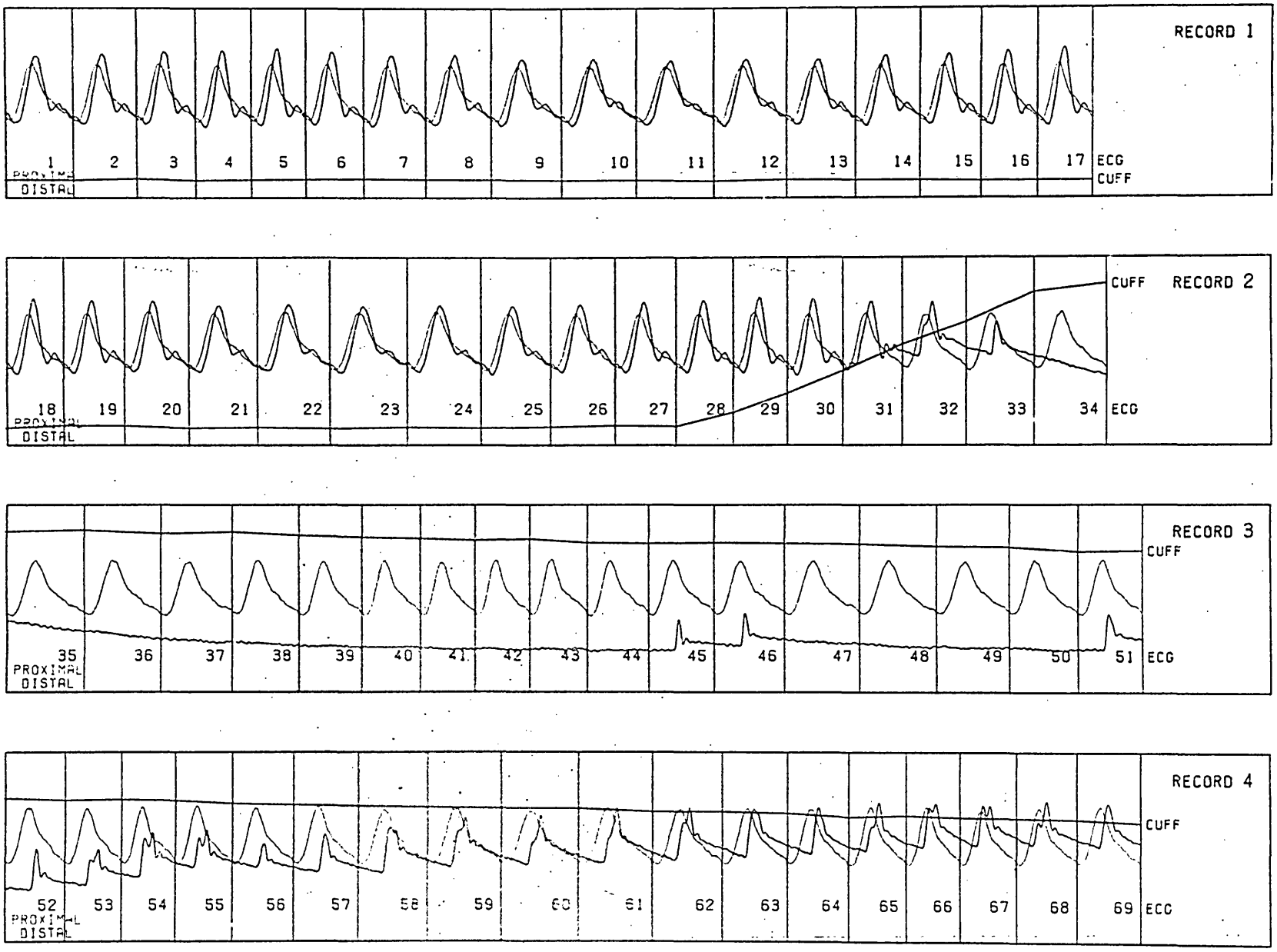


Fig. 5-23 (page 1)

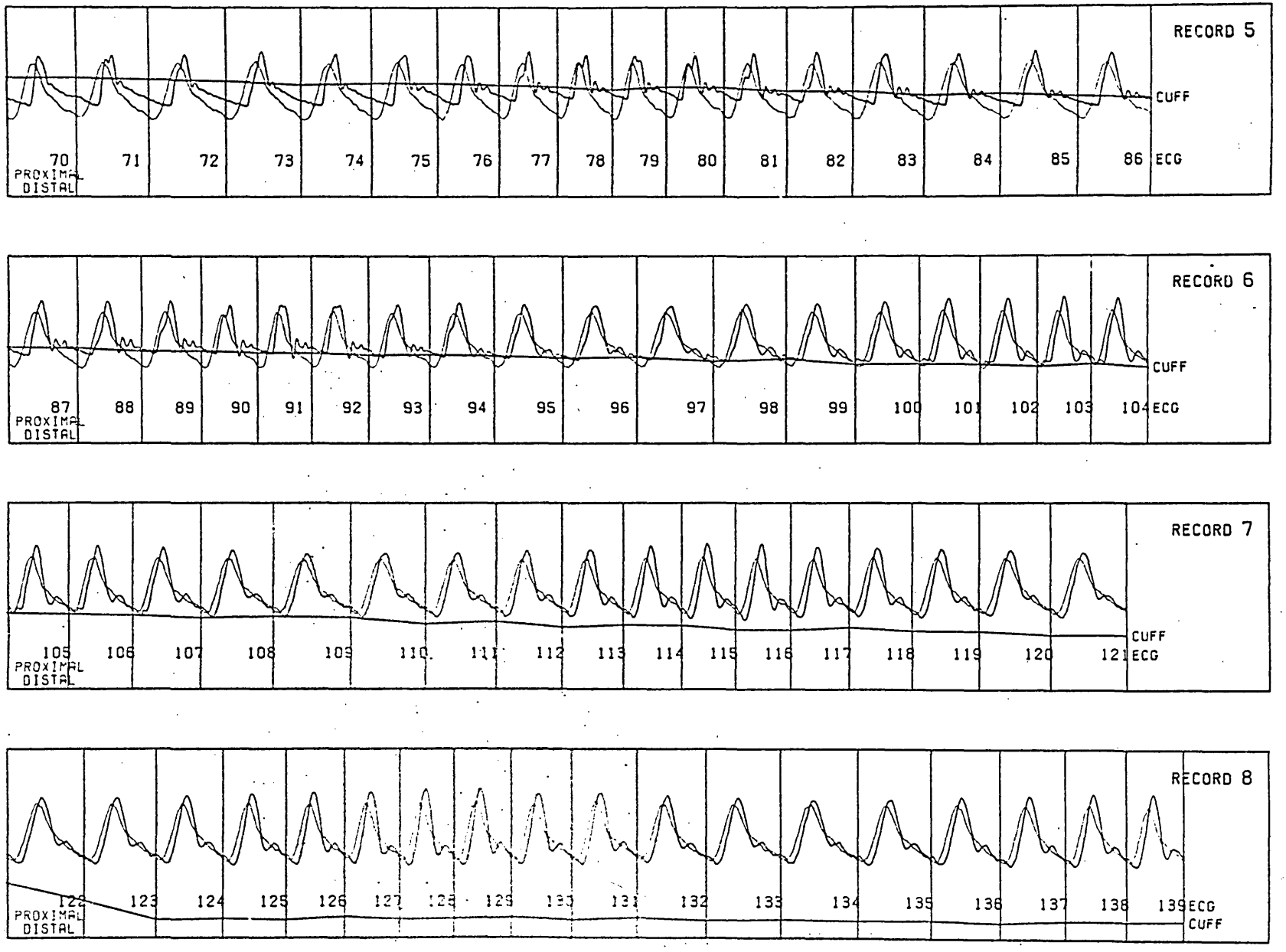


Fig. 5-23 (page 2)

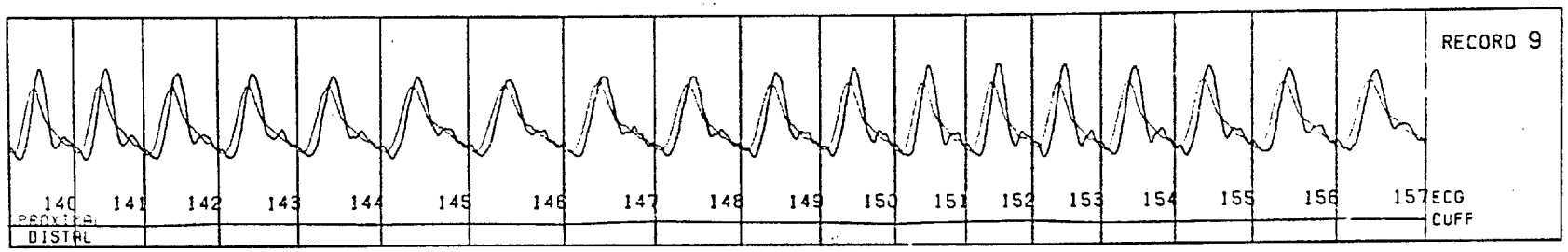


Fig. 5-23 (page 3) : Waveforms with variable interbeat intervals recorded during a simulation of an indirect blood pressure measurement.

interbeat interval as the period of the fundamental frequency (Section 3.3.5). Therefore the simulation discussed in this section is of limited value. However, the simulation proved useful for demonstrating the effects of systolic pressure variations and for showing that the application of the phase-correction algorithm reduces the amount of irregularity in the phase difference curves of the fundamental component.

The input waveform to the model is constant in amplitude but variable in frequency: as a result of the changes in frequency the peripheral waveforms vary also in amplitude. This is shown in Fig. 5-25, in which the systolic, diastolic, and cuff pressures are plotted from the data of Fig. 5-23. Except during the period of cuff pressurization, the triangular variation in interbeat interval is manifested by a triangular modulation of the distal systolic pressure curve. On the other hand, the corresponding distal diastolic pressures remain virtually constant. This is a fortuitous consequence of the phase relationships of the harmonics in this particular case, as subsequent analyses showed that all the harmonics of the distal waveform were modulated triangularly in both amplitude and phase angle. Therefore in the present simulation the modulation of the interbeat interval introduces effects due to changes in the systolic pressure.

The cuff systolic point occurs at beat 51 (Fig. 5-23). The momentary arterial openings at beats 45 and 46 are not artefactual, but indicate that for these beats the brachial systolic pressure has exceeded the instantaneous cuff pressure. The cessation of distal pulses during beats 47 to 50 occurs because the lengthening of the interbeat interval at this

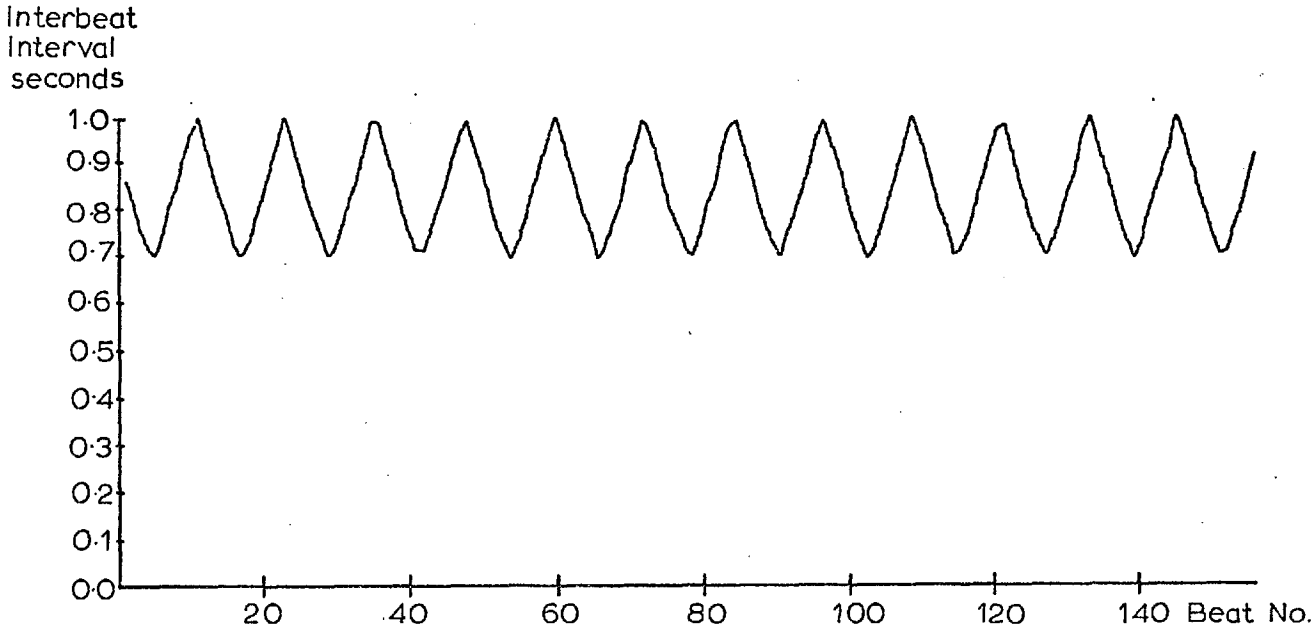


Fig. 5-24: Variation of interbeat intervals during the simulation.

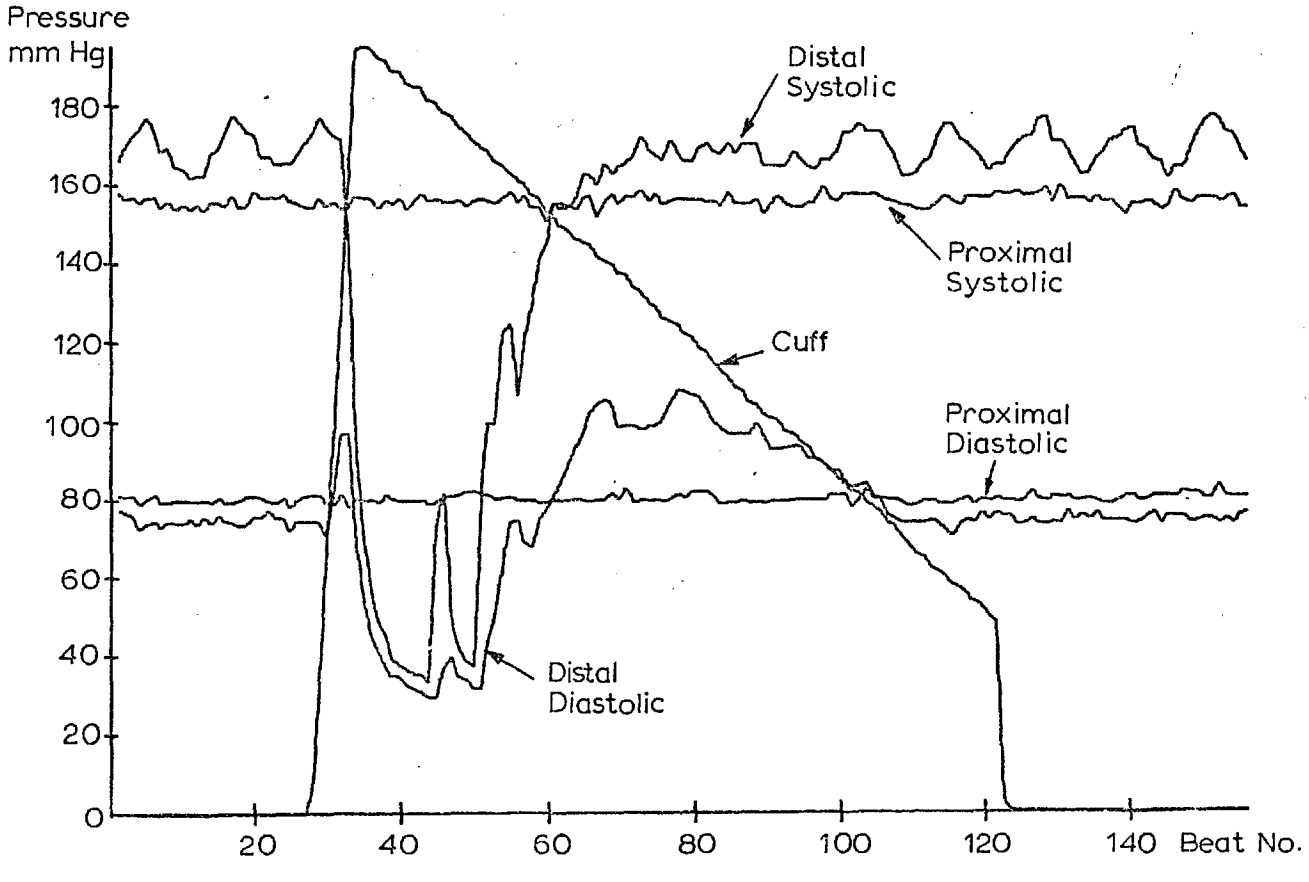


Fig. 5-25: Systolic, diastolic, and cuff pressures recorded during a simulation using variable interbeat intervals.

period causes the brachial systolic pressure to decrease at a rate that is faster than the depressurization rate of the cuff. (Similar gaps are encountered during practical indirect blood pressure measurements if the systolic pressure decreases significantly subsequent to the first penetration under the cuff). The depression of the distal wave at beat 56 is additional evidence that the variation of brachial systolic pressure influences the distal waveform during an indirect blood pressure measurement. This is a possible explanation for occasional irregularities in the Korotkoff sounds, known as "auscultatory gaps" (Bellville and Weaver, 1969).

The frequency spectra of the data of Fig. 5-23 are shown in Fig. 5-26. For this analysis, the interbeat interval was taken as the period of the fundamental frequency according to the procedure described in Section 3.3.5. From Fig. 5-26 it can be seen that the spectra of the distal waveforms are marked by triangular variations synchronized with the changes of interbeat interval shown in Fig. 5-24. These variations are caused by the response of the model. The effect on the second harmonic is greater than on the fundamental frequency because the frequencies covered by the second harmonic (2-2.8 Hz) are closer to the peak of the first resonance in the response (3.5 Hz, refer Fig. 5-8). The presence of similar resonances in the response of the living system would therefore be a factor contributing to the unreliability of the second harmonic compared with the fundamental frequency.

Because the spectra of the distal waveforms fluctuate with the interbeat intervals, the location of the cuff diastolic point from the amplitude ratio and phase difference curves is

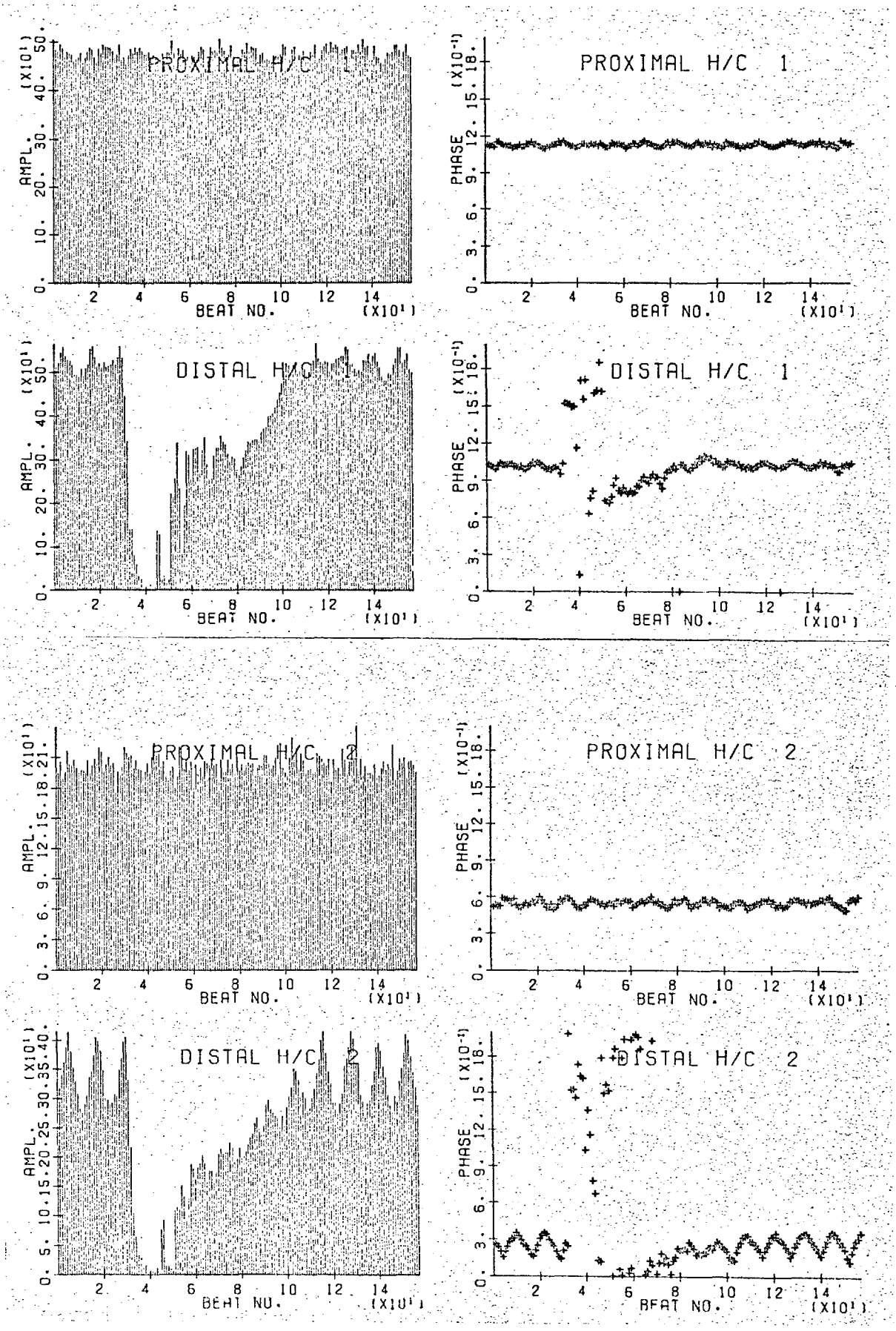


Fig. 5-26: Spectra computed during a simulation of an indirect blood pressure measurement (variable interbeat interval).

made more difficult than if the interbeat interval is constant. In Fig. 5-27 it is seen that, consistent with the results of the simulation using a constant interbeat interval (Fig. 5-22), the amplitude ratios of the fundamental frequency continue to increase during the period of phase difference overshoot (approximately beats 80 to 100). Of the four plots shown in Fig. 5-27, the amplitude ratio curve of the fundamental frequency has the least amount of irregularity and the most distinct stabilization, with a corner point in the trend at beat 102. This point compares well with the cuff diastolic point (beat 106, Fig. 5-25), confirming that the amplitude ratio of the fundamental frequencies of the distal and proximal waveforms may be used to indicate the cuff diastolic point even in cases where the interbeat interval varies considerably.

The irregularity in the phase difference curves may be smoothed significantly by applying the algorithm which computes time delays from phase differences (refer Section 3.3.5). Fig. 5-28 shows the results for the phase differences of Fig. 5-27b. The compensation for variations in interbeat interval is most noticeable for the fundamental frequency, in which the stabilization of the curve at the cuff diastolic point is made clearer than in Fig. 5-27b. However, the corner point is not marked distinctly because changes in this region are gradual, as the time delay reverts to its pre-occlusion value after the period of overshoot (beats 87 to 106). The improvement in the second harmonic curve is not as great as in the fundamental because, although the correction factor is proportional to the harmonic period, the response of the model is not as linear over the range of second harmonic frequencies

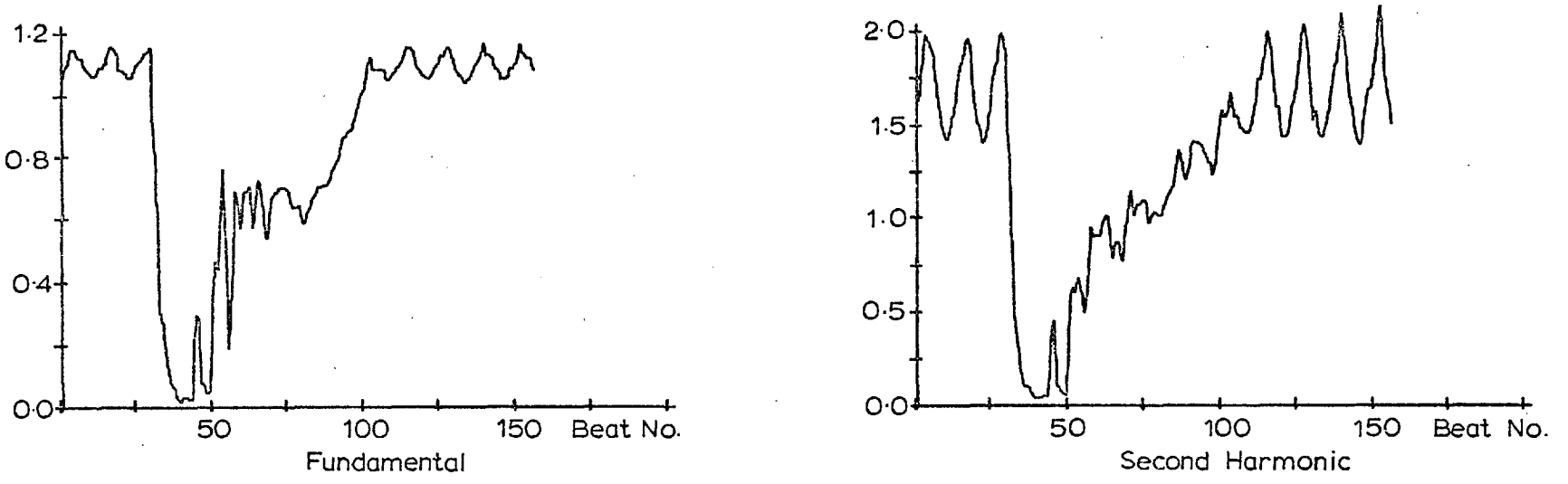


Fig. 5-27a : Distal : Proximal Amplitude Ratios

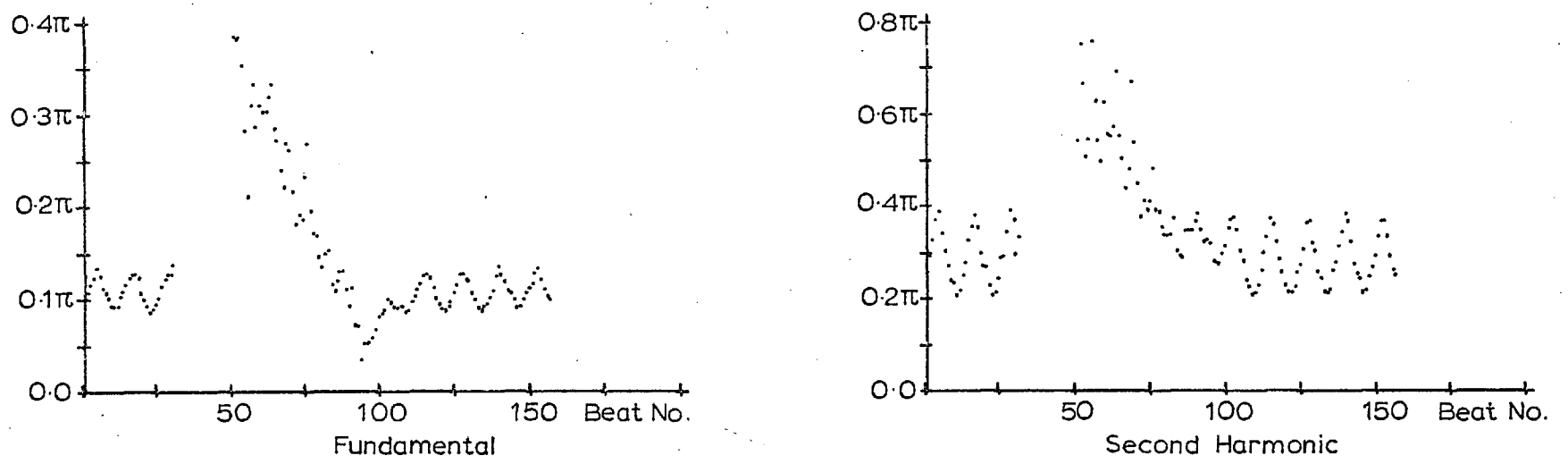


Fig. 5-27b: Proximal - Distal Phase Differences
(Simulation with variable interbeat intervals).

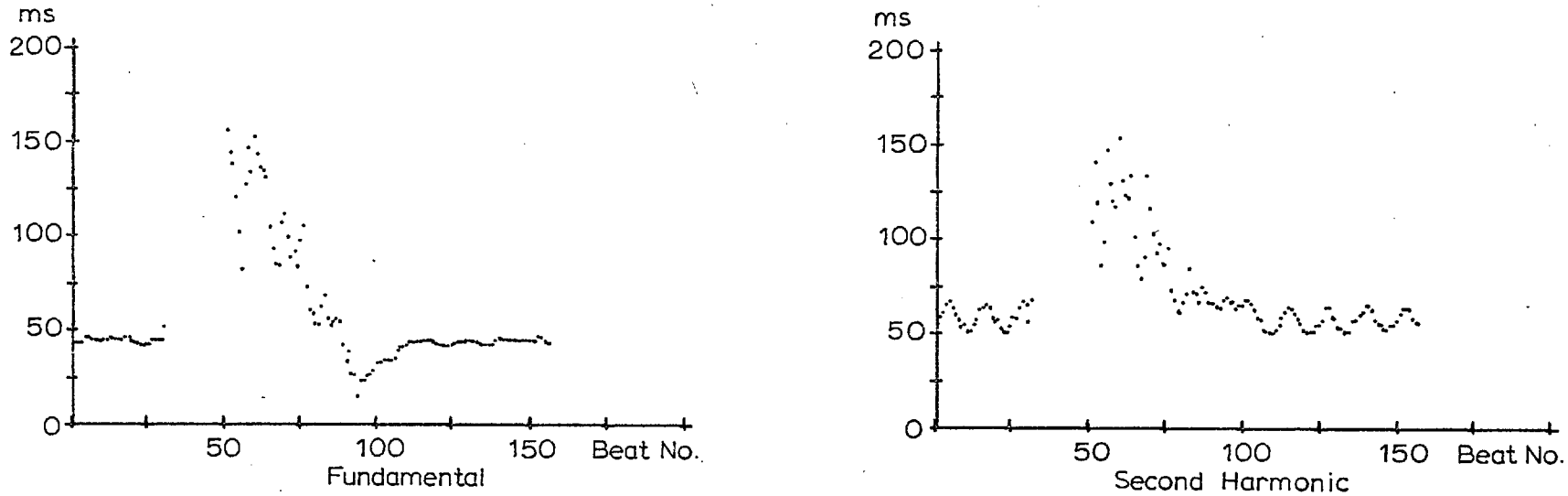


Fig. 5-28 : Harmonic time delays computed from phase differences.
(Simulation with variable interbeat intervals).

as it is over the range of fundamental frequencies.

The simulation using an input waveform with variable interbeat intervals has shown that the distal fundamental frequency is not affected to the same extent as the second harmonic. In addition, it appears that the first harmonic amplitude ratios of the distal and proximal waveforms may be used to indicate the cuff diastolic point, whereas the corresponding phase differences are difficult to interpret unless compensations are made for interbeat interval variations. The simulation has also shown that variations in systolic pressure can cause irregularities in the distal waveform when the cuff pressure is close to the systolic pressure.

5.5 SUMMARY

The simulation of an indirect blood pressure measurement using an electrical analogue model of the arm has provided waveforms which exhibit many of the features observed in the recordings of direct arterial pressures discussed in Chapter 3. By using a repetitive input signal it has been possible to examine the waveforms without effects caused by variations in interbeat interval and systolic and diastolic pressures. The modelling of the effects of a cuff by series switches has shown that an unstable situation exists whereby the brachial artery closes intermittently after flow has begun to pass beneath the cuff. Although the oscillations observed in the model occur at a frequency much greater than could be expected in the living system, the presence of instability provides an explanation for inflections seen in the systolic upstrokes of the distal waveforms in the practical recordings.

The use of a switch to simulate venous occlusion has shown that the venous pressure can rise significantly towards the end of the indirect measurement. Although this rise did not influence the arterial waveforms of the simulation, venous congestion could lead to an erroneous diastolic pressure measurement if the rate of cuff depressurization was significantly less than recommended. However, a more rigorous estimate of the venous compliance is required if the effects of the cuff on the distal venous system are to be examined critically.

It has been shown that in the model the cuff diastolic point can be located from a plot of successive time intervals measured from the QRS peak of the simulated E.C.G. to a defined point on the systolic upstroke of the distal waveform. These measurements are less meaningful in practical waveforms because there are beat-to-beat changes of waveshape due to variations in the higher harmonics which obscure the corner point in the trend.

The spectra of waveforms recorded during a simulation of an indirect blood pressure measurement have been computed and compared with the results of the analyses of the practical waveforms described in Chapter 3. As previously, it was found that the fundamental was the most reliable component and that the cuff diastolic point could be located with reasonable accuracy from a plot of successive amplitude ratios of the distal and proximal fundamental frequencies. On the other hand, it was found that the plot of the first harmonic phase differences of the proximal and distal waveforms showed an anomalous overshoot when near the cuff diastolic point which was not observed in the analyses of the practical waveforms. The reliability of the

amplitude ratio parameter has been confirmed by the simulation using waveforms with variable interbeat interval. In this simulation it was shown that the cuff diastolic point could be located with reasonable accuracy from the plot of the first harmonic amplitude ratios even though successive amplitudes related to different absolute frequencies. A detailed discussion of the sensitivity of the amplitude ratio and phase difference parameters to changes in waveshape follows in Chapter 6.

6. DISCUSSION

6.1 Partial-Beat Analyses

6.2 Evaluation of the Simulation

6.3 Theoretical Basis of the Waveform Analysis

6.4 Results of the Analyses

6. DISCUSSION

The simulation of an indirect blood pressure measurement has provided waveforms for analysis by computer programs used previously with corresponding practical waveforms. A comparison of the results of the analyses in the two cases showed close agreement between the first harmonic amplitude ratios of waveforms distal and proximal to the cuff but discrepancies were observed between the corresponding phase differences. The implications of these results are discussed in this chapter. A review of the simulation is given and the theoretical basis of the analysis is examined. The chapter concludes with a discussion of the results of the analyses with respect to the objective detection of the cuff diastolic point.

6.1 Partial-Beat Analyses

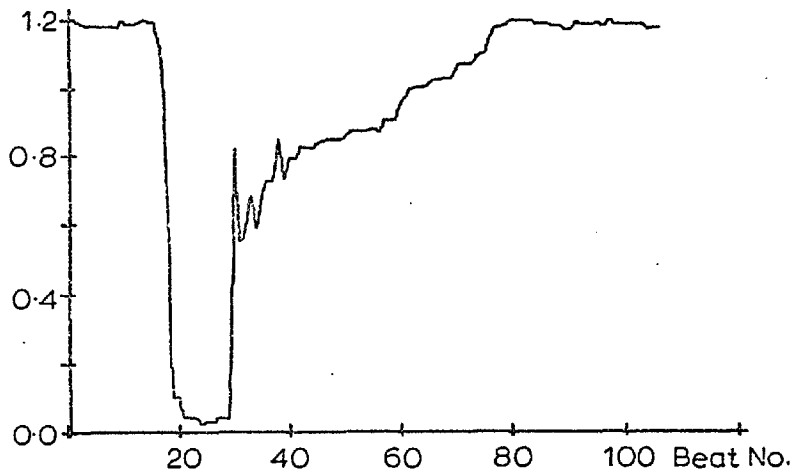
The major discrepancy between the first harmonic phase difference plots of the simulated and practical waveforms was the difference in the shapes of the curves for values occurring prior to the cuff diastolic point. For the practical waveforms, the phase difference decreased to its approximate pre-occlusion value when the distal diastolic pressure was still elevated above systemic diastolic pressure, with very little change in value occurring after this point (Fig. 3-16b). In contrast, during the corresponding period in the simulation the phase difference decreased to considerably less than its pre-occlusion value with a reversal in the slope of the trend occurring before the phase difference returned to its normal value at the cuff diastolic point (Fig. 5-22b). To investigate this discrepancy, the

simulated waveforms were examined for indications of the cause of this overshoot, and it was found that during the period in question undulations emerged in the distal waveforms during diastole (beats 57 to 77, Fig. 5-16). As such undulations did not occur in the practical recordings, it seemed likely that their presence in the simulated waveforms could account for the anomaly in the phase difference plots. Consequently, the analysis was repeated using a truncated period which excluded the undulations but was sufficiently long so as to include the main pulse of the waveform.

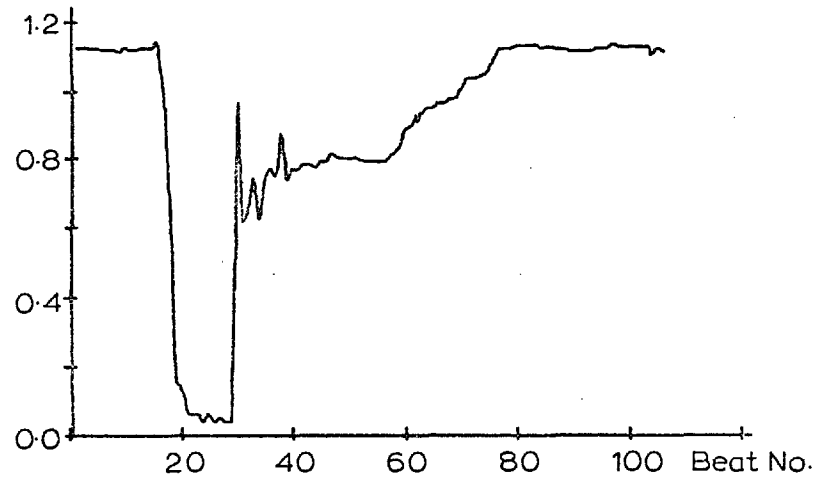
An inspection of the data (Fig. 5-16) showed that a period equal to 0.6 of the interbeat interval (beginning at the QRS peak of the E.C.G.) retained the bulk of the waveform but excluded the undulating portion. An analysis of the truncated waveforms was carried out, and the resulting first harmonic phase differences and amplitude ratios are shown in Fig. 6-1a. A comparison of the phase difference plot of Fig. 6-1a with the corresponding plot for the analysis using the full interbeat interval as period (Fig. 5-22b) clearly shows that the shape of the curve during beats 57 to 77 has changed from a slight overshoot to a monotonically decreasing trend. The change in shape suggests that the phase angle of the fundamental component is influenced significantly by small waveform irregularities. This is not surprising; the emergence of even brief irregularities will certainly introduce spectral power into the signal at the fundamental frequency. Furthermore, because the phase difference curves of Fig. 6-1a and 5-22b approach their pre-occlusion values at the cuff diastolic point with slopes of opposite sign, analyses using periods of intermediate lengths would produce

results more closely following those of the practical case. This was confirmed by carrying out analyses using periods equal to 0.7, 0.8, and 0.9 of the interbeat interval of the simulation. The results for the 0.8 interbeat interval analyses are shown in Fig. 6-1b. In each case, it was found that the initial portions of the phase difference curves were similar (beats 30 to 56) but the shape of approach to the cuff diastolic point was variable (beats 57 to 77). Such sensitivity to small variations of waveshape shows that the results obtained in the practical cases could well be variable in the region near the cuff diastolic point.

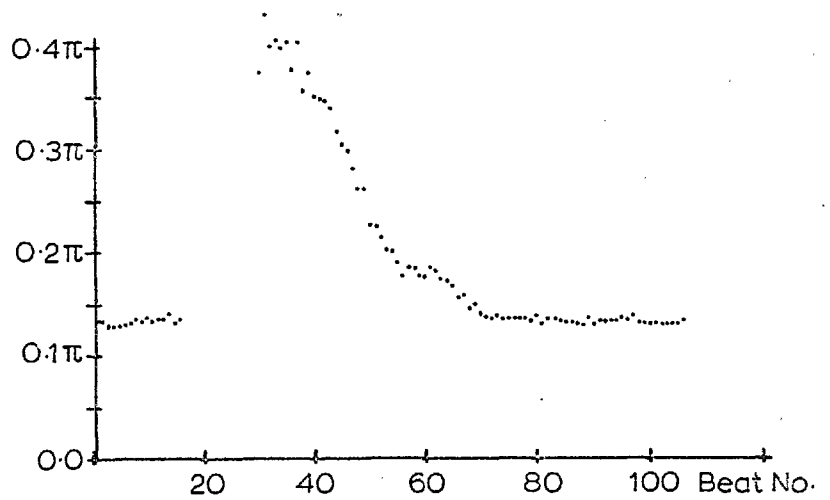
A comparison of the first harmonic amplitude ratio plots of the partial-beat analyses (Fig. 6-1) with that of the analysis using the full beat as the period (Fig. 5-22a) shows that their shapes are very similar. In particular, the position of the cuff diastolic point (beat 77) is marked by a distinct change of slope as the ratio stabilizes from a progressive increase, to its pre-occlusion value. The reason stated previously for the steady increase of this ratio prior to the cuff diastolic point was the steady decrease of the distal diastolic pressure from its elevated value (Section 5.4.4). It might be thought that shortening the period of analysis would affect the amplitudes because the beat has been truncated during diastole. However, a truncated beat beginning at the QRS peak of the E.C.G. includes the termination of the diastolic decline in pressure of the preceding beat, and even a period as short as 0.6 of the interbeat interval still contains the full amplitude of the pressure pulse. Consequently the increasing pulse pressure which occurs prior to the cuff diastolic point is seen as a



(a) Period = 0·6 interbeat interval



(b) Period = 0·8 interbeat interval



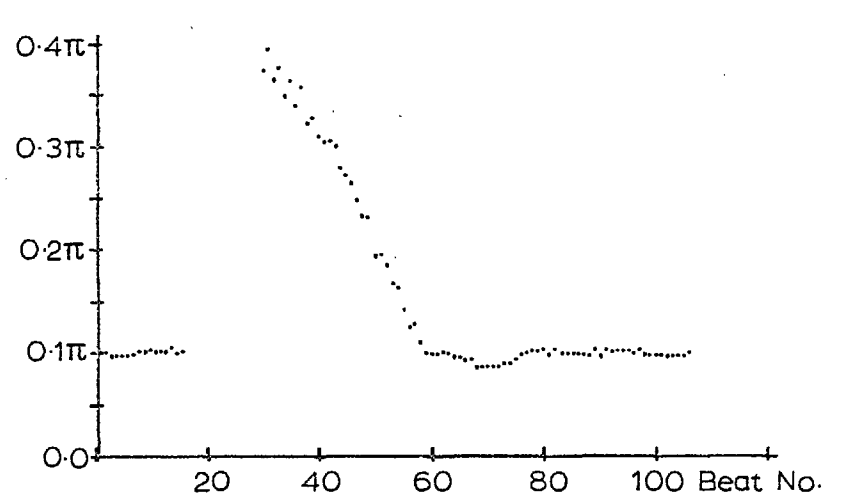
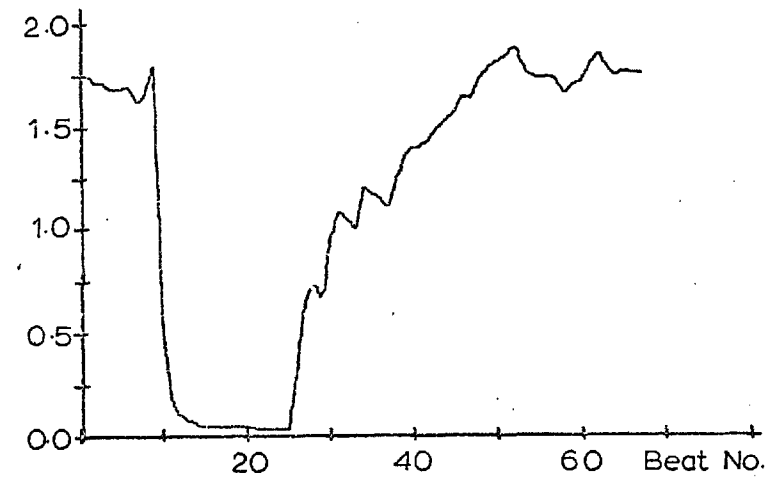


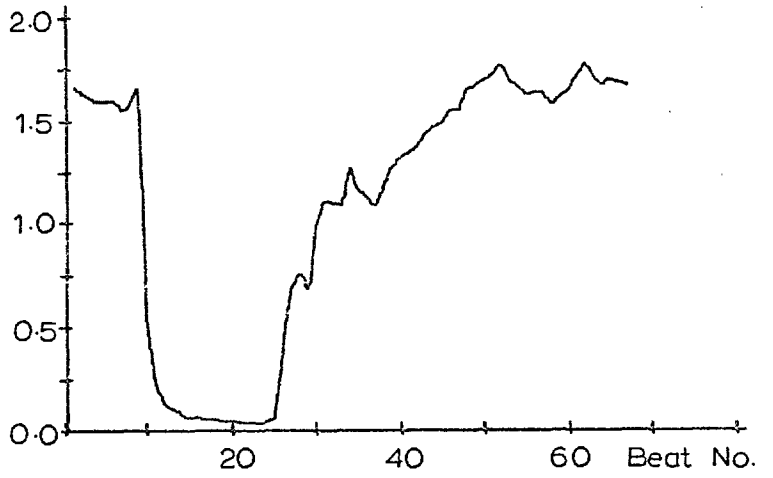
Fig. 6-1 : First harmonic amplitude ratios (upper) and phase differences (lower) of partial-beat analyses using simulated waveforms (data of Fig. 5-16).

corresponding increase in the fundamental amplitude ratio plots of the partial-beat analyses.

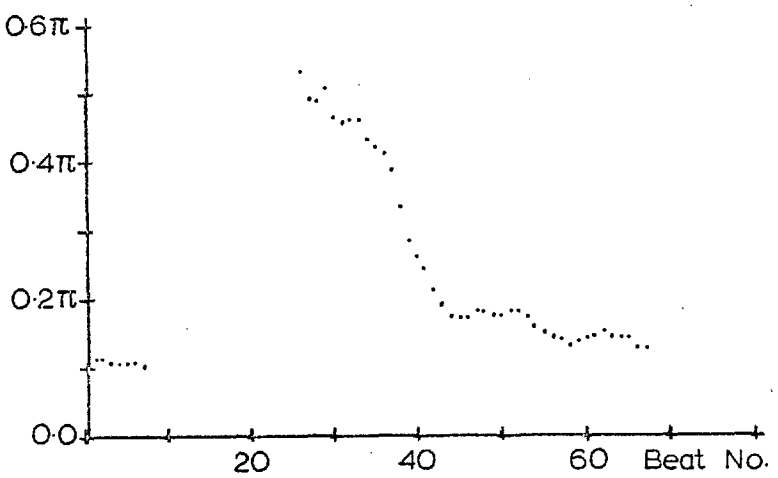
The partial-beat analyses of the model waveforms have provided evidence of two important characteristics of the first harmonic parameters of the proximal and distal waveforms. Firstly, that the phase difference parameter is sensitive to small waveshape details and is useful only for representing trends when the delay is changing rapidly; and secondly, that the amplitude ratio parameter is relatively insensitive to the length of the period and stabilizes at the cuff diastolic point in a well defined manner. To check the validity of these findings, partial-beat analyses were carried out using the practical waveforms of Fig. 3-2. The results of analyses using periods of 0.5 and 0.6 seconds are shown in Fig. 6-2a and 6-2b, respectively. These plots may be compared with those of the previous analysis using a fixed period of 0.7 seconds (Fig. 3-16). As the average interbeat interval in the record is approximately 0.8 seconds (the minimum being 0.725 seconds, refer Fig. 3-9) the three analyses use periods of about 62%, 75%, and 87% of the average interbeat interval. As expected, the three amplitude plots are very similar in shape, particularly so in the region of the cuff diastolic point (beat 52). Moreover, although the initial trends in the phase difference curves are similar (beats 33 to 43), there are variations in the shapes for the subsequent beats and there is no clear identification of the cuff diastolic point. However, the differences in the shapes of the curves in the latter region are not so marked as those of the partial-beat analyses using the model waveforms. This is because undulations during diastole are not present in the practical data to the same



(a) Period = 0·5 second



(b) Period = 0·6 second



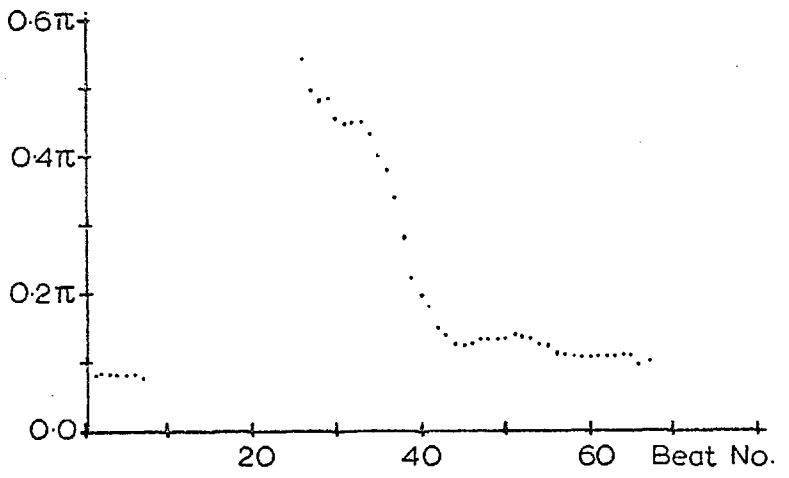


Fig. 6-2: First harmonic amplitude ratios (upper) and phase differences (lower) of partial-beat analyses using practical waveforms (data of Fig. 3-2).

extent as in the simulated waveforms. Nevertheless, there are many factors which influence the shape of the diastolic portion of the pressure wave, and published records show considerable variation in this region (Schultz, 1972). It is therefore concluded that the phase difference parameter is unreliable and the fundamental amplitude ratio is the most useful parameter for locating the cuff diastolic point.

6.2 Evaluation of the Simulation

The simulation of indirect blood pressure measurement was undertaken using an electrical analogue model composed of a number of arterial segments and peripheral terminations. Each arterial segment contained three elements designed according to the transmission line analogy using published arterial data. The peripheral terminations were designed to imitate the damping of the pressure pulse in the peripheral vessels. The input impedance of the model was found to be similar to that of a model of the leg described in the literature, except that the variations with frequency tended to be greater. This is thought to be due to the omission of correction networks compensating for true velocity profiles and wall viscoelasticities in the arterial segments.

The effects of the cuff were modelled by electronic switches inserted in the brachial and venous paths. Simulations of indirect blood pressure measurement were carried out using an input representing the aortic arch blood pressure waveform, and the recordings were compared with practical data. The simulation has led to a far greater understanding of the events which take place during an indirect blood pressure measurement.

Oscillations of the arterial switch in the model showed that the artery under the cuff is unstable and produces inflections in the systolic upstrokes of the distal waveforms. The model also exhibited the elevation of the distal diastolic blood pressure prior to the cuff diastolic point, matching what was observed in the practical recordings. The large rise in the simulated blood pressure in the venous system distal to the cuff illustrates the need for a cuff deflation rate not less than the recommended rate; otherwise, venous congestion could cause an erroneous measurement of the diastolic blood pressure.

The least satisfactory point in the design of the model is the representation of the cuff. As described in Section 5.3.1, the use of switches to simulate the effects of the cuff does not account for states of partial arterial occlusion. The simulation also does not include representations of the impedance of the cuff and its action in occluding a length of artery. Only if these features were included in the model would it be worthwhile improving the arterial segments by the addition of the correction networks discussed in Section 4.3. In this event, the variations with frequency of the response of the improved model would be reduced, enabling the use of more realistic input waveforms containing higher harmonics. As a consequence, the distal waveforms during the simulation would become more authentic with the largest changes occurring when the brachial artery is constricted and represents a high resistance to flow, i.e. during the period immediately following the cuff systolic point. No great changes would be expected in waveforms near the cuff diastolic point except for the reduction in amplitude of the undulations during diastole. Therefore it is doubtful if a more

complex model would lead to any difference in the conclusions reached concerning the location of the cuff diastolic point by signal analysis techniques. For this reason, it would be unnecessary to refine the model, as the simulation carried out has proved adequate for the purposes of the present study.

The results of the analyses of the simulated waveforms have greatly helped in the interpretation of those obtained from the practical recordings. Except for the period immediately following the cuff systolic point, the amplitude ratios of the first harmonics of the distal and proximal waveforms showed similar variations in both the simulated and practical recordings, and confirmed that the trend stabilizes in a distinct manner at the cuff diastolic point. In contrast, the corresponding variations of the first harmonic phase differences of the analysis using the simulated waveforms were inconsistent with those obtained using the practical data. Partial-beat analyses showed that the discrepancies were due to undulations in the distal waveform of the model. Although the undulations were thought to be caused by insufficiently damped resonances in the model, this action does not affect the validity of the first harmonic amplitude ratio parameter as a means of locating the cuff diastolic point in the indirect measurement cycle. The simulation has therefore proved valuable in diverting the emphasis of the analysis away from the characterization of a decreasing delay between the proximal and distal waveforms by means of the phase difference parameter. In addition, it has shown that the phase difference parameter is consistent only when the delay between the waveforms is changing by a relatively large amount with each successive beat. Unfortunately, in the region of interest (approaching the cuff

diastolic point) the change of delay is small and the variation of the first harmonic phase difference becomes confused with other changes caused by minor alterations in waveshape. The interest in the analysis now concerns the first harmonic amplitude ratio parameter, which behaves in a dependable manner as the cuff pressure decreases towards the value of the diastolic blood pressure. It is therefore concluded that the results of the practical waveform analyses discussed in Chapter 3 were not atypical. The simulation has established confidence that similar results would be obtained in the general case.

6.3 Theoretical Basis of the Waveform Analysis

Harmonic analysis has provided simple parameters with which successive beats may be compared. However, the approach is not as simple as it might superficially appear and it is important to understand the underlying principles of signal analysis on which it depends.

The most direct approach to the analysis of a single beat would be to consider it as a transient signal, successive beats being members of an ensemble. Each beat may therefore be represented by a repetitive signal multiplied by a rectangular time window having unity amplitude for the duration of the beat and zero amplitude elsewhere. In the frequency domain this is equivalent to taking the line spectrum of the repetitive waveform and convolving it with the $\frac{\sin x}{x}$ spectrum of the window, resulting in a continuous spectrum. If the continuous spectrum was computed for each beat, then successive spectra could be compared at any number of corresponding frequencies. Obviously this procedure would require a large amount of computation which would make it

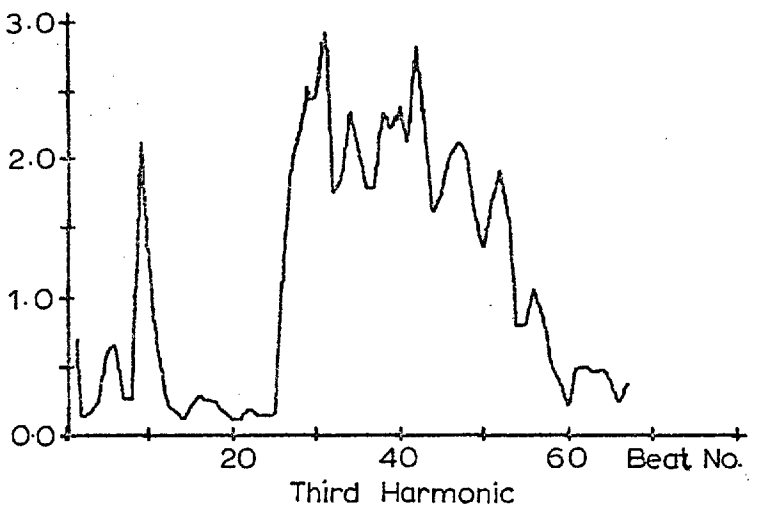
difficult to implement in a practical instrument. It might be thought that a simplification could be effected by assuming that the waveform is indeed repetitive but attention is to be paid to it only during one interbeat interval, ignoring the waveform outside this time. In this case each beat could be represented in the frequency domain by a line spectrum but since beats do not necessarily have the same interval, spectral lines will occur at different frequencies making comparisons between spectra theoretically impossible. In practice, some form of comparison can be made between like harmonic numbers, as described in Section 3.3.5. The difficulty is paralleled in the time domain in that successive beats having different periods cannot be compared beyond the end of the shortest beat.

A realistic approach to comparing waveforms of different periods is to define them over a constant period less than the minimum interbeat interval found in the record. This form of analysis is similar to the treatment of evoked responses in neurological studies. In such studies successive responses are compared by isolating sections of a recording beginning at the time of occurrence of the stimulus and terminating after an arbitrary time interval has elapsed. In the cardiovascular system the QRS peak of the E.C.G. can be considered to be a stimulus which evokes a response in the form of a cardiac contraction causing the arterial blood pressure to rise from diastolic pressure to systolic pressure. As time proceeds during the relaxation phase of the cardiac cycle the shape of the blood pressure wave becomes relatively featureless as the response decays. Hence the truncation of beats with a long interbeat interval does not destroy information of much

significance. The analysis can proceed on the basis that each beat is a transient signal starting at the QRS peak of the E.C.G. and terminating after the fixed period. As before, this analysis will yield continuous spectra. However, if repetitive waveforms are assumed rather than transients, the resulting line spectra now have the same frequencies for each beat and form a valid basis for comparison. These spectral lines coincide with the continuous spectra of the transient signals at the specific frequencies involved and therefore provide a limited number of 'samples' of the continuous spectra. The simplification afforded is obtained at the expense of the number of comparisons that can be made between spectra. In practice, it has been found that only the low frequencies provide reliable information and a single frequency is adequate for comparisons.

6.4 Results of the Analyses

As the circulatory system is relatively stable, the pressure waveforms should be regular in shape except for differences due to interbeat interval variations, changes in the contractile force of the heart, and reflections. As a result the higher harmonics of the waveforms would be expected to be less repeatable than the lower frequencies. This was found to be the case with both practical and simulated waveforms and hence the discussions in this thesis largely concern the fundamental and second harmonic components. The variability of the third and fourth harmonics may be judged from the plots of amplitude ratios shown in Fig. 6-3a and 6-3b for the practical and simulated waveforms, respectively. Each of these figures shows a considerable amount of noise and there are no significant



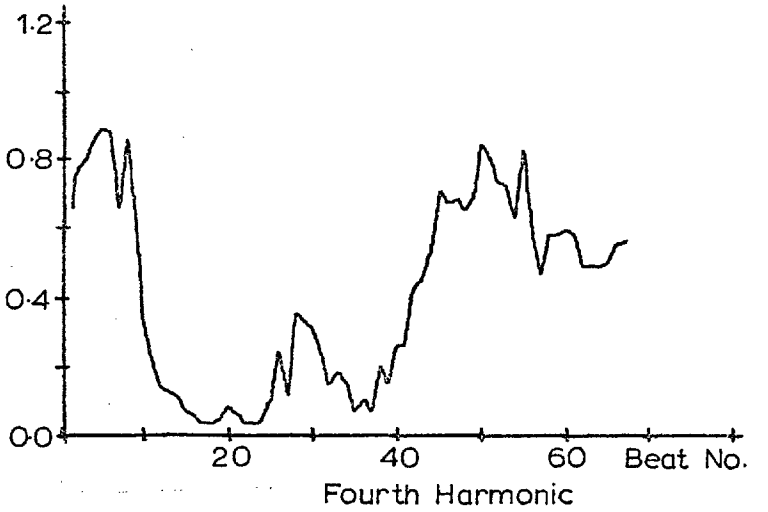
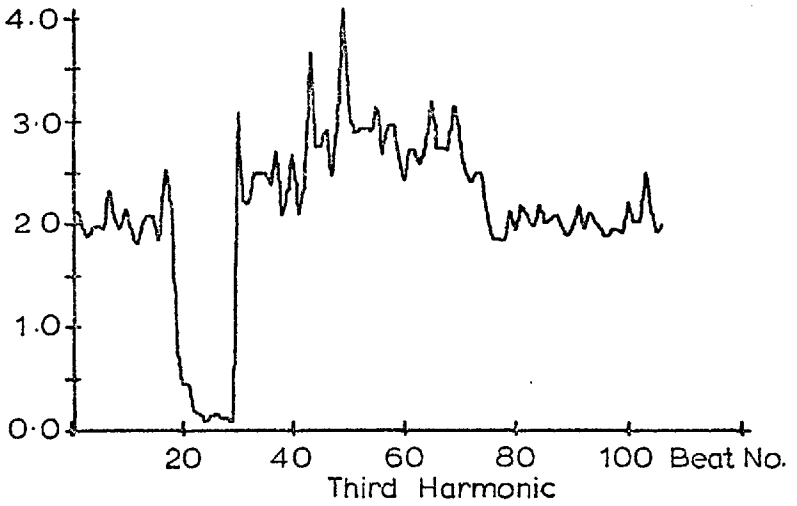


Fig. 6-3a: Third and fourth harmonic amplitude ratios of practical waveforms (data of Fig.3-2).



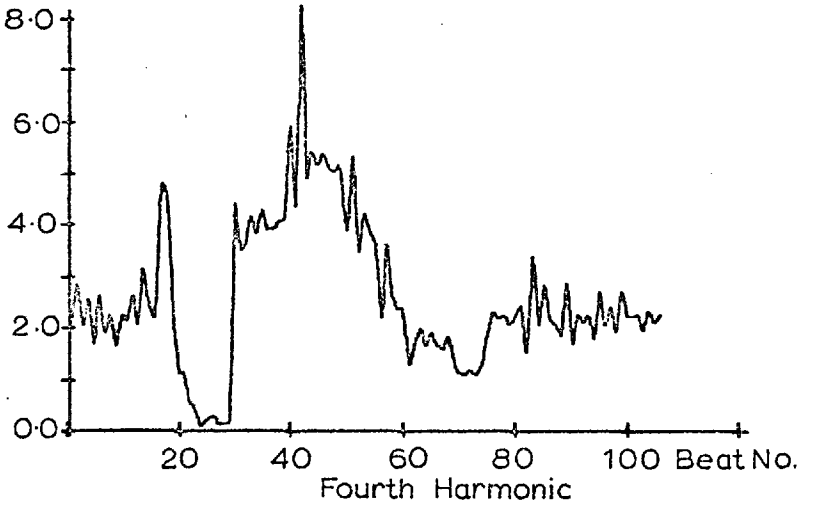


Fig. 6-3b: Third and fourth harmonic amplitude ratios of simulated waveforms (data of Fig.5-16).

features except for the suppression of the ratios during the period of total arterial occlusion. Certainly there are no distinct changes occurring by which the cuff diastolic point may be identified.

The variability of the higher harmonics is in accord with the random delays reported to occur between the two photoplethysmographic waveforms obtained with a finger cuff apparatus (refer Section 1.3). For the measurement of these delays, the waveforms from the transducer were high-pass filtered to remove low-frequency drift and partially differentiate the pulse to obtain suitable signals for timing purposes. The time constants used in the filtering were such that the fundamental components were largely suppressed and hence the time delay measurements were based on signals which contained a high proportion of the higher harmonics. It is therefore not surprising that the measurements did not clearly indicate the cuff diastolic point in the indirect measurement cycle.

The results of the analyses have not yielded any fresh information concerning the cuff systolic point: this point is indicated clearly by the first distal pulse after total arterial occlusion. However, several interesting details have emerged concerning the trends of successive amplitude ratios and phase differences, particularly as the cuff diastolic point is approached. It has been shown that there is a decreasing delay between the fundamental components of waveforms proximal and distal to the cuff as the cuff pressure is reduced, but contrary to what was originally expected, this delay (represented by the phase difference parameter) does not stabilize at the cuff diastolic point but rather at some previous time. In contradistinction to

the trend in the phase differences, the trend in the first harmonic amplitude ratios has been shown to indicate the cuff diastolic point in a well defined manner. This arises because the distal pulse pressure increases steadily just prior to complete arterial patency, causing the stabilization of the amplitude ratio to be distinct. The simulation using the model has shown that this phenomenon also occurs in the analysis of generalized waveforms. This gives confidence that waveform analysis can be used to locate the point in the indirect blood pressure measurement cycle when the major features of an indirect distal wave are no longer modified by the effects of the cuff, thus providing an objective method of measuring diastolic blood pressure indirectly.

7. CONCLUSION

7.1 Summary of the Research

7.2 Considerations for an Instrument

7.3 Proposals for Further Work

7. CONCLUSION

7.1 Summary of the Research

The research described in this thesis forms part of a general study of biological signal processing being carried out in the Engineering in Medicine laboratory. Within this context signal analysis concepts and techniques have been applied to a clinical measurement problem, with the ultimate aim of developing an instrument for the indirect measurement of blood pressure. It was intended also that this work should have an applicability outside the immediate range of the specific problem concerned by contributing to the general repertoire of techniques being developed to handle all manner of biological signals. This has been achieved in so far as several data handling procedures developed in the course of this work are now in general use in the laboratory.

The measurement of blood pressure in the traditional indirect manner using Korotkoff sounds specifies the waveform by the maximum (systolic) and minimum (diastolic) pressures reached during the heart beat cycle. It is therefore appropriate that an alternative method of measuring blood pressure should be directed towards measuring the same two parameters, which are now well established as standard clinical indices. A study of the literature indicated that the task of developing a theoretical basis for describing the haemodynamic conditions occurring beneath an occlusive cuff would be complex. It was therefore decided to investigate the nature of the blood pressure waveform and the manner in which it varies during an indirect blood pressure measurement cycle by examining data recorded from a live subject.

The work followed reports of a decreasing delay observed between waveforms proximal and distal to the cuff as the measurement proceeds. Whilst apparatus based on the measurement of this delay has achieved some success in measuring blood pressure, there is uncertainty in locating the point where the delay disappears, thus making it a poor indicator of the cuff diastolic point. For the current study it was decided that signal analysis techniques should be used to characterize the delay phenomenon in more detail, with the aim of establishing an alternative method of locating the cuff diastolic point.

Waveforms for analysis were obtained by simultaneously recording direct arterial blood pressures in the ascending aorta and radial arteries while indirect blood pressure measurements using a cuff were performed in the normal manner. Simple measurements of time intervals made on these data confirmed that they were unreliable for indicating the cuff diastolic point although a general pattern of decreasing delay could be seen. Representation of the waveforms in the frequency domain yielded better results. It was found that there were several ways in which frequency analysis could be applied. The best method was to modify each beat by truncating it to a fixed period so that all beats had the same duration and could be treated as an ensemble. The continuous frequency spectrum of an isolated beat was reduced to a simple line spectrum by assuming the beat to be a single cycle of a repetitive signal. Since the spectra of all beats contained the same frequencies they could be compared at each harmonic. It was found that the first harmonic showed the most consistent behaviour and little significance could be attached to the higher harmonics. During the course of a blood

pressure measurement the trend in the first harmonic phase differences of the proximal and distal waveforms showed that a decreasing phase shift occurred as the cuff pressure decreased from systolic blood pressure but there was an anomalous corner point where the trend stabilized to the pre-occlusion value prior to, rather than at, the cuff diastolic point. In contrast, the corresponding trend in the first harmonic amplitude ratios of the distal and proximal waveforms was found to stabilize consistently at the cuff diastolic point.

The characterization of the cuff by its notional impulse response was investigated but the interpretation of the results was found to be subjective.

To test the generality of the results and obtain further insight into the problem an electrical model of the arm was constructed using the transmission line analogy of the arterial system. Complex arterial terminations were designed to simulate the damping of the pressure pulse in peripheral vessels. The effects of the cuff were represented by switches in the arterial and venous lines. Waveforms recorded during simulations of indirect blood pressure measurements were analysed and the results were compared with those obtained using the practical data. Inconsistencies in the phase results led to a further investigation which revealed that the phase difference parameter was not well defined when the delay between the proximal and distal waveforms became small. However, it was found that in each of the analyses performed the amplitude ratio parameter could be used to locate the cuff diastolic point with confidence. The objectivity with which this point is indicated suggests that the amplitude ratio parameter might be exploited successfully in

an instrument designed to recognize the times at which the cuff pressure is equal to the systolic and diastolic blood pressures.

7.2 Considerations for an Instrument

From the start of the project it was realized that for use in a clinical environment a blood pressure measurement apparatus would need to utilize indirect waveforms. The detection of the cuff diastolic point by harmonic analysis would require two such waveforms to be recorded, at sites proximal and distal to the occlusive cuff. As the measurement proceeds there will be a relationship between the proximal and distal waveforms which relates to the action of the cuff. It is expected that harmonic analyses of these waveforms will reveal trends similar to those observed in the results of the analyses of the proximal and distal pressure waves. If the indirect waveforms bear a constant relationship to the direct waveforms, the first harmonic amplitude ratio is probably the only parameter required to be computed because, as shown in this thesis, this parameter for direct pressure waveforms is well defined throughout the entire measurement cycle. The phase difference parameter may prove useful as a coarse gate for the period in which the delay between the waveforms is large, i.e. for the period immediately following the cuff diastolic point, if the amplitude ratio is not well defined in this region.

On the assumption that the indirect waveforms will show an objective behaviour of the first harmonic amplitude ratio similar to that of direct pressure waveforms, several predictions can be made as to the probable form of a practical instrument designed to locate the cuff systolic and diastolic points. The instrument

will require three input waveforms, namely the E.C.G. and the two pulsatile waveforms detected by transducers either side of the occlusive cuff. The E.C.G. will be amplified and processed by analogue circuits to provide a timing pulse at the QRS peaks. The transducer waveforms will require more complicated processing to extract the first harmonic amplitude ratio. Low frequency analogue filtering is not appropriate because of the wide range of heart rates likely to be encountered (3 to 1). A more effective method of isolating the fundamental frequency is digital filtering. Although a general-purpose computer could well be used for handling large amounts of recorded data, it is envisaged that the processing tasks could be performed by special-purpose digital circuitry. Four basic functions are required: analogue to digital conversion, harmonic analysis, amplitude ratio calculation, and logic to recognize the cuff systolic and diastolic points. The manner in which these functions may be undertaken is discussed as follows.

The time of the analysis period is obtained by taking a suitable fraction (e.g. $\frac{3}{4}$) of the average of several interbeat intervals occurring prior to the cuff inflation. Using the QRS timing pulse as an initiating trigger, the transducer waveforms are sampled by ADC circuits for this period and the samples are held in a digital store. It may be possible to use a single ADC circuit for both transducer waveforms without subsequent demultiplexing if the harmonic processing is programmed for indexing alternate samples in the store. Although tests would be required to determine the optimum digitization rate, the number of samples to be stored is not likely to be large; a sampling rate of 100 Hz per channel is more than adequate.

Analysis of the stored samples would proceed immediately the period is complete. It may be possible to simplify this task to reduce the number of calculations. For example, as an alternative to Fourier analysis the coefficients of the first harmonic may be estimated by multiplying the waveform by a square wave rather than a sine wave of the fundamental frequency. The multiplications of the trigonometric terms in the DFT equations (Eq. 3.6 and 3.7) therefore reduce to additions or subtractions according to the sign of the square wave at each sample in the data sequence. Because the energy in the higher harmonics of the pulse wave is small, the error in performing this estimation could well be quite low, e.g. the fundamental frequency of a pressure wave containing as high as 10% of third harmonic would be estimated with an error of the order of 3% since the square wave contains no second harmonic and only 33% of third harmonic. If the estimation of the first harmonic in this manner was found to be satisfactory, the signal processing requirements for a clinical instrument could be reduced significantly.

The amplitudes of the harmonics are calculated as twice the square root of the sum of the squares of the real and imaginary Fourier coefficients. For the instrument, the computation of the square roots could be omitted, so that the amplitude ratio is replaced by the power ratio. This ratio is likely to be an even sharper indicator of the cuff diastolic point than the amplitude ratio. This is because the maximum amplitude ratio is slightly greater than unity and amplitude ratios calculated during the occlusive period are less than unity; hence their squares will be even smaller, and the stabilization of the power ratio will be made more distinct.

For real-time operation, the cuff diastolic point could be recognized by the increase of the power ratio to say 95% of the average value calculated for several beats prior to the occlusion. Alternatively, successive ratios could be stored and subsequently examined to find the point of stabilization; this would require additional trend detection circuitry and would add considerably to the complexity of the instrument.

The recognition of the cuff systolic point would not necessarily be performed by the digital circuits utilizing the power ratio. It could well be simpler to use analogue circuits to detect the first distal pulse during the cuff depressurization.

It therefore appears that the processing tasks would not prove an insurmountable barrier to the implementation of the amplitude, or power, ratio parameter in an instrument. The factor requiring careful attention is the nature of the indirect waveforms to be processed. An associated problem is the design of the transducers used in their detection.

7.3 Proposals for Further Work

It is suggested that the next stage of the research be orientated towards the use of indirect waveforms recorded from a variety of subjects. The use of photoplethysmographic waveforms is a possibility that needs to be explored, as such waveforms can be detected non-invasively by simple apparatus. Ultrasonic blood velocity transducers could be considered also, but these devices are more complicated and require additional electronic circuits for their operation. Irrespective of the type of pulse detector employed, the placement of the transducers with respect to the cuff needs to be investigated to determine the optimum positions.

As the blood pressure retains its pulsatile waveshape even in the small arteries, it should be possible to make valid measurements with the cuff on an extremity smaller than the arm, e.g. the finger. Because of the augmentation of the pulse pressure as it travels peripherally, the systolic pressure in the extremity is higher than systemic and the diastolic pressure is lower. Nevertheless, measurements at the extremities are likely to be useful in following trends in the blood pressures.

The practical design of an instrument should not be attempted until the behaviour of the indirect waveforms has been assessed and the transducers have been developed to a satisfactory stage. The data processing tasks of the instrument can be simulated on a small computer until a settled procedure has been formulated.

As the usefulness of any indirect method of blood pressure measurement is judged by comparison of its results with those obtained in the normal clinical manner, simultaneous recordings of Korotkoff sounds should be taken in future experiments using indirect waveforms.

APPENDICES

A. THE MODEL OF THE ARM

A.1 The Arterial Segments

A.2 The Peripheral Terminations

A.3 Practical Construction of the Model

B. ANCILLARY CIRCUITS

B.1 The Cuff Pressure Generator

B.2 The Arterial and Venous Switches

B.3 The Buffer Amplifiers

C. COMPUTER PROGRAMS

C.1 Data Processing Procedure

C.2 Main Programs

C.3 Subroutines

C.4 Ancillary Routines

A. THE MODEL OF THE ARM

This appendix contains details of the design and construction of the electrical analogue model of the vasculature of the arm. Calculations relating to the arterial segments and the peripheral terminations are described and tables of arterial data and component values are provided. A circuit diagram of the model is given and constructional details are outlined.

A.1 The Arterial Segments

The model of the arterial system of the upper limb comprises 19 segments representing the subclavian, vertebral, axillary, brachial, ulnar, radial, and interosseous arteries. The connections of the arterial segments (coded according to the notation used by Westerhof et al., 1969) are shown in Fig. A-1. Each segment is specified by four parameters, namely the length, internal radius, wall thickness, and Young's modulus of the wall material. These data (listed in Table 1) are taken from the table of physiological data in Westerhof et al. (1969).

Each segment is modelled by the symmetrical (Pi) network shown in Fig. A-2. It is to be noted that this circuit is the basic electrical analogue of a short section of an artery (refer Section 4.2) except that the shunt conductance has been omitted, i.e. the leakage through side branches is ignored. The values of resistance R, inductance L, and capacitance C are given by the following equations (refer Section 4.2.2).

$$R = \frac{8\mu}{\pi r^4} l \qquad L = \frac{\rho}{S} l \qquad C = \frac{3S(\alpha+1)^2}{E(2\alpha+1)} l$$

where $S = \pi r^2$

r = internal radius

$a = \frac{r}{h}$

h = wall thickness

E = Young's modulus

l = segment length

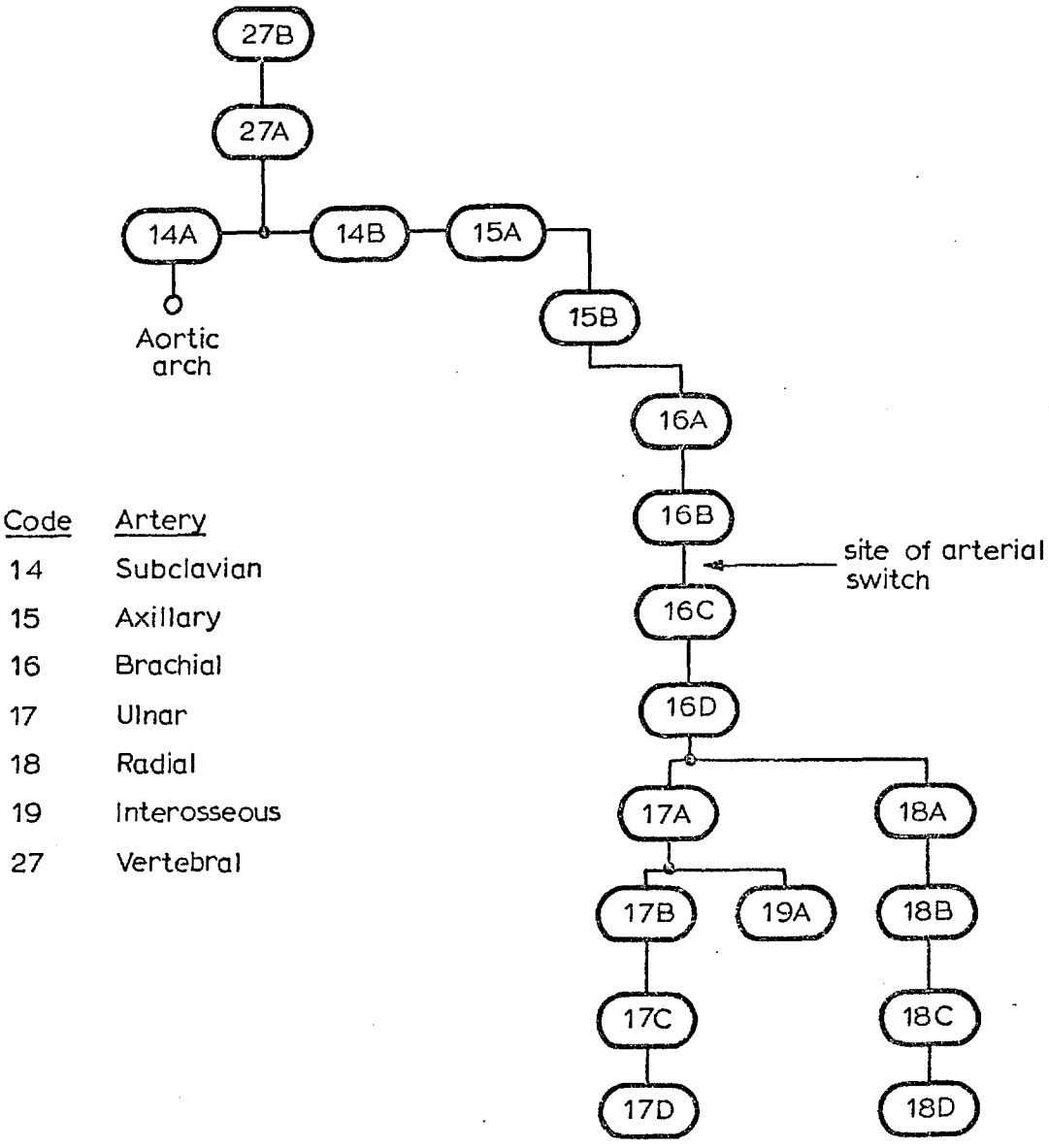
μ = viscosity of blood

ρ = density of blood

Working in the CGS system of units, and assuming that the viscosity and density of blood are 0.03 Poises and 1.05 g/cm^3 respectively (Westerhof et al., 1969), calculations using the above equations with the data of Table 1 give the component values listed in Table 2. From a practical standpoint, the resistances lie within a convenient range, varying from 8Ω in the subclavian to 8800Ω in the interosseous segment. For a time scaling of 1000 times real frequency, the values of the reactive components also lie in convenient ranges. The inductances range from 6 mH in the subclavian to 318 mH in the interosseous segment, and the capacitances range from 9945 pF to 93pF respectively in the same arteries. For the practical construction of the model the capacitances of adjacent networks are summed to form one capacitor at each junction, the values of which are listed in Table 3.

A.2 The Peripheral Terminations

The model of the damped peripheral resistance comprises four sections representing the small arteries, the arterioles, the capillaries, and the venous system (Fig. A-3). The total resistances in the peripheral circuits were taken from Noordergraaf et al. (1963), the values being 126 KΩ for the ulnar and vertebral arteries, 202 KΩ for the radial artery, and 400 KΩ for the interosseous artery. For the three arteries of



Code	Artery
14	Subclavian
15	Axillary
16	Brachial
17	Ulnar
18	Radial
19	Interosseous
27	Vertebral

Fig. A-1 : Arterial segments of the arm (after Westerhof et al., 1969).

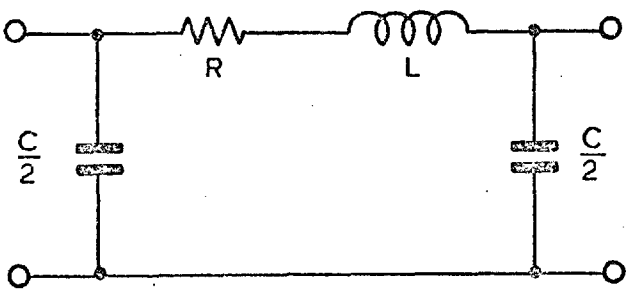


Fig. A-2 : The segment components.

ARTERIAL DATA
****

SEGMENT IDENTIFICATION ********** CODE	NAME OF ARTERY	SEGMENT LENGTH (CM)	INTERNAL RADIUS (CM)	WALL THICKNESS (CM)	YOUNGS MODULUS (X10**6)
14A	SUBCLAVIAN	3.4	0.423	0.067	4.0
14B	SUBCLAVIAN	6.8	0.403	0.066	4.0
15A	AXILLARY	6.1	0.364	0.062	4.0
15B	AXILLARY	5.6	0.314	0.057	4.0
16A	BRACHIAL	6.3	0.282	0.055	4.0
16B	BRACHIAL	6.3	0.266	0.053	4.0
16C	BRACHIAL	6.3	0.250	0.052	4.0
16D	BRACHIAL	4.6	0.236	0.050	4.0
17A	ULNAR	6.7	0.215	0.049	8.0
17B	ULNAR	6.7	0.203	0.047	8.0
17C	ULNAR	6.7	0.192	0.046	8.0
17D	ULNAR	3.7	0.183	0.045	8.0
18A	RADIAL	7.1	0.174	0.044	8.0
18B	RADIAL	7.1	0.162	0.043	8.0
18C	RADIAL	7.1	0.150	0.042	8.0
18D	RADIAL	2.2	0.142	0.041	8.0
19A	INTEROSSEOUS	7.9	0.091	0.028	16.0
27A	VERTEBRAL	7.1	0.188	0.046	8.0
27B	VERTEBRAL	7.7	0.183	0.045	8.0

Table 1 : Arterial data (after Westerhof et al., 1969).

VISCOSITY OF BLOOD = 0.03 POISE
DENSITY OF BLOOD = 1.05 GM/CC

SEG.	C	L	R
14A	5626	6.351	8.113
14B	9945	13.994	19.695
15A	7055	15.387	26.545
15B	4586	18.983	44.008
16A	3937	26.478	76.104
16B	3447	29.759	96.134
16C	2947	33.690	123.209
16D	1891	27.604	113.285
17A	1083	48.444	239.542
17B	954	54.340	301.406
17C	833	60.745	376.644
17D	410	36.927	252.034
18A	697	78.379	591.729
18B	584	90.421	787.516
18C	483	105.467	1071.407
18D	131	36.466	413.362
19A	92	318.348	8800.815
27A	833	67.140	434.199
27B	853	76.847	524.503

FOR 1000 X REAL-TIME FREQUENCY SCALING...

C IS IN PICOFARADS
L IS IN MILLIHENRIES
R IS IN OHMS

Table 2 : Segment component values.

Junction	Capacitance (pF)
14A, 14B, 27A	8202
27A, 27B	844
27B, peripheral circuit	427
14B, 15A	8500
15A, 15B	5820
15B, 16A	4260
16A, 16B	3690
16B, switch	1723
switch, 16C	1474
16C, 16D	2420
16D, 17A, 18A	1836
17A, 17B, 19A	1065
17B, 17C	894
17C, 17D	622
17D, peripheral circuit	205
18A, 18B	642
18B, 18C	534
18C, 18D	307
18D, peripheral circuit	65.5
19A, peripheral circuit	46.5

Table 3 : Circuit capacitor values.

	Ulnar Vertebral	Radial	Interosseous
Resistances (KΩ)			
R1	15.5	25	49.5
R2	71.5	114	227
R3	26	42	82.5
R4	13	21	41
Total	126	202	400
Capacitances (μF)			
C1	.015	.01	.0047
C2	.047	.033	.01
C3	.47	.28	.15

Table 4 : Peripheral resistance component values.

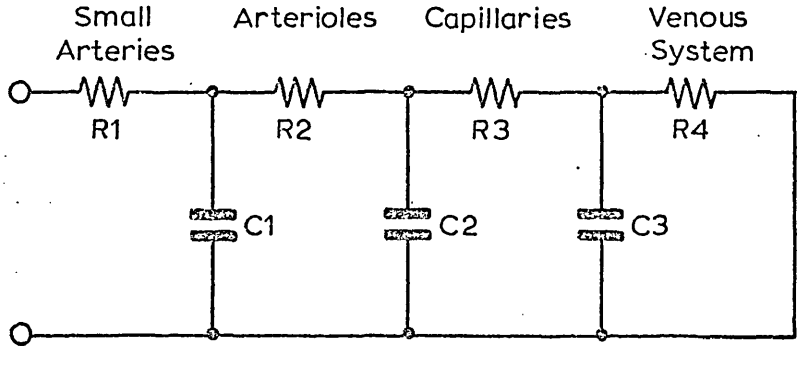


Fig. A-3 : Model of the peripheral circulation.

the forearm, the equivalent parallel resistance to flow is 65 KΩ. According to the scaling used by Noordergraaf et al. (1963), if a voltage of 'b' V represents a pressure of 'a' mm Hg, then the blood flow in cm^3/s is equal to 1.33 $\frac{a}{b}$ times the current flow in mA. Therefore if a=b=1 and the mean pressure at the periphery is taken to be 97 mm Hg (Guyton, 1966), then by Ohm's law the total forearm blood flow is equal to $1.33 \times \frac{97}{65}$ cm^3/s, i.e. 1.98 cm^3/s. This figure compares well with that given by Guyton (1966) for forearm blood flow measured with a plethysmograph (1.5 cm^3/s). The resistance values of the arterial terminations are therefore considered to be realistic.

The basis for the subdivision of the peripheral resistance into four sections representing the small arteries, arterioles, capillaries, and venous system is discussed in Section 5.2. In summary, it was concluded that each terminating resistance should be divided into four parts (R1, R2, R3, and R4) with ratios of 12:55:20:10 so that the approximate mean pressure drop occurring in each section is represented in the model. In addition, two damping capacitors (C1 and C2) are added, one at the junction of the small artery and arteriole resistors, the other at the junction of the arteriole and capillary resistors. Using a 1.2 KHz sinusoidal input to the model (representing the fundamental of a pressure wave at a scaled heart rate of 72 beats per minute) the values of these capacitors were chosen to give 50% and 98% attenuation respectively at the two junctions (the waveform being considered to have an amplitude of 100% at the input to the peripheral circuit). With these capacitors in position, the damping of the pressure pulse as it passes through

the peripheral vessels and microcirculation is simulated realistically.

To represent the compliance of the venous system, a third capacitor (C3) is added to each peripheral circuit at the junction of the capillary and venous resistors. The estimate of the total compliance of the veins distal to the cuff (900×10^{-6} $g^{-1}cm^4sec^2$) is converted to analogue units (900 μF) and divided by 1000 to give a total capacitance of 0.9 μF for the frequency scaling of the model. This value is subdivided into three parts in the ratio of the ulnar, radial, and interosseous peripheral flows, i.e. in the inverse ratio of the venous resistances ($\frac{1}{13}:\frac{1}{21}:\frac{1}{41}$). Since the ulnar and vertebral peripheral resistors have the same values, the capacitor representing the vertebral venous compliance was made equal to that of the ulnar peripheral circuit; the value of this capacitor is not critical as the vertebral artery is sited proximal to the cuff and its corresponding venous pressure is represented by a D.C. voltage. The values of the components of the peripheral networks are given in Table 4.

A.3 Practical Construction of the Model

The complete circuit of the model of the arteries and their terminations is shown in Fig. A-4. The capacitances of the arterial segments were formed by parallel combinations of standard value silver-mica capacitors (1%, 500V). Similarly, the resistances were formed by parallel combinations of standard value carbon-film resistors (5%, ¼W). The inductors were wound on 35 mm diameter adjustable pot-core assemblies

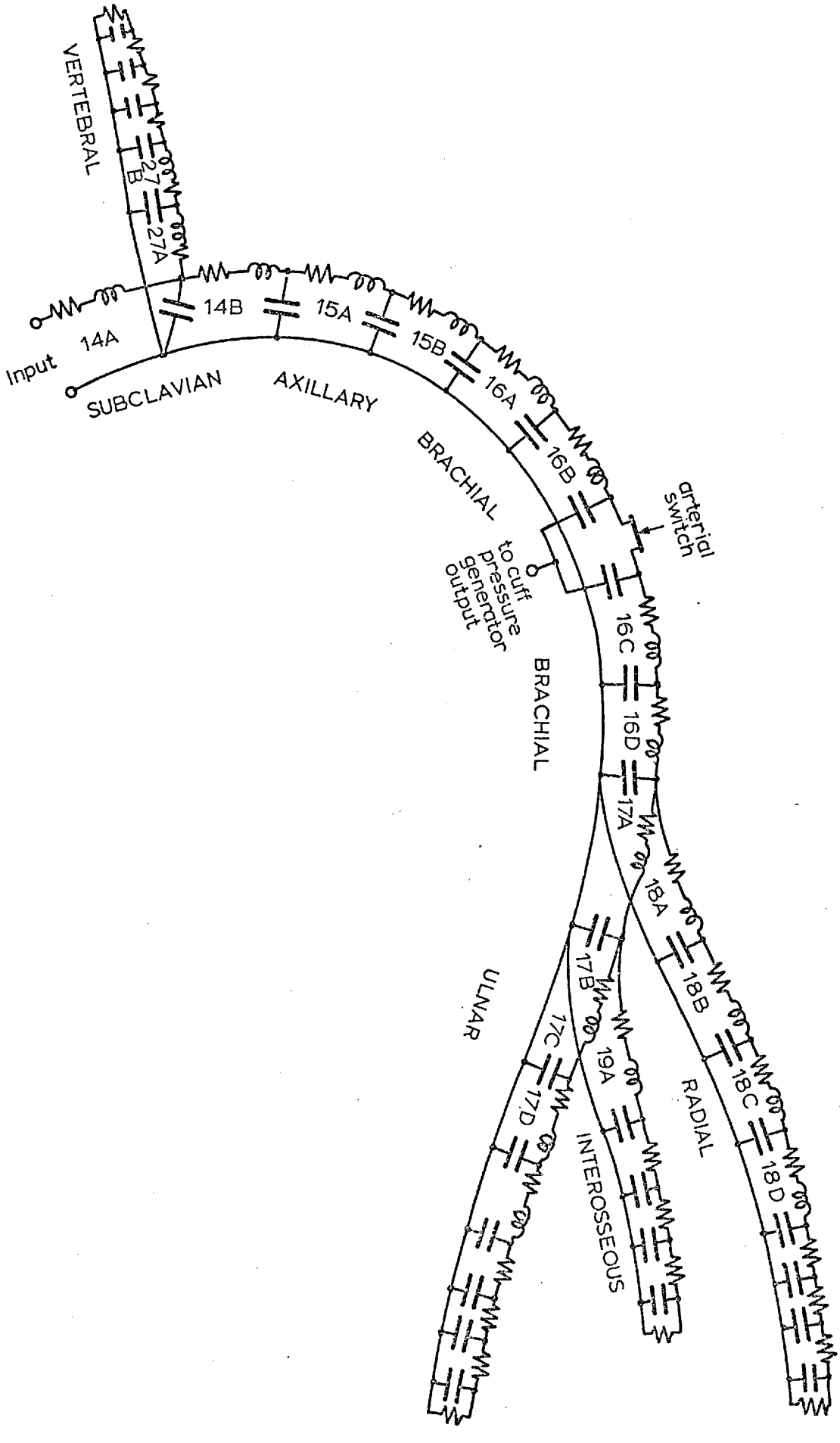


Fig. A-4 : Electrical analogue model of the arm.

(Mullard Vinkor LA1210) and individually trimmed to the required values of inductance. The high Q-factor of the pot-core inductors (typically 250 at 1000 Hz) ensured that the coil resistances were negligible compared with the series resistances of the segments. The resistors and capacitors were mounted in order on a strip of tagboard with their associated inductors on adjacent boards. The capacitors either side of the arterial switch were not connected to the circuit earth but were returned to the output terminal of the cuff pressure generator, because the outer walls of these segments are subjected to the cuff pressure rather than the atmosphere. In the present model, this connection is immaterial as the resistance, compliance, and inertance of the cuff are not modelled and the cuff generator output has negligible impedance to earth at the scaled heart rate frequency.

The choice of the pressure/voltage scale factor is arbitrary; for convenience in making measurements from the oscilloscope screen a factor of 50 mm Hg/V was chosen, with zero voltage representing zero pressure (relative to atmospheric). With this scale factor, a current flow of 1 mA represents a blood flow of $1.33 \times 50 = 66.5$ cm^3/s (refer Section A.2). If the input voltage to the model is maintained at a D.C. level of 2 V (equivalent to a mean arterial pressure of 100 mm Hg) the total current drain is 44 μA (representing a mean arterial flow of 2.92 cm^3/s). Because the current has such a small value, the monitoring of waveforms along the line was carried out using high impedance buffer amplifiers. However, having a low current flowing along the line enabled a semiconductor switch to be used for the simulation of the cuff, as described in Section 5.3.

For the simulation of an indirect blood pressure measurement, the time scaling of 1000 times real frequency permitted successive determinations to be observed as a stable oscilloscope display, compressing the action of one minute into 60 ms. Waveforms were monitored on a 4-channel oscilloscope.

B. ANCILLARY CIRCUITS

In addition to the model of the arm, several circuits were required to implement the simulation of an indirect blood pressure measurement. This appendix contains details of the cuff pressure generator, the arterial and venous switches, and the buffer amplifiers used to link the model to the tape recorder.

B.1 The Cuff Pressure Generator

The circuit diagram and output waveform of the cuff pressure generator are shown in Fig. B-1. The circuit comprises an astable multivibrator with unequal mark:space ratio (T1 and T2), a dual-slope reversing integrator (IC1), a wide hysteresis Schmitt trigger (IC2), and a unity-gain output buffer stage (IC3).

The repetition rate of the modelled cuff pressure cycle is set by the frequency of oscillation of the astable multivibrator. The basic repetition period is 300 ms (representing 5 minutes real time), but if capacitor C2 is removed from the circuit by opening switch S1, the repetition period reduces to 100 ms (1.7 minutes real time). The shorter period was used when it was desirable to reduce the flicker on the oscilloscope screen. Independent of which repetition period is used, the astable multivibrator is designed so that transistor T2 remains cut off for 55 ms in every cycle. In addition, diode D1 is used to isolate the collector of T2 from the capacitor discharge resistor R4 so that a square wave with sharp edges is available for driving the gate of the field-effect transistor (FET) switch via R11. The waveform at the collector of T1 was used to

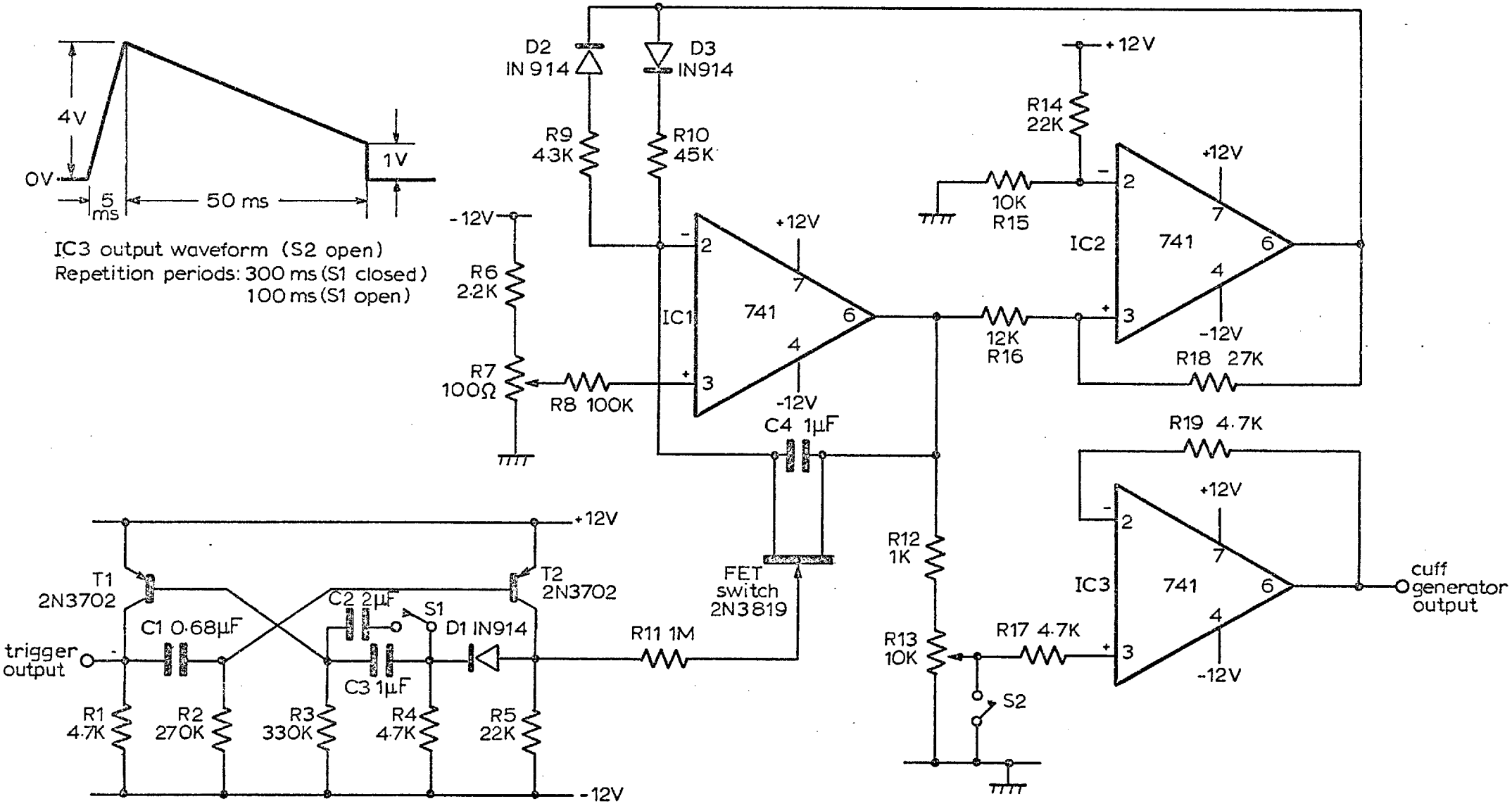


Fig. B-1 : The cuff pressure generator.

trigger the timebase of the oscilloscope.

When T2 is saturated, the FET short-circuits C4 and IC1 is connected as a unity-gain voltage follower. The output voltage of IC1 therefore remains equal to the voltage at the positive input, which is set by variable resistor R7 so that the output of buffer stage IC3 is at zero volts D.C. Whilst IC1 remains clamped at approximately zero volts, the Schmitt trigger IC2 is saturated in the positive direction (about +12 V) and diode D2 is reverse-biassed. However, when the astable multivibrator changes state (thus switching the FET to an open circuit) IC1 is able to begin integrating and its output voltage rises at a rate determined by the current flowing in R10 until it reaches the upper threshold of the Schmitt trigger. At this point (approximately +10 V) the output of IC2 becomes saturated in the negative direction (about -12 V) and D3 becomes reverse-biassed so that the integration changes sign with the rate determined by the current flowing in R9. As long as the FET remains open circuit the integration proceeds with a negative slope and the output of IC1 would eventually fall below the lower threshold of the Schmitt trigger (approximately +1 V). If this point was reached, the Schmitt trigger would change state and reverse the slope of the integration, thus repeating the cycle and generating a triangular waveform at the output of IC1. However, before the negative integration has reached the lower threshold of the Schmitt trigger, the astable multivibrator changes state and the FET is switched to a low resistance. Hence C4 is discharged to zero volts, the Schmitt trigger is fired prematurely, and IC1 again becomes a unity-gain

voltage follower until a new cycle is initiated by the next oscillation of the astable multivibrator.

Variable resistor R13 is used to attenuate the output of IC1 so that the maximum output of IC3 may be set to a calibrated level. Switch S2 is used to short the input of IC3 to ground thus effectively switching off the cuff pressure generator by clamping the output voltage to zero.

B.2 The Arterial and Venous Switches

As outlined in Section 5.3, the action of a cuff in occluding the brachial artery and veins is modelled by semiconductor switches inserted in series with the arterial and venous lines. FETs used to perform the switching were individually selected for a low 'on' resistance (120 Ω) to ensure that their insertion did not cause any significant change in normal transmission along the line. During the simulation of an indirect blood pressure measurement, comparators monitoring the proximal waveform and the output of the cuff pressure generator were used to control the switching of the FETs. To achieve a wide output voltage swing (approximately ± 12 V) with a high slew rate (about 60 V/μs), open-loop uncompensated operational amplifiers were used as the comparators. In addition, it was found necessary to drive the comparators from low impedance sources in order to obtain fast switching times with negligible hysteresis.

The circuit of the arterial switch (Fig. B-2) comprises a comparator (IC1) and voltage followers proximal and distal to the switch (IC2 and IC3). Both voltage followers are FET-input operational amplifiers; these devices draw negligible input bias

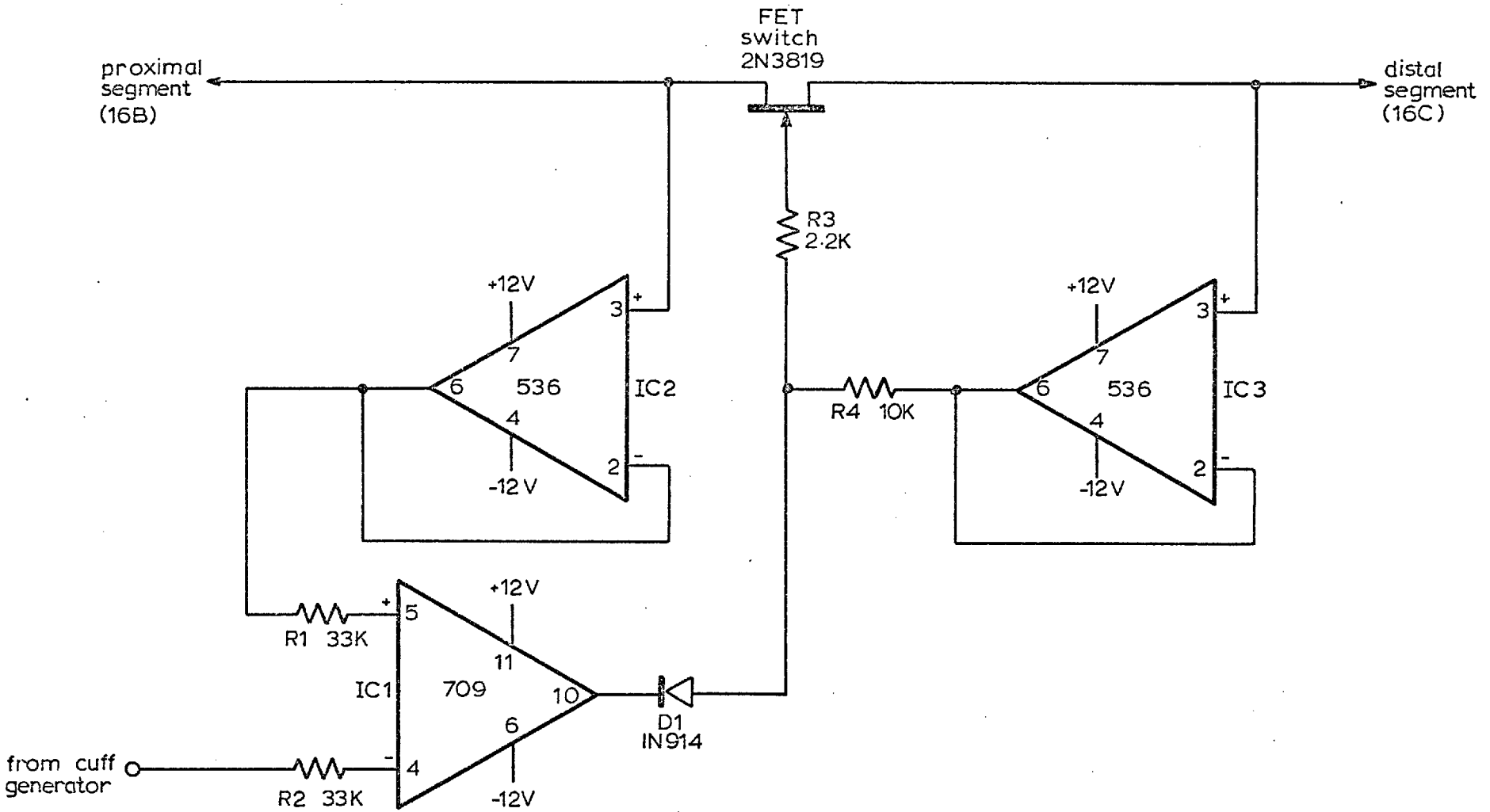


Fig. B-2: The arterial switch.

current and therefore do not load the line. The waveform immediately proximal to the switch is followed by IC2, which provides a low output impedance drive for the comparator. The other input to the comparator is connected to the output of the cuff pressure generator, which is a similar low output impedance source. Resistors R1 and R2 are necessary to limit the input current and prevent the comparator from being damaged. Diode D1 is necessary to prevent the FET junction from becoming forward-biassed when the output of the comparator is positive. If this component were not in circuit, it would be possible for gate current to flow when the FET was in the conducting state, thus interfering with the normal current flow in the line. However, so as not to leave the FET gate at a floating potential when diode D1 is reverse-biassed, the voltage follower IC3 is used to clamp the gate to the distal waveform. Resistor R4 is used to break the clamp when the output of the comparator becomes negative and forward-biasses diode D1 to switch the FET to its non-conducting state.

The circuit of the venous switch (Fig. B-3) is similar except that a high input impedance voltage follower is not required on account of the low impedances in this part of the model: a bipolar-input device is adequate. It is also unnecessary to use a second voltage follower to clamp the FET gate voltage when diode D1 is reverse-biassed, as the circuit position of the FET switch is such that if any gate current flows it is dissipated into the circuit earth without affecting venous flow. Although a single capacitor and resistor could be used to model the total venous compliance and resistance of the

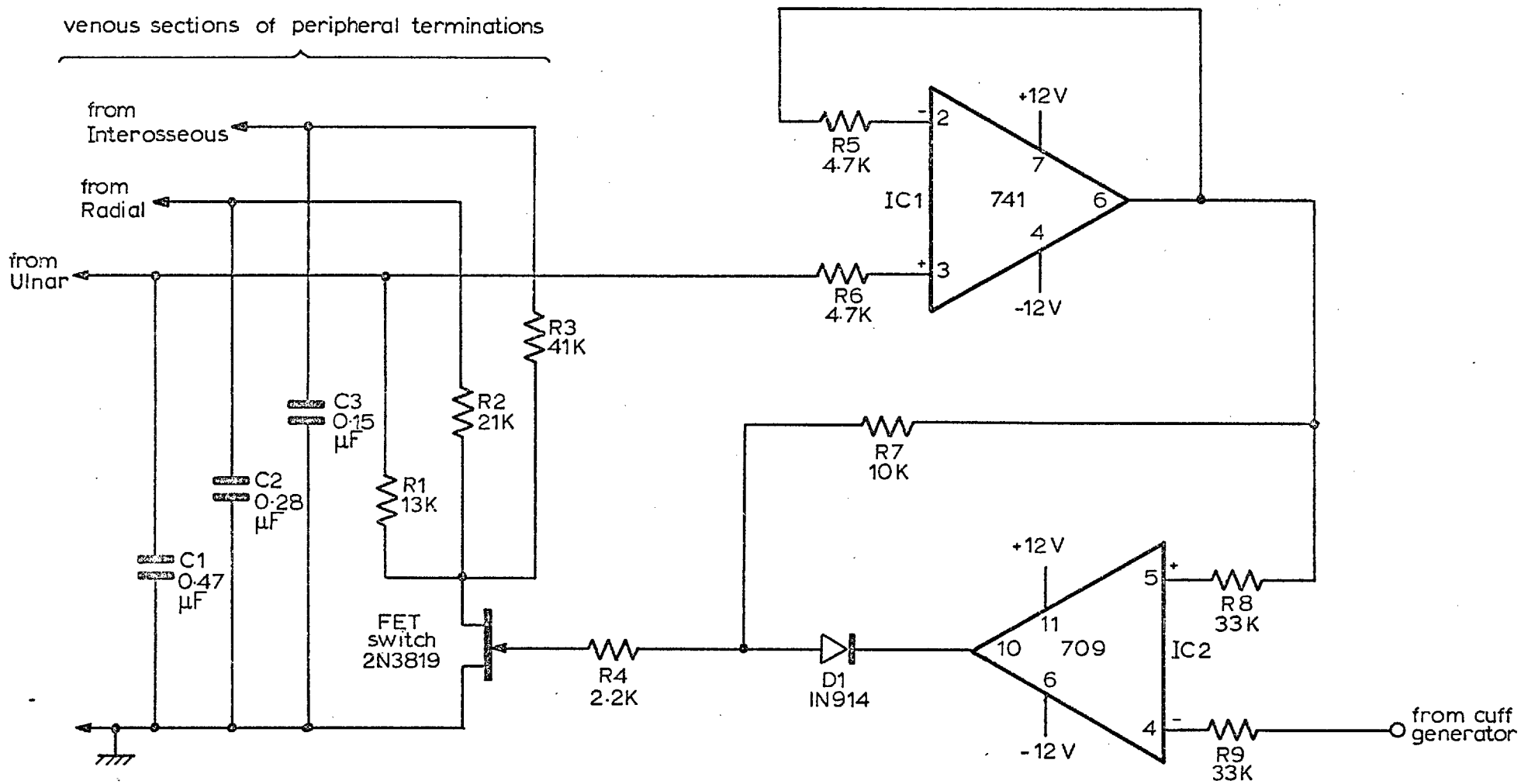


Fig. B-3: The venous switch.

lower arm, for the sake of completeness the venous sections of each peripheral termination are separated. The venous resistances of the ulnar, radial, and interosseous peripheral circuits (R1, R2, and R3) are connected together at the FET switch which, when conducting, forms the link to the circuit earth. As the waveforms representing the distal venous pressure are identical in each peripheral circuit, a single voltage follower (IC1) monitoring the ulnar venous voltage is used to provide an input for the comparator (IC2) controlling the action of the venous switch.

B.3 The Buffer Amplifiers

As described in Chapter 5, practical input waveforms for the model were generated by the IBM 1800 computer at 100 times real frequency and recorded in frequency modulated mode on an instrumentation tape recorder at a speed of 3.75 inches per second. The tape was then played at a speed of 37.5 inches per second to reproduce the waveforms at the time scale of the model, i.e. 1000 times real frequency. A buffer amplifier (Fig. B-4) was used to calibrate the waveform (from $\pm$1.4 V peak-to-peak at the recorder output terminal) to the voltage scale of the simulations (0 V = 0 mm Hg, 4 V = 200 mm Hg). The signal circuit comprises a variable input attenuator (R1), a differential amplifier (IC1), and an output power stage (T1 and T2). The differential amplifier uses a high slew rate device giving a large undistorted output (15 Vp-p) at high frequencies (50 KHz). The amplifier has a gain of 11, and the output D.C. voltage may be set to the desired value by variable resistor R3. Hence the mean level and peak-to-peak amplitude of the output signal may be

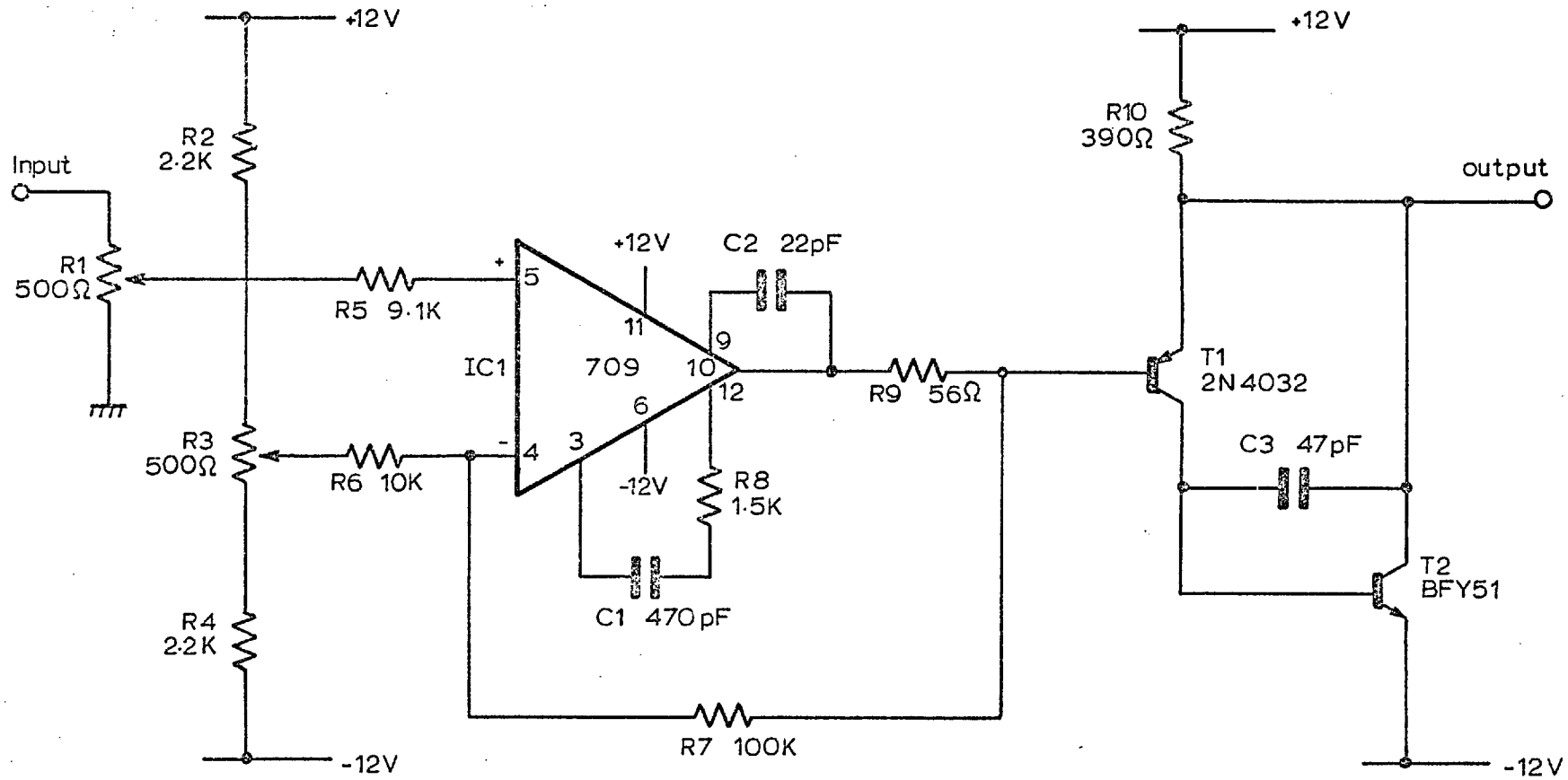


Fig. B-4 : The input buffer amplifier.

varied independently. The PNP-NPN transistor pair was used as an output stage to provide not only a low output impedance but also sufficient current drive at frequencies for which the input impedance of the model approaches the minimum (300Ω). As well as during simulations of indirect blood pressure determinations, the input buffer amplifier was used with variable frequency sine waves for input impedance and transmission measurements.

As with practical waveforms, there are four signals that need to be recorded during the simulation of an indirect blood pressure measurement, namely the input waveform to the model, the waveform at the radial peripheral resistance, the E.C.G., and the cuff pressure waveform. Although the model input and E.C.G. waveforms have been recorded previously, both waveforms need to be re-recorded in order to maintain synchronization with the other two channels, since the record and reproduce heads of the tape recorder are in different positions. To take advantage of the full recording range, three buffer amplifiers were constructed (Fig. B-5) having a fixed gain of 2 and a D.C. offset control (R5) so that voltages from the model (which ranged from 0 V to 4 V) could be calibrated symmetrically about zero (-4 V to 4 V). As with the input buffer amplifier, externally compensated operational amplifiers (IC2) were used to obtain large undistorted output waveforms at high frequencies. In addition, voltage followers (IC1) were used to obtain high input impedances.

Before recordings were taken, the three pressure waveform channels were identically calibrated so that no subsequent calibration was required before or after digitization. The

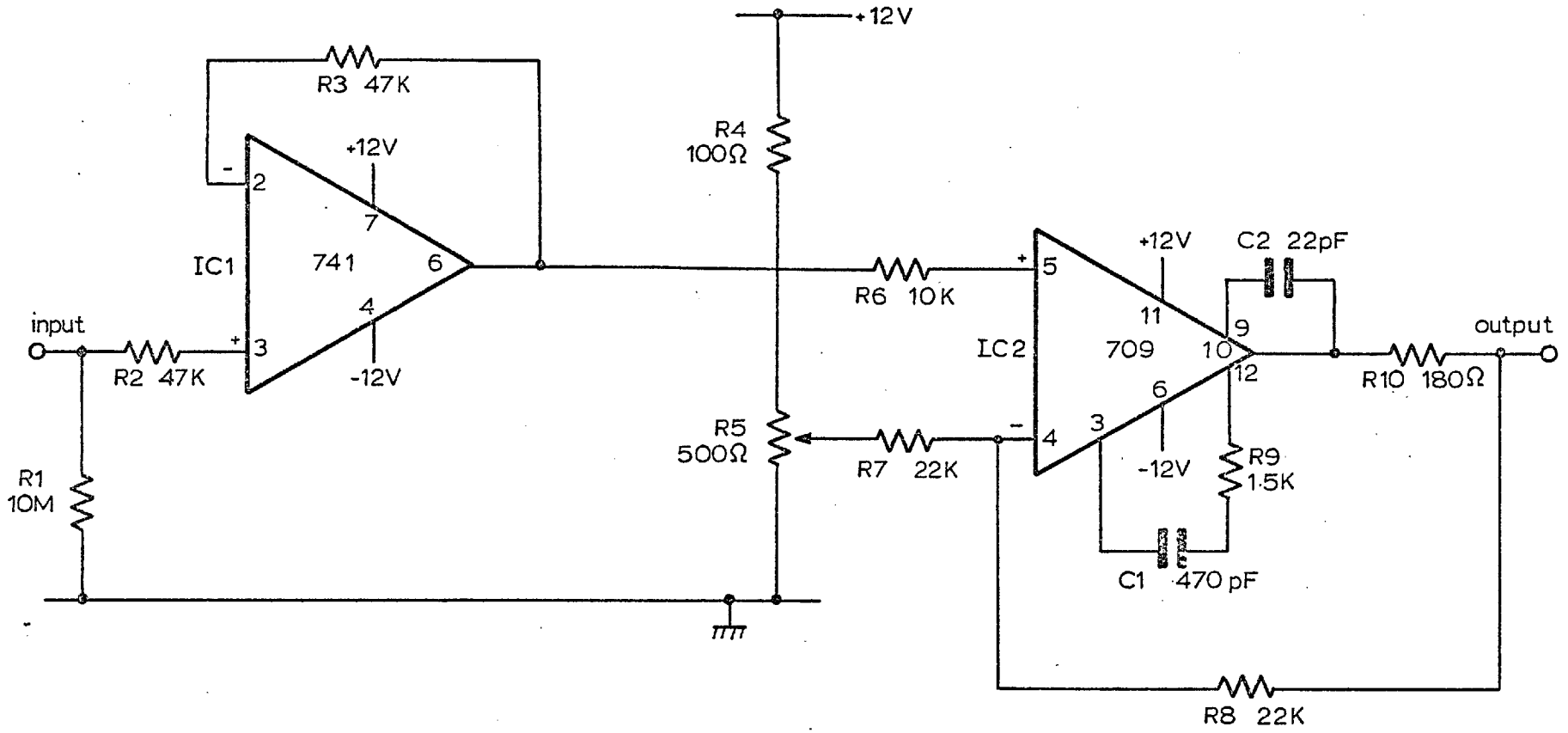


Fig. B-5 : The recording buffer amplifiers.

E.C.G. waveform was recorded by direct connection between the reproduce and record channels.

C. COMPUTER PROGRAMS

As the work described in this thesis forms part of a wider study of the applications of computers to biological signal analysis being carried out in the Engineering in Medicine Laboratory, considerable emphasis has been given to the development of programs and techniques for handling data. This appendix contains details of the main programs and subroutines that were written specifically for this project, as well as a list of other general-purpose ancillary routines. The appendix begins with a brief review of the data processing procedure so that an impression may be gained of the relative importance of the programs discussed.

C.1 Data Processing Procedure

As outlined in Chapter 3, two computers were used to perform the data processing: (i) an IBM 1800 in the Engineering in Medicine Laboratory, and (ii) a CDC 6400 in the Imperial College Computer Centre. Most of the programs were written in Fortran, except for certain oscilloscope display routines, which were written in the Assembler language for the IBM 1800 machine. Wherever possible, use was made of programs already available, including the analogue to digital conversion program, the Fast Fourier and Chirp-Z transform subroutines, and several of the plotting subroutines.

The sequence of the main programs is shown schematically in Fig. C-1. Waveform digitizing and editing were carried out on the IBM 1800 machine, and selected data were transferred to the CDC 6400 on binary punched cards. After calibration of the

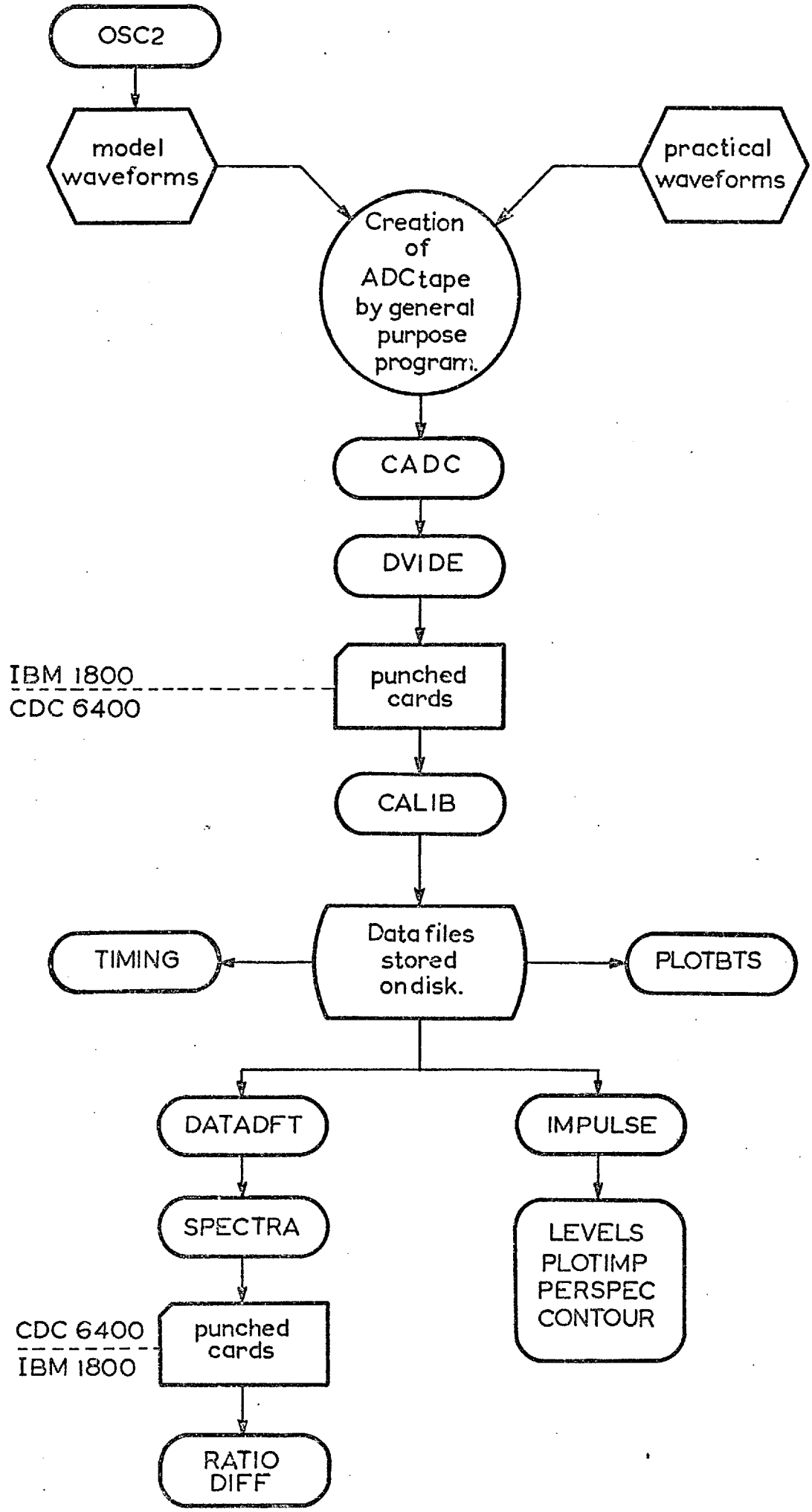


Fig. C-1 : Data processing procedure.

two pressure waveforms, the data were stored on disk files and plotted for visual observation and reference. The data were now available for beat by beat time measurements, frequency analyses, and impulse response analyses. In most cases the results were both plotted and tabulated. Plotting by the CDC 6400 was usually carried out on a Kingmatic flat-bed drafting machine (paper size A2, four pen colours). Alternatively, the same programs could be used for plotting on a Calcomp microfilm plotter (35mm film). In addition, the results of certain programs were copied to punched cards for transfer back to the IBM 1800 machine for further processing or plotting on a Bryans X-Y plotter (paper size A4).

C.2 Main Programs

The following main programs were written to perform the major processing stages. They are listed in an order corresponding to the sequence indicated in Fig. C-1.

OSC2

IBM 1800 Fortran main program to generate two simultaneous waveforms which are recorded for use with the analogue model of the arm. Digitized blood pressure and E.C.G. data for a selected beat are read from binary punched cards, transformed into the frequency domain (subroutine SLOWF) for filtering, and inverse transformed to obtain time waveforms containing the requisite number of harmonics. Continuous digital to analogue conversion is initiated by data channel operation at a rate determined by external synchronization (subroutine AOXY).

CADC

IBM 1800 Assembler main program for oscilloscope display of digitized waveforms stored on magnetic tape. The program is general purpose in that the tape positioning and channel selection details are requested from the computer keyboard. One or two channels may be displayed if the data are multi-channel. The tape is scanned at a rate convenient to the user, and to assist in editing, the block number of the current display may be typed out on command.

DVIDE

IBM 1800 Fortran main program for the creation of binary punched card records of blood pressure, E.C.G., and cuff pressure data. Six 1200-word blocks of 4-channel multiplexed data are read from the ADC tape, demultiplexed, scaled (subroutine MANIP), and placed in separate data arrays. The E.C.G. array is scanned by an algorithm locating the indices of the QRS peaks. These points are shown brightened in oscilloscope displays of (i) the E.C.G. and cuff pressure arrays, and (ii) the aortic and radial blood pressure arrays (subroutine SELEK). After the operator has noted any waveform abnormalities (and corrected the QRS peak indices, if necessary), three records of binary punched cards are produced (subroutine PCARD). The first record contains the QRS peak indices and the cuff pressure samples at these instants, relating to the following two records of aortic and radial blood pressure data. The sequence is repeated until the required sections of data have been copied to punched cards for transfer to the CDC 6400 computer.

CALIB

CDC 6400 Fortran main program for adjusting the two blood pressure channels and the cuff pressure data to the same calibration levels. The data are read from the punched cards produced by the DVIDE main program, converted, and stored on a disk file in card image format. In this manner each 60-bit disk word contains five 12-bit data words, enabling a five-fold reduction in data storage.

PLOTBTS

CDC 6400 Fortran main program for plotting the data (e.g. Fig. 3-2). The aortic and radial blood pressure waveforms are differentiated by colour when using the Kingmatic drafting machine, or by line thickness when plotting on microfilm. The positions of the QRS peaks are indicated by vertical divisions, and the level of the cuff pressure is shown by joining up the cuff pressure samples taken at the occurrence of the QRS peaks. Each beat in the data is sequentially numbered.

TIMING

CDC 6400 Fortran main program for measuring time intervals from the occurrence of the QRS peak to (i) the point located one quarter of the way up the systolic upstroke, and (ii) the end-diastolic point. For each beat the points of maximum and minimum pressure are located, and in the case of the radial waveform, the beat is checked for the presence of a pulse. The position of the desired point on the systolic upstroke is then found by searching the data from the minimum (diastolic pressure)

to the maximum (systolic pressure). The end-diastolic point is located by searching down the systolic upstroke until a point of inflection is found. The results are copied to binary punched cards for plotting by a minor program on the IBM 1800.

DATADFT

CDC 6400 Fortran main program for the frequency analysis of successive beats in the blood pressure waveforms. The indices of the QRS peaks and the two blood pressure waveforms are read from a disk file into the appropriate data arrays, from which beats are sequentially transferred to a working array for processing. The requisite number of low order Fourier harmonic coefficients are computed by subroutine SLOWF (Section C.3) except if 12 or more harmonics are required, when subroutines SETWT and CHRFT are used (Monro, 1972). The amplitudes and phases are calculated from the real and imaginary parts of the harmonics, and the results for each beat are suitably scaled and written to a disk file in compressed binary form. The processing sequence is repeated until all the beats have been analysed.

SPECTRA

CDC 6400 Fortran main program to plot the harmonic amplitudes and phase angles during the period of analysis (e.g. Fig. 3-14). The results of program DATADFT are read and re-arranged in order to show the harmonic variations throughout the data. The re-ordered results are copied to binary punched cards for further analysis and plotting on the IBM 1800.

RATIO and DIFF

IBM 1800 Fortran main programs to compute and plot the harmonic amplitude ratios and phase angle differences of the aortic and radial waveforms (e.g. Fig. 3-16). Corrections are made for phase angle discontinuities at the zero and 2 Pi borders, and non-significant phase angle differences are suppressed for the period of total arterial occlusion.

IMPULSE

CDC 6400 Fortran main program to compute the filtered impulse response of the cuff for successive beats. The aortic and radial waveforms for each beat are transformed into the frequency domain in the manner described for DATADFT. This is followed by complex division of the radial spectrum by the aortic spectrum, and inverse transformation to the time domain to obtain the impulse response filtered to contain the harmonics of interest. To improve the visual presentation, the two halves of the impulse response are transposed to place zero time (relative to the Fourier coefficients of each beat) in the central position before writing the array to a disk file.

LEVELS, PLOTIMP, PERSPEC, CONTOUR

CDC 6400 Fortran main programs to graphically present the successive impulse responses computed by program IMPULSE. Program LEVELS utilizes the line printer to produce a quick estimate of the shape of the set of responses. This is done by printing contours with grey-scale subroutines having ten levels of intensity. The outputs of the other programs are drawn on

microfilm or the flat-bed plotter. Program PLOTIMP is used to show the responses separately for detailed examination (e.g. Fig. 3-25). Program PERSPEC is used for a 3-dimensional representation of the responses considered as a deck of cards (e.g. Fig. 3-26). Program CONTOUR is used to plot the height contours of this imaginary deck as if viewed from a directly vertical position (e.g. Fig. 3-29).

C.3 Subroutines

Although the following subroutines were written specifically for use with the main programs described above, all have been used for similar applications in other research projects.

AOXY

IBM 1800 Assembler subroutine to initiate continuous digital to analogue conversion under external synchronization. The subroutine creates chained data channel tables by transferring the data in reverse order to specific areas in the COMMON part of core storage and adding the control coding, comprising table word count, scan control bits, analogue output addresses, and table chaining addresses. The last table is chained to the first, and execution is returned to the calling program immediately after conversion has been initiated. In this manner very high conversion rates are possible (about 240 KHz) whilst the central processor continues execution independently.

SELEK

IBM 1800 Assembler subroutine for the simultaneous display of two integer data arrays with selected data points brightened. The subroutine positions the beam of the oscilloscope by performing digital to analogue conversion of 3 channels under direct program control. Two channels are used for the data, whilst the third is used to provide the oscilloscope timebase. The indices of the data points to be brightened are held in an ancillary integer array, and the timebase is halted momentarily whenever the beam is displaying one of these points. The phosphor screen is therefore energized for a longer period to brighten the display at the selected indices. Further indices may be selected (or unwanted ones deleted) by bringing a movable spot on to the screen and shifting it to the desired positions. The control of this spot is by manual operation of the Process Interrupt switches, which are checked by the subroutine before the display is refreshed with another horizontal sweep.

PCARD

IBM 1800 Assembler subroutine to punch a record of 80-column cards with seventy-five 12-bit integer data words per card compatible with the CDC 6400 format for binary card input. As well as the data, each card contains a word count and a sequence number. Before punching, the subroutine checks that the card is blank, and any non-blank cards encountered are rejected to the second stacker. After the required number of data words have been transferred to cards, the record is terminated by punching a CDC 6400 End-of-Record card.

LCARD

IBM 1800 Assembler subroutine to read binary data cards produced by subroutine PCARD, or punched by the CDC 6400 machine. End-of-Record cards are ignored, but if a CDC 6400 End-of-File or End-of-Information is encountered, reading is terminated and a flag is set for the calling program to take appropriate action.

MANIP

IBM 1800 Assembler subroutine for scaling integer data values between the specific ranges used by the display, ADC, and binary card routines. Fast operation is achieved by bit-shifting the data instead of multiplication or division.

SLOWF

IBM 1800 and CDC 6400 Fortran subroutine to compute the Fourier coefficients of a given number of low-order harmonics, using Equations 3.6 and 3.7. The subroutine operates only on a real data sequence. The real parts of the complex harmonic coefficients are overwritten into the data array, whereas a separate array is required for the imaginary parts. This was done to provide compatibility with Monro's (1972) FFT subroutines.

AMPHASE

CDC 6400 Fortran subroutine to compute the amplitudes and phase angles of a specified number of complex coefficients calculated by the DFT or FFT routines. No change is made to the first term (the D.C. level). The amplitudes are calculated as twice the

square root of the sum of the squares of the real and imaginary parts. The phase angles are computed as the inverse tangents of the ratio of the imaginary and real parts, expressed as coefficients of Pi. To avoid division by zero in the computation of the phase angle, the absolute value of the denominator is compared with 0.001. If it is less than this the division is not carried out and the angle is set to 0.5 Pi or 1.5 Pi according to the sign of the numerator, or if the numerator is less than 0.001, the angle is set to zero. For each harmonic, the amplitude and phase results are overwritten in the locations of the respective real and imaginary coefficients.

HIST

IBM 1800 Assembler subroutine to display an integer data array as a bar graph. The subroutine positions the beam of the oscilloscope by performing digital to analogue conversion of two channels under direct program control, one channel for the data, the other to provide the oscilloscope timebase. Each bar is formed by a discrete number of dots with a height proportional to the magnitude of the data word. The maximum height is 50 dots, representing the largest integer of the machine (32767). This subroutine is useful for displaying data containing large differences in magnitude between adjacent values, e.g. spectral amplitudes.

MULT2

IBM 1800 Assembler subroutine to double the magnitudes of data held in an integer array. Each data word is first checked to

see if it lies within the range -16384 to 16383. If this is the case, the data word is shifted left one bit, i.e. multiplied by two. If the data word is greater than 16383 or less than -16384 the number is replaced by 32767, -32768 respectively. By using this subroutine, spectral amplitudes may be magnified for display by subroutine HIST without erroneous results being shown for data which, if doubled in magnitude, would exceed the integer range of the machine.

RAST

IBM 1800 Assembler subroutine to display the analogue output voltage limits as an oscilloscope raster. Two analogue output channels are used, one to display horizontal levels representing the integers 0, 16384 and 32767 (i.e. zero, half maximum height, and maximum height), the other to show the screen width boundaries represented by the integers 0 and 32767.

C.4 Ancillary Routines

Numerous other subroutines and main programs were written for both machines, many of which have been usefully applied in other areas of biological signal processing. For this reason they were written to be as versatile as possible in order to meet the requirements of a wide variety of needs in data handling, processing, and the presentation of results. Some of the more useful general-purpose routines developed during the course of this work are given in the following list.

IBM 1800

AOEXT, AOX, AOHLT	Data channel analogue output subroutines
DISK	To read or write data on disk
GREYP, GREYS, GREYK	Grey-scale printing subroutines
RD11S, RD11Y	Tape reading subroutines
SKIP, SKIPB	Tape positioning subroutines
SGNLS	General-purpose FFT and Chirp-Z program
TDATA	To request an unformatted integer from the keyboard
WINDO	To apply Hanning taper to data array

CDC 6400

CHECK, SCAN, CHECKF	To print structure of data files
SECTORS, RENEW, TOTAL	Housekeeping programs for permanent files

REFERENCES

Anliker, M. and Raman, K.R. (1966)
Korotkoff Sounds at Diastole - A Phenomenon of Dynamic Instability of Fluid-Filled Shells
International Journal of Solids and Structures Vol. 2, 467-491

Attinger, E.O. (1966)
Hydrodynamics of Blood Flow
Advances in Hydroscience Vol. 3, 111-152

Attinger, E.O. (1968)
Analysis of Pulsatile Blood Flow
Advances in Biomedical Engineering & Medical Physics Vol. 1, 1-59

Bellville, J.W. and Weaver, C.S. (1969)
Techniques in Clinical Physiology
Collier-Macmillan, London

Bergel, D.H. (1961a)
The Static Elastic Properties of the Arterial Wall
Journal of Physiology Vol. 156, 445-457

Bergel, D.H. (1961b)
The Dynamic Elastic Properties of the Arterial Wall
Journal of Physiology Vol. 156, 458-469

Bordley, J., Connor, C., Hamilton, W., Kerr, W., Wiggers, C.J. (1951)
Recommendations for Human Blood Pressure Determinations by Sphygmomanometers
Circulation Vol. 4, 503-509

Burton, A.C. (1951)
On the Physical Equilibrium of Small Blood Vessels
American Journal of Physiology Vol. 164, 319-329

Burton, A.C. (1965)
Physiology and Biophysics of the Circulation
Year Book Medical Publishers, Chicago

Clark, P.W. and Gowen, R.J. (1969)
Digital Indirect Blood Pressure Measurement
Proceedings of the 8th International Conference on Medical and Biological Engineering, Chicago

Clist, R.S. (1970)
Indirect Measurement of Blood Pressure from the Finger
presented at National Electronics Convention, Auckland

Conrad, W.A. (1969)
Pressure-Flow Relationships in Collapsible Tubes
I.E.E.E. Transactions on Bio-Medical Engineering Vol. 16, 284-295

De Dobbeleer, G.D.P. (1963)
Measurement of the Systolic and Diastolic Blood Pressure by means of Phase Shift
Proceedings of the 5th International Conference of Medical Electronics, Liege, 229-250

De Dobbeleer, G.D.P. (1965)
Measurement of Systolic and Diastolic Blood Pressure by means of Phase Shift
World Medical Electronics Vol. 3, 122-126

De Pater, L. (1966)
An Electrical Analogue of the Human Circulatory System
Ph.D. Thesis, Groningen

De Wit, B., Wesseling, K.H., Beneken, J.E.W. (1973)
Arm Arterial Parameters Determined from Noninvasively Measured Pulse Waves, using Parameter Estimation
Digest of the 10th International Conference on Medical and Biological Engineering, Dresden, paper 27-2

Fry, D.L. (1959)
The Measurement of Pulsatile Blood Flow by the Computed Pressure Gradient Technique
I.R.E. Transactions on Medical Electronics Vol. 6, 259-264

Gabe, I.T. (1965a)
Arterial Blood Flow by Analogue Solution of the Navier-Stokes Equation
Physics in Medicine and Biology Vol. 10, 271-280

Gabe, I.T. (1965b)
An Analogue Computer Deriving Oscillatory Arterial Blood Flow from the Pressure Gradient
Physics in Medicine and Biology Vol. 10, 407-415

Geddes, L.A. (1970)
The Direct and Indirect Measurement of Blood Pressure
Year Book Medical Publishers, Chicago

Gowen, R.J. (1963)
Automatic Electronic Measurement of Blood Pressure during Exercise
I.E.E.E. International Convention Record Vol. 11, Part 9, 132-140

Greatorex, C.A. (1971)
Indirect Methods of Blood Pressure Measurement
I.E.E. Medical Electronics, Monographs 1-6, 43-72
Peregrinus, London

Greenfield, J.C. (1966)
The Pressure Gradient Technique
Methods in Medical Research, Vol. 11, 83-93
Year Book Medical Publishers, Chicago

Greenfield, J.C. and Fry, D.L. (1965)
Relationship between Instantaneous Aortic Flow and the Pressure Gradient
Circulation Research Vol. 17, 340-348

Guyton, A.C. (1966)
Textbook of Medical Physiology, 3rd Edition
W.B. Saunders Co., Philadelphia

Hales, Stephen (1733)
Statical Essays: containing Haemostaticks
in Classics in Arterial Hypertension, edited by Ruskin, 1956
Charles C. Thomas, Springfield

Hamilton, W.J. (1956)
Textbook of Human Anatomy
Macmillan and Co. Ltd., London

Harvey, William (1628)
The Circulation of the Blood
Everyman's Library, 1968
Dent, London

Horeman, H.W. and Noordergraaf, A. (1958)
Numerical Evaluation of Volume Pulsations in Man
1. The Basic Formula
Physics in Medicine and Biology Vol. 3, 51-58

Jager, G.N., Westerhof, N., Noordergraaf, A. (1965)
Oscillatory Flow Impedance in Electrical Analog of Arterial System
Circulation Research Vol. 16, 121-133

Johnston, T.B. and Whillis, J. (1947)
Gray's Anatomy, 29th Edition
Longmans, Green and Co., London

Karvonen, M.J., Telivuo, L.J., Jarvinen, E.J.K. (1964)
Sphygmomanometer Cuff Size and the Accuracy of Indirect
Measurement of Blood Pressure
American Journal of Cardiology Vol. 13, 688-693

Kirkendall, W.M., Burton, A.C., Epstein, F.H., Freis, E.D. (1967)
Recommendations for Human Blood Pressure Determination by
Sphygmomanometers
Circulation Vol. 36, 980-988

Kitney, R.I. and Sheldrake, A. (1973)
An Algorithm to Evaluate the Time Response of a Linear Biological
System from its Transfer Function
Computers and Biomedical Research Vol. 6, 570-577

Korotkoff, N.S. (1905)
A Contribution to the Problem of Methods for the Determination
of the Blood Pressure
in Classics in Arterial Hypertension, edited by Ruskin, 1956
Charles C. Thomas, Springfield

Lambert, J.W. (1958)
On the Non-Linearities of Fluid Flow in Non-Rigid Tubes
Journal of the Franklin Institute Vol. 266, 83-102

Lathi, B.P. (1965)
Signals, Systems, and Communication
John Wiley & Sons, New York

London, S.B. and London, R.E. (1967)
Comparison of Indirect Pressure Measurements (Korotkoff) with Simultaneous Direct Brachial Artery Pressure Distal to the Cuff
Advances in Internal Medicine Vol. 13, 127-142

Lynn, P.A. (1973)
An Introduction to the Analysis and Processing of Signals
Macmillan Press, London

Monro, D.M. (1971)
Implementing the Fast Fourier Transform
Application Report No. 3, Engineering in Medicine Laboratory,
Imperial College, London

Monro, D.M. (1972)
Algorithm : Fast Fourier Transform
Application Report No. 5, Engineering in Medicine Laboratory
Imperial College, London

McCutcheon, E.P. and Rushmer, R.F. (1967)
Korotkoff Sounds - An Experimental Critique
Circulation Research Vol. 20, 149-161

McDonald, D.A. (1955)
The Relation of Pulsatile Pressure to Flow in Arteries
Journal of Physiology Vol. 127, 533-552

McDonald, D.A. (1960)
Blood Flow in Arteries
Edward Arnold (Publishers) Ltd., London

Noordergraaf, A. (1956)
Physical Basis of Ballistocardiography
Ph.D. Thesis, Utrecht

Noordergraaf, A. (1969)
Hemodynamics
in Biological Engineering, edited by H.P. Schwan
McGraw Hill, New York

Noordergraaf, A., Verdouw, P.D. and Boom, H.B.K. (1963)
The Use of an Analog Computer in a Circulation Model
Progress in Cardiovascular Diseases Vol. 5, 419-439

Nyquist, H. (1928)
Certain Topics in Telegraph Transmission Theory
Journal of the American I.E.E. Vol. 47, 214-216

Patel, D.J. and Vaishnav, R.N. (1972)
The Rheology of Large Blood Vessels
in Cardiovascular Fluid Dynamics, edited by D.H. Bergel
Academic Press, London

Raines, J.K. (1972)
Diagnosis and Analysis of Arteriosclerosis in the Lower Limbs
Ph.D. Thesis, Massachusetts Institute of Technology

Raines, J.K., Jaffrin, M.Y., Shapiro, A.H. (1971)
A Computer Simulation of the Human Arterial System
Proceedings of the Summer Computer Simulation Conference,
Boston, Mass. 890-900

Riva-Rocci, Scipione (1896)
A New Sphygmomanometer
in Classics in Arterial Hypertension, edited by Ruskin, 1956
Charles C. Thomas, Springfield

Sacks, A.H., Raman, K.R., Burnell, J.A. (1963)
A Study of Auscultatory Blood Pressures in Simulated Arteries
Proceedings of the 4th International Congress in Rheology,
Providence, Part 4, 215-230

Schultz, D.L. (1972)
Pressure and Flow in Large Arteries
in Cardiovascular Fluid Dynamics, edited by D.H. Bergel
Academic Press, London

Selkurt, E.E. (1966)
Physiology, 2nd Edition
Little, Brown and Company, Boston

Shirer, H.W. (1962)
Blood Pressure Measuring Methods
I.R.E. Transactions on Bio-Medical Engineering Vol. 9, 116-125

Simpson, J.A., Jamieson, G., Dickhaus, D.W., Grover, R.F. (1965)
Effect of Size of Cuff Bladder on Accuracy of Measurement of
Indirect Blood Pressure
American Heart Journal Vol. 70, 208-214

Singleton, R.C. (1969)
An Algorithm for Computing the Mixed Radix Fast Fourier Transform
I.E.E.E. Transactions on Audio Electroacoustics Vol. 17, 93-103

Skilling, H.H. (1952)
Electric Transmission Lines; Distributed Constants, Theory and
Applications
McGraw Hill, New York

Snyder, M.F., Rideout, V.C., Hillestad, R.J. (1968)
Computer Modelling of the Human Systemic Arterial Tree
Journal of Biomechanics Vol. 1, 341-353

Streeter, V.L., Keitzer, W.F., Bohr, D.F. (1963)
Pulsatile Pressure and Flow through Distensible Vessels
Circulation Research Vol. 13, 3-30

Streeter, V.L., Keitzer, W.F., Bohr, D.F. (1964)
Energy Dissipation in Pulsatile Flow through Distensible Tapered
Vessels
in Pulsatile Blood Flow 149-177, edited by E.O. Attinger
McGraw Hill, New York

Stuart, R.D. (1961)
An Introduction to Fourier Analysis
Methuen & Co. Ltd., London

Taylor, M.G. (1959)
The Influence of the Anomalous Viscosity of Blood upon its Oscillatory Flow
Physics in Medicine and Biology Vol. 3, 273-290

Vander Werff, T.J. (1971)
Studies in Cardiovascular Fluid Dynamics
Ph.D. Thesis, Oxford

Vierhout, R.R. (1963)
Indirect and Direct Blood Pressure Measurements
Proceedings of the 5th International Conference of Medical Electronics, Liege, 151-165

Weinman, J. (1972)
An Appraisal of some Noninvasive Cardiovascular Techniques
Medical and Biological Engineering Vol. 10, 496-503

Weinman, J., Hayat, A., Raviv, G. (1973)
Relationship Between Blood Volume and Light Intensity in Reflection Photoplethysmography
Digest of the 10th International Conference on Medical and Biological Engineering, Dresden, paper 7-1

Westerhof, N., Bosman, F., De Vries, C.J., Noordergraaf, A. (1969)
Analog Studies of the Human Systemic Arterial Tree
Journal of Biomechanics Vol. 2, 121-143

Westerhof, N. and Noordergraaf, A. (1970a)
Errors in the Measurement of Hydraulic Input Impedance
Journal of Biomechanics Vol. 3, 351-356

Westerhof, N. and Noordergraaf, A. (1970b)
Arterial Viscoelasticity : A Generalized Model
Journal of Biomechanics Vol. 3, 357-379

Womersley, J.R. (1955a)
Method for Calculation of Velocity, Rate of Flow, and Viscous Drag in Arteries when the Pressure Gradient is Known
Journal of Physiology Vol. 127, 553-563

Womersley, J.R. (1955b)
Oscillatory Motion of a Viscous Liquid in a Thin-Walled Elastic Tube 1. The Linear Approximation for Long Waves
Philosophical Magazine Vol. 46, 199-221

Womersley, J.R. (1957a)
An Elastic Tube Theory of Pulse Transmission and Oscillatory Flow in Mammalian Arteries
Wright Air Development Centre Technical Report TR 56-614

Womersley, J.R. (1957b)
Oscillatory Flow in Arteries : the Constrained Elastic Tube as a Model of Arterial Flow and Pulse Transmission
Physics in Medicine and Biology Vol. 2, 178-187